Thèse n° 7764

On the compressive and bond strength of reinforced concrete as structural properties

Présentée le 26 février 2021

Faculté de l'environnement naturel, architectural et construit
Laboratoire de construction en béton
Programme doctoral en génie civil et environnement

pour l'obtention du grade de Docteur ès Sciences

par

Francesco Rafael Alberto MOCCIA

Acceptée sur proposition du jury

Dr A. Vassilopoulos, président du jury
Prof. A. Muttoni, Dr M. Fernández Ruiz, directeurs de thèse
Prof. S. J. Foster, rapporteur
Prof. A. Sharma, rapporteur
Dr P. Lestuzzi, rapporteur

École
polytechnique
fédérale
de Lausanne

2021

To my dear parents,

Annamaria and Alberto.

Foreword

The uniaxial compressive strength of concrete has traditionally been considered as the most relevant parameter characterizing the response of this material. This value is, other than used to define the compressive resistance, also considered to characterize in an indirect manner the response of concrete in tension or with respect to its stiffness and toughness. The consideration of the compressive resistance as a material parameter presumes it to be constant within a structural member, and that it can be characterized on the basis of simple tests on specimens with given geometries (such as cubes, prisms or cylinders). The reality is however significantly more complex, and the concrete strength in a structure shows deviations with respect to simple material tests. Some relevant phenomena associated to these differences are the local casting conditions (influencing the local water content and early micro-cracking due to plastic settlement during concrete hardening), the presence of disturbances (such as ducts or large reinforcement, creating stress concentrations) and other structural effects influencing the state of cracking. Such phenomena also show strong influences on the response of bond between concrete and reinforcement, as experimentally observed in the past and traditionally considered by means of empirical efficiency factors.

In this context, the present research work aims at providing a comprehensive overview and scientific understanding of the physical phenomena locally governing the structural response of concrete compressive strength and bond. This is performed on the basis of a detailed experimental programme, instrumented with state-of-the-art measurement techniques (such as Digital Image Correlation or tomography) allowing to track in an accurate manner the displacement field under different conditions or investigating the cracking disturbances at selected locations. The results of this investigation are applied to a number of structural elements considering potential stress redistributions and its eventual strength. Such results are used to validate in a clear manner modern design approaches for reinforced concrete columns accounting for the interaction of longitudinal and confinement reinforcement as well as concrete brittleness. In particular, these results have been used for validation of the proposed formulations for the future revision of Eurocode 2. Also, detailed physical models are proposed and validated for the bond resistance governed by spalling of the concrete cover, outlining a comprehensive frame for treatment of bond in structural concrete.

This thesis has been partially funded by the Swiss Federal Road Authority, whose support is greatly appreciated.

Lausanne, October 2020

Prof. Aurelio Muttoni Dr Miguel Fernández Ruiz

Acknowledgements

During the almost five years spent at the Structural Concrete Laboratory (IBETON) of the Ecole Polytechnique Fédérale de Lausanne (EPFL), I had the chance of being surrounded by extraordinary people that supported and helped me in numerous ways.

First of all, my most sincere gratitude goes to my thesis directors Prof. Aurelio Muttoni and Dr Miguel Fernández Ruiz for giving me this incredible opportunity. Their expertise in the field, their passion and their energy motivated me to constantly improve myself and to push my boundaries. The daily discussions as well as their guidance helped me to enhance my knowledge and to develop a rigorous and efficient approach.

I would also like to acknowledge the members of the jury, namely Prof. Stephen J. Foster, Prof. Akanshu Sharma, Dr Anastasios Vassilopoulos and Dr Pierino Lestuzzi for their engagement and the time spent reading the manuscript. In addition, this research project would not have been possible without the funding provided by the Ecole Polytechnique Fédérale de Lausanne and by the Swiss Federal Road Authority (OFROU). Their financial support is greatly appreciated. During my staying at EPFL, I also had the chance to work with Prof. Giovanni Plizzari and Prof. Giovanni Metelli from the University of Brescia. I want to express my gratitude for this valuable collaboration.

I would also like to offer my special thanks to my officemates Filip Niketic and Raffaele Cantone. The experiences we shared (at work and outside EPFL) were truly amazing and certainly created an everlasting bond between us. My most sincere gratitude goes to my dear friends João Pacheco Almeida and Michele Godio. Their positivity, their great humour and their brilliant advices were truly helpful. Their attitude and personality surely inspired me significantly.

Special thanks to Yvonne Buehl-Brauch for being the kindest secretary and for providing with administrative and personal support. I would also like to thank Dr Olivier Burdet for the IT support and for the suggestions on laboratory and research work. Thanks also to Emma Sorrentino for her goodwill and openness.

I would like to express the deepest gratitude to all my colleagues from IBETON. I will certainly miss the interesting discussions and this dynamic environment. Special thanks goes to the senior generation of IBETON: Francisco, Jürgen, Marie-Rose, Fabio, Francesco (Cavagnis), Filip, Ioannis, João, Darko, Raffaele, Patrick and Max. I would also like to thank the younger generation of IBETON that brought new energy and motivation to the team: Diego, Xhemsi, Marko, Qianhui, Enrique and Frédéric. Special thanks goes to my dear friend Elizam Banla for his help in carrying out experimental tests and for the joy he brought to work every day. Thanks also to the new post-doc Andri as well as the numerous exchange students that joined us throughout the past years: Ondrej, Jesper, Hayami, Eduardo, Quentin, Andrea, Aurélie, Damjan and Aleksandar. I would also like to acknowledge Stefano Campana, Eckart Hars, Richard Thürler, Patrick Buchs, Dario Redaelli and Damien Dreier for sharing their valuable knowledge and expertise. Many thanks to Fabio Brantschen for always being available and providing with precious recommendations on laboratory work, but also for the various trips we did together around Europe and beyond.

The numerous experimental programmes carried out at the structural laboratory of EPFL would not have been possible without the precious help and experience of all technicians: Gilles, Serge, Gérald, Frédérique, Gary, Armin, Sylvain and François. Thank you very much to all of you.

The dynamic environment of EPFL also allowed me to meet several wonderful persons from other laboratories. Special thanks goes to all colleagues of EESD: Bastian, Angelica, Alessandro (Paparo), Ivana, Mahmoud, Amir, Igor, Francesco (Vanin), Danilo, Shenghan, Maria Pia, Lisandro and Giorgia. In addition, many thanks to Julien and Aryan of IBOIS, with whom I shared the hazardous life of the laboratory but also numerous hilarious moments. I would also like to thank the team of LMC, in particular Lionel Sofia and Antonino Costarella. Thanks also to Davide and Severin of LCH as well as Philippe, Imane, Gianni and Bartek from the MCS laboratory.

I would like to express my deepest gratitude to Dr Michel Gonzalez and Dr Sébastien Déglise from CHUV that saved my life on several occasions in 2018 by performing flawless and accurate surgeries.

Big thanks to Paul Biju-Duval for all the help he provided me during my stay in Austin and for the motivation in starting a PhD. I would also like to acknowledge Michele Frigerio for the opportunity that he gave me a few years ago to work with him. The collaboration was truly valuable and interesting.

In addition, I would like to thank Mikhail and Chris for the time spent together trying to develop a surfboard with a hydrofoil. It definitely was an intriguing project, even though it did not succeeded.

I would like to acknowledge all the support and positive energy received from the numerous friends that studied with me during the Bachelor and Master programmes: Melisa & Hugues, Ilham, Luca & Lila, Lucien & Cynthia, Geoffroy & Martina, Guillaume, Sarah & Quentin, Samuel (Rochat), Lucas, Emeline & Antoine, Benoit, Elodie, Tom, Clara & Samuel (Grangier), Jochua, Nikita, Marc-André, Charly, Arnaud, Laure, Pietro, Quentin and Etienne.

In addition, I sincerely thank my dear friends from Ticino: Giovanni, Orlando, Alessandro, Matteo, Franco, Annick, Jan, Charlotte, Gianluca, Davide, Giuseppe and David. They all showed me that, despite the distance separating us, I could always count on them. I also want to take this opportunity to thank Zeno and Giacomo for their goodwill and friendship.

Finally, I want to express all my gratitude to my family and Laura. Thanks to my brothers Alden and Christian for the encouragement and motivation throughout the past years. They clearly represent for me a source of admiration and an example to follow. My most sincere gratitude goes to Laura for the incredible support and infinite love that she gives me. I will never forget the kindness and endless patience she demonstrated in all circumstances. She definitely brought light into my life and I am thrilled to continue this journey together with her. Special thanks also to her family that welcomed me heartily and made me feel at home. My deepest gratitude goes to my dear parents Annamaria and Alberto for their unconditional love and generosity. They were always by my side when I needed them and they supported me in all life challenges. I have always felt blessed to be their son. This thesis is dedicated to them.

Lausanne, October 2020

Francesco Moccia

Abstract

Traditionally, the concrete strength is measured on cubes or cylinders having normalized dimensions, suitable vibration and curing conditions and their strength is assessed in laboratory under fast loading rates. However, the in-situ strength of structural elements can considerably differ from that of a small and homogenous control specimen due to a number of issues.

Notably, phenomena taking place during the consolidation process of fresh concrete may affect the compressive resistance of tall members as well as the bond strength of reinforcing bars located in top layers. During concrete consolidation, water migrates in the direction of the free surface while concrete settles downwards, phenomena referred as concrete bleeding and plastic settlement respectively. Under these circumstances, a decrease in the concrete properties near the upper surface is observed as well as a development of cracks and voids surrounding horizontal reinforcing bars, causing potential disturbances on the compressive stresses and affecting the mechanical engagement between bars and concrete.

In addition, the response of structural concrete may differ from that of material samples due to non-uniform stress states, the material brittleness, the cracking induced by imposed strains, the rheological response of concrete and the presence of embedded disturbances. As a result, the strength measured in material samples needs to be corrected with strength reduction factors to ensure suitable structural analysis.

In this thesis, an in-depth investigation is performed on the different phenomena affecting the compressive and bond strength of structural members. These aspects are assessed by means of several testing programmes instrumented with refined measurements techniques such as tomography and Digital Image Correlation.

An extensive experimental programme comprising 76 column and prism tests was carried out to evaluate the influence of casting position, loading direction and bar disturbances on the compressive resistance of structural elements. The detailed measurements performed at the fresh and hardened state resulted in the proposal of consistent design rules accounting for the investigated phenomena.

Focus was also given on the influence of material brittleness and the implications of internal stress redistributions on the structural response of reinforced concrete columns and compression zones of members in bending. The pertinence of the investigations were validated based on more than 400 column tests collected from the literature.

The implications of casting conditions on pull-out and spalling failures were also assessed by means of 137 pull-out tests on reinforcing bars presenting variable diameter, concrete cover, casting height and embedded length. The investigations resulted in the proposal for a physically-consistent approach, evaluating the pull-out resistance as function of casting conditions and reinforcement characteristics.

Finally, the phenomenon of cover spalling was examined with respect to the action of a radial inner pressure, as originated by bond engagement or associated to the volumetric expansion of corroded reinforcement. The mechanisms inducing spalling were analysed by means of a comprehensive experimental programme comprising 56 specimens instrumented with Digital Image Correlation. A mechanical model is eventually proposed to evaluate bond-related cases of cover spalling.

Keywords: structural concrete resistance, compression, bond, spalling, bleeding, plastic settlement, casting position effects, strength reduction factors, Digital Image Correlation, tomography.

Résumé

La résistance du béton est généralement mesurée sur des cubes ou cylindres dont les dimensions sont normalisées. La confection et la cure de ces échantillons sont réalisés dans les règles de l'art, puis leur résistance est déterminée en laboratoire sous des taux de chargement rapides. Cependant, la résistance in-situ d'un élément structural peut diverger considérablement par rapport à celle d'un échantillon normalisé de petites dimensions et cela pour plusieurs raisons.

En effet, des phénomènes liés au processus de consolidation du béton frais peuvent nuire à la résistance à la compression, mais aussi à l'adhérence des barres d'armature situées dans la partie supérieure d'un élément structural. En particulier, au cours de la consolidation du béton, l'eau a tendance à remonter vers la surface, alors que le béton se tasse progressivement, phénomènes nommés respectivement « ressuage » et « tassement plastique ». Cela conduit à une diminution des propriétés mécaniques du béton situé près de la surface supérieure ainsi qu'au développement de fissures et de vides autour des barres d'armature horizontales, provoquant des perturbations du champ de compression et du transfert d'efforts d'adhérence entre l'acier et le béton.

De plus, après durcissement, la réponse structurale du béton diffère également de celle d'un échantillon normalisé, du fait du développement de champs de contraintes non-uniformes, mais aussi de par la fragilité et le comportement rhéologique du béton, la présence de fissures ou d'éléments perturbateurs (tels que gaines de précontrainte par exemple). Par conséquent, la résistance mesurée sur échantillon doit être corrigée avec des facteurs de réduction, afin d'assurer une analyse structurale appropriée.

Dans la présente thèse, une étude approfondie a été menée sur ces phénomènes qui peuvent nuire à la résistance à la compression du béton et à l'adhérence acier-béton. Ces aspects sont caractérisés au travers de plusieurs campagnes expérimentales équipées de systèmes de mesure de haute précision, tels que la tomographie ou la corrélation d'images numériques.

Une vaste série d'essais a notamment été effectuée sur 76 colonnes et prismes en béton, afin d'évaluer l'influence sur la résistance à la compression de la position de bétonnage, de la direction de chargement et de la présence d'éléments perturbateurs. Des mesures détaillées ont été réalisées sur le béton à l'état frais et à l'état durci, ce qui a permis la définition de nouvelles règles de calcul pour les éléments structuraux.

Une attention particulière a par ailleurs été accordée au rôle joué par la fragilité du béton et les redistributions internes d'efforts sur la réponse structurale de colonnes en béton armé et des zones comprimées de poutres fléchies. La pertinence des résultats a été validée, pour ces cas, à partir de plus de 400 tests sur colonnes recueillies dans la littérature scientifique.

De plus, les implications de la position et orientation des barres d'armature sur l'adhérence et sur l'éclatement de l'enrobage ont été étudiées sur la base de 137 essais d'arrachement de barres d'armature. Les variables principales retenues ont été le diamètre des barres d'armature, l'épaisseur de l'enrobage, la hauteur des éléments et la longueur d'ancrage. De cette étude découle alors la proposition d'une approche mécanique qui permet l'évaluation de l'adhérence en fonction de la position des barres d'armature à l'intérieur d'un élément structural et des caractéristiques de leurs nervures.

Finalement, le phénomène d'éclatement de l'enrobage a été examiné sous l'application d'une pression radiale interne, comme cela apparaît par exemple lors de la dilatation volumétrique due à la corrosion de barres d'armature ou lors de l'activation de l'adhérence acier-béton. Les mécanismes qui provoquent ce mode de rupture ont été analysés à travers une campagne expérimentale constituée de 56 spécimens, lesquels ont été examinés au moyen de la corrélation d'images numériques. Un modèle mécanique a ensuite été dérivé, permettant la caractérisation de l'adhérence en cas d'éclatement de l'enrobage.

Mots clés: résistance du béton structural, compression, adhérence, éclatement de l'enrobage, ressuage du béton, tassement plastique, position de bétonnage, facteurs de réduction de résistance, corrélation d'images numériques, tomographie.

Riassunto

La resistenza del calcestruzzo è generalmente misurata su provini cubici o cilindrici di dimensioni nominali, i quali sono sottoposti a condizioni di vibrazione e stagionatura adeguate. In seguito, la loro resistenza è determinata in laboratorio seguendo spesso una procedura di carico rapida. Tuttavia, la resistenza in situ di elementi strutturali può differire considerevolmente rispetto a quella misurata su provini di piccole dimensioni e relativamente omogenei e ciò per diversi motivi.

Infatti, fenomeni legati al consolidamento del calcestruzzo fresco possono incidere sulla resistenza a compressione come pure sull'aderenza dell'armatura situata nella parte superiore di una struttura. Durante il consolidamento del calcestruzzo, l'acqua tende a risalire verso la superficie mentre il calcestruzzo si assesta, fenomeni comunemente chiamati essudazione e assestamento plastico rispettivamente. Ciò provoca un peggioramento delle proprietà meccaniche del calcestruzzo situato nella parte superiore di un elemento e porta inoltre alla sviluppo di fessure e vuoti attorno all'armatura orizzontale, con possibili effetti negativi sul trasferimento di sforzi di compressione e sull'ingranamento acciaio-calcestruzzo.

Inoltre, il comportamento del calcestruzzo di una struttura può discostarsi rispetto a quello di un provino per via di stati di sforzo non uniformi, della presenza di fessure o elementi perturbatori e della fragilità del calcestruzzo. Di conseguenza, la resistenza misurata su campioni deve essere corretta con specifici coefficienti al fine di garantire un'adeguata analisi strutturale.

In questa tesi sono esaminati diversi fenomeni che possono avere un impatto negativo sulla resistenza del calcestruzzo strutturale, in particolare sulla resistenza a compressione e sull'aderenza. Questi aspetti sono stati valutati tramite diverse campagne sperimentali dotate di sistemi di misura di elevata precisione, quali la tomografia e la correlazione digitale di immagini.

Un'ampia serie di test è stata effettuata su 76 colonne e prismi in calcestruzzo per esaminare l'influenza sulla resistenza a compressione della posizione durante il getto, della direzione del carico e della presenza di elementi perturbatori. Misure dettagliate sono state effettuate sia sul calcestruzzo fresco che indurito, permettendo la definizione di nuove regole per la progettazione e il calcolo di elementi strutturali.

È inoltre stato approfondito il ruolo della fragilità del calcestruzzo e delle possibili ridistribuzioni di sforzi interni sulla risposta stutturale di colonne in calcestruzzo armato e di zone compresse di travi in flessione. La pertinenza dei risultati è, in questo caso, stata validata sulla base di più di 400 test su colonne ricavate da adeguata letteratura scientifica.

Gli effetti legati alla posizione dell'armatura durante il getto sulla resistenza dell'aderenza sono inoltre stati esaminati attraverso 137 prove di estrazione su barre. Le principali variabili sono il diametro delle barre, le dimensioni del copriferro, l'altezza dell'elemento strutturale e la lunghezza dell'ancoraggio. Dallo studio ne è conseguita la proposta di un approccio meccanico che permette la valutazione della resistenza all'estrazione di una barra in base alla sua posizione all'interno di un elemento strutturale e alle caratteristiche delle sue nervature.

Infine, è stato esaminato il fenomeno dell'espulsione del copriferro in seguito all'applicazione di una pressione radiale interna, come si può riscontrare in seguito alla corrosione di barre d’armatura o all’attivatione dell’aderenza acciaio-calcestruzzo. I meccanismi che provocano tale rottura sono stati analizzati tramite una campagna sperimentale costituita di 56 provini, i quali sono stati studiati con l’uso della correlazione digitale di immagini. Un modello meccanico è stato inoltre proposto per la valutatione della resistenza d’aderenza in caso di espulsione del copriferro.

Parole chiave: resistenza strutturale del calcestruzzo, compressione, aderenza, espulsione copriferro, essudazione, assestamento plastico, posizione durante il getto, coefficienti di riduzione della resistenza, correlazione digitale di immagini, tomografia.

Zusammenfassung

Traditionell wird die Betonfestigkeit an Würfeln oder Zylindern mit normalisierten Abmessungen und geeigneten Vibrations- und Aushärtungsbedingungen gemessen und ihre Festigkeit im Labor unter schnellen Belastungsraten bestimmt. Die in-situ-Festigkeit von Strukturelementen unterscheidet sich jedoch aufgrund mehrerer Ursachen erheblich von der einer kleinen und homogenen Probe.

Insbesondere können Phänomene, die während des Verfestigungsprozesses von Frischbeton auftreten, den Druckwiderstand von hohen Bauteilen sowie die Verbundfestigkeit von Bewehrungsstäben in den oberen Schichten beeinflussen. Während der Betonverfestigung wandert Wasser in Richtung der freien Oberfläche, während sich der Beton nach unten absetzt; diese Phänomene werden als Betonbluten bzw. plastisches Absetzen bezeichnet. Folglich wird eine Abnahme der Betoneigenschaften in der Nähe der oberen Oberfläche sowie eine Entwicklung von Rissen und Hohlräumen um horizontale Bewehrungsstäbe herum beobachtet, was zur potenziellen Störung der Druckspannung führt und die Verbundwirkung von Stäben und Beton beeinträchtigt.

Darüber hinaus kann sich die Reaktion des Konstruktionsbetons aufgrund ungleichmässiger Spannungszustände, der Sprödigkeit des Materials, der durch aufgezwungene Dehnungen induzierten Rissbildung, der rheologischen Reaktion des Betons und des Vorhandenseins von eingebetteten Störungen von der Reaktion der Materialproben unterscheiden. Darum muss die in Materialproben gemessene Festigkeit mit Reduktionsfaktoren korrigiert werden, um eine geeignete Strukturanalyse zu gewährleisten.

In dieser Arbeit wird eine eingehende Untersuchung der verschiedenen Phänomene durchgeführt, die die Druck- und Verbundfestigkeit von Bauteilen beeinflussen. Diese Aspekte werden mit Hilfe mehrerer Versuchsprogramme beurteilt, die mit verfeinerten Messtechniken wie Tomographie und digitaler Bildkorrelation untersucht wurden.

Eine umfangreiche Untersuchung mit 76 Versuchen wurde auf Stützen- und Prismenelemente durchgeführt, um den Einfluss von Gussrichtung, Belastungsrichtung und Stabstörungen auf die Druckfestigkeit von Druckgliedern zu bewerten. Die detaillierten Messungen, die im frischen und ausgehärteten Beton durchgeführt wurden, führen zu einem Vorschlag konsistenter Konstruktionsregeln für die untersuchten Phänomene.

Der Schwerpunkt lag auch auf dem Einfluss der Materialsprödigkeit und den Auswirkungen von internen Spannungsumverteilungen auf das Bauteilverhalten von Stahlbetonstützen und Biegedruckzonen von Balken. Die Relevanz der Untersuchungen wurde anhand von mehr als 400 aus der Literatur gesammelten Stützenversuchen validiert.

Die Auswirkungen der Giessbedingungen auf Auszugs- und Abplatzungsbrüche wurden ebenfalls anhand von 137 Auszugsversuchen an Bewehrungsstäben mit variablem Durchmesser, Betonüberdeckung, Giesshöhe und Einbettungslänge bewertet. Diese Untersuchung führte zu dem Vorschlag für einen physikalisch konsistenten Ansatz, bei dem der Auszugswiderstand als Funktion der Betonierungsbedingungen und der Bewehrungseigenschaften bewertet wurde.

Schliesslich wurde das Phänomen des Abplatzens der Betondeckung im Hinblick auf die Einwirkung eines radialen Drucks untersucht, wie er durch den Verbund entsteht oder durch die volumetrische Zunahme korrodierter Bewehrung verursacht wird. Die Mechanismen, die Abplatzungen verursachen, wurden mit Hilfe eines umfassenden Versuchsprogramms analysiert, das 56 mit digitaler Bildkorrelation instrumentierte Proben umfasste. Eine mechanische Analogie wird schliesslich vorgeschlagen, um haftungsbedingte Fälle von Abplatzungen der Abdeckung zu bewerten.

Schlüsselwörter: struktureller Betonwiderstand, Druck, Verbund, Abplatzen, Ausbluten, plastische Setzung, Auswirkungen der Giessposition, Festigkeitsreduzierungsfaktoren, digitale Bildkorrelation, Tomographie.

Resumen

Tradicionalmente, la resistencia del hormigón se mide en cubos o cilindros de dimensiones normalizadas, con unas condiciones de vibrado y curado apropiadas, y su resistencia se determina en laboratorio bajo la aplicación rápida de cargas. Sin embargo, la resistencia in-situ de los elementos estructurales puede diferir considerablemente de la obtenida en especímenes pequeños y homogéneos debido a una serie de razones.

Notablemente, ciertos fenómenos que ocurren durante el proceso de consolidación del hormigón fresco pueden afectar a la resistencia a compresión de elementos de cierta altura, así como a la resistencia a la adherencia de barras de armadura localizadas en capas superiores. Durante la consolidación, el agua migra hacia la superficie libre mientras el hormigón se asienta, fenómenos conocidos como sangrado y asiento plástico del hormigón, respectivamente. Bajo estas circunstancias, se observa una reducción de las propiedades del hormigón cerca de la superficie libre, además de la aparición de fisuras y huecos alrededor de las barras de armadura horizontales, perturbando potencialmente las tensiones de compresión y afectando a la interacción mecánica entre las barras y el hormigón.

Además, la respuesta del hormigón estructural puede diferir de la de muestras del material debido a estados de tensiones no uniformes, la fragilidad del material, la fisuración inducida por deformaciones impuestas, el comportamiento reológico del hormigón y la presencia de perturbaciones en el material. Como resultado, la resistencia medida en muestras del material ha de ser corregida mediante factores de reducción de la resistencia para garantizar un análisis estructural apropiado.

En esta tesis se ha llevado a cabo una investigación en profundidad de los distintos fenómenos que afectan la resistencia a la compresión y la adherencia en elementos estructurales. Estos aspectos han sido evaluados a través de varios programas experimentales instrumentados detalladamente mediante técnicas tales como la tomografía y la Correlación Digital de Imágenes (DIC).

Un extenso programa experimental constituido por 76 ensayos de columnas y prismas se ha llevado a cabo para evaluar la influencia de la posición de hormigonado, la dirección de las cargas y las perturbaciones en las barras de armadura en la resistencia a la compresión de elementos estructurales. Las mediciones detalladas obtenidas en estado fresco y tras endurecer han permitido proponer reglas de diseño relativas a los fenómenos investigados.

Asimismo, se ha puesto énfasis en la influencia de la fragilidad del material y en las implicaciones de las redistribuciones internas de tensiones en el comportamiento estructural de columnas de hormigón armado y en las zonas comprimidas de miembros en flexión. La relevancia de la investigación ha sido validada en base a más de 400 ensayos de columnas recopilados de la literatura.

Las implicaciones de las condiciones de hormigonado en roturas por arrancamiento de barras o desconchamiento han sido asimismo analizadas mediante 137 ensayos pull-out de barras de armadura con distintos diámetros, recubrimientos, posición de hormigonado y longitud anclada. Como resultado de la investigación se ha propuesto un método físicamente congruente que evalúa la resistencia al arrancamiento de barras en función de las condiciones de hormigonado y las características de la armadura.

Finalmente, el desconchamiento del recubrimiento ha sido examinado en relación a la acción de la presión radial, originada por adherencia o asociada a la expansión volumétrica de armadura corroída. Los mecanismos que inducen al desconchamiento han sido analizados mediante una extensa campaña experimental que incluye 56 especímenes instrumentados con DIC. Una analogía mecánica ha sido propuesta para evaluar situaciones de desconchamiento relativas a problemas de adherencia.

Palabras clave: resistencia del hormigón estructural, compresión, adherencia, desconchamiento, sangrado (exudación), asientos plásticos, efectos de la posición de hormigonado, factores de reducción de la resistencia, Correlación Digital de Imágenes (DIC), tomografía.

Contents

Foreword ... i

Acknowledgements ... iii

Abstract ... v

Résumé ... vii

Riassunto ... ix

Zusammenfassung ... xi

Resumen ... xiii

Chapter 1. Introduction ... 1

1.1. Aims of the research ... 3

1.2. Scientific contributions of the thesis ... 4

1.3. Structure of the thesis ... 5

1.4. List of publications ... 5

1.5. References ... 6

Chapter 2. The influence of casting position and disturbance induced by reinforcement on the structural concrete strength ... 9

2.1. Abstract ... 10

2.2. Introduction ... 10

2.3. In-situ structural concrete resistance: a review of the state-of-the-art ... 11

2.3.1. Plastic settlement and bleeding ... 11

2.3.2. In-situ concrete strength as function of the casting position ... 12

2.3.3. Influence of presence of bars on compressive strength ... 15

2.3.4. In-situ structural concrete strength in codes of practice ... 16

2.4. Experimental programme on the measurement of settlements in fresh concrete ... 17

2.4.1. Specimen description ... 17

2.4.2. Main experimental results ... 19

2.5. Experimental programme on the influence of casting position on the concrete resistance ... 22

2.5.1. Specimen description ... 22

2.5.2. Main experimental results ... 25

2.6. Discussion on implications for design ... 31

2.6.1. Members with confinement or with controlled propagation of cracking ... 32

2.6.2. Unconfined members or without controlled propagation of cracking ... 33

2.7. Conclusions ... 36
2.8. References ... 37
2.9. Annexes ... 40
2.9.1. Annex A: Failure modes ... 40
2.9.2. Annex B: Stress-strain responses ... 41
2.9.3. Annex C: Effect of disturbances on the resistance of concrete ... 44
2.10. Notation ... 48
Chapter 3. Concrete compressive strength: from material characterization to a structural value ... 50
3.1. Abstract ... 51
3.2. Introduction ... 51
3.3. Structural concrete strength: background and implications ... 52
3.4. Response of axially-loaded reinforced concrete columns ... 55
3.4.1. Response of reinforced concrete columns in pure compression and design approaches 56
3.4.2. Discussion of design idealizations and comparison to test results ... 57
3.4.3. Design idealization accounting for material brittleness ... 60
3.4.4. Influence of casting conditions ... 61
3.5. Response of eccentrically-loaded columns ... 62
3.5.1. Stress distribution in compression zones subjected to strain gradients ... 62
3.5.2. Design idealization of eccentrically-loaded columns ... 63
3.6. Design values and partial safety factor for concrete ... 67
3.7. Conclusions ... 68
3.8. References ... 69
3.9. Annexes ... 74
3.9.1. Annex A: Structural strength reductions for material resistance accounted in codes of practice… ... 74
3.9.2. Annex B: Determination of the partial safety factor of concrete for members in compression ... 75
3.9.3. Annex C: Database on column tests without eccentricity ... 77
3.9.4. Annex D: Database on column tests with load eccentricity ... 77
3.9.5. Annex E: confinement effect in reinforced concrete columns ... 77
3.10. Notation ... 78
Chapter 4. Casting position effects on bond performance of reinforcement bars ... 81
4.1. Abstract ... 82
4.2. Introduction ... 82
4.3. Influence of casting position on bond response ... 84
4.3.1. Phenomena before concrete hardening ... 84

4.3.2. Implications of casting conditions on pull-out resistance ... 85
4.3.3. Implications of casting conditions on spalling failure ... 88
4.4. Experimental programme ... 88
4.4.1. General overview ... 88
4.4.2. Materials ... 91
4.4.3. Instrumentation and setup ... 92
4.5. Experimental results ... 93
4.5.1. Short pull-out tests ... 93
4.5.2. Tests with anchorage length 10ϕ ... 95
4.5.3. Tests with anchorage length 20ϕ ... 97
4.6. Discussion of results ... 99
4.6.1. Role of the void under the bar on pull-out and spalling failures ... 99
4.6.2. Design implications ... 100
4.7. Conclusions ... 101
4.8. References ... 102
4.9. Annexes ... 104
4.9.1. Annex A: Evaluation of spalling strength ... 104
4.10. Notation ... 107
Chapter 5. Spalling of concrete cover induced by reinforcement ... 109
5.1. Abstract ... 110
5.2. Introduction ... 110
5.3. Review of the state-of-the-art ... 111
5.3.1. Influence of internal pressures inside concrete ... 111
5.3.2. Spalling induced by bond ... 112
5.4. Experimental programme ... 113
5.4.1. Description of test series ... 114
5.4.2. Materials ... 116
5.4.3. Instrumentation and setup ... 117
5.5. Experimental results ... 118
5.5.1. Inner-pressure tests with the hydraulic inflator device ... 119
5.5.2. Pull-out tests ... 123
5.6. Analysis of spalling failures based on detailed measurements of crack development ... 126
5.6.1. Tests with stable crack propagation ... 126
5.6.2. Tests with unstable crack propagation ... 127
5.7. Design approach for spalling failures due to the application of an internal pressure ... 128

5.7.1. Geometrical parameters ... 128
5.7.2. Stress distribution and equilibrium of forces ... 128
5.7.3. Consideration of size effect ... 129
5.7.4. Considerations on casting position and tensile strength ... 130
5.7.5. Consideration of multiple disturbances ... 130
5.7.6. Comparison to test results ... 131
5.8. Design proposal for pull-out spalling failures ... 133
5.9. Conclusions ... 135
5.10. References ... 136
5.11. Notation ... 140
Chapter 6. Conclusions and outlook ... 142
6.1. General conclusions ... 142
6.2. Detailed findings ... 143
6.3. Outlook and future work ... 145
6.4. References ... 148
Appendices ... 149
Appendix A: Database on column tests without eccentricity ... 149
Appendix B: Database on column tests with load eccentricity ... 162
Appendix C: DIC measurements of series ML10 ... 165
Curriculum Vitae ... 193

Chapter 1.
Introduction

The evaluation of the concrete strength is of paramount importance in the design and assessment of concrete structures. The concrete strength of new structures is often based on measurements performed on cylinders or cubes having normalized dimensions [1] and cast with the same batch as the structural members [2] (unless a continuous quality control is performed), see Figure 1.1a-b. These control specimens are then tested following standardized procedures in order to obtain the concrete compressive strength (Figure 1.1a), the concrete tensile strength (Figure 1.1b) and other material properties (such as modulus of elasticity or density) [3]–[6]. In addition, testing of the material samples is typically performed under relatively fast loading rates and at a specific reference age (refer for instance to [3] for compression tests).

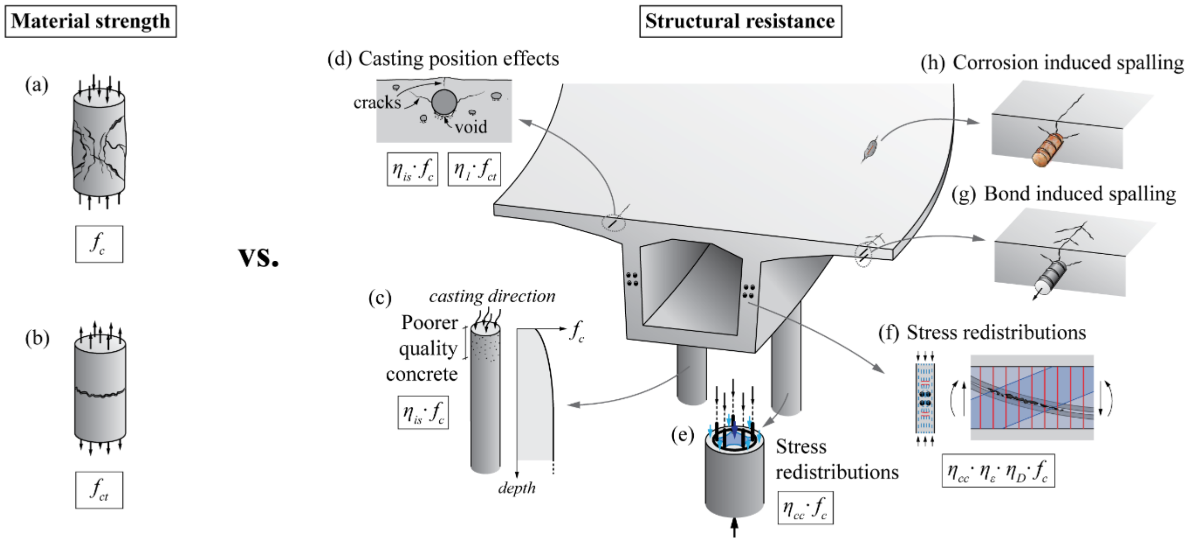

Figure 1.1: Evaluation of concrete strength based on control specimens: (a) compression test; and (b) tensile test. Actual concrete strength in a structure: (c) effect of bleeding and plastic settlement on the compressive strength of concrete; (d) casting position effects near a top bar; (e) response of a reinforced concrete column with different load-carrying actions and stress redistributions; (f) reduced compressive strength in a web due to disturbances related to the presence of post-tensioning ducts and imposed transverse strains; (g) spalling of the concrete cover as function of orientation and position of bar during casting; and (h) spalling resistance of the cover subjected to radial inner pressure exerted by corrosion products.

Although accurate for material characterization, these tests do not account for a number of phenomena influencing the in-situ structural resistance (Figure 1.1c-h). In fact, the control specimens have different casting and curing conditions than those encountered in actual structures [7]. Also, ambient conditions such as temperature, moisture and curing duration may affect the in-situ strength [8], [9]. In addition, cast-in place structural elements (such as columns or walls, Figure 1.1c) can be relatively high and subjected to different pressure and vibration conditions [10]. This can lead to more favourable compacting conditions in the bottom parts of a structural member compared to those on top (Figure 1.1c).

At the fresh state, two phenomena related to the consolidation process of fresh concrete potentially affect the concrete strength and the interface characteristics between concrete and reinforcing bars. These phenomena refer to the migration of water to the top surface – referred as concrete bleeding – and the plastic settlement of fresh concrete [11]. Bleeding is at the source of an enhanced porosity of the concrete located in the upper region of an element and is responsible for the development of cavities or voids under solid disturbances, such as coarse aggregates or reinforcement bars (Figure 1.1d). The plastic settlement phenomenon however leads to the development of voids under top bars in case the latter are restrained from any vertical movement (Figure 1.1d) and to internal and surface cracks [12], [13]. This results in reduced mechanical properties of concrete, affecting not only the compressive strength but also the tensile strength, the elastic modulus and the density in the uppermost part of a structural element [14].

At the hardened state of concrete, the situation encountered in structural elements (Figure 1.1c-h) also differs from that of control specimens (Figure 1.1a-b) as the response can be affected by the brittleness of concrete, with regions in the softening regime before others attain their peak strength [15]–[17]. Moreover, reinforcement bars may represent physical discontinuities that locally disturb the stress state in their surroundings [18]–[20]. This leads to a complex global response, where stress redistributions occur between concrete and reinforcement as well as among different regions of concrete [17]. It is typically the case in concrete columns, where redistributions take place between concrete core, concrete cover and longitudinal reinforcement (Figure 1.1e), or in members designed with strut-and-tie or stress fields where idealized compression fields are assumed (Figure 1.1f) [21]–[23].

The response in compression may also differ to that of material samples due to the development of transverse cracking from imposed tensile strains due to reinforcing bars (Figure 1.1f) [24], the rheological response of concrete (continuous cement hydration with time and sensitivity to sustained loadings) [25], [26], and the presence of embedded disturbances such as ducts or large reinforcement (Figure 1.1f). It should be noted that the response in compression is also affected by spalling of the concrete cover [27], [28], the less-than proportional increase of the tensile strength for increasing compressive strength [23] and the unfavourable effect of transverse tensile stresses on the compressive strength for increasing material strength [29]. As a result, the concrete compressive strength measured in material samples has to be modified in order to be used for structural analyses [15]–[17]. For design purposes, this is normally performed by considering a number of strength reduction factors (refer for instance to [23], [30]–[32]).

Another significant phenomenon of reinforced concrete structures refers to the bond between steel bars and concrete. It allows for the transfer of forces from the reinforcement to the surrounding concrete and is also dependent on structural properties (Figure 1.1d,g). In fact, bond is not an intrinsic attribute of a reinforcing bar but is influenced by the geometry of the structural member, strain and size effects, material properties, stress states as well as rib characteristics [13], [33], [34]. Moreover, the mechanical engagement between deformed bars and concrete is also affected by the phenomena of bleeding and plastic settlement. The enhanced porosity and weaker mechanical properties of the concrete located near to the free-surface due to bleeding [14] and the development of voids beneath top bars related to the settlement of concrete [35] can severely reduce the quality of the rebar-to-concrete interface (Figure 1.1d). As a result, the bond strength is strongly dependent on the position and orientation of the bars, the depth of the concrete member and the concrete composition and consistency [34], [36]–[41]. Furthermore, the phenomena of bleeding and plastic settlement may also influence in different manners the failure mechanisms of bond (pull-out, splitting or spalling). Based on these considerations, current design codes [23], [30], [42] account for casting position effects by reducing the bond strength of embedded reinforcement located in top layers (top bar effect) by means of strength reduction factors (for instance η_1 in EN 1992-1-1:2004 [30]).

With respect to the spalling of the concrete cover induced by reinforcing bars (Figure 1.1g-h), this failure mode also depends upon a number of structural factors, such as the spacing and dimensions of the reinforcing bars, the thickness of the cover, the concrete tensile strength and the casting position [13], [43]–[47]. These considerations are valid whether spalling is related to bond (Figure 1.1g) [43], [45], reinforcement corrosion (Figure 1.1h) [48], [49], or deviation forces [50].

In this thesis, the aspects related to the compressive and bond strength as structural properties are investigated by means of theoretical considerations and multiple experimental programmes. In this respect, targeted testing programmes were performed on compression members (such as columns and prisms), anchorages with different casting conditions and embedded lengths as well as specific tests on cover spalling induced by reinforcement. The structural response is studied both at the fresh and hardened state using state-of-the-art measurement techniques such as tomography and Digital Image Correlation. These measurements techniques allow for a precise and phenomenological explanation of the structural response of the investigated concrete elements. In addition, the aim is to provide theoretical and practical justifications for different strength reduction factors, such as the brittleness factor for concrete in compression (η_{cc}), the coefficients considering for casting position effects (η_{is} for compression and η_1 for bond) and the factor accounting for the presence of embedded disturbances (η_D). Finally, the mechanisms triggering spalling failures are investigated using detailed measurements techniques and simple mechanical analogies suited for bond-related cases are proposed.

1.1. Aims of the research

The aim of this work is to provide an accurate evaluation of the structural resistance, both in the case of compression and rebar-to-concrete bond. The main objectives of this research are as follows:

- Investigate the phenomena of bleeding and plastic settlement using detailed measurement techniques such as tomography and Digital Image Correlation both at the fresh and hardened state of concrete. The implications of these phenomena on reinforcing bars restrained from any vertical movement are additionally evaluated.
- Investigate in a detailed manner the influence of the depth of concrete under the bars on the concrete compressive resistance.
- Determine the potential disturbances induced by reinforcing bars placed transversely to the loading direction on the concrete compressive strength.
- Evaluate the influence of the casting direction with respect to the loading direction on the compressive resistance of structural members.
- Derive consistent design rules to correct the strength of control samples to consider for the influence of casting position and the disturbance induced by reinforcing bars.
- Examine the influence of concrete brittleness in compression and its implications with respect to potential stress redistributions occurring within structural members.
- Determine appropriate stress distributions occurring within the compression region of beams and columns with bending moments and evaluate the suitability of adopting the parabola-rectangle diagram for their design.
- Investigate the influence of casting position effects on the bond strength of reinforcement bars.
- Assess the influence of bleeding and plastic settlement phenomena on the failure modes related to bond (pull-out, spalling and splitting).
- Perform pull-out tests representative of the bond conditions encountered in actual structural members.

- Evaluate the bond strength reductions for poor bond conditions as indicated in EN 1992-1-1:2004 [30] and ACI 318-19 [42].
- Investigate the cover spalling mechanism induced by the reinforcement using Digital Image Correlation.
- Assess the influence of structural properties such as casting position, size effect and group effect on the resistance to cover spalling.
- Investigate the spalling failure mechanism by applying pressure within openings embedded in concrete using hydraulic inflator devices.

1.2. Scientific contributions of the thesis

The main contributions of the work undertaken are:

- Extensive experimental programme comprising 76 column and prism tests on the influence of casting position, loading direction and disturbance induced by transverse reinforcement on the compressive resistance.
- Detailed tomography measurements of voids and internal cracking surrounding reinforcement bars due to bleeding and plastic settlement phenomena.
- Precise measurements of concrete settlement in the first hours after casting using Digital Image Correlation.
- Accurate description of the structural response of columns and prisms by means of Digital Image Correlation.
- Consistent design rules are proposed for the consideration of casting position effects and presence of embedded disturbances for members under pure compression.
- Extensive database of more than 400 column tests (with and without eccentricity) gathered from relevant scientific literature used to assess the pertinence of considering a brittleness factor for the calculation of columns and compression zones of beams.
- Detailed investigations on the influence of material brittleness and internal stress redistributions on the structural response of reinforced concrete members based on theoretical and experimental evidence.
- Comprehensive experimental programme consisting of 137 pull-out tests (performed both at the Ecole Polytechnique Féférale de Lausanne and at the University of Brescia) having different casting conditions, embedment lengths, loading setup, cover thickness and bar diameter.
- Proposal for a physically-consistent approach, previously derived for bond in cracked conditions, to compute the pull-out strength of reinforcing bars subjected to casting position effects.
- Design recommendations for the evaluation of casting position effects on spalling and pull-out failures.
- Extensive testing programme comprising 12 pull-out tests and 44 tests with hydraulic inflator devices on the phenomenon of cover spalling induced by reinforcement. The series of tests investigated a number of parameters relevant to spalling failures using Digital Image Correlation.
- Proposal for a simple mechanical approach suited for bond-related cases failing by cover spalling.

1.3. Structure of the thesis

After the introduction, the thesis is structured in four main chapters each corresponding to a different scientific publication. A general conclusion and appendices are given at the end of the document. The topics treated in each chapter are the following:

- Chapter 2: presents the results of an experimental investigation on the effective structural strength consisting of 76 column and prism tests. The effects related to casting position and presence of disturbances are evaluated both at the fresh and hardened state using refined measurements techniques (tomography and Digital Image Correlation). Design rules are also proposed to account for the effects of the previous phenomena on the resistance of structural members.
- Chapter 3: gives a detailed description of the influence of material brittleness and stress redistributions on the structural response of concrete members. The work is based on theoretical considerations supported with experimental results of more than 400 column tests taken from the literature.
- Chapter 4: presents an investigation on the influence of casting position effects on the bond performance of reinforcing bars. The results of an extensive experimental programme comprising 137 pull-out tests are outlined. The implications of bleeding and plastic settlement on bond-related failure modes are also discussed.
- Chapter 5: describes an investigation on the phenomenon of cover spalling induced by bond or by the action of an inner pressure (such as corrosion). The mechanisms triggering spalling are analysed by means of a comprehensive experimental programme consisting of 56 specimens instrumented with Digital Image Correlation.
- Chapter 6: outlines the main conclusions of the thesis and gives an outlook on potential future research.
- Appendices: it is resumed the complete database of column tests used to evaluate the necessity of the brittleness factor for concrete in compression (η_{cc}). In addition, it is also shown the results of DIC measurements performed on pull-out tests of reinforcing bars.

It should be noted that since the thesis is a collection of different scientific publications, each chapter presents its own introduction, state-of-the-art, conclusions, notations and references.

1.4. List of publications

The research performed at the Structural Concrete Laboratory (IBETON) of the Ecole Polytechnique Fédérale de Lausanne resulted in the following publications (reverse chronological order):

- F. Moccia, M. Fernández Ruiz, A. Muttoni, *Spalling of concrete cover induced by reinforcement*, Engineering Structures. [submitted for review, October 2020]
- F. Moccia, M. Fernández Ruiz, G. Metelli, A. Muttoni, G. Plizzari, *Casting position effects on bond performance of reinforcement bars*, Structural Concrete. [submitted for review, September 2020]
- F. Moccia, Q. Yu, M. Fernández Ruiz, A. Muttoni, *Concrete compressive strength: from material characterization to a structural value*, Structural Concrete, 2020, pp. 1-20.
- F. Moccia, X. Kubski, M. Fernández Ruiz, A. Muttoni, *The influence of casting position and disturbance induced by reinforcement on the structural concrete strength*, Structural Concrete, 2020, pp. 1-28.

- A. Muttoni, M. Fernández Ruiz, F. Moccia, *Strength reduction factor for concrete in compression*, Background document to prEN 1992-1-1:2018, European Committee for Standardization (CEN), Brussels, Belgium, 2018, pp. 9-26.
- F. Moccia, M. Fernández Ruiz, A. Muttoni, *Efficiency Factors for Plastic Design in Concrete: Influence of Brittleness in Compression*, High Tech Concrete: Where Technology and Engineering Meet, Springer International Publishing, 2018, pp. 1234-1242.

1.5. References

[1] EN 12390-1:2012, "Testing hardened concrete - Part 1: Shape, dimensions and other requirements for spcimens and moulds," European Committee for Standardization (CEN), Brussels, Belgium, 13 p., 2012.

[2] EN 206+A1:2016-11, "Concrete - Specification, performance, production and conformity," European Committee for Standardization (CEN), Brussels, Belgium, 102 p., 2016.

[3] EN 12390-3:2019, "Testing hardened concrete - Part 3: Compressive strength of test specimens," European Committee for Standardization (CEN), Brussels, Belgium, 20 p., 2019.

[4] EN 12390-6:2012, "Testing hardened concrete - Part 6: Tensile splitting strength of test specimens," European Committee for Standardization (CEN), Brussels, Belgium, 11 p., 2012.

[5] EN 12390-13:2013, "Testing hardened concrete: Part 13: Determination of secant modulus of elasticity in compression," European Committee for Standardization (CEN), Brussels, Belgium, 14 p., 2013.

[6] EN 12390-7:2019, "Testing hardened concrete - Part 7: density of hardened concrete," European Committee for Standardization (CEN), Brussels, Belgium, 11 p., 2019.

[7] N. Petersons, "Strength of concrete in finished structures," Transactions of the royal Institute of Technology, Stockholm, Sweden, 189 p., 1964.

[8] F. M. Bartlett and J. G. MacGregor, "Variation of In-Place Concrete Strength in Structures," *ACI Materials Journal*, vol. 96, no. 2, pp. 261–270, 1999.

[9] W. K. Tso and I. M. Zelman, "Concrete Strength Variation in Actual Structures," *ACI Journal Proceedings*, vol. 67, no. 12, pp. 981–988, 1970.

[10] M. Kanda and H. Yoshida, "The distributing condition of water-cement ratio in the member section after concrete placing," *RILEM Symposium on Quality Control of Concrete Structures*, pp. 85–92, 1979.

[11] T. C. Powers, "The properties of fresh concrete," John Wiley & Sons, Hoboken, NJ, United States, 664 p., 1968.

[12] R. Combrinck, L. Steyl, and W. P. Boshoff, "Interaction between settlement and shrinkage cracking in plastic concrete," *Construction and Building Materials*, vol. 185, pp. 1–11, 2018.

[13] International Federation for Structural Concrete, "fib Bulletin 10: Bond of reinforcement in concrete," State-of-art report prepared by Task Group Bond Models, Lausanne, Switzerland, 439 p., 2000.

[14] G. Giaccio and A. Giovambattista, "Bleeding: Evaluation of its effects on concrete behaviour," *Materials and Structures*, vol. 19, no. 4, pp. 265–271, 1986.

[15] H. Exner, "On the effectiveness factor in plastic analysis of concrete," *IABSE reports of the working commissions*, pp. 35–42, 1979.

[16] E. Thorenfeldt, "Design Properties for High-Strength Concrete," *Nordisk Betong, No. 1-2*, pp. 71–73, 1986.

[17] A. Muttoni, "The applicability of the theory of plasticity in the design of reinforced concrete ('Die Andwendbarkeit der Plastizitätstheorie in der Bemessung von Stahlbeton')," PhD thesis, ETH, Zürich, 164 p., 1990.

[18] R. D. Gaynor, "Effect of Horizontal Reinforcing Steel on the Strength of Molded Cylinders," *Journal of the American Concrete Institute*, vol. 62, no. 7, pp. 837–840, 1965.

[19] F. Leonhardt, "Abminderung der Tragfähigkeit des Betons infolge stabförminger, rechtwinklig zur Druckrichtung angeordneter Einlagen," *Festschrift Rüsch*, pp. 71–78, 1969.

[20] A. Muttoni, O. L. Burdet, and E. Hars, "Effect of Duct Type on Shear Strength of Thin Webs," *ACI Structural Journal*, vol. 103, no. 5, pp. 729–735, 2006.

[21] A. Muttoni, M. F. Ruiz, and F. Niketic, "Design versus assessment of concrete structures using stress fields and strut-and-tie models," *ACI Structural Journal*, vol. 112, no. 5, pp. 605–615, 2015.

[22] M. Rupf, M. Fernández Ruiz, and A. Muttoni, "Post-tensioned girders with low amounts of shear reinforcement: Shear strength and influence of flanges," *Engineering Structures*, vol. 56, pp. 357–371, 2013.

[23] International Federation for Structural Concrete, "fib Model Code for Concrete Structures 2010," Ernst & Sohn, Berlin, Germany, 434 p., 2013.

[24] F. J. Vecchio and M. P. Collins, "The Modified Compression-Field Theory for Reinforced Concrete Elements Subjected to Shear," *ACI journal*, vol. 83, no. 2, pp. 219–231, 1986.

[25] H. Rüsch, "Researches Toward a General Flexural Theory for Structural Concrete," Journal of the American Concrete Institute, 28 p., 1960.

[26] D. Tasevski, M. Fernández Ruiz, and A. Muttoni, "Assessing the compressive strength of concrete under sustained actions: From refined models to simple design expressions," *Structural Concrete*, vol. 20, no. 3, pp. 971–985, 2019.

[27] S. J. Foster, J. Liu, and S. A. Sheikh, "Cover Spalling in HSC Columns Loaded in Concentric Compression," *Journal of Structural Engineering*, vol. 124, no. 12, pp. 1431–1437, 1998.

[28] S. J. Foster, "On Behavior of High-Strength Concrete Columns : Cover Spalling, Steel Fibers, and Ductility," *ACI Structural Journal*, vol. 98, no. 4, pp. 583–589, 2001.

[29] H. Kupfer, H. K. Hilsdorf, and H. Rüsch, "Behavior of Concrete Under Biaxial Stresses," *ACI Journal*, vol. 66, no. 52, pp. 656–666, 1969.

[30] EN 1992-1-1:2004, "Eurocode 2: Design of Concrete Structures - Part 1: General Rules and Rules for Buildings," European Committee for Standardization (CEN), Brussels, Belgium, 225 p., 2004.

[31] GB 50010-2010, "Code for Design of Concrete Structures," Ministry of Housing and Urban-Rural Development of the People's Republic of China, Beijing, 427 p., 2010.

[32] ABNT NBR 6118:2014, "Projeto de Estruturas de Concrete - Procedimento," Associação Brasileira de Normas Técnicas, Rio de Janeiro, Brazil, 238 p., 2014.

[33] J. Cairns, "Bond and anchorage of embedded steel reinforcement in fib Model Code 2010," *Structural Concrete*, vol. 16, no. 1, pp. 45–55, 2015.

[34] F. Brantschen, D. M. V. Faria, M. Fernández Ruiz, and A. Muttoni, "Bond behaviour of straight, hooked, U-shaped and headed bars in cracked concrete," *Structural Concrete*, vol. 17, no. 5, pp. 799–810, 2016.

[35] A. Castel, T. Vidal, K. Viriyametanont, and R. François, "Effect of reinforcing bar orientation and location on bond with self-consolidating concrete," *ACI Structural Journal*, vol. 103, no. 4, pp. 559–567, 2006.

[36] D. A. Abrams, “Tests of bond between concrete and steel,” University of Illinois Bulletin No. 71, University of Illinois at Urbana-Champaign, Urbana, IL, USA, 240 p., 1913.

[37] C. A. Menzel, “Some Factors Influencing Results Of Pull-Out Bond Tests,” *Journal of the American Concrete Institute, Journal Proceedings*, vol. 35, no. 6, pp. 517–542, 1939.

[38] A. P. Clark, “Bond of concrete reinforcing bars,” *Journal of the American Concrete Institute*, vol. 46, no. 11, pp. 161–184, 1949.

[39] G. Rehm, “Über die Grundlagen des Verbunds zwischen Stahl und Beton,” *Deutscher Ausschuss für Stahlbeton*, vol. 138, pp. 1–59, 1961.

[40] J. O. Jirsa and J. E. Breen, “Influence of Casting position and shear on development and splice length - design reccomendations,” Report No. 242-3F, Centre for Transportation Research, The University of Texas at Austin, Austin, TX, USA, 45 p., 1981.

[41] J. Cairns, “Influence of casting position on lap and anchorage strength,” Heriot Watt University, Edinburgh, UK, 40 p., 2018.

[42] ACI Committee 318, “Building Code Requirements for Structural Concrete (ACI 318-19) and Commentary,” American Concrete Institute, Farmington Hills, USA, 624 p., 2019.

[43] R. Tepfers, “A theory of bond applied to overlapped tensile reinforcement splices for deformed bars,” PhD Thesis, Division of Concrete Structures, Chalmers University of Technology, Göteborg, Sweden, 328 p., 1973.

[44] R. Tepfers, “Cracking Of Concrete Cover Along Anchored Deformed Reinforcing Bars,” *Magazine of Concrete Research*, vol. 31, no. 106, pp. 3–12, 1979.

[45] J. Cairns and K. Jones, “The splitting forces generated by bond,” *Magazine of Concrete Research*, vol. 47, no. 171, pp. 153–165, 1995.

[46] J. Cairns, “An Analysis of The Ultimate Strength Of Lapped Joints Of Compression Reinforcement,” *Magazine of Concrete Research*, vol. 31, no. 106, pp. 19–27, 1979.

[47] E. Giuriani, G. Plizzari, and C. Schumm, “Role of stirrups and residual tensile strength of cracked concrete on bond,” *Journal of Structural Engineering*, vol. 117, no. 1, pp. 1–18, 1991.

[48] K. Bhargava, A. K. Ghosh, Y. Mori, and S. Ramanujam, “Analytical model for time to cover cracking in RC structures due to rebar corrosion,” *Nuclear Engineering and Design*, vol. 236, no. 11, pp. 1123–1139, 2006.

[49] I. Balafas and C. J. Burgoyne, “Modeling the Structural Effects of Rust in Concrete Cover,” *Journal of Engineering Mechanics*, vol. 137, no. 3, pp. 175–185, 2011.

[50] M. Fernández Ruiz, S. Plumey, and A. Muttoni, “Interaction between bond and deviation forces in spalling failures of arch-shaped members without transverse reinforcement,” *ACI Structural Journal*, vol. 107, no. 3, pp. 346–354, 2010.

Chapter 2.

The influence of casting position and disturbance induced by reinforcement on the structural concrete strength

This chapter is the postprint version of the article *The influence of casting position and disturbance induced by reinforcement on the structural concrete strength* published in the journal *Structural Concrete*. The authors of this publication are Francesco Moccia (PhD Candidate), Xavier Kubski (Master Student), Miguel Fernández Ruiz (Senior lecturer and thesis co-director) and Aurelio Muttoni (Professor and thesis director). The complete reference is the following:

> F. Moccia, X. Kubski, M. Fernández Ruiz, A. Muttoni, *The influence of casting position and disturbance induced by reinforcement on the structural concrete strength*, Structural Concrete, 2020, pp. 1-28. (DOI: https://doi.org/10.1002/suco.201900562)

The work presented in this article was performed by Francesco Moccia under the supervision of Miguel Fernández Ruiz and Aurelio Muttoni, who gave constant and valuable feedback as well as performed several proof readings of the manuscript. In this paper, it is also included one series of columns (12 specimens) tested and analysed by Xavier Kubski in the framework of his master thesis.

The main contributions of Francesco Moccia are the following:

- Measurements of the plastic settlement of fresh concrete in the first hours after casting using Digital Image Correlation (test series BM2).
- Tomography measurements on 10 cores containing embedded reinforcing bars extracted from a wall (test series WM1) as well as compressive tests on 4 additional plain cores.
- Casting and testing of 36 concrete prisms with embedded transverse reinforcement (test series PM1, PM2, PM3) as a preliminary experimental programme. The results are presented in Annex C.
- Casting and testing of 12 reinforced concrete columns with hoops (test series CM1).
- Casting and testing of 6 concrete prisms with embedded transverse reinforcement saw-cut from a concrete column (test series CM2).
- Casting and testing of 12 concrete prisms with embedded transverse bars saw-cut from a concrete beam (test series BM1).
- Supervision of the column tests (series CK1) and analysis performed by Xavier Kubski during his master thesis.
- Detailed measurements of the compressive response of the members investigated by means of Digital Image Correlation.
- Measurements of cover spalling by means of Digital Image Correlation and assessment of its influence on the resistance and failure mechanism of the studied elements.
- Design rules proposal for the consideration of casting position effects and presence of embedded disturbances for members under pure compression.
- Production of the figures included in the article.
- Writing of the manuscript of the article.

2.1. Abstract

It is well known that control specimens used to assess the concrete strength of new structures have different casting and curing conditions than those of actual structures. Notably, after pouring of the concrete and before its hardening, a number of phenomena such as concrete bleeding and plastic settlement occur, influencing the in-situ strength with respect to that of small and homogeneous control specimens (cubes or cylinders). In addition, the development of these phenomena and their structural implications are influenced by the presence of reinforcing bars, disturbing the settlement and bleeding of fresh concrete. In this paper, these aspects, with particular emphasis on the effective structural strength, are investigated by means of a testing programme performed with refined measurement techniques such as tomography and Digital Image Correlation. On that basis, consistent design rules are derived to correct the strength of control specimens in order to calculate the resistance of a structural concrete member.

2.2. Introduction

Traditionally, the compressive strength of concrete measured on cubes or cylinders cast and cured under potentially different conditions than those of actual members has been used to characterize the compressive resistance of a new structural concrete member. These control specimens have normalized dimensions (with a height between 100 and 300 mm), are subjected to good vibration conditions and their strength is assessed in laboratory under relatively high loading rates (typically 1-2 min test duration [1]). However, cast-in place structural elements can be relatively high (as columns or walls) and with regions where the concrete can be subjected to different pressure, curing and handling conditions. This leads to regions with potentially more favourable compacting conditions in the bottom parts compared to those on top. This is related to the consolidation process of fresh concrete which behaves like a saturated soil where water migrates from the bottom to the top surface and concrete settles downwards, phenomena usually named as “concrete bleeding” and “plastic settlement” respectively.

These phenomena have also a potential interaction with the reinforcement bars arranged in structural concrete members. This is justified by the fact that the fresh concrete settlement is potentially restraint by horizontal reinforcement bars, disturbing the homogeneity of concrete. In addition, these bars are physical discontinuities that can locally disturb the stress state in their vicinity once concrete hardens.

Significant scientific literature exists on this topic and will be reviewed in the next section. These studies cover the variation of the in-situ concrete strength according to the casting position and also the influence of transverse reinforcing bars on the compressive capacity of concrete members. However, no specific series has been found on their combined influence.

In this paper, an in-depth investigation on the different phenomena and their interaction is presented. This research is based on an extensive literature review and on the results of a new experimental programme. This programme takes advantage of state-of-the-art measurement techniques, such as Digital Image Correlation and tomography, and is addressed both to unconfined concrete (representing the typical case of walls) and to confined concrete (as for columns with hoop reinforcement). Its results provide a clear description of the phenomena occurring during the fresh state of concrete (bleeding, plastic settlement, vertical density variation) and allows understanding their significance and implications on the structural concrete design.

2.3. In-situ structural concrete resistance: a review of the state-of-the-art

Although the concrete strength of new structures is often assessed on the basis of standard cubes or cylinders, it has been argued in the past that such specimens can potentially not represent adequately the actual material strength in a structure. The difference between the in-situ concrete strength in structures and the uniaxial strength on control cylinders is largely related to differences in casting and curing processes. In addition, particularly when control specimens are not cast on construction site, additional differences exist related to transportation, unexpected addition of water on the construction site or to pumping/movement in buckets [2]. With respect to casting, several potential differences also exist related to the presence of reinforcement, to the manner in which concrete is poured or how it is vibrated (other sources can also exist, as a non-uniform supply of material with differences between batches of an element).

Concerning ambient conditions such as temperature, moisture and curing duration, they can also have a significant effect on the in-situ strength [3], [4]. With respect to curing of control specimens, several works have shown non-negligible differences between air-cured or moist-cured specimens (the latter being more resistant, and showing potentially higher differences between the in-situ strength and the control specimens [5], [6]). For this reason, in the comparisons presented below, air-cured control specimens will be considered (stored and cured in a similar manner as the structural member).

2.3.1. Plastic settlement and bleeding

After pouring of concrete, the differences between control specimens and actual structures are related to the behaviour of fresh concrete, which varies according to the casting position and direction. With this respect, Powers [7] gave a detailed description on the properties of fresh concrete. He observed that, due to gravitational forces, the solid particles in fresh concrete settle, displacing water upwards. This phenomenon, called plastic settlement, starts after concrete is poured and remains active until cement hydration begins (the development of hydration products fills the gaps between the solid particles, interrupting their settlement). Powers also observed that the amount of settlement was directly related to the depth of the freshly placed mass. Following this work, Clear and Bonner [8] described the two major components of plastic settlement. First, a rapid settlement in response to the applied load that compresses the pore water and the solid particles. Second, a gradual settlement resulting from the dissipation of pore water with time that slowly increases the effective stress on the inter-granular structure. The settlement of the free surface associated to these processes can be significant, reaching several millimetres depending on the height of the member and time of initiation of the hardening process [9], [10].

The upward displacement of water related to the settlement of solid particles, in case the formwork is watertight, is called bleeding and leads to the accumulation of water on the surface [7]. In case of significant bleeding, water migrating upwards can accumulate under coarse aggregates, leading to air pockets in hardened concrete (the so-called “internal bleeding”), or it can reach the free surface (the so-called “external bleeding”, or “surface bleeding”). In this latter case, a layer of water can be observed on the concrete surface if the bleeding rate is higher than the evaporation rate (Figure 2.1a). For high bleeding velocities, vertically-oriented channels develop (as for internal erosion in soils occurring when seepage velocity is high enough [11]) and fine particles are washed out and transported to the surface (creating aureoles around the lips of the channels). Measuring the amount of water reaching the surface is claimed as a procedure to quantify the bleeding phenomenon according to ASTM C232 [12]. Since bleeding and settlement are both associated to the consolidation process, the volume of displaced water can be related to the volume of settlement.

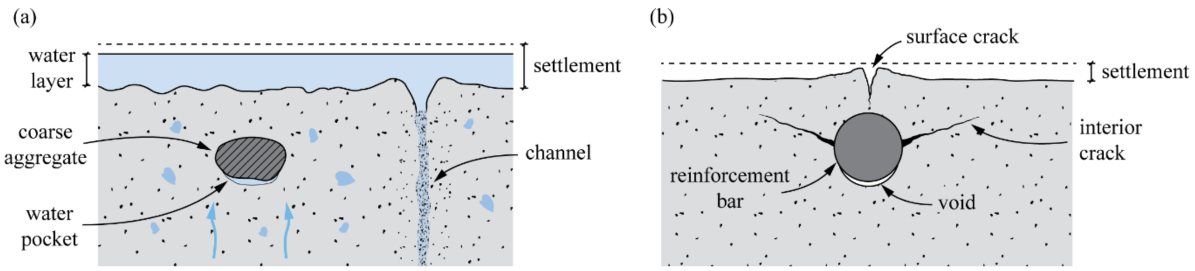

Figure 2.1: Schematic representation of the phenomena related to: (a) bleeding; and (b) cracking associated to plastic settlements.

Tan et al. [13] showed that bleeding is a process mostly governed by consolidation rather than by segregation/sedimentation as previously thought. They observed that, due to the high concentration of fresh paste, forces develop and particles interact between them. Such forces can be considered as the effective stresses in soil mechanics, meaning that bleeding represents in fact a self-weight consolidation. Since consolidation is slowed down or stopped by the hardening process, a part of the bleeding water cannot reach the free surface [9]. Thus, the temperature and presence of admixtures (for instance retarder) can influence the amount of bleeding. Furthermore, during casting and compaction, heavier and larger aggregates tend to settle (potential segregation process). As a result of both consolidation and segregation, the bottom part of concrete has a larger content of coarse aggregates and the upper part contains more fine particles and water.

Powers [7] indicated that objects fixed in the formwork, such as reinforcing steel, interfere with the settlement as they are unable to follow the descending movement of the fresh paste. Settlement and bleeding lead potentially to a layer of water under each bar which is later absorbed by the hydration of the cement paste or evaporates, leading to a permanent void, which can also have implications for corrosion issues. Since the amount of settlement is related to the depth of the element, larger voids can be expected under horizontal bars placed closer to the top surface of concrete. Castel et al. [14] confirmed the presence of such voids using video-microscope and validated this observation for various types of concrete. Recently, Combrinck et al. [15] stated that plastic settlement may result in two different types of cracks: tensile cracks at the surface (surface cracks) and shear-induced cracks near the reinforcement bars (interior cracks), Figure 2.1b. Similar studies on the crack pattern due to the restraint plastic settlement related to steel bars were carried out by [16], [17].

2.3.2. In-situ concrete strength as function of the casting position

The previous phenomena were observed since the beginning of reinforced concrete practice and engineers were concerned by the potential reduction of concrete strength in its upper regions. In addition, it was not clear to what extend concrete control specimens (cubes, prisms or cylinders) produced to verify the specified compressive strength of concrete were suitably representing the actual resistance of a structural member cast with the same concrete. For these reasons, several researches were devoted to these topics already at the beginning of the last century. In 1915, Berndt and Preuss [18] compared the strength of cast cubes with that of saw-cut cubes from concrete monoliths. They reported a larger variability of concrete strength in actual structures compared to control specimens and confirmed that the concrete strength in the upper parts of concrete monoliths was lower than that in bottom parts. In 1931, Slater and Lyse [19] conducted tests on reinforced and unreinforced concrete columns. The crushing failures of unreinforced columns occurred always in the upper part, but this was attributed to load eccentricity. In addition, the unreinforced columns exhibited a resistance corresponding to only 85% of the compressive strength measured on control cylinders. As a consequence, this ratio of strength was later adopted by the ACI code for reinforced concrete at that time [20] and is still applied nowadays in the design of members in compression [21]. In the following decades, several researchers investigated the resistance of vertically cast columns and walls. Some of them showed that the strength reduction factor to be applied for calculating the crushing axial force of columns (as a function of the uniaxial concrete strength measured on control cylinders) decreases as the concrete strength increases, see [22]–[24].

The research of Petersons [5] represent one of the most systematic and comprehensive studies on the difference between in-situ compressive strength and control specimens. He reported tests on 37 square columns produced with different water/cement ratios and different concrete consistencies. Cylinders were drilled in vertical direction at different depths, whose strength was compared to control cylinders with the same size and cast with the same concrete batch. Figure 2.2 shows the distribution of the in-situ compressive strength $f_{c,is}$ in vertically-cast columns by Petersons [5] compared to the cylinder strength $f_{c,cyl}$. The in-situ strength $f_{c.is}$ in Figure 2.2 is calculated by multiplying the reported core strength $f_{c,core}$ by a coefficient 1.04 in order to account for damage sustained during drilling (according to Bartlett and MacGregor [25] for 150 mm cores). One can observe that, compared to the cylinder strength $f_{c,cyl}$ (dotted vertical lines), the in-situ strength $f_{c,is}$ in the upper part of the column (0.30-0.60 m, corresponding to 10-20% of the column's height) is usually lower. Below this weaker zone, the in-situ compressive strength is however normally higher (up to 20-30% higher than the cylinder strength). In that investigation, the variation over the column height seems to be higher for concretes produced with a small water/cement (*W/C*) ratio and the variation seems to be independent of the consistency class. Furthermore, Petersons [5] observed that cores drilled from the upper part of horizontally-casted columns had similar strength as that of cores drilled from the uppermost portions of vertically-poured columns.

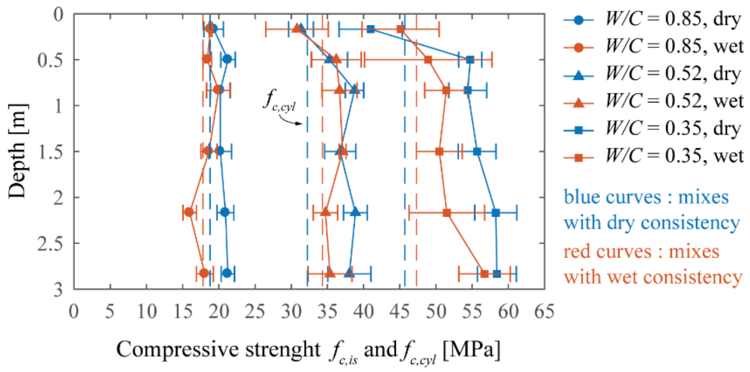

Figure 2.2: Tests by Petersons [5]: distribution of in-situ strength $f_{c,is}$ in vertically-cast columns obtained from vertically-drilled cores as a function of the core location (depth) and cylinder strength $f_{c,cyl}$ (error bars refer to the standard deviation calculated for the 4 columns produced with the same mix, but with four different batches).

Similar tests by other researchers have shown significant strength variations over the depth also for high *W/C* ratios and some influence of the fresh concrete consistency, Figure 2.3. Kanda and Yoshida [26] studied the variation of the *W/C* ratio in columns and slabs after concrete placing as a function of time and depth. This research confirmed that the content of water in the bottom part of slabs and columns decreases continuously before the hardening process starts (Figure 2.4a). In the top part, the water content increases in the first 60 minutes (as a result of the upward water movement due to bleeding), but then decreases again since the bleeding water moves to the free surface. The investigation also showed that the final water increase in the top layer is practically independent from the initial water content

(Figure 2.4b). This is in agreement to the fact that the compressive strength reduction in the upper layers is more pronounced for concretes with low *W/C* ratios (associated to higher concrete strengths) since these concretes are more sensitive to a variation in water content.

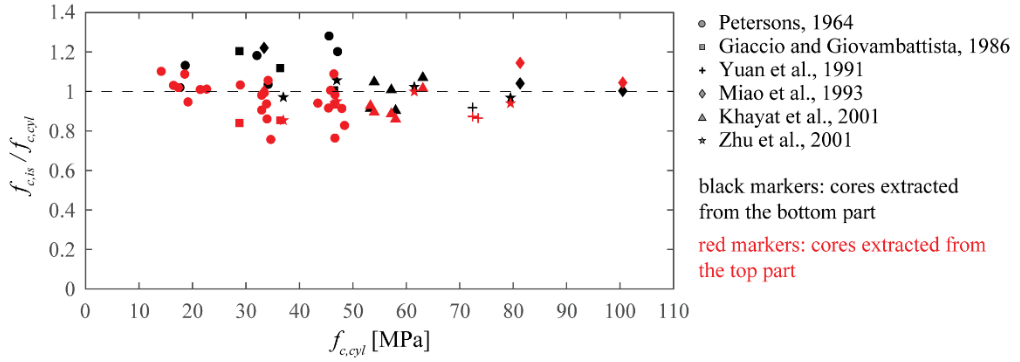

Figure 2.3: In-situ concrete compressive strength $f_{c,is}$ in bottom and top layers of columns related to the cylinder strength $f_{c,cyl}$ (data from Petersons [5], Giaccio and Giovambattista [11], Yuan et al. [6], Miao et al. [27], Khayat et al. [28], Zhu et al. [29]).

In addition, Kanda and Yoshida [26] also investigated the influence of vibration time on the variation of water and coarse aggregate content in the different layers of a column. As shown in Figure 2.4c-d, a reasonable vibration time (< 60 min) has little influence, but an increase of vibration can trigger a segregation process in the top layer.

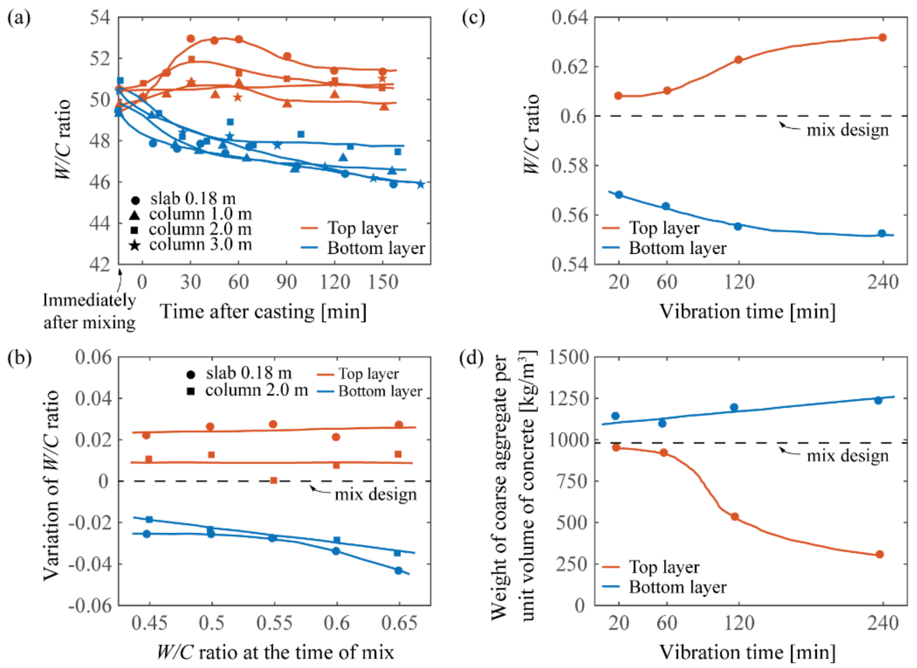

Figure 2.4: Tests by Kanda et al. [26]: (a) *W/C* ratio in top and bottom layers of concrete as a function of time after casting; (b) variation of *W/C* content as a function of this ratio at time of mixing; (c) final *W/C* ratio; and (d) weight of coarse aggregate in the top and bottom layers as a function of vibration time.

Following these observations, the strength increase in the bottom layer can also be justified by the enhanced amount of force that can be carried by direct contact between aggregates (releasing the transfer of forces through the matrix). With this respect, Takahashi and Nakane [30] found that the concrete compressive strength was significantly related to the consolidation pressure, the weight per unit volume and the air void content.

With respect to the influence of bleeding on the mechanical properties of structural concrete, Giaccio and Giovambattista [11] investigated this issue not only for the compressive strength, but also for the tensile strength, the elastic modulus and the mass per unit weight, showing poor mechanical performance and mass per unit weight on the top part (Figure 2.5). In some cases, similar strength reductions in the upper part were observed in the cores drilled vertically and horizontally, but in other cases, a significant anisotropy was observed. This is relevant for the tensile strength where, according to the observed voids under coarse aggregates (Figure 2.1a), the tensile strength in the vertical direction was significantly lower than in the horizontal one. Their research [11] also showed that the bleeding test on small concrete volumes (as according to ASTM C232 [12]) is not necessarily representative for the phenomena in larger structural members [31], [32].

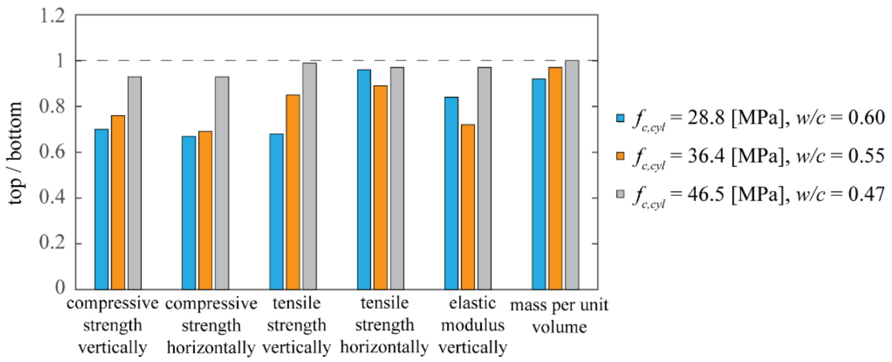

Figure 2.5: Tests by Giaccio and Giovambattista [11]: ratios between the measured properties at top and bottom of columns for different concrete mixes.

Tests conducted with concretes containing admixtures, with self-compacting concrete (SCC), or with slag, have shown almost systematically lower differences between the top and the bottom layers (see tests with $f_{c,cyl}$ between 50 and 110 MPa in Figure 2.3 by Yuan et al. [6], Miao et al. [27], Khayat et al. [28], Zhu et al. [29]). For instance, Ranjbar et al. [33] noticed that the amount of variation from top to bottom regions was lower in case of walls produced with SCC mixes. On the other hand, cores extracted from large columns cast with such concrete type have shown non-negligible differences in the strength over the cross section (the central part being stronger than the zones near to the surfaces, see [20], [34]).

2.3.3. Influence of presence of bars on compressive strength

The effects of embedded steel bars on the compressive resistance of concrete members has been investigated in the past by few researchers. Gaynor [35] studied the influence of placing one or two steel bars perpendicular to the loading direction in concrete cylinders (casting height 300 mm). He observed that the presence of the bars reduced the compressive strength of cylinders and that the reduction depended mainly on the amount of steel placed within the specimens. The location of the bar in the cylinders, however, did not seem to affect the compressive strength. Following these works, Plowman [36] tested specimens with horizontal steel bars in concrete cylinders to evaluate the influence of such inclusions, varying the diameter of the bars and their position with respect to the vertical axis. In the case of bars placed in the middle of the cylinders, the higher strength reductions corresponded to bars located at mid-height of the specimens. On the other hand, for offset bars, the highest strength reductions took place for bars placed near the top of the specimens. These results were in good agreement with the work performed by Gaynor. More recent works have also been performed on this topic [37], [38].

A comprehensive investigation comprising the influence of post-tensioning ducts and steel bars on the compressive capacity of concrete panels was performed by Leonhardt [39]. The case of injected ducts is relevant as they might have a similar influence as reinforcement bars in disturbing a compression field. Leonhardt [39] noticed that, in presence of post-tensioning ducts, the resistance of panels was reduced by a factor of approximately 0.86-0.89 with respect to control panels without ducts. Leonhardt explained that the strength reduction could be caused by the development of transverse tensile stresses related to the stress deviation induced by the different stiffness between steel and concrete. In addition, it was observed that the eccentricity and inclination of the tendons had only a small influence on the panel strength, while the distance between two post-tensioning ducts seemed to play a significant role. Other tests on panels were performed by Muttoni et al. [40] (16 panels with various types of post-tensioning ducts) and Wald [41] (testing 100 concrete panels).

The outlined researches highlight the detrimental effect of transverse bars or ducts on the compressive capacity of concrete cylinders or panels. This effect has been traditionally associated to the disturbance in the stress flow originated by the presence of the reinforcement. However, the potential influence of concrete bleeding and plastic settlement of fresh concrete (refer to Figure 2.1b) has to date not been investigated in depth. In this paper, such relationship will be discussed by means of a specific testing programme.

2.3.4. In-situ structural concrete strength in codes of practice

As already stated in Section 2.3.2, the ACI 318 code for structural concrete considers explicitly a strength reduction factor to account for the difference between the in-situ concrete resistance measured in structural members and the material strength measured on control cylinders. This factor is given in the ACI code a value equal to 0.85 [21]. Besides the phenomena related to casting, a strength reduction factor can also be required to account for other issues such as: (i) processes taking place between concrete production (when specimens for determining concrete strength are produced) and the beginning of on-site casting; (ii) different curing conditions; and (iii) different loading conditions (as for instance different loading rates as described by Tasevski et al. [42]).

As summarized in Table 2.1 for the case of a centrally-loaded column, other codes also account for the difference between the in-situ structural strength and the cylinder strength. This consideration can be explicit (with specific strength reduction factors) or implicit (by its consideration within the partial safety factors). In addition, this effect is in some cases more severely considered for higher strength concrete. For other members and loading conditions (e.g. compression zones in beams or compression field in webs) or for sustained loading effects, additional strength reduction factors can be required.

Table 2.1: Strength reduction factor $\eta_{is} = f_{c,is} / f_{c,cyl}$ in different codes of practice (case of an axially loaded column).

Code	$\eta_{is} = f_{c,is} / f_{c,cyl}$	Commentary
EN 1992-1-1:2004 (Europe) [43]	0.85	Accounted for implicitly in γ_C = 1.5 (see [44]). An additional strength reduction factor k_t = 0.85 is recommended in case the detrimental effect of sustained loading is not compensated by the strength increase due to continued cement hydration (see clause 3.1.2(4)).
ACI 318-19 (USA) [21]	0.85	Accounted for explicitly in strength formulae (see for instance clause 22.4).
AS3600:2018 (Australia) [45]	0.90 (general case) For columns: - 0.85 for $f_c' \leq 50$ MPa - 0.72 for $f_c' \geq 93$ MPa - linear interp. in-between	0.90 according to clause 3.1.1.2 (accounts for differences between structural elements and control cylinders related to curing environments, loading rate, shape and size). Strength reduction factor α_1 for axially loaded columns according to clause 10.6.2.2 contains previous factor 0.90 and an additional strength reduction to account for cover spalling [46].
GB50010-2010 (China) [47]	$0.88 \cdot \alpha_2$ where: - α_2 = 1.0 for $f_{ck} \leq 40$ MPa - α_2 = 0.87 for $f_{ck} \geq 80$ MPa - linear interp. in-between	0.88 accounted for in definition of f_{ck}, see commentary to clause 4.1.3.
fib MC2010 [48]	Not accounted for explicitly, despite the fact that the same partial safety factor γ_C = 1.5 as in EN 1992-1-1:2004 [43] is defined (but with a different explanation).	

2.4. Experimental programme on the measurement of settlements in fresh concrete

Concrete settlement is investigated in this section using state-of-the-art measurement techniques such as tomography and Digital Image Correlation (DIC). The phenomenon is investigated both during hardening of the concrete as well as on the resulting (hardened) state.

2.4.1. Specimen description

2.4.1.1. Geometry

One beam and one wall element were cast and used to obtain a number of smaller test specimens (see Figure 2.6):

- The beam was cast with 20 mm transverse bars (beam BM2, Figure 2.6a) with variable concrete covers (denoted by letters A-E, refer to Table 2.2). During casting, the upper surface of the beam was monitored with DIC in order to measure the settlements of fresh concrete.
- The wall was cast with 16 mm transverse bars (wall WM1, Figure 2.6b) located at different depths. From this wall, ten cores with a diameter of 73 mm were drilled (specimens WM1A1-10). Each core was centred on the bars and prepared for tomography scanning. In addition, four

plain cores (named WM1B1-4) located at different depths were extracted horizontally from the same wall. Once their density was determined, they were tested in pure compression (failure reached in approximately 2 minutes).

The geometry of the investigated specimens is described in Figure 2.6 and Table 2.2. All bars were fixed to the vertical formworks to avoid their movement during casting and concrete consolidation.

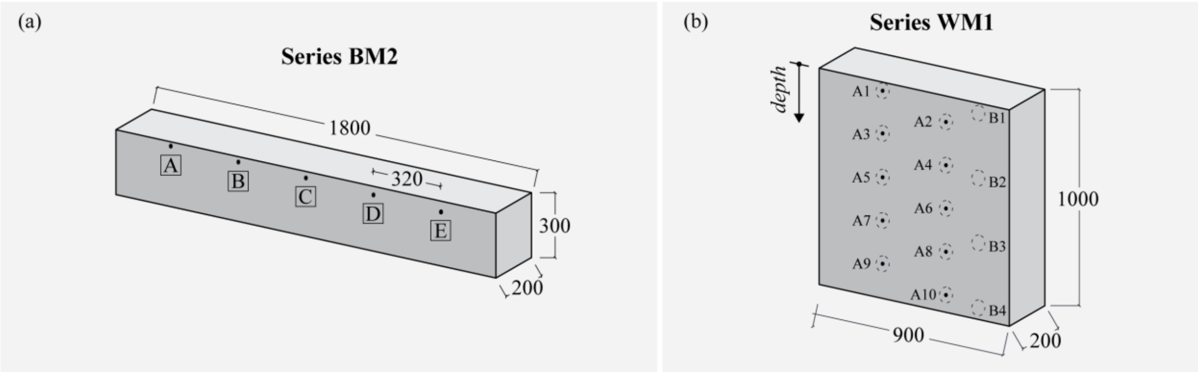

Figure 2.6: Geometry and reinforcement of the investigated specimens: (a) beam BM2; and (b) wall WM1. Casting direction vertical in all cases.

Table 2.2: Main parameters and results of the investigated specimens: depth refers to the distance from the top surface to the centre of gravity of each element; *ø* to the diameter of the transverse rebar; *c* to the concrete cover (upper surface); *Δ* to the average thickness of the void measured under the bars; f_R to the structural resistance (applied load divided by gross cross section).

Specimen	Depth [m]	*ø* [mm]	*c* [mm]	*Δ* [mm]	f_R [MPa]
WM1A1	0.04	16	-	0.87	-
WM1A2	0.12	16	-	0.51	-
WM1A3	0.24	16	-	0.41	-
WM1A4	0.32	16	-	0.48	-
WM1A5	0.44	16	-	0.57	-
WM1A6	0.52	16	-	0.23	-
WM1A7	0.64	16	-	0.24	-
WM1A8	0.72	16	-	0.20	-
WM1A9	0.84	16	-	0.12	-
WM1A10	0.92	16	-	0	-
WM1B1	0.05	-	-	-	32.9
WM1B2	0.35	-	-	-	35.1
WM1B3	0.65	-	-	-	39.2
WM1B4	0.95	-	-	-	37.7
BM2A	-	20	10	-	-
BM2B	-	20	15	-	-
BM2C	-	20	20	-	-
BM2D	-	20	30	-	-
BM2E	-	20	40	-	-

2.4.1.2. Material properties

The test series were cast with similar ready-mix concrete from a local supplier. Cement type of series BM2 was CEM II/B-M (T-LL) 42.5N while for series WM1 was CEM II/B-LL 32.5R, according to [49]. For both series, the maximum aggregate size was 16 mm. Slump and flow tests were performed to evaluate the consistency of fresh concrete, in conformity with [50]–[52]. A curing time of 14 days was respected for both specimens (in accordance with [53]) except on the surface over which DIC measurements on fresh concrete were performed (beam BM2). In this case, curing started 24 hours after casting. The concrete composition and the results of the fresh concrete tests are summarized in Table 2.3.

Table 2.3: Concrete properties.

Series	*c* [kg/m³]	*W/C* [-]	Aggregates [kg/m³] 0/4	4/8	8/16	Retarder [kg/m³]	Superpl. [kg/m³]	Slump [mm]	Flow [mm]	$f_{c,cyl}$ [MPa]	CoV [%]
WM1	342	0.57	893	394	687	1.35	1.70	140 (S3)	480 (F3)	36.8	4.2
BM2	344	0.53	830	380	671	0.95	1.30	200 (S4)	515 (F4)	-	-

2.4.2. Main experimental results

2.4.2.1. Tomography measurements

The concrete cores extracted from the wall were scanned in a tomograph (UltraTom from Rx-Solutions). This method allows for a precise evaluation of the porosity and presence of voids in the concrete samples. It was targeted on the region near the transverse reinforcement bars in order to detect any void produced by bleeding and concrete settlement. The main findings of the tomography imaging are presented in Figure 2.7, with reference to cores extracted at three different depths (top, middle and bottom regions).

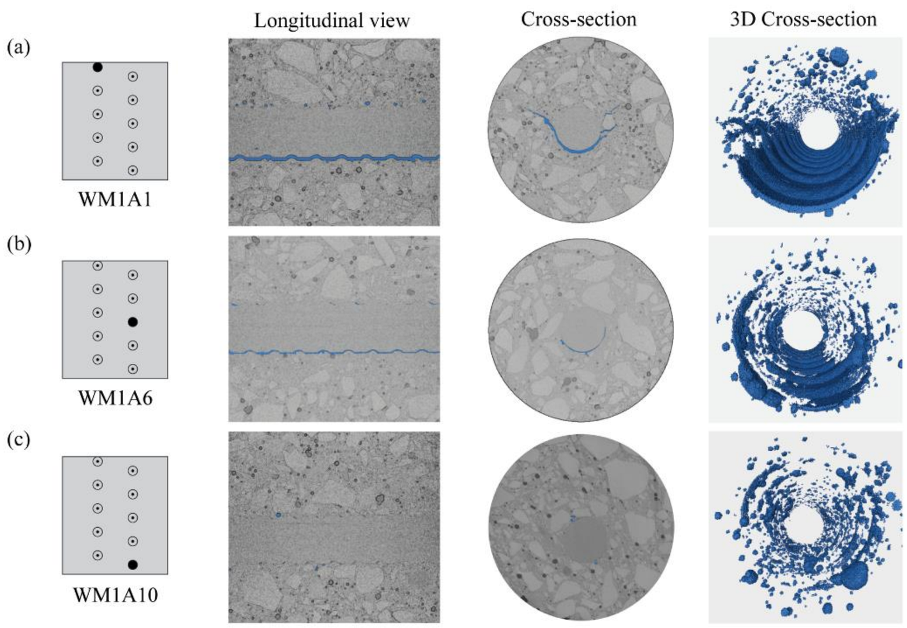

Figure 2.7: Tomography sectioning of concrete cores extracted from the wall element WM1. The blue zones indicate the presence of voids or porosity: (a) top region; (b) middle region; and (c) bottom region.

It is interesting to observe that a clear void is located directly under the transverse bars in the top and middle regions of the wall (as shown in Figure 2.1b). The void is shown to develop along the bottom surface of the reinforcing bars and increases in dimensions as the reinforcement is located closer to the top surface. In the lower part of the wall, however, almost no voids are observed in the vicinity of the bars (with a homogeneous porosity distribution). These observations clearly outline the interaction between fresh concrete consolidation and fixed elements, with two phenomena occurring. First, fresh concrete settles while the reinforcing bars remain fixed to the formwork and, second, bleeding water movement is obstructed by the reinforcement (both phenomena yield to the development of voids below the bars). In addition, as shown in Figure 2.7a, the presence of bars also disturbs the settlement of adjacent coarse aggregates, favouring the development of cracks below them (see interior crack in Figure 2.1b).

The tomography results are further analysed in Figure 2.8a, showing the average thickness of the voids located under the bars. The results consistently show increasing void depth for locations closer to the top surface (refer to Powers [7]), confirming the findings of Castel et al. [14].

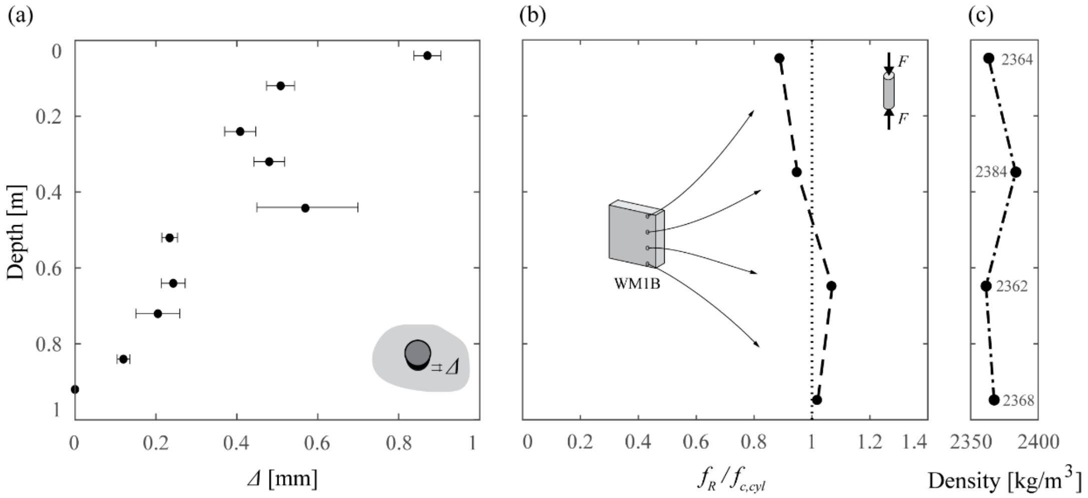

Figure 2.8: Main results of core tests: (a) average void thickness under the bars measured with tomograph as function of the depth (error bars indicate standard deviation); (b) ratio between the structural resistance and the concrete compressive strength measured on cores as function of the depth; and (c) density of the cores tested in compression.

2.4.2.2. Compression tests

The plain cores (WM1B1-4) were used to determine the influence of the location in the wall on the density variation and the compressive strength. With respect to density (Figure 2.8c), it appears to be roughly constant regardless of the depth at which the cores are extracted, with no particular trend in the performed tests. Regarding the compressive strength (Figure 2.8b), the tests show a clear increase for higher distances to the top surface (this topic will be examined later more in detail).

2.4.2.3. DIC measurements

The digital image correlation was additionally used to investigate the plastic settlement and horizontal displacement of fresh concrete at the upper surface of beam BM2 containing 20 mm transverse rebars. The DIC measurements started one hour after concrete casting (preparation of DIC speckle) and lasted for 24 hours (1 picture per minute in the first hour, 1 picture each 2 minutes in the second and third hours and 1 picture each 5 minutes thereafter). The upper surface was white-painted and speckled with random black patterns. This procedure was possible as surface bleeding was almost negligible. For a more refined evaluation of concrete settlement and horizontal displacement, the vertical displacement w and longitudinal displacement u are computed along the beam at the mid-section of the investigated surface. The results are presented in Figure 2.9. It should be noted that the reference time is set to 1 hour after casting (beginning of the measurements) and, therefore, the initial plastic settlement (as described by Clear and Bonner [8]) was not recorded.

Figure 2.9a shows that the concrete settlement is relevant with values of approximately 1 mm for a 300 mm-high beam with most of the plastic settlement occurring over the first 5 hours after casting (Figure 2.9b). The location of the bars is clearly noticeable, with maximum concrete settlements between bars and lower settlements at the location of the bars. This effect was in addition more pronounced for lower concrete covers.

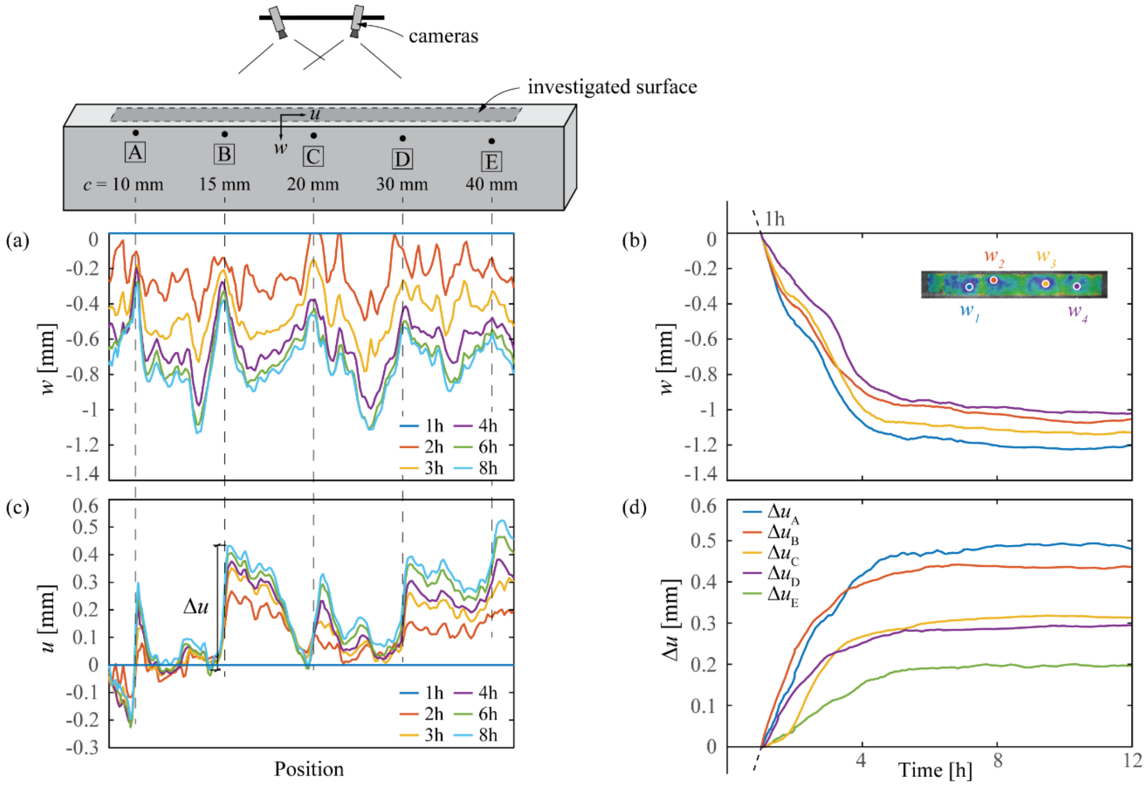

Figure 2.9: Fresh concrete settlement measurements: (a) vertical settlement *w* of fresh concrete at the mid-section of the top surface at different times after casting; (b) vertical settlement *w* of the regions representing the largest vertical displacements; (c) horizontal displacement *u* of fresh concrete at the mid-section of the top surface; and (d) relative horizontal displacement at the location of the transverse bars.

With respect to the horizontal displacement u, a considerable discontinuity is measured at the location of the transverse reinforcement (Figure 2.9c), indicating that fresh concrete flows in two opposite directions. This response is in agreement to the development of surface cracks aligned with the bar axis (refer to Figure 2.1b). As shown in Figure 2.9d, the difference of displacement is higher for small concrete covers (approximately 0.4-0.5 mm for c = 10 mm and 15 mm) and lower for large concrete covers (down to 0.2 mm for c = 40 mm). This phenomenon, combined with the progressive hardening of the concrete, induces cracking along the transverse reinforcement and represents one of the main sources of concrete cracking at early age, as previously described by Combrinck et al. [15].

2.5. Experimental programme on the influence of casting position on the concrete resistance

A second experimental programme was performed to investigate in a detailed manner the influence of the previous phenomena (distance with respect to the casting surface, disturbance of reinforcement, influence of casting direction) on the concrete compressive resistance of concrete elements.

2.5.1. Specimen description

2.5.1.1. Geometry

Four different series of specimens were cast:

- Series CK1 (Figure 2.10a) consisted of 3 columns of 3 m-high cast vertically and also a column of 0.75 m-high cast horizontally. Cross section dimensions were 250 × 250 mm and three different reinforcement layouts were investigated: plain concrete (cross section A), and 30 mm transverse bars in one direction (cross section B), 30 mm transverse bars in two directions (cross section C). The transverse reinforcement was fixed to the vertical formwork and no vertical reinforcement was arranged. After curing, the specimens were demoulded and saw-cut into four pieces (750 mm high) for testing in compression.
- Series CM1 (Figure 2.10b) was composed of 3 vertically-cast columns with a height of 2.25 m. Three additional elements with a length of 0.75 m were casted horizontally. For comparison purposes, the cross section was identical to the CK1 series. The reinforcement layout was however different: all column elements had 4 × 10 mm longitudinal bars and stirrups with 150 mm spacing. The stirrups, fixed to the longitudinal reinforcement during casting, were 8 mm diameter for cross section A, 12 mm for cross section B and 16 mm in the case of cross section C. The concrete cover was kept constant for all specimens and was equal to 20 mm. After curing and demoulding, the columns were saw-cut into three pieces of 750 mm high.
- A small column of 1.05 m high (series CM2, Figure 2.10c) was also cast and subsequently saw-cut into prisms of 0.35 m high. The column contained 20 mm transverse bars fixed to the formwork during casting and no vertical reinforcement was arranged.
- Finally, series BM1 (Figure 2.10d) consisted of a beam with a cross section 0.15 × 0.3 m and a length of 1.8 m. The specimen had two layers of transverse bars fixed to the formwork with variable concrete cover to the top and bottom surfaces. The beam was eventually saw-cut into prisms of 0.3 m high. The prisms were either plain or contained transverse bars.

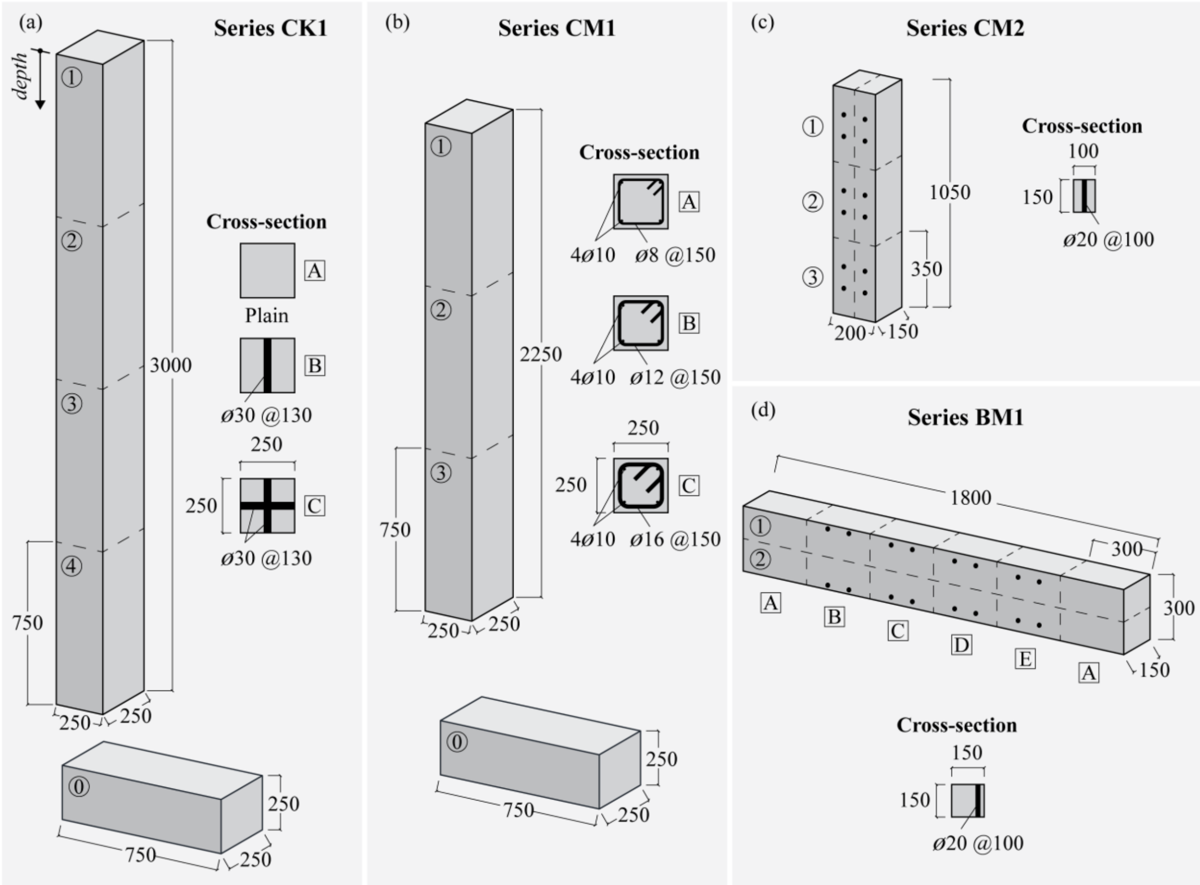

Figure 2.10: Geometry, reinforcement and cutting planes for each investigated series (dimensions in [mm]): (a) series CK1; (b) series CM1; (c) series CM2; and (d) series BM1. Casting direction vertical in all cases.

Control concrete cylinders (160 mm diameter, 320 mm high) were cast at the same time. All elements followed the same curing period and were stored in the laboratory at an average temperature of 22°C and an average relative humidity of approximately 50%.

The main properties of the tested specimens and casting direction with respect to the loading conditions is indicated in Table 2.4. The specimens are named according to their series name followed by the cross section type (letter) and the casting position (number). If the casting position number is followed by .1 or .2, this indicates that two specimens with identical characteristics are present in the test series.

2.5.1.2. Material properties

The casting of each series took place at different dates with slightly different concrete, using ordinary ready-mix concrete from a local supplier. The cement type of series BM1, CM1 and CM2 was CEM II/B-M (T-LL) 42.5N while, for series CK1, it was CEM II/B-LL 32.5R, according to [49]. The maximum aggregate size in all cases was 16 mm. The concrete was poured in layers of a maximum height of 400 mm and vibrated before pouring a new layer of concrete (vibration and casting according to [53]). At the end of each casting, the exposed surfaces of the specimens (top surfaces) were protected with plastic films to ensure suitable curing conditions during at least 14 days, in accordance with [53].

Table 2.4: Main parameters of test specimens: depth refers to the distance from the top casting surface to the centre of gravity of each element; // testing direction parallel to the casting direction; ⊥ testing direction perpendicular to the casting direction; ø diameter of the transverse rebar, *c* concrete cover (size of prisms for compression tests: 250 x 250 x 750 mm for series CK1 and CM1; 100 x 150 x 350 mm for series CM2; 150 x 150 x 300 mm for series BM1).

Specimen	Depth [m]	Testing	ø [mm]	*c* [mm]	Specimen	Depth [m]	Testing	ø [mm]	*c* [mm]
CK1A0	0.125	⊥	-	-	CM1C1	0.375	//	16	20
CK1A1	0.375	//	-	-	CM1C2	1.125	//	16	20
CK1A2	1.125	//	-	-	CM1C3	1.875	//	16	20
CK1A3	1.825	//	-	-	CM21.1	0.175	//	20	40
CK1A4	2.625	//	-	-	CM21.2	0.175	//	20	40
CK1B1	0.375	//	30	110	CM22.1	0.525	//	20	40
CK1B2	1.125	//	30	110	CM22.2	0.525	//	20	40
CK1B3	1.825	//	30	110	CM23.1	0.875	//	20	40
CK1B4	2.625	//	30	110	CM23.2	0.875	//	20	40
CK1C1	0.375	//	30	110	BM1A1.1	0.075	⊥	-	-
CK1C2	1.125	//	30	110	BM1A1.2	0.075	⊥	-	-
CK1C3	1.825	//	30	110	BM1A2.1	0.225	⊥	-	-
CK1C4	2.625	//	30	110	BM1A2.2	0.225	⊥	-	-
CM1A0	0.125	⊥	8	20	BM1B1	0.075	⊥	20	10
CM1A1	0.375	//	8	20	BM1B2	0.225	⊥	20	10
CM1A2	1.125	//	8	20	BM1C1	0.075	⊥	20	20
CM1A3	1.875	//	8	20	BM1C2	0.225	⊥	20	20
CM1B0	0.125	⊥	12	20	BM1D1	0.075	⊥	20	30
CM1B1	0.375	//	12	20	BM1D2	0.225	⊥	20	30
CM1B2	1.125	//	12	20	BM1E1	0.075	⊥	20	40
CM1B3	1.875	//	12	20	BM1E2	0.225	⊥	20	40
CM1C0	0.125	⊥	16	20					

The compression tests of control cylinders were performed at 7, 14, 21, 28 days and during the test programme with loading rates leading to failure in approximately 1-2 minutes. Details of the concrete cylinder strength ($f_{c,cyl}$) at the days of prism tests are shown in Table 2.5. The concrete composition as well as the results of the fresh concrete tests are summarized in Table 2.5.

Table 2.5: Concrete properties.

Series	*c* [kg/m³]	*W/C* [-]	Aggregates [kg/m³] 0/4	4/8	8/16	Retarder [kg/m³]	Superpl. [kg/m³]	Slump [mm]	Flow [mm]	$f_{c,cyl}$ [MPa]	CoV [%]
CK1	340	0.45	732	402	713	1.36	1.70	240 (S5)	690 (F6)	36.4	2.5
CM1 CM2	340	0.57	819	375	674	1.02	1.36	120 (S3)	440 (F3)	35.2 34.3	3.7
BM1	341	0.54	920	360	660	0.93	1.33	85 (S2)	380 (F2)	48.2	3.9

Conventional hot-rolled ribbed bars with characteristic yield strength of f_{yk} = 500 MPa were used in all specimens. Tension tests were also performed on the reinforcement of series CM1, in accordance with [54]. The mean values of the yield and ultimate strength are given in Table 2.6. With respect to the other test series, the transverse bars were not tested since no yielding was expected during prism tests.

Table 2.6: Reinforcing steel properties of stirrups and longitudinal reinforcement of series CM1 (average values for three samples, values in brackets refer to standard deviations).

Diameter [mm]	f_y [MPa]	f_u [MPa]
8	496 (12.1)	601 (6.6)
10	539 (4.2)	613 (5.0)
12	531 (11.3)	601 (4.7)
16	474 (11.0)	588 (1.2)

2.5.1.3. Testing and measurements

All specimens were tested in pure compression. Two testing machines were used: series CK1 and CM1 were tested in a 10 MN hydraulic Schenck-Trebel machine while series CM2 and BM1 were tested in a 2.5 MN hydraulic Schenck machine. The specimens were loaded under controlled displacement conditions. Typical duration of tests was about 30-40 minutes for column elements (CK1, CM1) and 2-3 minutes for prisms (CM2, BM1), refer to Table 2.7. All specimens were mechanically-polished before testing to ensure planar and parallel loading surfaces. In addition, a thin layer of epoxy resin was placed underneath and on top of each element to avoid any stress concentration at the load introduction regions. The columns of series CK1 and CM1 were externally confined with a steel ring to avoid failure at the load introduction. During the tests, continuous readings were recorded on the load and displacement of the jack.

Digital Image Correlation (DIC) pictures were taken at a frequency of 0.1 Hz, increased to 1 Hz near failure. The DIC was used at the sides of the specimens with reinforcing bars, in order to get an accurate description of the strain and displacement fields originated by the disturbances. The DIC was performed by applying a random and uniform speckle pattern on the entire surface of the specimens. Two high-resolution cameras were used (either Manta G504B with a resolution of 5 Megapixels or Manta with 4 Megapixel). The photos were post-processed using VIC-3D [55] providing the complete displacement field during the test. The maximum error corresponded to approximately 1/40 of a pixel (whose dimension were either 217×217μm^2 or 380×380μm^2, depending on the camera used).

2.5.2. Main experimental results

2.5.2.1. Structural resistance

A summary of the failure load, test duration and density is presented for each specimen in Table 2.7 (no results reported for specimens CK1B2, CM1A1 and CM1A3 due to damage during handling). In addition, Figure 2.11 illustrates for each test series the ratio between the structural compressive resistance (f_R) and the concrete strength measured in standard cylinder tests ($f_{c,cyl}$) as function of the depth. It has to be noted that the cylinder strength refers to rapid loading conditions (1-2 minutes before failure) while the series CK1 and CM1 have been performed with lower loading rates (typical test durations of approximately 30 minutes). For such loading durations, a reduction can be expected on the compressive strength of the material (approximately 4% for the investigated cases according to Tasevski et al. [42]). This effect is considered for series CK1 and CM1 (see Table 2.7 and Figure 2.11) by correcting the concrete strength measured in cylinders under rapid loading ($f_{c,cyl}$) with the factor k_t (equal to 0.96).

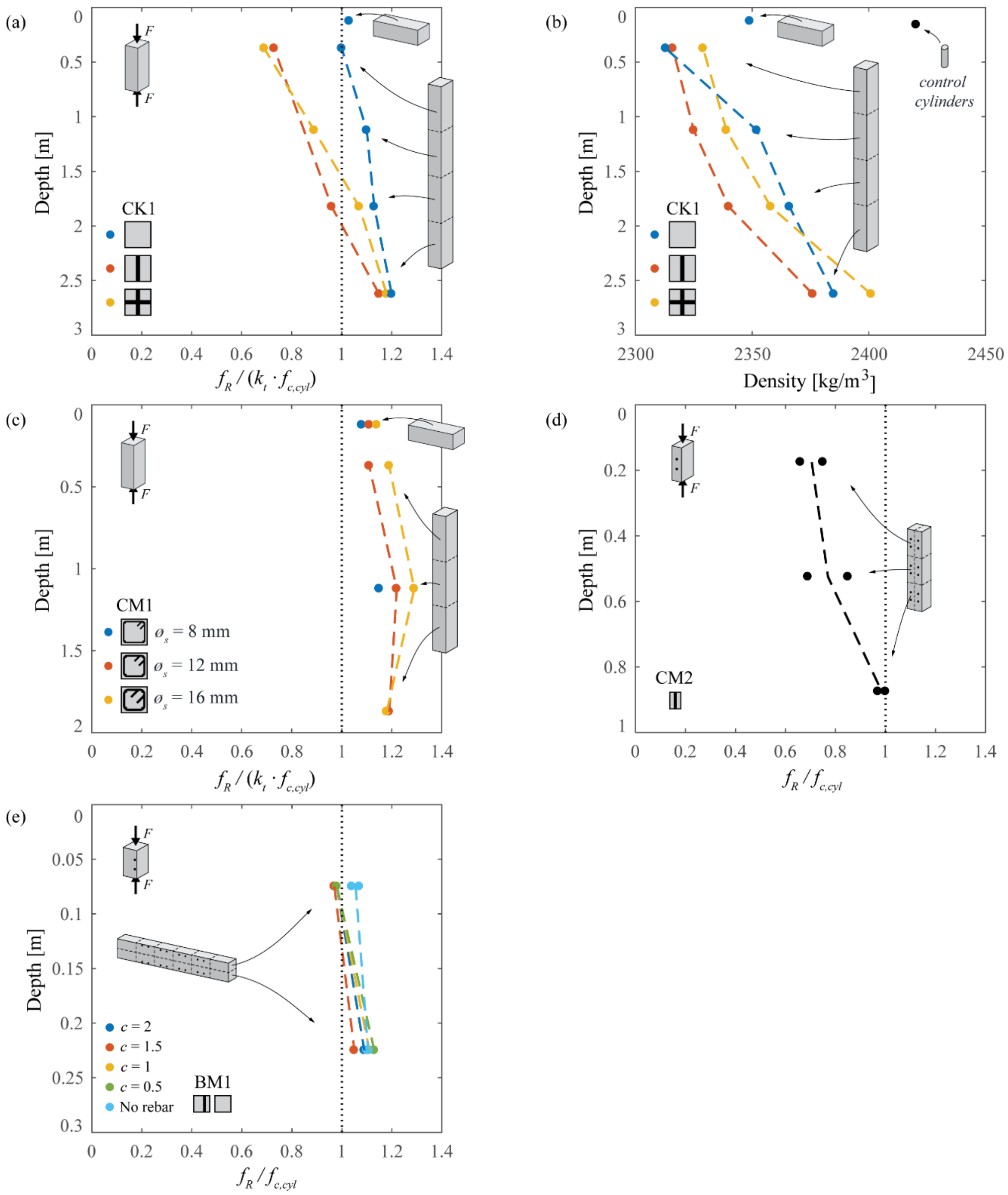

Figure 2.11: Main results of the experimental investigation in terms of the ratio between the structural resistance f_R and the cylinder compressive strength $f_{c,cyl}$ as function of the depth (for series CK1 and CM1, f_R is corrected to account for load duration with coefficient k_t): (a) series CK1; (c) series CM1; (d) series CM2; and (e) series BM1. Variation of volumetric mass density as function of the depth: (b) series CK1.

As Figure 2.11a indicates, the compressive resistance of series CK1 increases with increasing depth. The strength reduction with decreasing depth is more pronounced for specimens containing transverse bars, indicating that such reinforcement has an unfavourable effect on the compressive resistance. In addition, the plain specimen cast horizontally shows a similar resistance than the one measured in the top part of the plain column cast in vertical direction (and consequently similar strengths as the reference cylinders).

Table 2.7: Main experimental results (f_R structural resistance calculated as the applied force divided by gross cross section; k_t strength reduction factor accounting for low loading rates equal to 0.96 for loading duration of approximately 30 minutes [42]; ρ volumetric mass density).

Specimen	f_R [MPa]	f_R / ($k_t \cdot f_{c,cyl}$)	Duration [min]	ρ [kg/m^3]	Specimen	f_R [MPa]	f_R / $f_{c,cyl}$	Duration [min]
CK1A0	35.9	1.03	29.9	2349	CM21.1	22.6	0.66	2.83
CK1A1	34.9	1.00	31.4	2313	CM21.2	25.8	0.75	2.58
CK1A2	38.4	1.10	28.8	2352	CM22.1	23.5	0.69	2.63
CK1A3	39.6	1.13	34.3	2366	CM22.2	29.2	0.85	2.50
CK1A4	42.1	1.20	31.8	2385	CM23.1	34.4	1.00	3.18
CK1B1	25.5	0.73	23.1	2316	CM23.2	33.2	0.97	2.50
CK1B2	-	-	-	2325	BM1A1.1	51.5	1.07	3.08
CK1B3	33.7	0.96	29.2	2340	BM1A1.2	50.0	1.04	2.88
CK1B4	40.3	1.15	30.5	2376	BM1A2.1	53.0	1.10	3.02
CK1C1	24.2	0.69	29.9	2329	BM1A2.2	53.6	1.11	2.90
CK1C2	31.2	0.89	30.1	2339	BM1B1	47.3	0.98	2.90
CK1C3	37.5	1.07	33.2	2358	BM1B2	54.4	1.13	3.07
CK1C4	41.3	1.18	32.6	2401	BM1C1	47.2	0.98	2.93
CM1A0	36.5	1.08	28.6	-	BM1C2	53.6	1.11	3.12
CM1A2	39.0	1.15	37.6	-	BM1D1	46.8	0.97	2.88
CM1B0	37.6	1.11	32.2	-	BM1D2	50.8	1.05	3.38
CM1B1	37.4	1.11	34.2	-	BM1E1	47.3	0.98	3.03
CM1B2	41.3	1.22	35.2	-	BM1E2	52.6	1.09	2.73
CM1B3	40.1	1.19	33.7	-				
CM1C0	38.6	1.14	33.8	-				
CM1C1	40.2	1.19	34.4	-				
CM1C2	43.6	1.29	31.1	-				
CM1C3	39.8	1.18	28.9	-				

Density measurements (Figure 2.11b) indicate a good correlation between the density increase with depth and the strength variations observed in Figure 2.11a. Surprisingly, all investigated specimens present lower densities than those of reference cylinders. In the case of the plain column elements CK1A, the variation in density and compressive strength are most probably associated to the bleeding phenomenon (water migration to the casting surface, affecting the density). The arrangement of transverse bars (but not stirrups) increases the significance of the effects of plastic settlement on the compressive resistance (refer to specimens CK1B and CK1C in Figure 2.11a). This can be justified by the larger voids developing below the reinforcement. Although these voids are negligible in the bottom part of the column, they can reach significant dimensions in the top part, resulting in large discontinuities (as discussed in Figure 2.7). Such discontinuities disturb the flow of stresses and give rise to regions with tensile stresses and concentrations of compressive stresses (see Figure 2.12a), leading to the development of local cracking and crushing near the bar (refer to Figure 2.12b,c respectively) being thus associated to a decrease in the overall compressive resistance. This can presumably be the reason why, for column elements CK1B and CK1C, the strength decrease with decreasing depth is more pronounced compared to the plain column elements CK1A (this phenomenon will be discussed later on the basis of DIC-measurements).

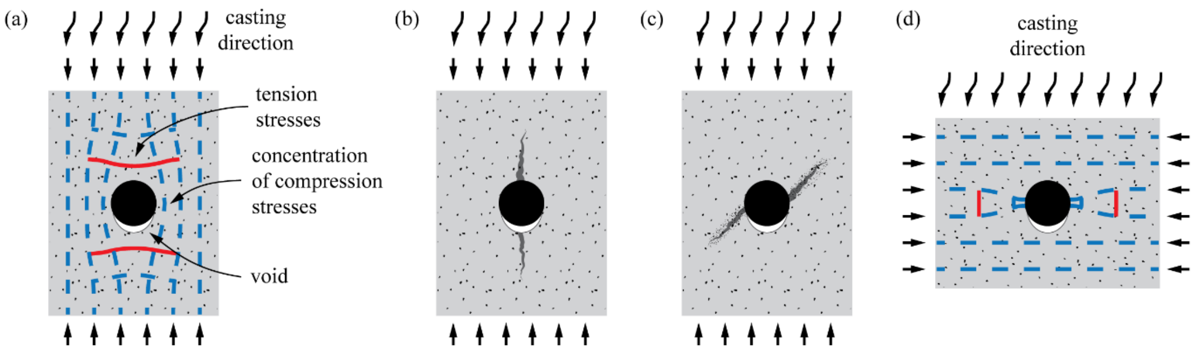

Figure 2.12: Influence of presence of voids on the compression field: (a) stress state for loading parallel to casting direction; (b) associated cracking near a bar; (c) crushing regions near the bar due to stress concentration; and (d) stress state for loading perpendicular to casting direction.

Interestingly, series CM1 (Figure 2.11c) where closed stirrups were arranged, does not show any significant variation of the resistance over the height of the column. For each column layout, the compressive resistance of the specimens is roughly constant, regardless of the casting depth and direction (vertical or horizontal). In addition, these specimens presented higher compressive resistances than those of reference cylinders (probably associated to the confinement provided by the stirrups). In this case, bleeding and plastic settlement should also occur over the height of the columns, decreasing the density in the top part and creating voids below the transverse reinforcement. However, these potentially negative effects seem compensated by the favourable action of the stirrups (for crack control and core confinement).

With respect to series CM2 (Figure 2.11d), a similar behaviour to series CK1 can be observed. The prisms in the bottom reach similar resistances than the control specimens, while the prisms of the top and middle region exhibit a lower resistance. In this case, bleeding should have a less pronounced impact on the compressive capacity of the prisms due to the relatively small height of the column. However, voids under the bars were observed in the top and middle reinforcements once the formwork was removed and plastic settlement influenced thus the compressive capacity of the specimens. This test series confirms additionally the observations of series CK1, namely that the presence of transverse reinforcement (when not arranged as stirrups providing confinement) weakens the compressive strength.

For series BM1, Figure 2.11e shows that the prisms extracted from the beam presented similar resistances in the top and bottom regions. It can be noted that the casting direction and the loading direction were perpendicular in this case. Thus, the potential voids under the bars during casting were not located under the reinforcement with respect to the loading direction, but at its side (Figure 2.12d). This condition, whose implications will be discussed later more in detail, seems also to reduce the disturbance induced by the reinforcement (smaller deviations of the compression field).

For further details, an extended description of the observed failure modes and surface cracking can be consulted in Annex A of this paper.

2.5.2.2. Stress-strain response

As previously explained, with the exception of specimens with confinement reinforcement, the casting position influenced the resistance of the specimen, leading to a decreasing strength for elements closer to the casting surface. Such strength decrease was also accompanied by a less brittle response. For instance, Figure 2.13 shows the longitudinal stress-strain curves for series CM2. For the specimens with the lowest strength (closest to the casting surface), the slope of the stress-strain curve in the softening part is clearly milder. Similar results were also recorded for comparable series (details on all measured stress-strain curves and corresponding Poisson's coefficients can be consulted in Annex B).

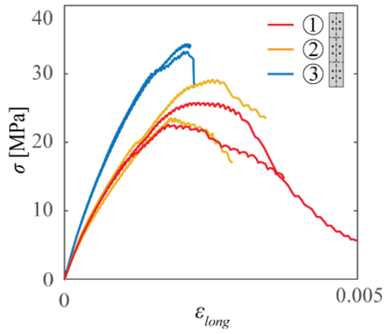

Figure 2.13: Stress-strain relationship of test series CM2.

2.5.2.3. Disturbance induced by the reinforcement

The influence of the reinforcement bars on the structural response is investigated in detail by means of DIC measurements in Figure 2.14. This figure plots the vertical displacements measured in the axis of the bars for two prisms of series CM2 and BM1.

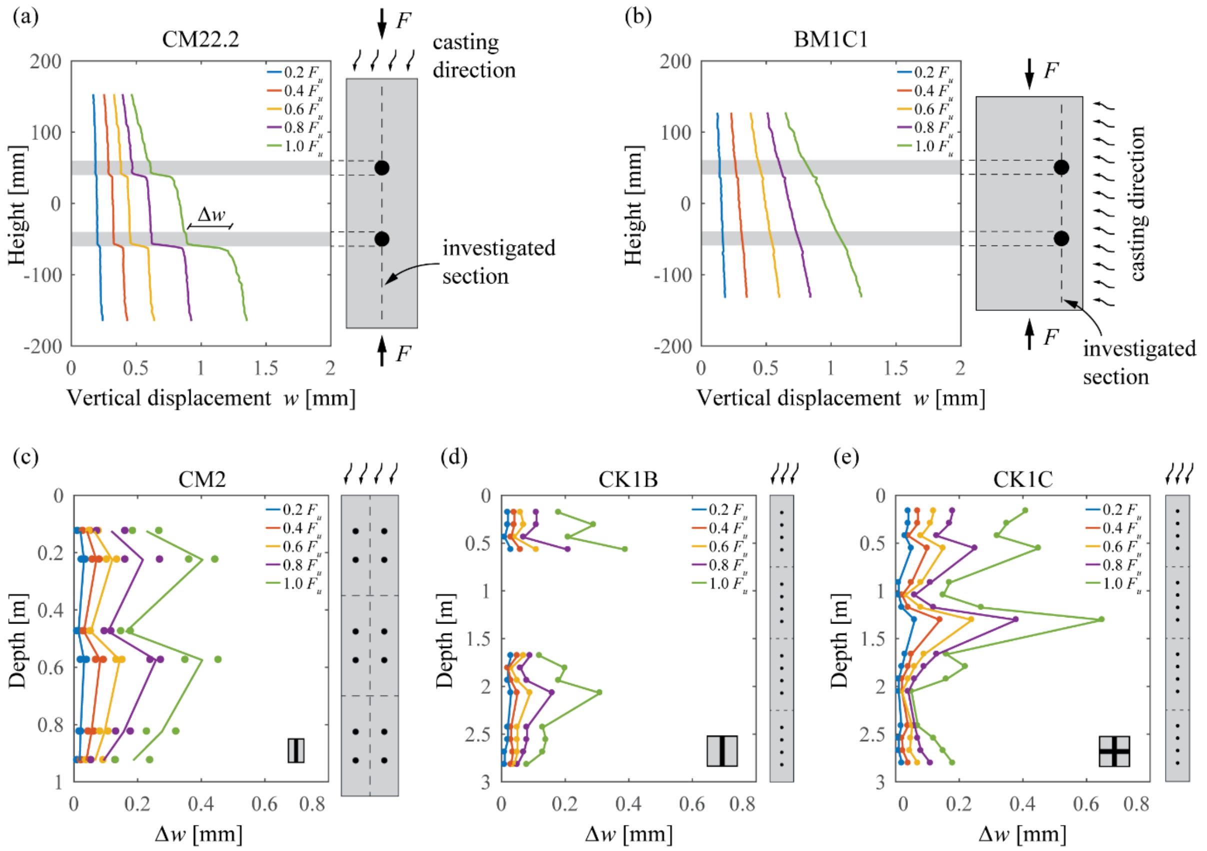

Figure 2.14: Disturbance induced by reinforcement: (a-b) vertical displacement at the axis of the transverse bars at different load levels; and (c-e) difference of vertical displacement.

With respect to specimen CM22.2 (Figure 2.14a), it can be noted that the increase of deformations concentrates in the region beneath the bars. This response can be explained by the closing of the void under the bars (see Figure 2.7) and the local crushing of the concrete where voids are not continuous. Such crushing can be associated to the poor quality of the concrete in this region, due to the bleeding and plastic settlements. In addition, crushing beside the bars as shown in Figure 2.12c related to stress concentrations (Figure 2.12a) is also possible.

In the case of specimen BM1C1 (Figure 2.14b), the vertical displacements measured in the axis of the bars are linear and do not show any noticeable disturbance associated to the reinforcement. This indicates a better and more homogenous concrete carrying compression near to the bars and is a direct consequence of the fact that the casting direction of the prisms is perpendicular to the applied load. The voids issued from plastic settlement are then located on the side of the bars (refer to the condition of Figure 2.12d).

The discontinuity of vertical displacement between points on top and on bottom of the bar (Δw) is plotted in Figure 2.14c-e for series CM2, CK1B and CK1C. It can be noted that, in general, the discontinuity of vertical displacement is more pronounced for specimens corresponding to the middle and top parts of the columns. This suggests that the voids below the reinforcing bars (closed and crushed during the loading process) are larger in the upper part of the elements. In addition, this discontinuity of vertical displacement is more pronounced for the lower bar of each specimen. This latter behaviour results from the larger bar spacing at the saw-cuts regions, inducing the concrete to settle over a higher height and developing larger voids under the lower bars.

2.5.2.4. Influence of concrete cover and spalling

The prisms of test series BM1 contained transverse bars with variable concrete cover. This parameter was varied with the aim of investigating its influence on the compressive capacity and failure mode of the investigated prisms (Figure 2.15a) and to compare it to the other test series (Figure 2.15b), with different casting direction and steel bars placed in the middle of the cross section (CK1, CM2) or with stirrups (CM1).

According to Figure 2.15a, the failure load of the prisms of BM1 (loaded perpendicular to the casting direction) shows no significant reduction in case of elements with transverse reinforcement. In addition, it remains constant regardless of the concrete cover variation, both for the prisms located in the top and bottom part of the beam. However, the concrete cover seems to influence the failure mechanisms of the investigated specimens, with low concrete covers associated to spalling failures of the cover and large covers associated to crushing of the prisms.

With respect to series CK1 and CM2 (loaded parallel to the casting direction, see Figure 2.15b), the specimens containing transverse bars were characterized by a splitting failure mode. For elements in the top and middle parts, the presence of transverse bars was clearly associated to a reduction of the compressive resistance.

For the columns with stirrups (series CM1, loaded parallel to the casting direction), an initiation of spalling of the concrete cover was observed before the maximum failure load was attained. After such spalling, an increase on the load was still possible until crushing of the core. The out-of-plane displacement related to spalling was measured with DIC and is depicted in Figure 2.16b for a representative specimen (displacement along the plane defined by the dashed white line in Figure 2.16a). With this respect, the progression of spalling can be favoured by the presence of voids under the bars (refer to Figure 2.14) in addition to other potential effects [56], [57].

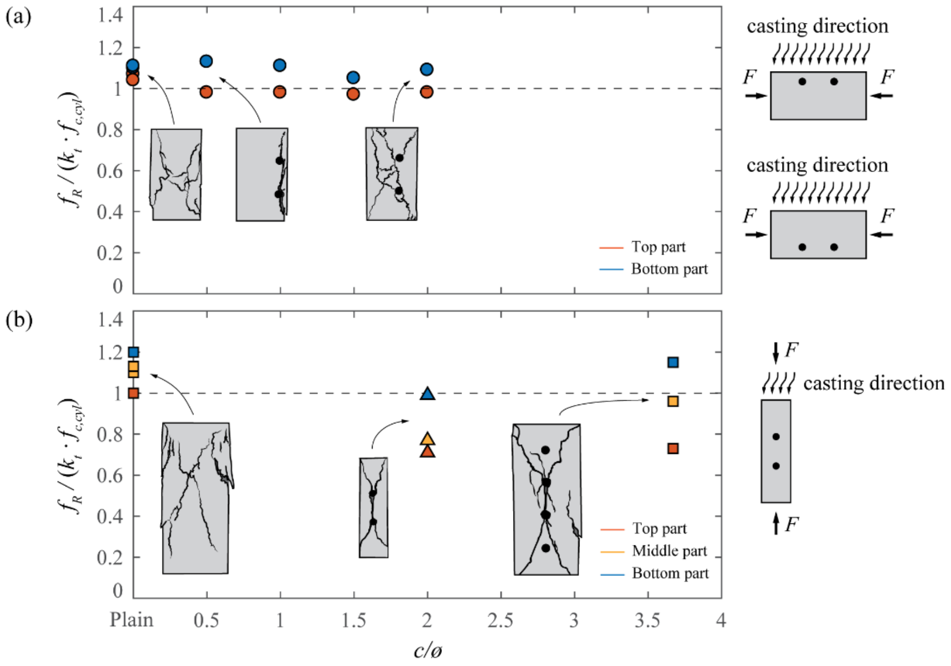

Figure 2.15: Influence of the ratio between concrete cover and bar diameter on the compressive resistance: (a) series BM1 (rapid loading conditions, k_t = 1.0); and (b) series CK1 (30 minutes of loading before failure, k_t = 0.96) and CM2 (rapid loading, k_t = 1.0).

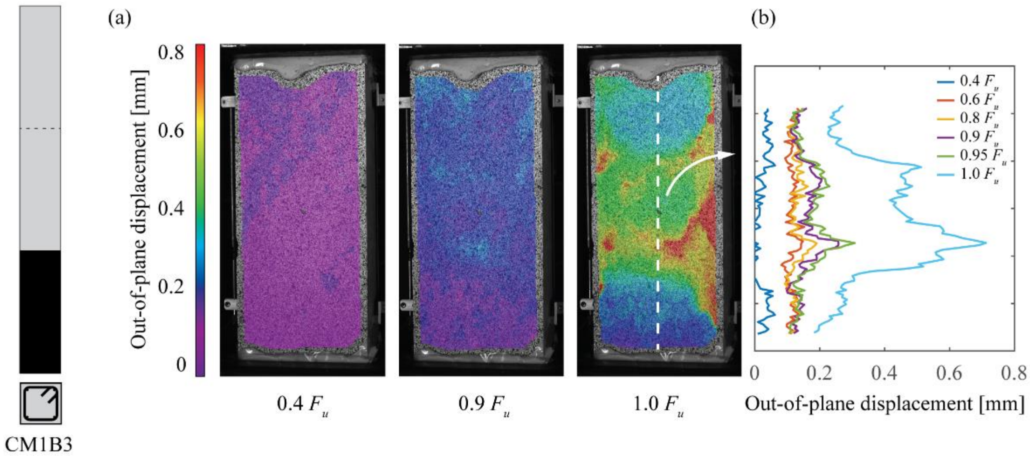

Figure 2.16: Spalling observed in test series CM1: (a) DIC measurements of the out-of-plane displacement at different load levels; and (b) out-of-plane displacement measured at the mid-section of the column.

2.6. Discussion on implications for design

As shown in the previous tests and by the review of the state-of-the-art, the casting depth and direction can potentially have an effect on the structural resistance (as also acknowledged in codes of practice, refer to Section 2.3.4). According to the tests presented in this paper, a distinction could be established between members where concrete is confined or where the propagation of cracking is controlled with respect to members without confinement or without a controlled propagation of internal cracking.

2.6.1. Members with confinement or with controlled propagation of cracking

For confined members or when the propagation of cracking is controlled by the presence of reinforcement, the influence of bleeding and plastic settlement on the structural resistance is more limited. It can be assumed that voids under coarse aggregates due to bleeding (Figure 2.1a) have similar effect as voids under bars due to settlement (Figure 2.1b). For both cases, the presence of confinement allows for a reduction of these effects. Nevertheless, a redistribution of internal forces occurs and such situation can be considered to be covered by standard design approaches of structural concrete. Suitable formulations of a strength reduction factor accounting for local stress redistributions were suggested by Muttoni [58] considering the influence of concrete brittleness (with more severe reductions associated to higher brittleness). Such approach is currently acknowledged in codes of practice for shear in members with stirrups or for design with stress fields [48], by reducing the compressive strength of concrete by means of a coefficient (η_{cc}) in the following form:

$$\eta_{cc} = \left(\frac{30}{f_c}\right)^{1/3} \leq 1 \tag{2.1}$$

In the tests presented in this paper, the behaviour of columns confined with hoop reinforcement corresponds typically to series CM1 (refer to Figure 2.11c), where hoops and longitudinal bars were arranged. This allowed for the combined response of the various load-carrying mechanisms (the unconfined concrete cover, the confined concrete core and the longitudinal bars, see Figure 2.17) with controlled stress redistributions potentially occurring between them.

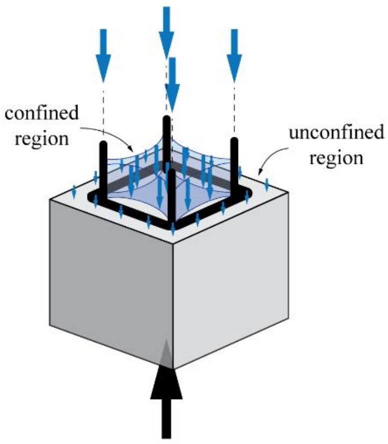

Figure 2.17: Idealized response for a column with hoops.

The structural resistance can in this case be determined in the following manner (where the concrete compressive strength is reduced by the strength reduction factor accounting for its brittleness):

$$N_{calc} = \eta_{cc} \cdot k_t \cdot f_{c,cyl} \cdot A_c + f_y \cdot A_s \tag{2.2}$$

where factor k_t, as previously discussed, accounts for the difference of test duration compared to the control specimens [42]. More refined estimates can also be obtained when considering the confinement provided by the stirrups. For instance, by considering the guidelines of *fib* MC2010 [48] for confined concrete, the compressive resistance results:

$$N_{calc} = \eta_{cc} \cdot k_t \cdot f_{c,cyl} \cdot A_c + 3.5 \cdot \left(k_t \cdot f_{c,cyl}\right)^{1/4} \cdot \sigma_2^{\ 3/4} \cdot A_{cs} + f_y \cdot A_s \tag{2.3}$$

where σ_2 is the effective lateral compressive stress due to confinement and A_{cs} is the concrete area within the confinement reinforcement (defined at the centreline of the external hoop).

The strength estimates of series CM1 (considering a value k_t = 0.96 as previously discussed) are summarized in Table 2.8 for the two approaches (with and without confinement). Consistent estimates of the resistance are obtained in both cases (slightly better when confinement stresses are accounted for), irrespective of the position of the specimen in the member.

Table 2.8: Comparison between measured and calculated failure load of series CM1 without consideration of confinement (Eq. (2.2)) and with consideration of confinement (Eq. (2.3)).

Specimen	N_R / N_{calc}	
	Eq. (2.2)	**Eq. (2.3)**
CM1A0	1.06	1.04
CM1A2	1.13	1.11
CM1B0	1.09	1.07
CM1B1	1.08	1.06
CM1B2	1.20	1.17
CM1B3	1.16	1.13
CM1C0	1.12	1.09
CM1C1	1.16	1.13
CM1C2	1.26	1.23
CM1C3	1.15	1.12
Average	**1.14**	**1.11**
CoV	**0.05**	**0.05**

2.6.2. Unconfined members or without controlled propagation of cracking

In the case of unconfined members or without a controlled propagation of internal cracking, the effects of bleeding and plastic settlement can be more severe. This is justified by the fact that splitting forces originated by the voids under the bars due to settlement (see Figure 2.12a) and voids under coarse aggregates due to bleeding yield potentially to the development of cracks parallel to the loading direction at early loading stages (Figure 2.12b). In this case, the lack of capacity to control the opening of the crack limits the potential redistribution of internal stresses and thus the resistance of the member, which depends upon the significance of the defects originated by bleeding and plastic settlement. This effect can for instance be clearly observed in the unconfined specimens tested in series CK1 and CM2 (refer to Figure 2.11a,d).

The complete consideration of the phenomenon implies in principle accounting for the casting position (effect of bleeding) as well as for an additional strength reduction factor considering the disturbance induced by the bars amplified by the effect of settlement (in a similar manner to those used when post-tensioning ducts are present in concrete panels and webs [40][59]). This is the case in practice for walls without confinement reinforcement loaded in compression (see Figure 2.18).

With respect to the influence of concrete bleeding on the compressive resistance of plain concrete, a reduction of the concrete strength at the top region shall be considered in unconfined situations. This can be performed by means of a specific strength reduction factor (η_{is}) accounting for the casting position. For such factor, and as discussed in Section 2.3.4, design approaches usually suggest values between 0.85 and 0.90 (refer to Table 2.1). In the following, a value η_{is} = 0.90 will be adopted, reasonably covering the average of available test results (see Figure 2.3).

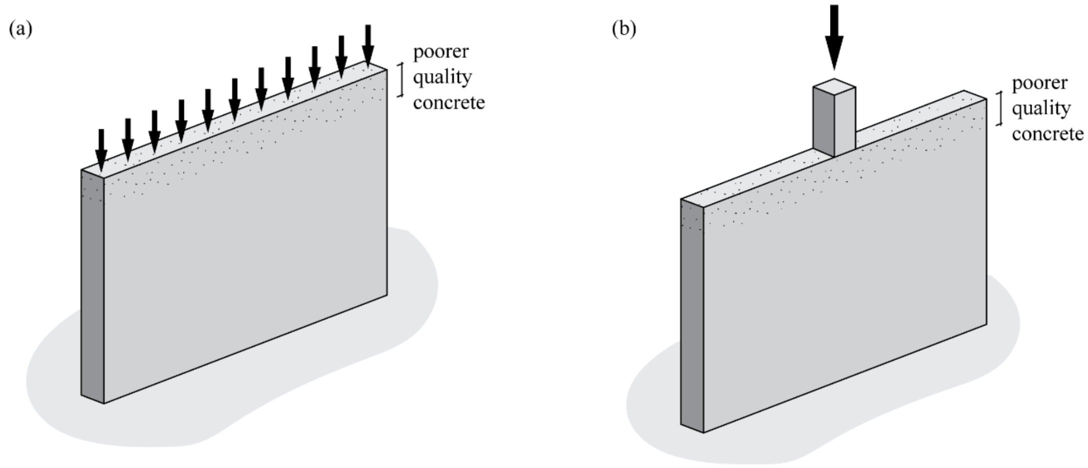

Figure 2.18: Instances of walls without transversal or confinement reinforcement: (a) subjected to linear loading; and (b) subjected to concentrated loading.

With respect to the influence of reinforcement (or ducts), specific strength reduction factors are usually adopted to account for their disturbance after concrete hardening. For instance, as suggested in codes of practice [43], [48] (see also [40]), this can be performed by considering a strength reduction factor in the following manner:

$$\begin{aligned} &\eta_D = 1 - k \cdot \sum \frac{ø}{t} \quad \text{for} \quad \frac{ø}{t} \geq \frac{1}{8} \\ &\eta_D = 1 \ \ \text{otherwise} \end{aligned} \tag{2.4}$$

where k is a diameter-correction factor, $ø$ is the duct diameter and t is the thickness of the member. A typical value of parameter k in grouted ducts is k = 0.5, while for empty ducts a value k = 1.2 is usually adopted [43], [48]. It shall be noted that this formulation of factor η_D [43], [48] does not account explicitly for the brittleness of concrete, although this phenomenon shall theoretically have an influence on the response of the member (capacity to redistribute internal stresses) and more refined approaches could be applied when determining this parameter [59]. Also, when control of the propagation of the splitting crack is provided (by means for instance of transverse reinforcement), this effect can be neglected (η_D = 1) as provisioned in codes of practice [43].

In the present case, voids can be present under the bar (Figure 2.12a) as it happens also for ducts. The response is consequently assumed to be similar to that of an injected duct and a value k = 0.5 will be adopted in the following. On the other hand, when voids are located laterally to the bar (due to different casting and loading directions, refer to Figure 2.12d), a lower disturbance can be considered and a value k = 0 will be adopted hereafter. It can be noted that, for practical cases, this reduction of the strength can be neglected (values $ø$ / t < 1/8 for most reinforced concrete members) except when very large bar diameters or ducts are used.

Accounting for both effects, the compressive resistance of members with limited or no stress redistribution capacity can thus be calculated as follows:

$$N_{calc} = \eta_{is} \cdot \eta_D \cdot k_t \cdot f_{c,cyl} \cdot A_c \tag{2.5}$$

where η_D = 1.0 for plain specimens and η_{is} = 0.90 is applied only for specimens extracted from the top layer of concrete. With respect to Equation (2.5), the disturbance due to the presence of bars is considered to be uncoupled from the effect of the casting position (η_{is}). This is justified by the fact that strength reductions due to the disturbance induced by bars occurs even at high distances from the surface or for panels with a casting direction perpendicular to the direction of loading [40].

The results of such approach are presented in Table 2.9 and show again very consistent agreement with reasonable scatter. For the strength calculation of series BM1, due to the small height of the element (300 mm), the negative effects of bleeding are considered negligible (similar as control specimens) and the η_{is} factor is set to 1.0.

Table 2.9: Comparison between measured and calculated failure load of series CK1, CM2 and BM1.

Specimen	η_{is}	η_D	k_t	N_R / N_{calc}	Specimen	η_{is}	η_D	k_t	N_R / N_{calc}
CK1A0	1.00	1.00	0.96	1.03	CM22.2	1.00	0.90	1.00	0.95
CK1A1	0.90	1.00	0.96	1.11	CM23.1	1.00	0.90	1.00	1.11
CK1A2	1.00	1.00	0.96	1.10	CM23.2	1.00	0.90	1.00	1.08
CK1A3	1.00	1.00	0.96	1.13	BM1A1.1	1.00	1.00	1.00	1.07
CK1A4	1.00	1.00	0.96	1.20	BM1A1.2	1.00	1.00	1.00	1.04
CK1B1	0.90	1.00	0.96	0.81	BM1A2.1	1.00	1.00	1.00	1.10
CK1B3	1.00	1.00	0.96	0.96	BM1A2.2	1.00	1.00	1.00	1.11
CK1B4	1.00	1.00	0.96	1.15	BM1B1	1.00	1.00	1.00	0.98
CK1C1	0.90	1.00	0.96	0.77	BM1B2	1.00	1.00	1.00	1.13
CK1C2	1.00	1.00	0.96	0.89	BM1C1	1.00	1.00	1.00	0.98
CK1C3	1.00	1.00	0.96	1.07	BM1C2	1.00	1.00	1.00	1.11
CK1C4	1.00	1.00	0.96	1.18	BM1D1	1.00	1.00	1.00	0.97
CM21.1	0.90	0.90	1.00	0.81	BM1D2	1.00	1.00	1.00	1.05
CM21.2	0.90	0.90	1.00	0.93	BM1E1	1.00	1.00	1.00	0.98
CM22.1	1.00	0.90	1.00	0.76	BM1E2	1.00	1.00	1.00	1.09
		Average					**1.02**		
		CoV					**0.12**		

Figure 2.19 plots the ratio between measured and calculated resistance for all investigated specimens in this paper (with and without confinement reinforcement). The analyses show consistent agreement for the range of investigated concrete compressive strengths, with an average of 1.05 and a coefficient of variation of 0.11 for all specimens. In case the effect of the strength reduction factors η_{cc}, η_{is}, η_D and k_t were ignored, the results would worsen, with an average of measured-to-predicted strength 0.99 and a coefficient of variation of 0.14 (significantly more scattered than previously). These results are promising, but future research is required to confirm their validity beyond the investigated range of compressive strengths (particularly for high-strength concrete).

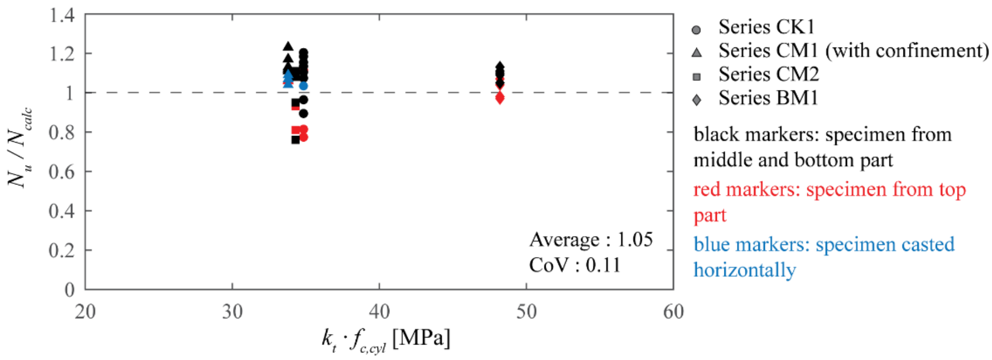

Figure 2.19: Proposed approach: ratio between measured failure load and axial load as function of the concrete compressive strength.

2.7. Conclusions

This paper presents the results of an investigation on the concrete compressive strength in structural members. The influence of the casting position, the loading direction with respect to the casting direction and the disturbance of transverse reinforcement are investigated by means of an experimental programme instrumented with refined measurements. The main findings of the paper are the following:

1. Tomography measurements confirm that plastic settlement of fresh concrete potentially leads to continuous voids under the reinforcement. This phenomenon is observed to be dependent on the distance of the bar both to the casting surface and to the closest vertical disturbances under the bar.

2. DIC measurements of concrete settlement in the first hours after casting show that this phenomenon can reach significant values (up to ~ 3 mm/m have been measured). The influence of the concrete cover is also observed to be relevant and influencing surface cracking along the reinforcement bars.

3. The experimental results performed confirm the dependence of the in-situ concrete strength on the distance to the casting surface in cases of plain concrete or for concrete with transversal bars not acting as confinement reinforcement. The loading direction with respect to the casting direction influences in this case the compressive resistance of the member as it governs the location of voids (formed due to plastic settlement under the reinforcement) with respect to the loading direction. Varying the concrete cover of the transverse reinforcement influences the failure mechanism (spalling or crushing) but it does not seem to influence the failure load.

4. The experiments show that the negative impact related to casting position and casting direction is virtually negligible when a confinement reinforcement is provided. The effects due to bleeding and plastic settlement seem to be compensated by the favourable action of stirrups or ties (due to the control of splitting cracks initiated by stress disturbances associated to the presence of voids under reinforcement bars).

5. For members without confinement reinforcement or when no control of internal cracking is provided, the effects of concrete bleeding and plastic settlements under the reinforcement are clearly perceptible in terms of member resistance. In this case, lower resistances are associated to locations closer to the top casting surface. A consistent design in such cases shall account for specific considerations of both effects (casting position and presence of reinforcement). For elements located in the top region, considering a strength reduction factor with a value 0.90

(consistently with those suggested in codes of practice) seems in agreement with the test results available in the scientific literature as well as with the specimens presented in this paper. When large reinforcement bars or large disturbances in the form of ducts are also present, specific strength reduction factors (as those usually considered in codes of practice) shall additionally be accounted for in the calculation of the resistance of the member.

2.8. References

[1] EN 12390-3:2019, "Testing hardened concrete - Part 3: Compressive strength of test specimens," European Committee for Standardization (CEN), Brussels, Belgium, 20 p., 2019.

[2] G. Koenig, D. Soukhov, and F. Jungwirth, "Safe concrete production for reinforced concrete strutures (in German: Sichere Betonproduktion für Stahlbetontragwerke)," Leipzig, 41 p., 1998.

[3] F. M. Bartlett and J. G. MacGregor, "Variation of In-Place Concrete Strength in Structures," *ACI Materials Journal*, vol. 96, no. 2, pp. 261–270, 1999.

[4] W. K. Tso and I. M. Zelman, "Concrete Strength Variation in Actual Structures," *ACI Journal Proceedings*, vol. 67, no. 12, pp. 981–988, 1970.

[5] N. Petersons, "Strength of concrete in finished structures," Transactions of the royal Institute of Technology, Stockholm, Sweden, 189 p., 1964.

[6] R. L. Yuan, M. Ragab, R. E. Hill, and J. E. Cook, "Evaluation of Core Strength in High-Strength Concrete," *Concrete International*, vol. 13, no. 5, pp. 30–34, 1991.

[7] T. C. Powers, "The properties of fresh concrete," John Wiley & Sons, Incorporated, Hoboken, NJ, United States, 664 p., 1968.

[8] C. A. Clear and D. G. Bonner, "Settlement of fresh concrete—an effective stress model," *Magazine of Concrete Research*, vol. 40, no. 142, pp. 3–12, 1988.

[9] L. Josserand, O. Coussy, and F. de Larrard, "Bleeding of concrete as an ageing consolidation process," *Cement and Concrete Research*, vol. 36, no. 9, pp. 1603–1608, 2006.

[10] H. J. Yim, J. H. Kim, H. G. Kwak, and J. K. Kim, "Evaluation of internal bleeding in concrete using a self-weight bleeding test," *Cement and Concrete Research*, vol. 53, pp. 18–24, 2013.

[11] G. Giaccio and A. Giovambattista, "Bleeding: Evaluation of its effects on concrete behaviour," *Materials and Structures*, vol. 19, no. 4, pp. 265–271, 1986.

[12] ASTM International, "C232/C232M-14 (2019) Standard Test Methods for Bleeding of Concrete." West Conshohocken, PA, 2019.

[13] T. S. Tan, T. H. Wee, S. A. Tan, C. T. Tam, and S. L. Lee, "A consolidation model for bleeding of cement paste," *Advances in cement research*, vol. 1, no. 1, pp. 18–26, 1987.

[14] A. Castel, T. Vidal, K. Viriyametanont, and R. François, "Effect of reinforcing bar orientation and location on bond with self-consolidating concrete," *ACI Structural Journal*, vol. 103, no. 4, pp. 559–567, 2006.

[15] R. Combrinck, L. Steyl, and W. P. Boshoff, "Interaction between settlement and shrinkage cracking in plastic concrete," *Construction and Building Materials*, vol. 185, pp. 1–11, 2018.

[16] R. E. Weyers, J. C. Conway, and P. D. Cady, "Photoelastic analysis of rigid inclusions in fresh concrete," *Cement and Concrete Research*, vol. 12, no. 4, pp. 475–484, 1982.

[17] P. Ghoddousi and A. A. S. Javid, "Effect of reinforcement on plastic shrinkage and settlement of self-consolidating concrete as repair material," *Materials and Structures*, vol. 45, no. 1–2, pp. 41–52, 2012.

[18] O. Berndt and E. Preuss, “Tests on the comparison between concrete compressive strength of cube specimens and obtained in-situ strength (in German: Versuche zum Vergleich der Würfeldruckfestigkeit des Betons zu der im Bauwerk erzielten Festigkeit),” Deutscher Ausschuss für Eisenbeton, vol. 36, 55 p., 1915.

[19] W. A. Slater and I. Lyse, “Second Progress Report On Column Tests Made At Lehigh University,” *Journal of the American Concrete Institute - Proceedings*, vol. 27, no. 3, pp. 791–835, 1931.

[20] J. G. Sanjayan and B. Sioulas, “Strength of Slag-Cement Concrete Cured in Place and in Other Conditions,” *ACI Materials Journal*, vol. 97, no. 5, pp. 603–611, 2000.

[21] ACI Committee 318, “Building Code Requirements for Structural Concrete (ACI 318-19) and Commentary,” American Concrete Institute, Farmington Hills, USA, 624 p., 2019.

[22] O. Graf, “Tests with Reinforced Concrete Columns (in German: Versuche mit Eisenbetonsäulen),” Deutscher Ausschuss für Eisenbeton, vol. 77, 67 p., 1934.

[23] W. R. Crawford and J. F. Fry, “The Strength of Plain Concrete Columns,” *Concrete and Constructional Engineering*, vol. 34, no. 8, pp. 443–449, 1939.

[24] B. M. F. Kaplan, “Compressive Strength and Ultrasonic Pulse Velocity Relationships for Concrete in Columns,” *Journal of the ACI*, vol. 29, no. 8, pp. 675–688, 1958.

[25] F. M. Bartlett and J. G. MacGregor, “Effect of Core Diameter on Concrete Core Strengths,” *ACI Materials Journal*, vol. 91, no. 5, pp. 460–469, 1994.

[26] M. Kanda and H. Yoshida, “The distributing condition of water-cement ratio in the member section after concrete placing,” *RILEM Symposium on Quality Control of Concrete Structures*, pp. 85–92, 1979.

[27] B. Miao, P.-C. Aitcin, W. D. Cook, and D. Mitchell, “Influence of Concrete Strength on In Situ Properties of Large Columns,” *ACI Materials Journal*, vol. 90, no. 3, pp. 214–219, 1993.

[28] K. H. Khayat, P. Paultre, and S. Tremblay, “Structural performance and in-place properties of self-consolidating concrete used for casting highly reinforced columns,” *ACI Materials Journal*, vol. 98, no. 5, pp. 371–378, 2001.

[29] W. Zhu, J. C. Gibbs, and P. J. M. Bartos, “Uniformity of in situ properties of self-compacting concrete in full-scale structural elements,” *Cement and Concrete Composites*, vol. 23, no. 1, pp. 57–64, 2001.

[30] H. Takahashi and S. Nakane, “Strength of Concrete in Structures and Factors Contributiong to Strength Differentials,” *RILEM Symposium on Quality Control of Concrete Structures*, pp. 183–190, 1979.

[31] C. K. Loh, T. S. Tan, K. Y. Yong, and T. H. Wee, “An experimental study on bleeding and channelling of cement paste and mortar,” *Advances in Cement Research*, vol. 10, no. 1, pp. 1–16, 1998.

[32] L. Josserand, “Bleeding of concrete (in French: Ressuage des bétons hydrauliques),” PhD thesis of l’Ecole Nationale des Ponts et Chaussées, 210 p., 2002.

[33] M. M. Ranjbar, M. H. Beygi, I. M. Nikbin, M. Rezvani, and A. Barari, “Evaluation of the strength variation of normal and lightweight self-compacting concrete in full scale walls,” *Materiali in Tehnologije*, vol. 45, no. 6, pp. 571–577, 2011.

[34] S. L. Mak, M. M. Attard, D. W. S. Ho, and P. L. P. Darvall, “Cross-sectional strength gradients in high strength concrete columns,” *Cement and Concrete Research*, vol. 24, no. 1, pp. 139–149, 1994.

[35] R. D. Gaynor, “Effect of Horizontal Reinforcing Steel on the Strength of Molded Cylinders,”

Journal of the American Concrete Institute, vol. 62, no. 7, pp. 837–840, 1965.

[36] J. M. Plowman, W. F. Smith, and T. Sherriff, “Cores, cubes and the specified strength of concrete,” *Struct. Eng*, vol. 52, no. 11, pp. 421–426, 1974.

[37] Y. H. Loo, C. W. Tan, and C. T. Tam, “Effects of embedded reinforcement on measured strength of concrete cylinders,” *Magazine of Concrete Research*, vol. 41, no. 146, pp. 11–18, 1989.

[38] H.-B. Ko, “Effect of the Embedded Reinforcing Bar of Specimens on the Compressive Strength of Concrete,” *Journal of the Korea Academia-Industrial cooperation Society*, vol. 17, no. 9, pp. 552–558, 2016.

[39] F. Leonhardt, “Abminderung der Tragfähigkeit des Betons infolge stabförminger, rechtwinklig zur Druckrichtung angeordneter Einlagen,” *Festschrift Rüsch*, pp. 71–78, 1969.

[40] A. Muttoni, O. L. Burdet, and E. Hars, “Effect of Duct Type on Shear Strength of Thin Webs,” *ACI Structural Journal*, vol. 103, no. 5, pp. 729–735, 2006.

[41] D. M. Wald, “Experimental Investigation of Crushing Capacity of I-Girder Webs Containing Post-Tensioning Ducts,” The University of Texas at Austin, USA, 228p., 2012.

[42] D. Tasevski, M. Fernández Ruiz, and A. Muttoni, “Assessing the compressive strength of concrete under sustained actions: From refined models to simple design expressions,” *Structural Concrete*, vol. 20, no. 3, pp. 971–985, 2019.

[43] EN 1992-1-1:2004, “Eurocode 2: Design of Concrete Structures - Part 1: General Rules and Rules for Buildings,” European Committee for Standardization (CEN), Brussels, Belgium, 225 p., 2004.

[44] European Concrete Platform, “Eurocode 2 Commentary,” European Committee for Standardization (CEN), Brussels, Belgium, 168 p., 2008.

[45] Standards Australia, “AS 3600:2018 : Concrete Structures,” Standards Australia Limited, Sydney, Australia, 264 p., 2018.

[46] S. J. Foster, “Personal communication.” 2018.

[47] GB 50010-2010, “Code for Design of Concrete Structures,” Ministry of Housing and Urban-Rural Development of the People’s Republic of China, Beijing, 427 p., 2010.

[48] International Federation for Structural Concrete, “fib Model Code for Concrete Structures 2010,” Ernst & Sohn, Berlin, Germany, 434 p., 2013.

[49] EN 197-1:2011, “Cement - Part 1: Composition, specifications and conformity criteria for common cements,” European Committee for Standardization (CEN), Brussels, Belgium, 38 p., 2011.

[50] EN 206+A1:2016-11, “Concrete - Specification, performance, production and conformity,” European Committee for Standardization (CEN), Brussels, Belgium, 102 p., 2016.

[51] EN 12350-2:2019, “Testing fresh concrete - Part 2: Slump test,” European Committee for Standardization (CEN), Brussels, Belgium, 8 p., 2019.

[52] EN 12350-5:2019, “Testing fresh concrete - Part 5: Flow table test,” European Committee for Standardization (CEN), Brussels, Belgium, 12 p., 2019.

[53] EN 13670:2013, “Execution of concrete structures,” European Committee for Standardization (CEN), Brussels, Belgium, 66 p., 2013.

[54] EN ISO 6892-1:2016, “Metallic materials - Tensile testing - Part 1: Method of test at room temperature,” European Committee for Standardization (CEN), Brussels, Belgium, 79 p., 2016.

[55] Correlated Solutions, “VIC-3D Digital Image Correlation.” Copyright 1998-2018 Correlated Solutions, Inc.

[56] S. J. Foster, J. Liu, and S. A. Sheikh, "Cover Spalling in HSC Columns Loaded in Concentric Compression," *Journal of Structural Engineering*, vol. 124, no. 12, pp. 1431–1437, 1998.

[57] S. J. Foster, "On Behavior of High-Strength Concrete Columns : Cover Spalling, Steel Fibers, and Ductility," *ACI Structural Journal*, vol. 98, no. 4, pp. 583–589, 2001.

[58] A. Muttoni, "The applicability of the theory of plasticity in the design of reinforced concrete ('Die Andwendbarkeit der Plastizitätstheorie in der Bemessung von Stahlbeton')," PhD thesis, ETH, Zürich, 164 p., 1990.

[59] E. Hars, "Zum Querkraftwiderstand von Stahl- und Spannbetonträgern mit dünnen Stegen," PhD Thesis, EPFL, Lausanne, Switzerland, 303 p., 2006.

2.9. Annexes

2.9.1. Annex A: Failure modes

Figure 2.20 illustrates the typical failure modes observed during the experimental programme for some representative specimens.

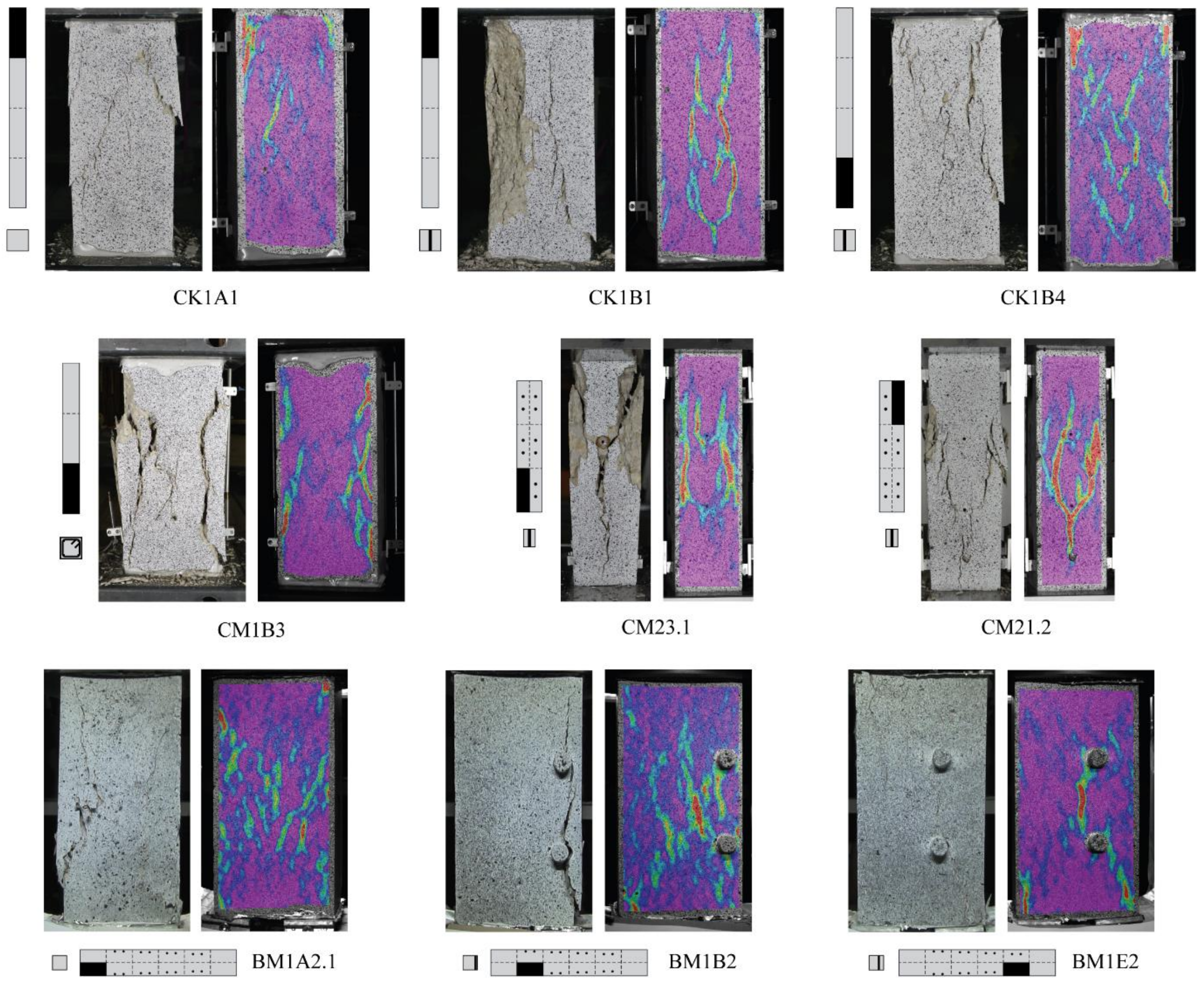

Figure 2.20: Photos of typical failure modes for some representative specimens and principal strains measured with DIC.

Series CK1 was influenced by the reinforcement layout as well as by the casting location of the elements, with failures characterized by formation of inclined failure surfaces in the case of plain specimens. For columns with transverse reinforcement, failures were characterized by a splitting failure crack developing along the plane of the bars, with cracks originated in the regions with larger voids under the bars.

With respect to members with closed stirrups (series CM1), the same failure pattern was consistently observed for the entire test series despite their different transverse reinforcement layout, casting position and casting direction. Failure was characterized by the spalling of the concrete cover prior to failure, followed by the crushing of the core.

For the specimens obtained from beam BM1, failure was influenced by the presence and position of the transverse reinforcement (Figure 2.20). Plain prisms (BM1A) were characterized by inclined failure planes. Prisms containing transverse bars presented two different modes of failure: spalling of the concrete cover in the case of small concrete covers (as for BM1B and BM1C) or inclined failure surfaces for larger covers (as for BM1D and BM1E).

2.9.2. Annex B: Stress-strain responses

The stress-strain curves for most of the specimens are presented in Figure 2.21. The results are given in terms of longitudinal stresses versus the longitudinal and transversal strains. The longitudinal strains are determined from the LVDTs measurements, while the transverse strains are derived from the DIC measurements. The lengths used for the calculation of strains are summarized in Table 2.10.

Table 2.10: Lengths for the calculation of average strains.

Test series	Measurement length [mm]	
	Longitudinal	Transverse
CK1	470	200
CM1	470	200
CM2	280	65
BM2	240	125

For the plain specimens of series CK1 (Figure 2.21a), the deformation capacity in the longitudinal and transverse direction is comparable independently of the casting position. However, when transverse bars are present in the cross section (Figure 2.21b-c), the decrease of failure load with increasing height is accompanied by a gradual increase of the transverse strains indicating a tougher response (particularly for series C, where transverse reinforcement bars can partly serve as confinement reinforcement). The specimens with stirrups (series CM1, Figure 2.21d-f) present overall similar stress-strain response despite the different casting positions, casting direction and stirrup diameter.

With respect to test series CM2, the stress-strain response is remarkably different according to the casting position of the specimens (Figure 2.21i). Bottom prisms exhibit a stiffer and more brittle response (explosive at failure) compared to top and middle prisms, which show a reduction of stiffness already at low levels of stresses and a less brittle response. This is probably a sign that local concrete crushing under the bars and closing of the voids due to plastic settlement take place even at low load levels and allows dissipating a fraction of the introduced energy. Two prisms of this series, located on top and on bottom of the column, are further investigated in detail in Figure 2.21g-h. Their transverse strains obtained from DIC are plotted at the level of the two transverse bars. In the bottom prism (Figure 2.21g), the increase of transverse strains at the top bar indicates that the splitting crack developed first in this region. Once the crack progresses and connects with the crack at the bottom bar, the general stiffness of the specimen drops dramatically leading to failure. Interestingly, the opposite crack development was observed for top and middle prisms.

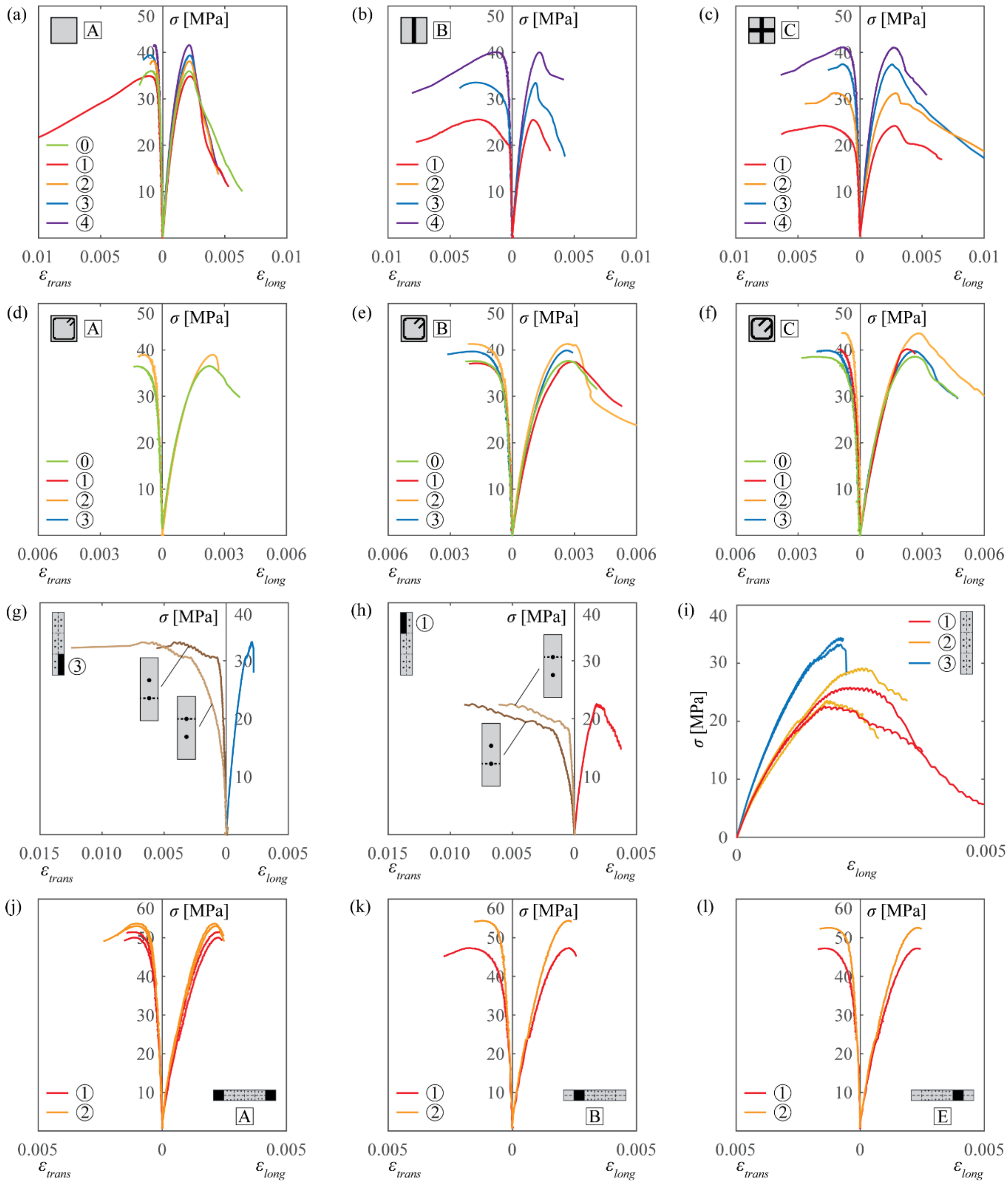

Figure 2.21: Stress-strain relationships of the investigated test series: (a) series CK1A; (b) series CK1B; (c) series CK1C; (d) series CM1A; (e) series CM1B; (f) series CM1C; (g) specimen CM23.1; (h) specimen CM21.1; (i) series CM2; (j) series BM1A; (k) series BM1B; and (l) series BM1E.

Plain prisms of series BM1 (Figure 2.21j) present comparable stress-strain responses, with larger failure loads for the bottom prisms but associated to a more brittle response. Prisms containing transverse bars (Figure 2.21k-l) exhibit a clear difference in the failure load according to their casting positions.

Additionally, it seems that prisms located on the top part of the beam and characterized by small concrete covers (for instance prism B, see Figure 2.21k) exhibit larger transverse strains at failure compared to the corresponding bottom prisms. This behaviour was however not observed for prisms with larger concrete covers (refer to prism E, see Figure 2.21l).

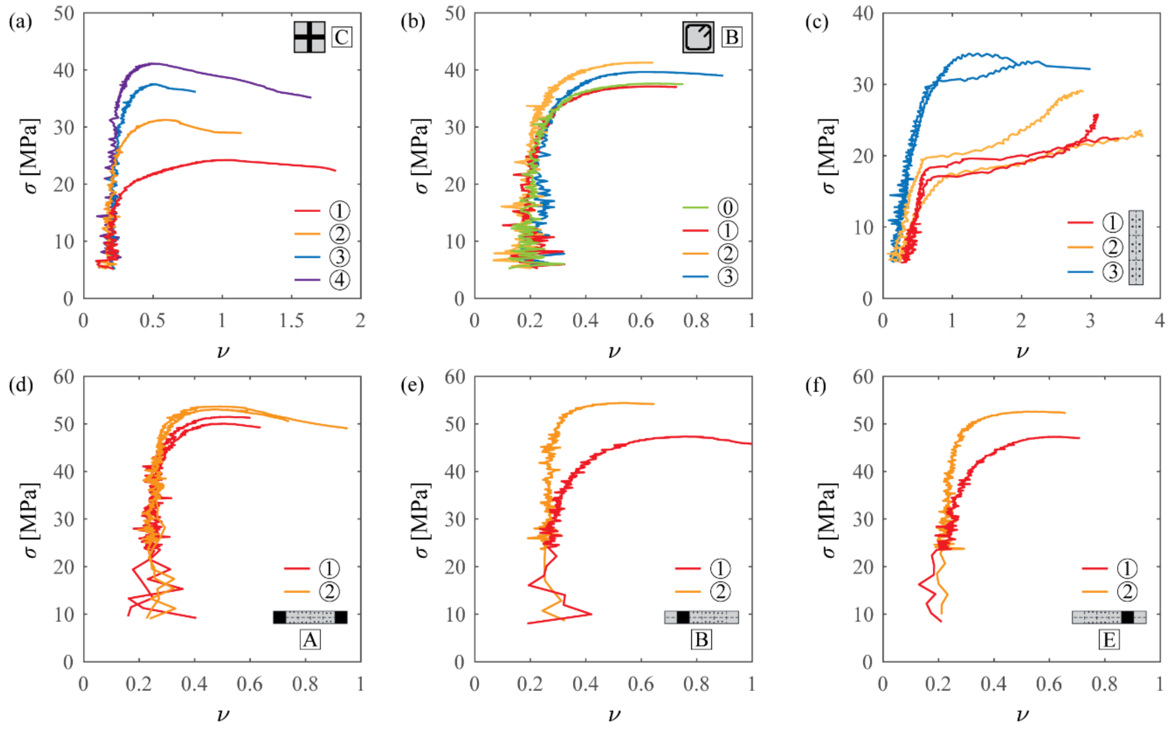

Figure 2.22: Poisson's ratio of some investigated elements: (a) series CK1C; (b) series CM1B; (c) series CM2; (d) series BM1A; (e) series BM1B; and (f) series BM1E.

A detailed investigation of the apparent Poisson's coefficient (calculated as $\nu = - \varepsilon_{trans} / \varepsilon_{long}$) is shown in Figure 2.22 for some selected specimens. It can be noted that, during the first loading stages, all specimens show consistently a value comparable to that of undisturbed concrete ($\nu \approx 0.2$). At maximum load, however, the apparent Poisson's coefficient varies according to the investigated series. In series CK1 (Figure 2.22a) the specimens containing transverse bars (for instance cross section C) experienced a relative increase of the Poisson's coefficient with decreasing distance from the upper surface. This indicates that, with such reinforcement configuration, the casting position not only affects the failure load but also the transverse expansion. On the contrary, test series CM1 (Figure 2.22b) shows at failure a roughly constant apparent Poisson's coefficient ($\nu \approx 0.5$) regardless of the casting direction and stirrup layout. With respect to series CM2 (Figure 2.22c), similar comments to series CK1 can be made. The plain prisms of series BM1 (Figure 2.22d) as well as the prisms with large concrete covers (for instance prisms E, Figure 2.22f) exhibit at failure a Poisson's coefficient of $\nu \approx 0.5$. However, for low concrete covers in this series (prisms B for example, Figure 2.22e), the top prisms experienced a relatively larger expansion compared to the corresponding bottom prisms, indicating that the casting direction plays a role in this parameter.

2.9.3. Annex C: Effect of disturbances on the resistance of concrete

This annex presents a preliminary experimental programme carried out on concrete prisms that was not published in the paper "The influence of casting position and disturbance induced by reinforcement on the structural concrete strength". The aim of this study was to investigate the influence on the compressive resistance of placing embedded steel bars perpendicular to the loading direction. The experimental programme consisted of 36 concrete prisms with varying levels of disturbances and made with normal and high-strength concrete.

2.9.3.1. Prisms specimens

Three series of prisms were tested comprising a total of 36 specimens. The dimensions of the prisms were selected in order to have a longitudinal direction (parallel to the loading direction) of 2÷3.5 times the minimum transversal dimension. This allowed avoiding confinement effects by the load introduction plates, to avoid potential second-order effects and to have similar dimensions as the control specimens (standard cylinders Ø160 mm with a height of 320 mm).

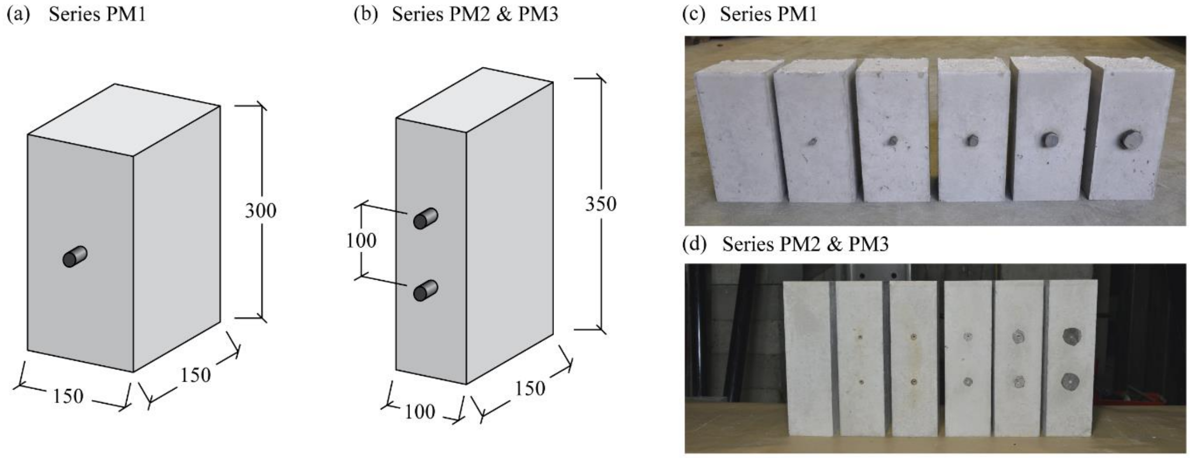

Figure 2.23: Geometry and reinforcement of the investigated specimens (dimensions in [mm]): (a) series PM1; and (b) series PM2 and PM3. Overview of the tested prisms: (c) series PM1; and (d) series PM2 and PM3.

Except for reference specimens (without embedded bars), the specimens presented one or two bars, with values of parameter δ above or below the threshold of 1/8. These bars (called in the following transverse bars) are placed perpendicular to the loading direction and in a position so that the disturbance effect is more dominant than the confinement effect. Beside the diameter of the reinforcement bars, the concrete strength was also varied, from normal strength concrete with $f_{c,cyl}$ = 45-48 MPa to high-strength concrete with $f_{c,cyl}$ = 72.3 MPa. The main characteristics of the specimens are listed below (details can be consulted in Table 2.12):

- Series PM1 (Figure 2.23a,c) consisted of 12 prisms cast vertically in normal strength concrete with the dimensions shown in Figure 2.23a. The specimens were plain or contained bars with diameter varying from 10 mm up to 40 mm. The reinforcement was fixed to the formwork during casting and no vertical nor confinement reinforcement was arranged.
- Series PM2 (Figure 2.23b,d) consisted of 14 prisms cast vertically in normal strength concrete with the dimensions shown in Figure 2.23b. The specimens were either plain or contained two transverse bars spaced 100 mm. The diameter of the bars varied from 10 mm up to 40 mm.
- Series PM3 (Figure 2.23b,d) had identical dimensions and reinforcement layout as series PM2, but was cast with high-strength concrete.

The transverse bars were cleaned before installing and placed with the ribs aligned vertically. All specimens, together with the control specimens (cylinders 160×320mm), were stored and cured in laboratory conditions at an average temperature of 22°C and average relative humidity of approximately 50%.

2.9.3.2. Material properties

The three test series were cast at different dates using ready-mix concrete from a local concrete supplier. For the normal strength concrete (series PM1 and PM2), a cement CEM II/B-M (T-LL) 42.5N was used while for the high-strength concrete (series PM3), a cement CEM I 52,5 R was used [49]. The maximum aggregate size was 16 mm in all cases. Slump and flow tests were performed to evaluate the consistency of fresh concrete, in conformity with [50]–[52]. After casting, plastic sheets were used to protect the exposed surfaces of the specimens to ensure suitable curing conditions during 14 days, in accordance with [53]. Standard compression tests (monotonic loading lasting approximately two minutes to failure) were performed on the control cylinders at 7, 14, 21, 28 days and also during the testing programme. Details on the concrete mix, results of the fresh concrete tests and of the material tests ($f_{c,cyl}$ measured at the days of prism tests) are summarized in Table 2.11.

Table 2.11: Concrete properties.

Series	*c* [kg/m³]	*W/C* [-]	Aggregates [kg/m³] 0/4	4/8	8/16	Retarder [kg/m³]	Superpl. [kg/m³]	Slump [mm]	Flow [mm]	$f_{c,cyl}$ [MPa]	CoV [%]
PM1	341	0.54	920	360	660	0.93	1.33	85 (S2)	380 (F2)	48.2	3.9
PM2	344	0.53	830	380	671	0.95	1.30	200 (S4)	515 (F4)	44.9	2.9
PM3	375	0.40	957	272	724	1.88	4.88	195 (S4)	470 (F3)	72.3	5.4

The transverse bars consisted of conventional hot-rolled ribbed bars of variable diameter and with characteristic yield strength of f_{yk} = 500 MPa. They were not tested in tension since no yielding was expected during the specimen tests.

2.9.3.3. Testing procedure and main experimental results

All prisms were tested in pure compression in a 2.5 MN hydraulic Schenck machine. The prisms were rectified before testing to ensure planar and parallel loading surfaces and were perfectly centred in the testing machine with laser pointers. In addition, a thin layer of epoxy resin was placed on the top and bottom surface of each element to allow for a uniform introduction of the load. The typical duration of the tests was 2-3 minutes, leading to similar loading rate conditions as the control specimens.

Digital Image Correlation (DIC) measurements were performed at one side of the specimens perpendicular to the reinforcing bars. Pictures were taken at a frequency of 0.5 Hz and increased to 2 Hz near failure. High-resolution cameras were used (Manta G504B, 5 Megapixels resolution) and the photos were post-processed using VIC-3D [55]. The maximum error corresponded to approximately 1/35 of a pixel (whose dimension were 217×217μm²).

The test results in terms of measured failure loads are presented in Table 2.12 for each specimen. The failure mechanisms of the specimens was observed to be influenced by the presence or absence of the disturbance as shown in Figure 2.24. For plain specimens (Figure 2.24a,c), failure was characterized by the development of an inclined failure surface. When transverse bars were arranged (Figure 2.24b,d), high strains were recorded in the vicinity of the bars already at low load levels and failure was originated by a crack developing diagonally from the location of the disturbances.

For series PM1 and PM2 (made with normal strength concrete), it was observed that the response was increasingly brittle for larger bar diameters (Figure 2.24b,d). For the prisms made of high-strength concrete (series PM3), all failures were very brittle (explosive).

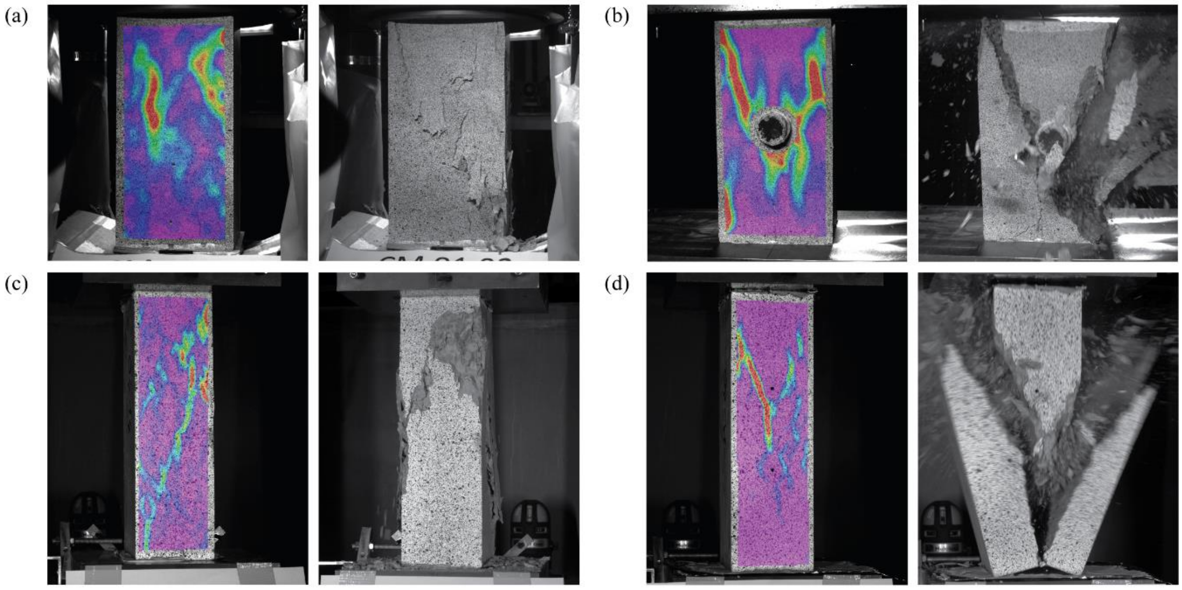

Figure 2.24: Influence of presence of transverse bars on the failure mechanism of the investigated prisms (left: principal strains measured with DIC; right: observed failure mode): (a) plain prism of series PM1; (b) prism with ø40 mm steel bar of series PM1; (c) plain prism of series PM2; and (d) prism with ø30 mm steel bar of series PM2.

2.9.3.4. Analysis of experimental results

The ratio between the structural compressive resistance (f_R, calculated by dividing the resistance N_R by the gross area of the specimen) and the concrete strength measured in standard cylinders tests ($f_{c,cyl}$) is plotted in Figure 2.25a as a function of the ratio between the diameter of the transverse bar and the thickness of the member. This ratio is also represented in Figure 2.25b as a function of the concrete cylinder compressive strength (see details in Table 2.12). For comparison purposes, tests with transverse reinforcement bars available from other experimental programmes [35], [37], [39] are also considered in the figure (for specimens by Loo et al. [37], only cylinders with a slenderness of 2.0 are considered to be comparable to the current programme). Figure 2.25a shows (in agreement to previous experimental programmes [35], [37], [39]) that the resistance of the prisms decreases with increasing diameter of the transverse bars.

The consideration of the strength reduction factor for large disturbances (η_D, Eq. (2.4) with k = 0.5) is presented in Figure 2.25c,d. The results show a better agreement. However, it can be noted that the influence of disturbances is slightly underestimated for low values of the ratio $ø / t$ (below the threshold of 1/8 which seems to be reasonable for simplifying practical verifications, but not from a theoretical point of view) and somewhat overestimated for higher ratios. Despite these trends, the results can be considered as overly acceptable. In addition, as shown in Figure 2.25d, the results show a trend with respect to the influence of $f_{c,cyl}$, with decreasing level of safety for increasing material strength. This is justified by the fact that factor η_D in Eq. (2.4) is based only on geometrical considerations and neglects the increased brittleness as well as the relative lower tensile strength of high strength concrete.

Table 2.12: Main results of the experimental programme (f_R structural resistance calculated as the applied force divided by the gross cross-section).

Specimen	ø [mm]	ø / t	$f_{c,cyl}$ [MPa]	η_D (Eq. 2.4 with k = 0.5)	f_R [MPa]	$f_R / f_{c,cyl}$	$f_R / (\eta_D \cdot f_{c,cyl})$
PM1-1	Plain	-	48.2	1.00	47.9	0.99	0.99
PM1-2	Plain	-	48.2	1.00	50.0	1.04	1.04
PM1-3	10	0.07	48.2	1.00	46.6	0.97	0.97
PM1-4	10	0.07	48.2	1.00	46.8	0.97	0.97
PM1-5	14	0.09	48.2	1.00	46.4	0.96	0.96
PM1-6	14	0.09	48.2	1.00	46.1	0.96	0.96
PM1-7	20	0.13	48.2	0.93	46.7	0.97	1.04
PM1-8	20	0.13	48.2	0.93	46.4	0.96	1.03
PM1-9	30	0.20	48.2	0.90	48.9	1.01	1.13
PM1-10	30	0.20	48.2	0.90	46.2	0.96	1.07
PM1-11	40	0.27	48.2	0.87	41.5	0.86	0.99
PM1-12	40	0.27	48.2	0.87	38.7	0.80	0.93
PM2-11	Plain	-	44.9	1.00	45.7	1.02	1.02
PM2-12	Plain	-	44.9	1.00	47.1	1.05	1.05
PM2-13	Plain	-	44.9	1.00	50.7	1.13	1.13
PM2-14	Plain	-	44.9	1.00	46.3	1.03	1.03
PM2-1	10	0.10	44.9	1.00	44.5	0.99	0.99
PM2-2	10	0.10	44.9	1.00	42.7	0.95	0.95
PM2-3	14	0.14	44.9	0.93	42.5	0.95	1.02
PM2-4	14	0.14	44.9	0.93	42.5	0.95	1.02
PM2-5	20	0.20	44.9	0.90	38.5	0.86	0.95
PM2-6	20	0.20	44.9	0.90	35.3	0.79	0.87
PM2-7	30	0.30	44.9	0.85	44.5	0.99	1.17
PM2-8	30	0.30	44.9	0.85	41.1	0.92	1.08
PM2-9	40	0.40	44.9	0.80	41.0	0.91	1.14
PM3-11	Plain	-	72.3	1.00	65.2	0.90	0.90
PM3-12	Plain	-	72.3	1.00	66.4	0.92	0.92
PM3-1	10	0.10	72.3	1.00	64.6	0.89	0.89
PM3-2	10	0.10	72.3	1.00	63.1	0.87	0.87
PM3-3	14	0.14	72.3	0.93	65.1	0.90	0.97
PM3-4	14	0.14	72.3	0.93	64.8	0.90	0.96
PM3-5	20	0.20	72.3	0.90	61.4	0.85	0.94
PM3-6	20	0.20	72.3	0.90	61.8	0.85	0.95
PM3-7	30	0.30	72.3	0.85	62.6	0.87	1.02
PM3-8	30	0.30	72.3	0.85	60.9	0.84	0.99
PM3-10	40	0.4	72.3	0.80	58.1	0.80	1.00
					Average	**0.93**	**1.00**
					(# spec.)	**(36)**	**(36)**
					CoV [%]	**8.2**	**7.2**

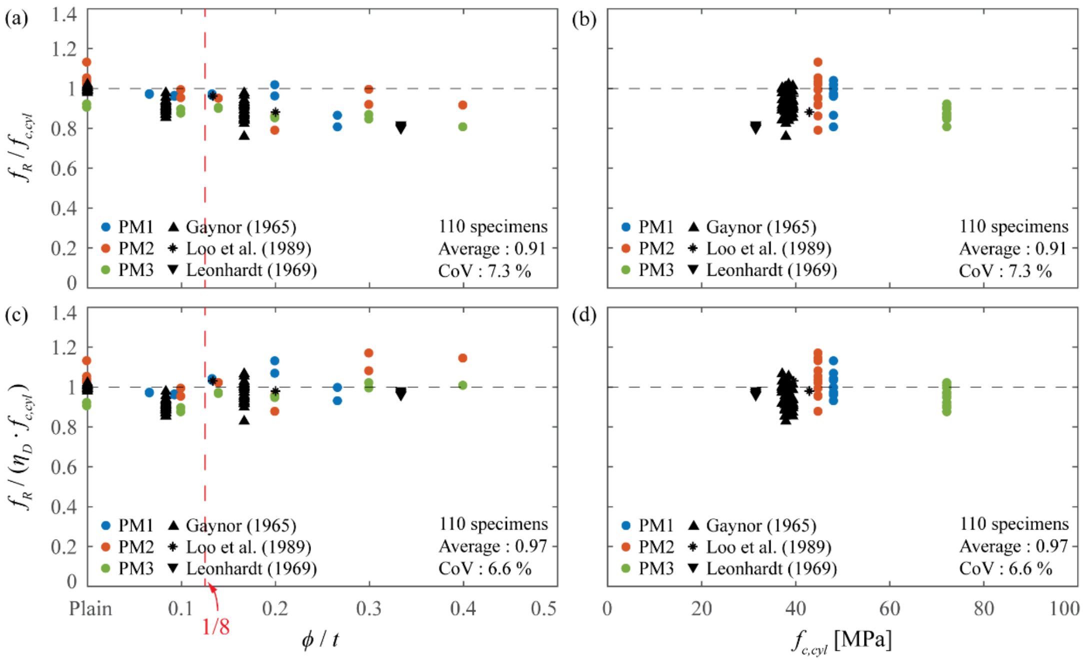

Figure 2.25: Results of the experimental programme and available tests from literature in terms of the ratio between the structural resistance f_R and the cylinder compressive strength $f_{c,cyl}$ as function of: (a) ratio between the diameter of the transverse bar and the thickness of the members; (b) the concrete cylinder compressive strength; (c-d) the same variables but correcting the cylinder compressive strength $f_{c,cyl}$ with the strength reduction factor η_D calculated according to Eq. (2.4).

2.10. Notation

A_c : cross section area of concrete

A_{cs} : cross section area of concrete within the confinement reinforcement

A_s : cross section area of longitudinal reinforcement

F : applied force

F_u : failure load

N_{calc} : axial force computed according to proposed model

N_u : axial force at failure

W/C : water / cement ratio

c : concrete cover

$f_{c,core}$: compressive strength of concrete core

$f_{c,cyl}$: compressive strength of concrete cylinder

$f_{c,is}$: compressive in-situ strength of concrete

f_c' : specified concrete strength

f_R : structural compressive resistance

f_u : mean value of tensile strength of reinforcement

f_{yk} : characteristic yield strength of reinforcement

f_y : mean value of yield strength of reinforcement

k : diameter correction factor

k_t : strength reduction factor accounting for loading rate

t : thickness of a member

u : longitudinal displacement

w : vertical displacement / settlement

γ_c : partial safety factor for concrete material

Δ : void thickness

ε_{long} : longitudinal strain

ε_{trans} : transverse strain

η_D : strength reduction factor to account for the presence of post-tensioning ducts or reinforcement

η_{cc} : strength reduction factor to account for concrete brittleness

η_{is} : strength reduction factor to account for difference between in-situ and control specimen compressive strength

ν : Poisson's ratio

ρ : volumetric mass density

σ : stress

σ_2 : effective lateral compressive stress due to confinement

$\varnothing$: diameter of a reinforcing bar

$\varnothing_s$: stirrup diameter

// : testing direction parallel to casting direction

$\perp$: testing direction perpendicular to casting direction

Chapter 3.

Concrete compressive strength: from material characterization to a structural value

In this chapter, it is presented the postprint version of the article *Concrete compressive strength: from material characterization to a structural value* published in the journal *Structural Concrete*. The authors of this publication are Francesco Moccia (PhD Candidate), Qianhui Yu (PhD Candidate), Miguel Fernández Ruiz (Senior lecturer and thesis co-director) and Aurelio Muttoni (Professor and thesis director). The complete reference is the following:

> F. Moccia, Q. Yu, M. Fernández Ruiz, A. Muttoni, *Concrete compressive strength: from material characterization to a structural value*, Structural Concrete, 2020, pp. 1-20. (DOI: https://doi.org/10.1002/suco.202000211)

The work presented in this article was performed by Francesco Moccia under the supervision of Miguel Fernández Ruiz and Aurelio Muttoni, who gave helpful feedback and valuable input during the entire work on this manuscript. In addition, Miguel Fernández Ruiz and Aurelio Muttoni proof-read the entire manuscript on several occasions. It should also be noted that the Section 3.6 and Annex B were written by Aurelio Muttoni with the help of Qianhui Yu.

The main contributions of Francesco Moccia are the following:

- Collection of an extensive database with 264 column tests subjected to pure compression as well as 156 column tests with load eccentricity. The tests are gathered from relevant scientific literature. The complete database has been made publicly available on the website of *Structural Concrete* and is also presented in the Appendix of this thesis.
- Review and comparison of the formulations accounting for material brittleness in structural analysis as accounted in several codes of practice.
- Theoretical background on the response of axially-loaded columns. Different design idealizations are discussed and a comparison to tests results is provided.
- Assessment of the pertinence of considering a brittleness factor for the calculation of reinforced concrete columns and compression zones of beams.
- Evaluation of the influence of casting conditions on the compressive resistance of the investigated columns.
- Theoretical background on the stress distribution in compression zones in beams and columns under eccentric loading.
- Comparison to tests results and validation of the parabola-rectangle diagram (corrected for material brittleness) as stress distribution for the compression zone of members in bending. A similar validation is also carried out for the simplified stress block distribution.
- Production of the figures included in the article.
- Writing of the manuscript of the article (except from Section 3.6 and Annex B, written by Aurelio Muttoni with the help of Qianhui Yu).

3.1. Abstract

The compressive resistance of concrete in new structures is usually characterized on the basis of tests performed on concrete cylinders or cubes under relatively rapid loading conditions. Although efficient for material characterization, these tests do not acknowledge a number of phenomena potentially influencing the compressive resistance of concrete in actual structures. For this reason, when performing a structural analysis, strength reduction factors are usually considered in codes of practice modifying the uniaxial strength of material tests.

In this paper, a detailed investigation of the influence of material brittleness and internal stress redistributions on the structural response of reinforced concrete members is presented. This work is based on a number of theoretical considerations and supported by the experimental results of more than 400 reinforced concrete columns tested with or without eccentricity and gathered from the literature. The results show the pertinence of considering a brittleness factor in the calculation of the structural resistance of reinforced concrete columns and compression zones of beams. The results of this work are eventually formulated in terms of code-like proposals, currently considered in the draft of the new Eurocode 2 (prEN 1992-1-1:2018).

3.2. Introduction

The uniaxial compressive strength of concrete (f_c) is the most significant parameter used to characterize the mechanical response of concrete in a structural member. It allows calculating the resistance of concrete members subjected to compressive forces, but is also used to characterize indirectly or to estimate many other material properties such as the modulus of elasticity or tensile strength. This value is also used, with appropriate corrections, for the verification of compression developing in members subjected to axial force, bending and shear, or in stress field and strut-and-tie analyses.

The value of the uniaxial compressive strength is normally assessed on the basis of small material samples (such as cylinders, or cubes with some adjustments) typically measuring between 100 – 300 mm and cast with the same batch as the structural members (although this might not be the case depending on the conditions for quality control). Yet, it should be noted that the material samples are often vibrated, stored and cured in a different manner than the actual conditions of the structure. In addition, testing of the material samples is typically performed under relatively fast loading rates (with failure occurring after one or two minutes of monotonic loading) and at a specific reference age that may be different to those of the actual structure.

Other than from differences in casting, curing, loading conditions and size and shape, the response of structural concrete may also differ to that of material samples due to a number of issues. These aspects may relate to non-uniform stress states (where stress redistributions can be affected by the material brittleness), to the development of cracking associated with strains imposed by the reinforcement, to the rheological response of concrete (related to continuous cement hydration and to its sensitivity to sustained actions) or to the presence of embedded reinforcement and disturbances (such as ducts or disturbances related to the casting position and conditions).

As a result of the previous aspects and considering also all uncertainties, the compressive strength of concrete measured in material samples has to be modified so that it can be used for structural analyses. For design purposes, this is normally performed by considering a number of efficiency factors in the following manner:

$$f_{cd} = \frac{f_{ck}}{\gamma_C} \cdot \prod_{i=1}^{n} \eta_i \tag{3.1}$$

Where symbol Π refers to a multiplication of factors and:

- f_{ck} refers to the characteristic value of the compressive strength of concrete (5% fractile of the measured material strength on normalized cylinders and specified stress rate).

- γ_C is the partial safety factor of concrete, which ensures a given level of reliability in the analyses. It accounts for the variability of the material properties (including the variability within the structural member due casting and curing procedure, see [1]), the variability of resistance models used for calculation of the strength, and the variability of geometrical dimensions [1].

- η_i refers to the different efficiency factors (allowing for strength reduction or enhancement) accounting for the influence on the structural resistance of concrete of various phenomena not directly considered in the material sample testing.

It should be noted that the influence of the efficiency factors (η_i) is considered following a multiplicative formulation. This presumes that the various phenomena are independent, which might be a simplification in some cases. Similar approaches can also be found in other codes of practice (refer for instance to the Chinese code GB 50010-2010 [2] or the Brazilian code ABNT NBR 6118:2014 [3]) while others are formulated with a partial safety factor $\phi < 1$ (ACI 318-19 [4], CSA A23.3 2014 [5] or AS 3600-2018 [6]), but with similar strength reduction factors accounting for the other effects.

In this paper, the influence of the material brittleness in compression and its implications with respect to potential stress redistributions occurring within a structural concrete member are investigated in detail. This aspect is instrumental for structural concrete design as it is required for a suitable applicability of typical design idealizations (as columns in compression, beams in bending and shear, or modelling with struts-and-ties). After a theoretical discussion of the basis of this approach and its formulation, its pertinence is validated by means of more than 400 tests on reinforced concrete columns from the literature. On this basis, a discussion is also presented on suitable stress distributions occurring within the compression region of beams and columns with bending moments. This discussion shows the complexity of these regions and the suitability of adopting parabola-rectangle diagrams for their design (accounting for the internal stress redistributions). These recommendations are eventually formulated in terms of design proposals (currently considered in the draft for new Eurocode 2 prEN 1992:1-1:2018 [7]) consistently covering the range of available experimental data.

3.3. Structural concrete strength: background and implications

As previously introduced, the material strength used for structural analyses should be modified accounting for actual conditions and ensuring safe application of design approaches. Following the formulation of Eq. (3.1), a number of phenomena can be addressed by means of the following efficiency factors (refer also to EN 1992-1-1:2004 [8] or *fib* MC 2010 [9] and the related factors in Table 3.1):

- η_{cc} (concrete brittleness factor): This factor accounts for the fact that concrete is not a perfectly plastic material, having a softening behaviour after its peak strength [10]–[13]. The consideration of this factor is typically required to cover the effect of stress redistributions considered implicitly in idealised stress states (as for instance constant stress distributions in axially loaded columns and parabola-rectangle or stress block distributions in compression zones of beams). It also allows accounting for the enhanced strength reduction in high-strength columns due to the phenomenon of cover spalling [14].

- η_{ε} (transverse strain factor): This factor refers to the influence of the transverse strain on the concrete strength. For members with imposed tensile strains (and thus to transverse cracking), this factor reduces the material strength as acknowledged by Vecchio and Collins [15] while it enhances the strength in case of confinement (transversal compressive stresses applied to the concrete).

- η_{is} (in-situ concrete strength factor): This factor accounts for the differences in casting and curing between control specimens and structural members. A typical phenomenon is, for instance, related to material consolidation of fresh concrete (associated to concrete bleeding, plastic settlement and segregation), particularly detrimental close to the free surface, it can be relevant for members without confinement reinforcement or other cracking control means [16].

- η_t (time-dependence factor): Two effects are normally considered with respect to the influence of time on the concrete strength: the increase of the compressive strength with time due to continuous cement hydration and the decrease of the compressive strength for high levels of sustained loads [17]. For conventional design of new structures, it is normally assumed that both phenomena compensate (although this may be arguable for early applications of permanent loads [17], [18]). As a consequence, it is normally assumed that $\eta_t = 1.0$ if the concrete strength is measured at a reference time of about 28 days [8], [9]. For assessment of existing structures, the concrete strength is measured on extracted cores when most of cement hydration has occurred; thus, more detailed considerations are needed accounting for the level of permanent loading and age of the structure [18].

- η_D (disturbance factor): The presence of significant disturbances (as inserts or post-tensioning ducts with a duct-to-member thickness ratio typically larger than 1/8 [8], [9]) has also been reported to reduce the compressive strength. The value of this factor depends on the material interface of the disturbance (e.g., plastic or steel ducts) and can also be applied to disturbances associated to large-diameter reinforcement [19]–[21].

Other phenomena should also be considered for specific analyses, for instance, effects related to low cycle fatigue [22], to size [23], to temperature [9] and shape effects in compression.

Table 3.1: Overview of strength reduction factors according to EN 1992-1-1:2004 [8] and *fib* MC 2010 [9].

		EN 1992-1-1:2004 [8]	*fib* MC 2010 [9]
η_{cc} (concrete brittleness factor)	For pure compression	Not considered	
	For compression zones due to bending	Not considered for parabola-rectangle stress distribution; considered for stress block distribution	
	For shear and strut-and-ties models	Considered within coefficient ν	Considered explicitly (coefficient η_{cc})
η_{ε} (transverse strain factor)		Considered within coefficient ν	Considered explicitly (coefficient k_c)
η_{is} (in-situ concrete strength factor)		Accounted for implicitly in γ_c (see [1])	-
η_t (time-dependence factor)		= 1.0 if $f_{c,cyl}$ is determined at 28 days = 0.85 otherwise	
η_D (disturbance factor)		Only for post-tensioning ducts	

The consideration of η_{cc} is discussed in the following with respect to a number of practical cases. Figure 3.1a presents a simple material test that can be assumed to have no disturbance with respect to a theoretical uniform stress field (disturbances are only at material level related to different behaviour of aggregates, cement paste and pores). On that basis, the value of the uniaxial compressive strength of the material ($f_c = f_{c,cyl}$) can be defined.

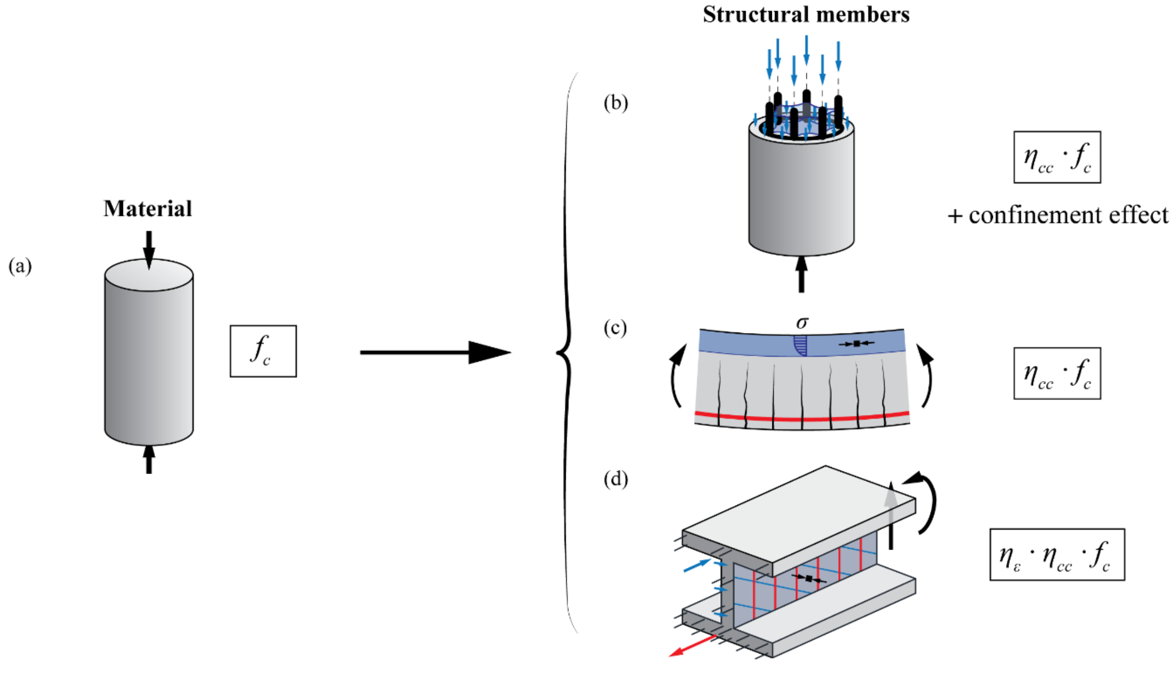

Figure 3.1: From material to structural concrete strength: (a) control specimens used to determine the material compressive strength; (b) axially-loaded column; (c) compression zone in beam in bending; and (d) compression stresses in web.

For structural elements, the situation differs from that of Figure 3.1a, as reinforcement bars are present and interacting with the concrete. This leads to potential stress redistributions between concrete and steel and also to redistributions between different regions of concrete (depending on its confinement and stress conditions). These cases are thus also affected by the brittleness of concrete, as some regions may be in the softening regime before others attain their maximum capacity. This is typically the case in concrete columns with or without eccentricity (Figure 3.1b, where redistributions between concrete core, concrete cover and longitudinal reinforcement occur), in compression zones subjected to bending (Figure 3.1c) or for elements designed with strut-and-tie or stress fields (Figure 3.1d, where idealized compression fields are assumed and the influence of transverse cracking shall be accounted for by means of coefficient η_ε).

In the cases related to the structural response of concrete (Figure 3.1b-d), the consideration of a brittleness factor influencing the material strength ($\eta_{cc} \cdot f_c$) has been demonstrated to be a suitable manner to account for the potential stress redistributions [12], [24], [25]. A consistent formulation for this coefficient was proposed by Muttoni [12] in the following form (currently used in shear design or for stress field analyses in *fib* MC 2010 [9]):

$$\eta_{cc} = \left(\frac{30}{f_c}\right)^{1/3} \leq 1 \tag{3.2}$$

Similar formulations accounting for material brittleness in the calculation of the structural resistance can also be found in codes of practice, as shown in Figure 3.2 (see also Annex A). As it can be seen, except for ACI 318-19 [4], the general trends seem to be reasonably comparable, indicating a lower nominal resistance for higher concrete grades (associated to higher material brittleness).

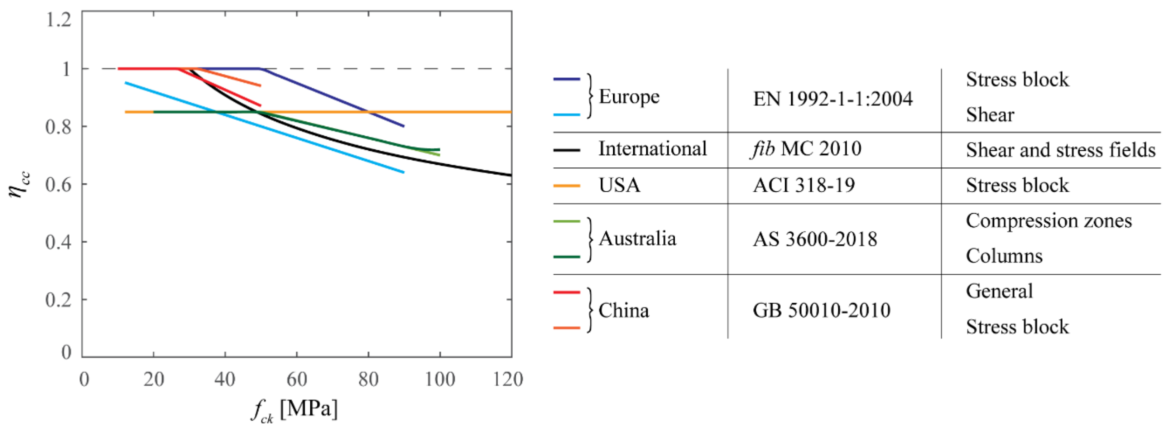

Figure 3.2: Comparison between the different formulations presented in codes of practice [2], [4], [6], [8], [9] to reduce the material compressive resistance as function of the material characteristic strength.

In the following, the importance of this coefficient will be investigated with reference to the design of reinforced concrete columns and compression zones of members in bending. As it will be shown, the consideration of the material brittleness is justified by the strong idealizations performed in the design models.

3.4. Response of axially-loaded reinforced concrete columns

In this section, the behaviour of concrete columns with longitudinal and confinement reinforcement is investigated. First, the complexity of the actual stress state and failure modes are presented and compared to typical design idealizations. On this basis, the need to consider the brittle response of concrete in the response of the member is verified.

3.4.1. Response of reinforced concrete columns in pure compression and design approaches

Reinforced concrete columns are amongst the most common structural elements and normally contain longitudinal reinforcement (parallel to the loading direction) and confinement reinforcement (hoops or spirals). Despite their apparent simplicity, the structural response of reinforced columns is relatively complex as a number of phenomena and load-carrying actions occur (Figure 3.3a-b):

- It is usually assumed that the concrete cover behaves under approximately uniaxial loading conditions (comparable to those of a material test) but it is potentially affected by spalling (Figure 3.3b). The development of cover spalling is a complex phenomenon related to the coalescence of longitudinal cracking due to the potential voids from bleeding and plastic settlement under the hoop reinforcement [16] and to the disturbance created by the presence of the hoops (restraint effect of the confinement reinforcement originating transverse tensile stresses near the hoops and thus reducing locally the compressive resistance [26], [27], Figure 3.3c,g). In addition, the response is highly dependent on the concrete cylinder strength, with a steeper post-peak response (refer to Figure 3.3e), the less-than-proportional increase of the tensile resistance (Figure 3.3f) and the higher detrimental influence of transverse tensile stress on the compressive strength for increasing material strength [28] (Figure 3.3g). It shall also be noted that the deformation capacity of concrete is sensitive to the speed of loading, with higher loading times associated to larger deformations at uniaxial concrete failure (typically, loading times higher than 30-60 minutes are usually associated to yielding of the longitudinal reinforcement prior to spalling of the cover) [18], [29].

- The concrete core behaves under confined conditions due to the presence of the hoops opposing the lateral dilatancy of the concrete. This allows for a tougher (less brittle) response [30] and with increased resistance (refer to Figure 3.3c-d for the core region). It should be noted that the actual effect of confinement is a complex phenomenon as the dispersion of the deviation forces of the hoop reinforcement within the core generates regions with higher confinement conditions (and associated resistance) than others (refer to the different strength profiles of Figure 3.3c-d associated to the variable confinement stresses within the core).

- The longitudinal reinforcement carries also a fraction of the load, with a response which can be described approximately as elastic-plastic (Figure 3.3b), provided that buckling of the reinforcement in compression is restraint by the hoops.

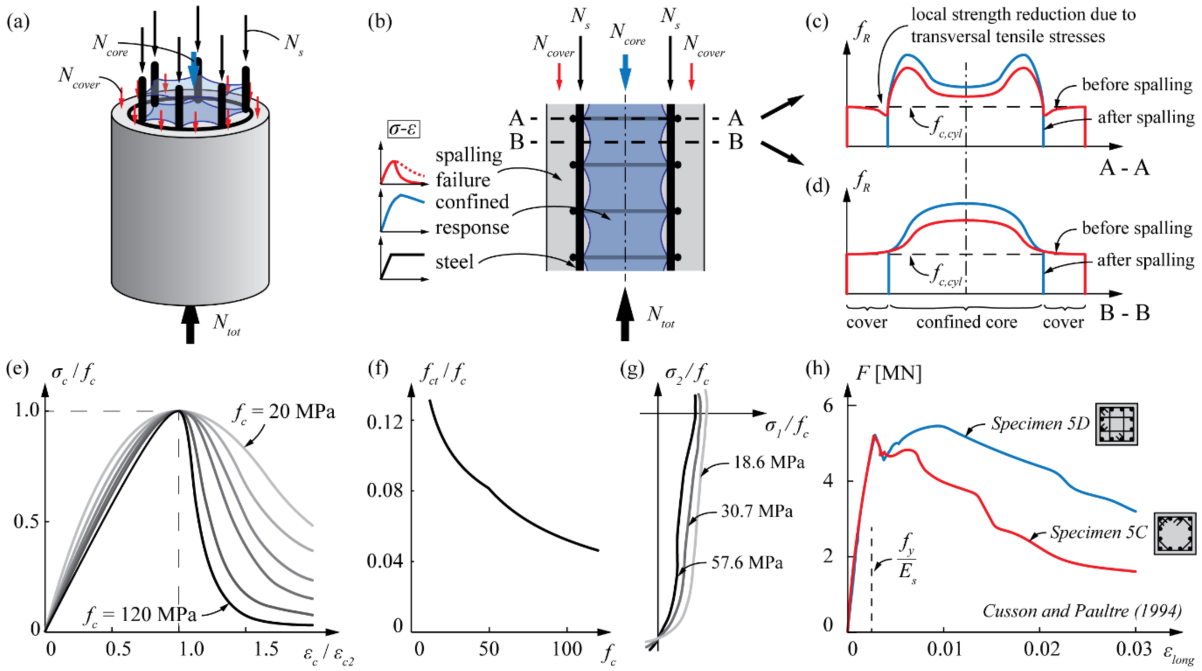

Figure 3.3: Response of a reinforced concrete column: (a) different load-carrying actions in a column; (b) material response of steel reinforcement, confined core and cover; (c) qualitative strength distribution along the cross section A-A due to transversal tensile or confinement stresses; (d) qualitative strength distribution along the cross section B-B; (e) normalized stress-strain relationships for concrete in uniaxial compression for different strengths; (f) ratio f_{ct} / f_c as a function of the compressive concrete strength (relationships calculated according to *fib* MC 2010 [9]); (g) interaction between transverse tensile stress and compressive strength for three concrete grades according to [28]; and (h) typical failure modes observed in tests (refer to [31]): maximum resistance reached at cover spalling (specimen 5C) and maximum resistance achieved after spalling of the cover and full activation of the confinement (specimen 5D).

It can be observed (Figure 3.3a-b) that the different responses (reinforcement, confined concrete, cover) give rise to a complex global response which is also highly dependent on the concrete cylinder strength (Figure 3.3e,f). At maximum load, some regions can be in a softening regime while others attain their maximum capacity. The global response is thus typically governed by two failure modes (Figure 3.3h). The first one relates to a case where the maximum resistance is reached at cover spalling (refer to specimen 5C [31] in Figure 3.3h) while the second one relates to reaching the maximum resistance after spalling of the cover (refer to specimen 5D [31] in Figure 3.3h).

Current design approaches are usually based on adopting one of these cases as governing. For instance, in EN 1998-1:2005 [32] referring to seismic design conditions, cover spalling is considered to occur (large deformation capacities and cyclic loading conditions) and only the confined concrete core and longitudinal reinforcement are used to assess the resistance. A similar consideration is also suggested in *fib* MC 2010 [9] where the enhancement conditions of the confined core may be considered only if the cover resistance is neglected. On the contrary, EN 1992-1-1:2004 [8] or ACI 318-19 [4] do not explicitly suggest the consideration of cover spalling, but do not give clear provisions on how to account for confinement.

3.4.2. Discussion of design idealizations and comparison to test results

The pertinence of current design idealizations based on the consideration of a full-cross section analysis (without cover spalling and without confinement enhancement) or of a reduced cross section (after cover spalling but with enhanced core strength) is investigated in this section with the help of 264 experimental results on reinforced columns subjected to pure compression. The tests are taken from the literature [16], [31], [41]–[50], [33]–[40] and details of the complete database considered are given in Annex C of this paper. All specimens had low slenderness (negligible second order effects) and presented variable concrete compressive strength (24 to 200 MPa), cross section (square or circular), longitudinal reinforcement ratio (0.8 to 6.8 %), confinement reinforcement ratio (0.1 to 4.5 %), tie arrangement and spacing, yield strength of the longitudinal reinforcement (260 to 820 MPa) and yield strength of the confinement reinforcement (300 to 1000 MPa).

3.4.2.1. Consideration of full cross section without enhancement of the core due to confinement

The first investigated approach corresponds to the consideration of the full cross section of a column neglecting the core enhancement due to confinement [4], [8]. To that aim, the resistance is calculated according to EN 1992-1-1:2004 [8] considering the concrete compressive strength $f_{c,cyl}$ (acting on the full cross section and neglecting the effect of concrete brittleness on the response) but accounting for a strain limit (ε_{c2}, which can potentially limit the activation of the longitudinal reinforcement):

$$N_{calc,f} = k_t \cdot f_{c,cyl} \cdot A_c + \sigma_s(\varepsilon_{c2}) \cdot A_s \tag{3.3}$$

Where $f_{c,cyl}$ refers to the mean value of the cylinder compressive strength of concrete, A_c is the cross-sectional area of the concrete (obtained by subtracting the longitudinal reinforcement area from the gross area of the cross section), A_s is the cross-sectional area of the longitudinal reinforcement and σ_s is the steel stress of the longitudinal reinforcement (with strain limit ε_{c2} as defined in EN 1992-1-1:2004 [8] and *fib* MC 2010 [9]). With respect to coefficient k_t in Eq. (3.3), it refers to the influence of loading rates on the concrete strength. When detailed information is available on the loading rate, a tailored value of k_t is used (according to the approach presented in [18]). In absence of specific data, factor k_t is set to 1.0 (corresponding to a fast loading rate, maximum difference expected for tests is lower than 4% [18]).

The comparison of the measured-to-predicted strength is shown as a function of the cylinder compressive strength of concrete ($f_{c,cyl}$) in Figure 3.4a. The results show a clear and marked trend, with decreasing levels of safety for increasing material resistance. As it can be observed, Eq. (3.3) clearly overestimated resistances for $f_{c,cyl}$ > 50 MPa, even if the effect of confinement is neglected. For $f_{c,cyl}$ < 50 MPa, however, the Eq. (3.3) provides too conservative values.

3.4.2.2. Consideration of a reduced cross section due to spalling and enhancement of the core due to confinement

As a second analysis, the responses of the same specimens are investigated by considering a design idealization where it is assumed that concrete cover is spalled but full activation of the confinement and longitudinal reinforcement is possible (hoops and longitudinal bars at yielding, refer to specimen 5D in Figure 3.3h). In this case, the resistance can be calculated as:

$$N_{calc,s} = k_t \cdot \left(f_{c,cyl} + \Delta f_{c,cyl} \right) \cdot A_{cs} + f_y \cdot A_s \tag{3.4}$$

Where A_{cs} is the concrete area within the confinement reinforcement (defined at the centreline of the external hoop [9], [32]) and the term $\Delta f_{c,cyl}$ refers to the enhancement on the strength of the core due to the confinement of the hoops.

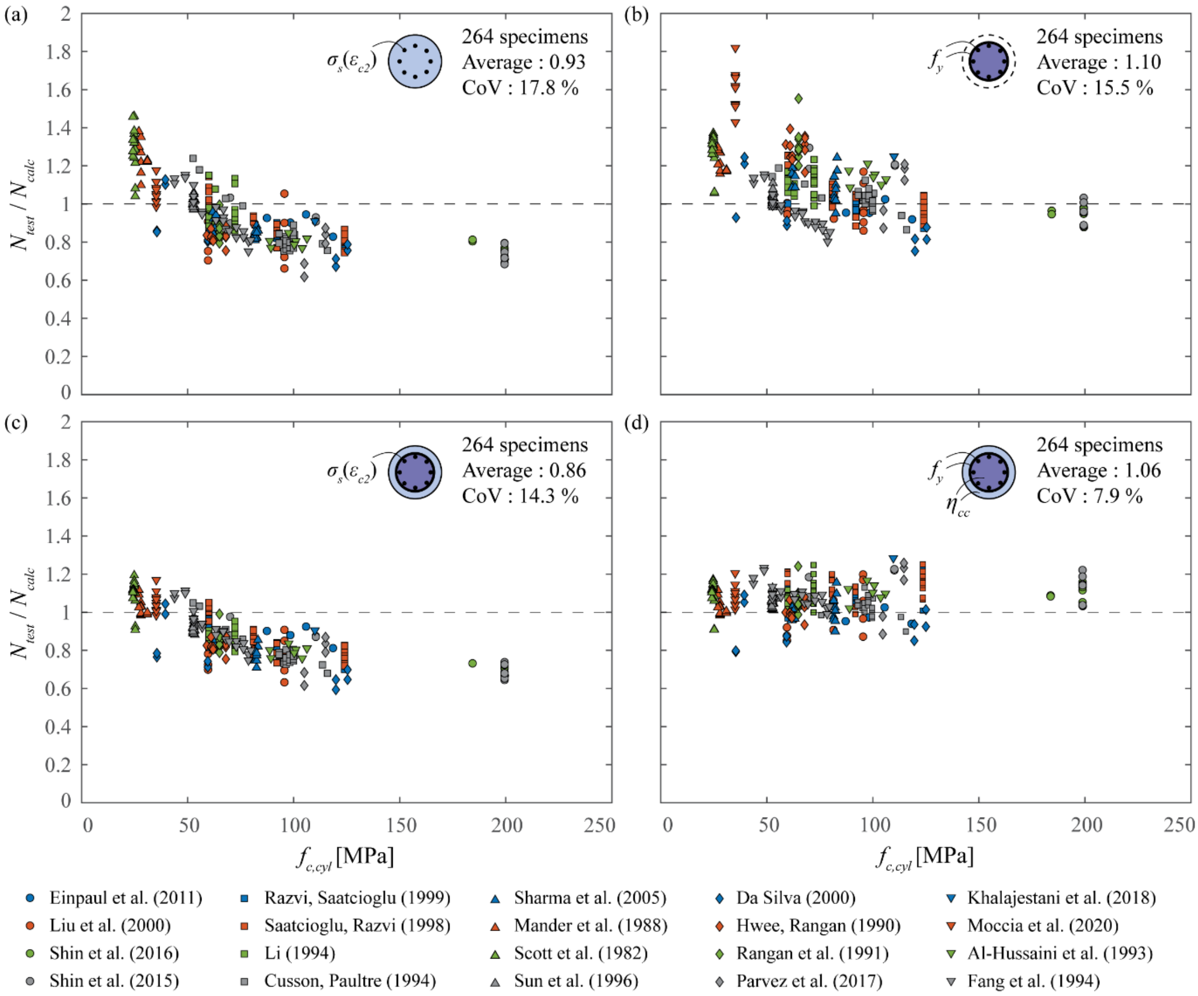

Figure 3.4: Ratio between the measured failure load and the calculated axial load as a function of the cylinder compressive strength of concrete $f_{c,cyl}$: (a) analysis according to EN 1992-1-1:2004 [8] without confinement (Eq. (3.3)); (b) analysis considering the spalling of the cover and full activation of the confinement and longitudinal reinforcement (Eq. (3.4)); (c) analysis considering the confinement enhancement in a full cross section (EN 1992-1-1:2004 [8] with confinement, Eq. (3.7)); and (d) analysis considering confinement enhancement and material brittleness (η_{cc}) without strain limit, Eq. (3.8).

The formulation of the confinement contribution of Eq. (3.5) is evaluated in the following by using prEN 1992-1-1:2018 [7] (the expression for this purpose suggested in *fib* MC 2010 [9] has been observed to be unsuitable for low levels of confinement [51]):

$$\Delta f_{c,cyl} = 4 \cdot \sigma_{c2} \qquad \text{for } \sigma_{c2} \leq 0.6 \cdot f_{c,cyl} \tag{3.5a}$$

$$\Delta f_{c,cyl} = 3.5 \cdot \sigma_{c2}^{3/4} \cdot f_{c,cyl}^{1/4} \qquad \text{for } \sigma_{c2} > 0.6 \cdot f_{c,cyl} \tag{3.5b}$$

Where σ_{c2} is the effective lateral compressive stress due to confinement [9] (see Annex E). As shown in Figure 3.4b, the results are relatively unsatisfactory. Overly conservative results are obtained for lower strength concretes, although the results seem more in agreement to test results (yet unsafe) for higher strength concrete.

3.4.2.3. Discussion of design idealizations

It can be noted that both previous idealizations (without cover spalling and without core confinement, Figure 3.4a, and with cover spalling and core confinement, Figure 3.4b) lead to unsatisfactory results. Also, considering the maximum of the two previous idealizations as the resistance (the maximum of the two peaks in Figure 3.3h):

$$N_{calc} = \max\left(N_{calc,f}\,; N_{calc,s}\right) \tag{3.6}$$

leads to unsatisfactory results as $N_{calc,f}$ is governing in almost all cases (Average = 0.92 and CoV = 16.5 %, similar trend as for Figure 3.4a).

In addition, the consideration of confinement enhancement in a full cross section would also be an unsuitable approach. This is shown in Figure 3.4c by using the following relationship:

$$N_{calc} = k_t \cdot \left(f_{c,cyl} \cdot A_c + \Delta f_{c,cyl} \cdot A_{cs} \right) + \sigma_s(\varepsilon_{c2}) \cdot A_s \tag{3.7}$$

This expression corrects to some extent the results for lower strength concrete ($f_{c,cyl}$ < 40 MPa) but worsens the prediction for higher strength concrete.

3.4.3. Design idealization accounting for material brittleness

A more consistent idealization of the global response of a column can be performed by considering the potential redistributions of stresses between the various load-carrying actions (Figure 3.3a-d). In this case, such redistributions are due to the different strains required to attain the peak strength in a material which is not plastic (refer to cover and core response in Figure 3.3b). In addition, stresses and strength are not homogeneous in the cover and the core (Figure 3.3c-d), so that previous approaches can be considered as a rough idealisation of the behaviour. To that aim, it is required to consider a brittleness factor for concrete (η_{cc}), reducing the strength of the most brittle components.

Different formulations for such an efficiency factor have been proposed in the past. Exner [10] was amongst the first to introduce an effectiveness factor to be considered when computing the resistance of a structural member using the theory of plasticity. Thorenfeldt [11] defined also different conversion factors to transform the uniaxial strength measured on control specimens to the strength of concrete in structures. Particularly, Thorenfeldt proposed considering a reduction factor for the structural strength of high-strength concretes. Also, Muttoni [12] proposed a general formulation considering the enhanced brittleness of concrete with increasing compressive strength (refer to Eq. (3.2)), originally developed for panels in shear but generally applicable [25], [52], [53]). Other definitions and formulations of the strength reduction factor η_{cc} are given in Figure 3.2 and Annex A.

The influence of the material brittleness is thus eventually considered by means of the following expression:

$$N_{calc} = k_t \cdot \left(\eta_{cc} \cdot f_{c,cyl} \cdot A_c + \Delta f_{c,cyl} \cdot A_{cs} \right) + f_y \cdot A_s \tag{3.8}$$

Where the factor η_{cc} (Eq. (3.2)) is influencing the unconfined response of concrete while the strength enhancement in the core is considered to follow a plastic response (and is thus not affected by η_{cc}). The results with this expression are shown in Figure 3.4d, showing sound agreement without any significant trend and a low scatter. Such good agreement results from the fact that the concrete contribution is more severely reduced in case of higher strength concrete (particularly reducing the contribution of the cover to the total strength in these cases). Despite its simplicity, the approach is shown to provide sound agreement on the complete range of investigated tests and confirms its pertinence [25].

It is also interesting to note that no trends are observed with reference to the main mechanical parameters concerned (Figure 3.5): core area-to-gross area ratio (A_{cs} / A_g), longitudinal and confinement reinforcement ratio ($\rho_{s,long}$, $\rho_{s,conf}$), or yield strength of longitudinal and confinement reinforcement ($f_{y,long}$, $f_{y,conf}$). A discussion on the influence of casting conditions is also presented in the next section.

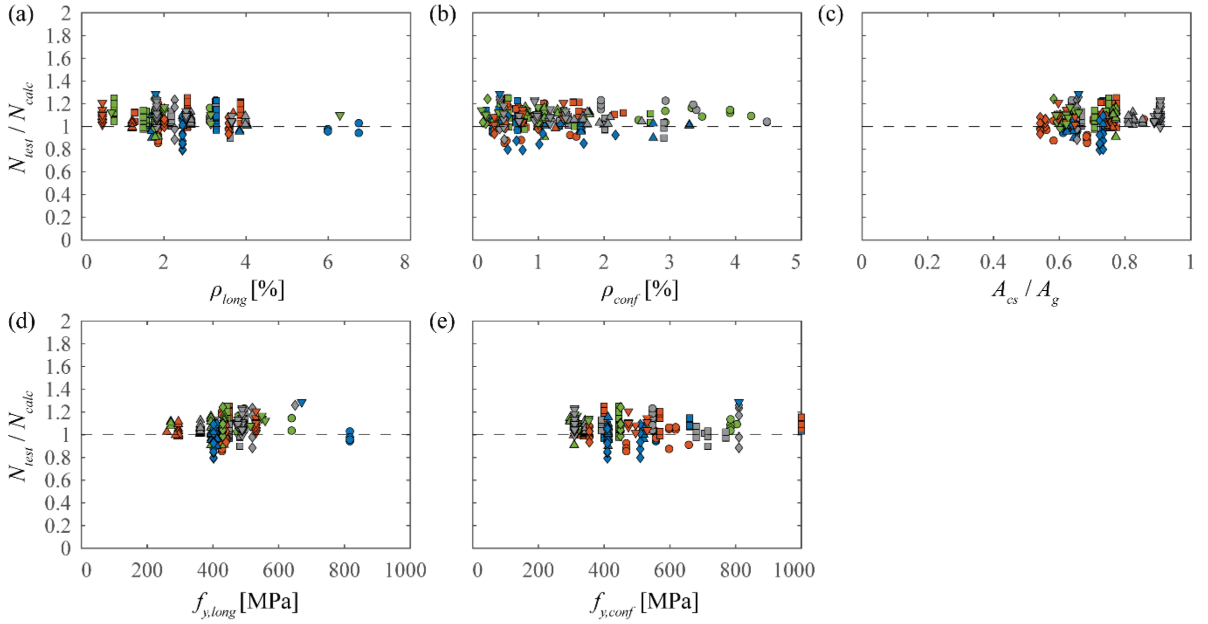

Figure 3.5: Main mechanical parameters investigated (according to Eq. (3.8)): (a) longitudinal reinforcement ratio; (b) confinement reinforcement ratio; (c) core area-to-gross area ratio; (d) yield strength of longitudinal reinforcement; and (e) yield strength of confinement reinforcement. For the legend of symbols, refer to Figure 3.4.

3.4.4. Influence of casting conditions

A detailed insight into potential effects due to casting conditions is presented in Figure 3.6a-b (strength prediction according to Eq. (3.8)) where specimens cast vertically and cast horizontally are considered separately. The analysis of the test results shows, on average, slightly safer calculations of the strength of specimens cast horizontally than for specimens cast vertically. One source for this difference could be found on the presence of voids developing under reinforcing bars just after casting due to bleeding and plastic settlement of fresh concrete [16]. For vertical casting conditions (Figure 3.6c), these voids develop under the hoops, while they develop at a side (with respect to loading direction) of the hoop for column elements cast horizontally (Figure 3.6d). The presence of these voids disturb the flow of stresses and can contribute to a premature spalling of the cover, with more unfavourable conditions when the voids are located under the hoops when cast vertically [16]. It can be observed that the difference due to casting conditions is limited (7 %) and smaller than that for members without reinforcement for crack control (which has been observed to be approximately 10 % [16]). This is associated to the fact that the disturbances due to the casting conditions are partly covered by η_{cc}, while additional differences and those related to on-site variability are usually accounted for in γ_C for design (this topic is treated in detail in Section 3.6).

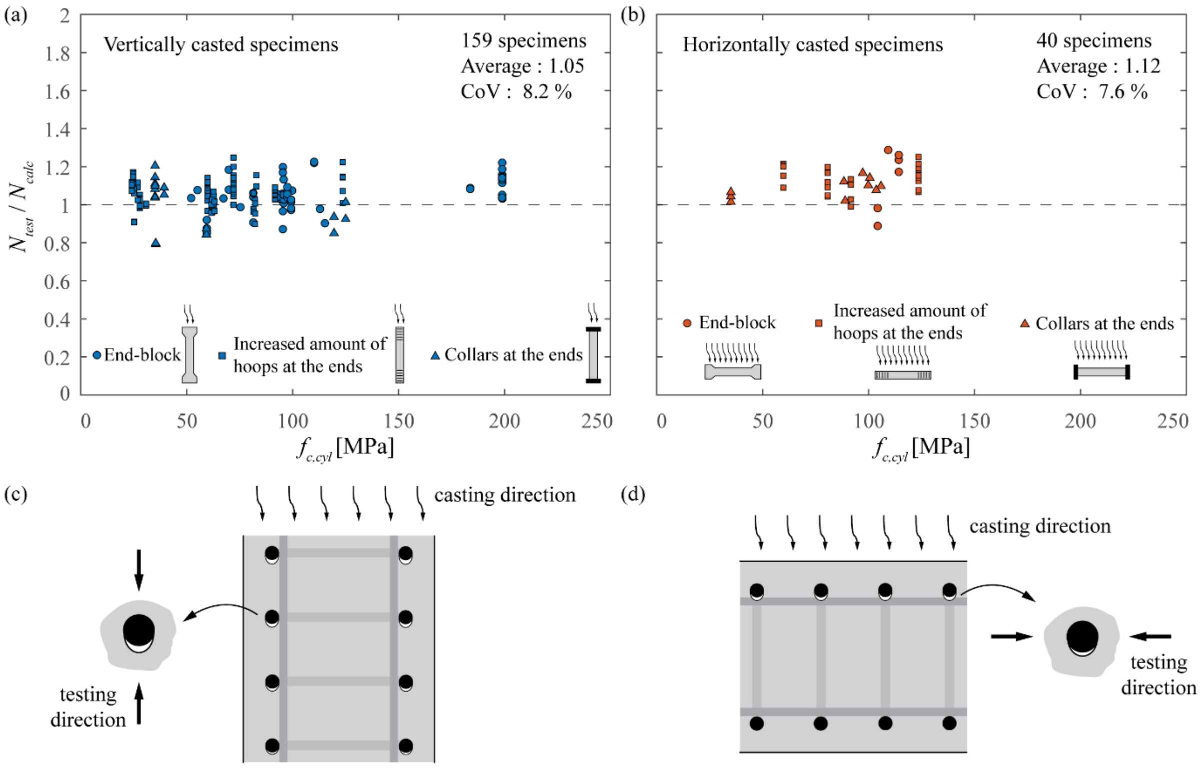

Figure 3.6: Influence of casting and boundary conditions: (a) measured-to-predicted strength for vertically-cast specimens (strength prediction according to Eq. (3.8)); (b) measured-to-predicted strength for horizontally-cast specimens (strength prediction according to Eq. (3.8)); (c) voids under hoops for vertically-cast members; and (d) voids at a side of the hoops for horizontally-cast members.

With respect to the boundary conditions during testing (also plotted in Figure 3.6), different cases can be found: end block, increased amount of hoops at the ends and collars at the load-introduction regions. No marked trend seems to appear (refer to Figure 3.6a-b), confirming that the specimens considered in the database are representative of actual structural elements and various potential load-introduction conditions.

3.5. Response of eccentrically-loaded columns

3.5.1. Stress distribution in compression zones subjected to strain gradients

Differently to columns in pure compression, where all fibres are subjected to a uniform strain level (when averaged over a certain length), compression zones in beams in bending or columns under eccentric loading show a strain gradient. In these cases, the determination of the stress profile is more complex. At early loading stages, plane sections can be assumed to remain plane and the associated stress profile can be determined on the basis of the material response under uniaxial conditions (Figure 3.7a). At higher loading stages, concrete reaches its maximum capacity at the outermost fibres. Under this situation, a significant lateral expansion of concrete occurs, leading eventually to the development of longitudinal cracking in a wedge-shaped region [54], [55] (Figure 3.7b). A suitable kinematical description of this phenomenon has been proposed by Kanellopoulos [55] on the basis of a triangular Rankine region (Figure 3.7c) where a constant distribution of longitudinal strains develops (contradicting at local level the hypothesis that plane sections remain plane). In addition, the stress state is also disturbed in this zone because the lever arm varies between regions with and without softening conditions (leading to a biaxial compressive stress state near the crack tip, as shown in Figure 3.7d according to Muttoni [12]). As a consequence of these processes, at ultimate limit state, the stress distribution cannot be derived any more from a stress-strain relationship for uniaxial material response and based on the assumption of plane section deformation (as for low loading stages, Figure 3.7a). For this reason, the stress distribution usually adopted by codes of practice were originally derived directly from tests on compression zones accounting for the described phenomena [17], [56]–[59]. They show a rather constant plateau at a certain distance from the crack tip, in agreement to the uniform strain state shown by Kanellopoulos. This is in most cases considered in design by means of a parabola-rectangle diagram, which does not actually refer to a stress-strain relationship for uniaxial material response but to a distribution of stresses within this disturbed region.

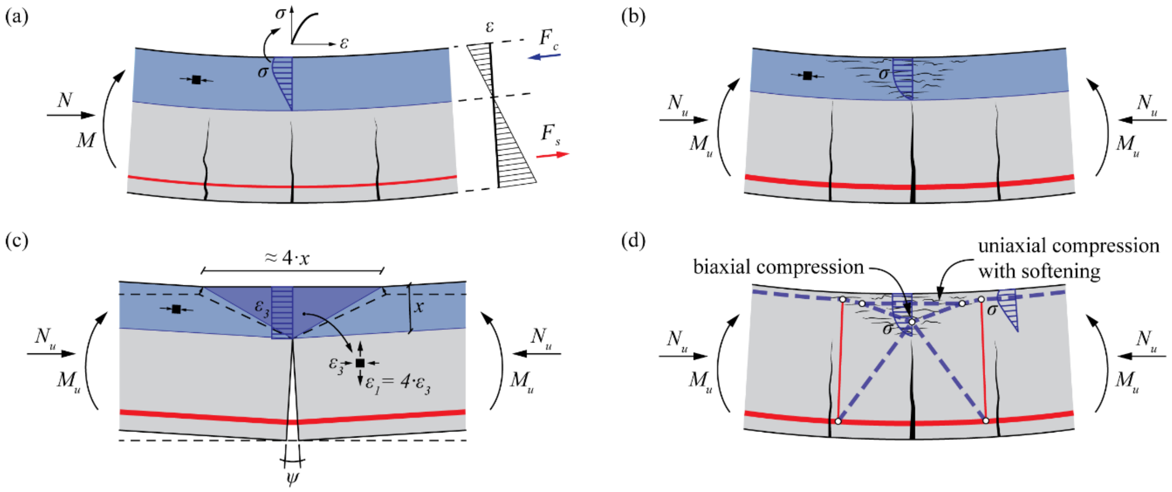

Figure 3.7: Stress distribution in compression zones subjected to strain gradients (blue: compression stresses; red: tensile stresses): (a) moderate loading, plane sections are assumed to remain plane and the stress profile is determined from the material constitutive law under uniaxial compression; (b) deformations concentrating in a wedge-shaped region in the compression zone with stress distribution comparable to parabola-rectangle diagram; (c) failure mechanism with Rankine deformation field [55]; and (d) detailed view of the stresses and corresponding strut-and-tie model [12].

In addition to these considerations, it can be theoretically observed that since some regions are in the softening phase while others not, the consideration of the brittleness strength reduction factor (η_{cc}) on the material strength is required for a consistent design. This fact is however not always acknowledged in design codes. In the next section, the necessity of accounting for this factor will be demonstrated by means of analysing experimental data.

3.5.2. Design idealization of eccentrically-loaded columns

Design approaches for members subjected to bending and normal forces are usually based on a nominal plane strain distribution, with varying neutral axis depth and respecting some conditions (see for instance [8],[9]). For each strain profile (Figure 3.8a), the corresponding steel and concrete stresses can be calculated (see Figure 3.8b-c) and eventually integrated over the height of the cross section to determine the resisting moment and normal force (Figure 3.8d).

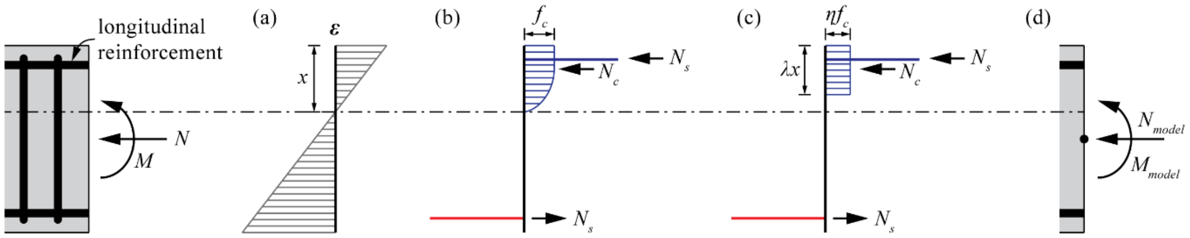

Figure 3.8: Idealization for the resistance of a column subjected to bending moment and axial compression (blue: compression stresses; red: tensile stresses): (a) assumed strain distribution; (b) parabola-rectangle stress distribution for concrete under compression; (c) stress block distribution; and (d) resisting force and moment at the reference axis of the cross section.

With respect to the stress distribution of concrete under compression, the EN 1992-1-1:2004 [8] proposes two possible idealizations (also suggested by *fib* MC 2010 [9]): a parabola-rectangle distribution (Figure 3.8b) and a stress block (Figure 3.8c). These two stress distribution diagrams will be discussed in the following and evaluated based on a database of eccentrically-loaded columns.

3.5.2.1. Parabola-rectangle stress distribution

As previously discussed, the distribution of compression stresses in a compression zone of beams subjected to bending can be assumed to be comparable to a parabola-rectangle profile (Figure 3.7b). This stress distribution is expressed in EN 1992-1-1:2004 [8] (and *fib* MC 2010 [9]) as a virtual stress-strain relationship defined in the following manner:

$$
\begin{aligned}
\sigma_c &= f_c \cdot \left[1-\left(1-\frac{\varepsilon_c}{\varepsilon_{c2}}\right)^n\right] && \text{for } 0 \le \varepsilon_c \le \varepsilon_{c2} \\
\sigma_c &= f_c && \text{for } \varepsilon_{c2} \le \varepsilon_c \le \varepsilon_{cu2}
\end{aligned}
\tag{3.9}
$$

where

- $\varepsilon_{c2} = 0.002$ for $f_c \le 50$ MPa and $\varepsilon_{c2} = 0.002 + 0.000085 \cdot (f_c - 50)^{0.53}$ for $50 < f_c \le 90$ MPa
- $n = 2.0$ for $f_c \le 50$ MPa and $n = 1.4 + 23.4\left[(90 - f_c)/100\right]^4$ for $50 < f_c \le 90$ MPa
- $\varepsilon_{cu2} = 0.0035$ for $f_c \le 50$ MPa and $\varepsilon_{cu2} = 0.0026 + 0.035\left[(90 - f_c)/100\right]^4$ for $50 < f_c \le 90$ MPa

It should be noted that this approach accounts for the influence of the material brittleness on the value of the limiting strains ε_{c2} and ε_{cu2}, but not on the concrete strength in the compression zone. The results obtained by considering this stress distribution are compared in Figure 3.9a to 156 specimens from the literature ([14], [42], [60]–[67]) as a function of the concrete compressive strength $f_{c,cyl}$ (assuming a constant eccentricity equal to the one of the tests). This analysis considers the deformation planes in accordance to the strain limits suggested in EN 1992-1-1:2004 [8] (pivot points in compression at ε_{c2} and ε_{cu2} and limiting strain $\varepsilon_{ud} = 0.02$ for steel in tension [8]). Details of the complete database considered are given in Annex D of this paper. As previously observed for columns subjected to pure compression, a decreasing level of safety can be observed for increasing concrete strength.

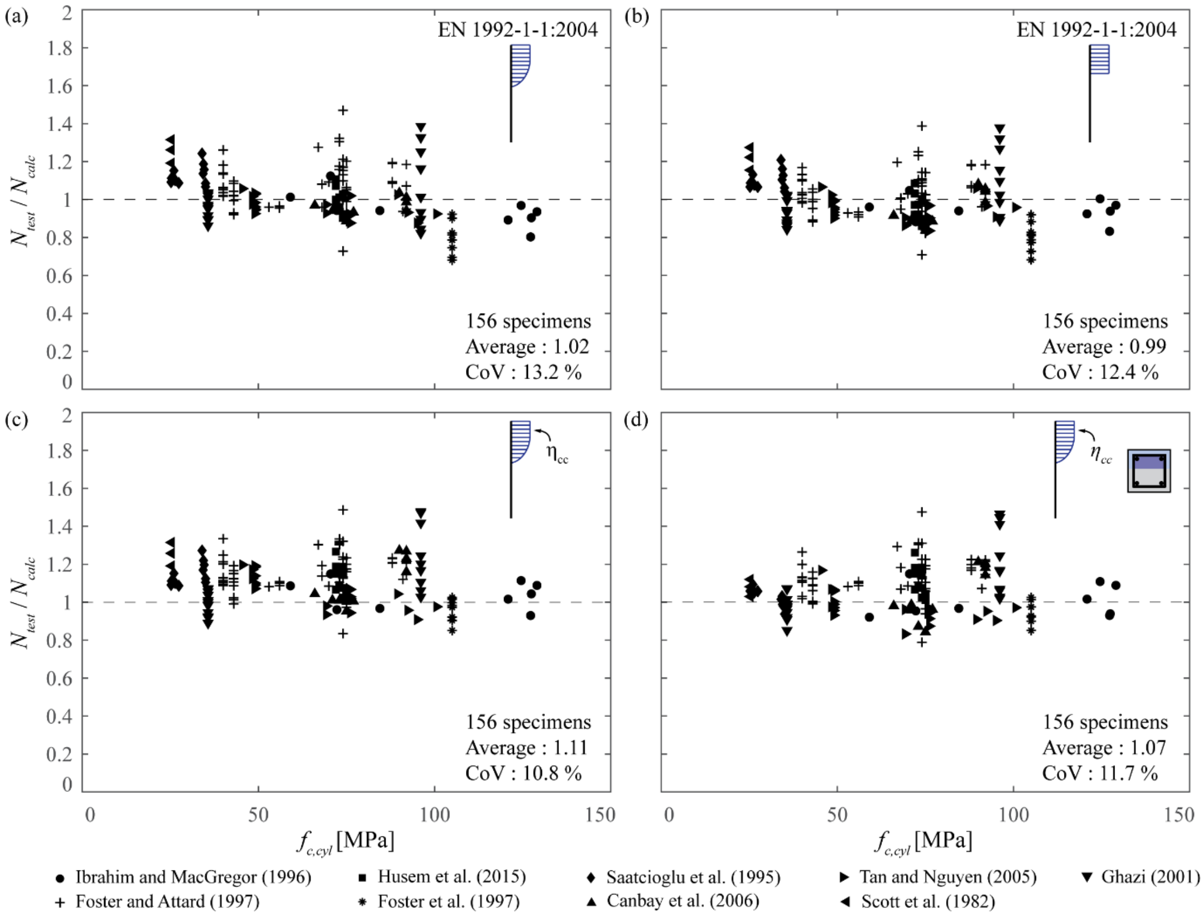

Figure 3.9: Ratio N_{test} / N_{model} as a function of the cylinder compressive strength of concrete $f_{c,cyl}$, analysis according to: (a) EN 1992-1-1:2004 [8], parabola-rectangle method; (b) EN 1992-1-1:2004 [8], stress-block method; (c) CEB-FIP MC 1990 [68], parabola-rectangle method corrected with η_{cc}; and (d) CEB-FIP MC 1990 [68], parabola-rectangle method corrected with η_{cc} and considering the confinement provided by the hoops in the compressed region.

For this reason, the EN 1992-1-1:2004 [8] approach is simplified and modified to consider the strength reduction factor η_{cc} presented in Eq. (3.2). To that aim, the simple parabola-rectangle stress distribution of CEB-FIP MC 1990 [68] is adopted with constant strain limits (ε_{c2} = 2.0 ‰ and ε_{cu2} = 3.5 ‰ and with a value of the exponent n = 2), but with a strength reduced to $\eta_{cc} \cdot f_{c,cyl}$. In addition, the definition of potential deformation planes is simplified with respect to EN 1992-1-1:2004 [8], by considering in the compression region only one limiting strain (pivot point) at ε_{cu2}. The comparison of this approach to the test results is shown in Figure 3.9c. The results are better, with a less marked trend and safer estimates for members with higher concrete strength. It can however be noted that the procedure still leads to somewhat safe estimates for normal strength concrete. This result, as for columns in pure compression, can be explained by the fact that the confinement effect of the core by the transverse reinforcement is neglected. When this contribution is accounted for (refer to Figure 3.9d, calculated with the provisions for confinement according to [9] and previously used for columns in compression), the results improve and present no trend with respect to the concrete strength (average 1.07 and coefficient of variation 11.7 %).

In addition, the proposed simplification of the parabola-rectangle method of EN 1992-1-1:2004 [8] with the one of CEB-FIP MC 1990 [68] with constant strain limits and η_{cc} (case without confinement) does not show any particular trend with regard the main mechanical parameters investigated (Figure 3.10).

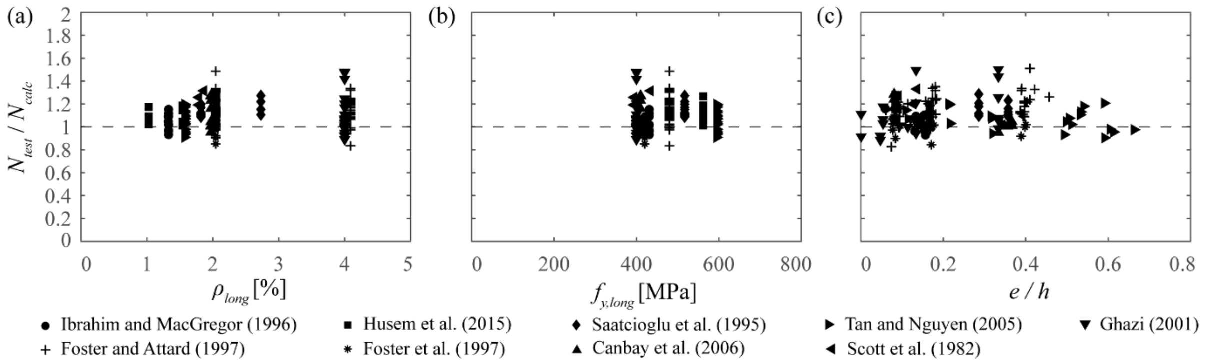

Figure 3.10: Main mechanical parameters investigated according to the parabola-rectangle of CEB-FIP MC 1990 [68] modified with η_{cc} without accounting for confinement: (a) longitudinal reinforcement ratio; (b) yield strength of longitudinal reinforcement; and (c) normalized load eccentricity.

3.5.2.2. Stress block stress distribution

For analyses undertaken by hand, the stress distribution within the compression zone of a member subjected to eccentric loading is often simplified to an equivalent rectangular stress distribution [59], usually referred to as the stress block method (Figure 3.8c). In this procedure, the compressive stresses are assumed to be uniformly distributed over a region of maximum compressive strain until a certain depth.

The EN 1992-1-1:2004 [8] defines the rectangular stress distribution by means of two coefficients: the λ-factor indicating the equivalent depth of the distribution, and the η-factor to be applied to the concrete compressive strength f_c to obtain an equivalent strength (Figure 3.8c). These factors also consider that the depth and value of the distribution vary for increasing concrete compressive strength (this was considered in the parabola-rectangle method by modifying the strain limits for f_c > 50 MPa). The λ and η coefficients are defined as follows:

$$\begin{aligned} &\lambda = 0.8 && \text{for } f_c \leq 50 \text{ MPa} \\ &\lambda = 0.8 - (f_c - 50)/400 && \text{for 50 MPa} < f_c \leq 90 \text{ MPa} \end{aligned} \tag{3.10}$$

and

$$\begin{aligned} &\eta = 1.0 && \text{for } f_c \leq 50 \text{ MPa} \\ &\eta = 1.0 - (f_c - 50)/200 && \text{for 50 MPa} < f_c \leq 90 \text{ MPa} \end{aligned} \tag{3.11}$$

The stress block method presented in EN 1992-1-1:2004 [8] is compared to the previous database of test results in Figure 3.9b as function $f_{c,cyl}$. It can be noted that this procedure leads to almost identical results as the parabola-rectangle distribution, showing again a decreasing level of safety with increasing concrete compressive strength.

In order to correct this trend, and to simplify the procedure, it is proposed to replace the η-factor of EN 1992-1-1:2004 [8] with the concrete brittleness factor η_{cc} (presented in Eq. (3.2)) and to set the λ-factor to a constant value of 0.8. This method provides almost identical results as the one of the parabola-rectangle of CEB-FIP MC 1990 [68] corrected with η_{cc} (average 1.08, coefficient of variation 10.7 %). If the procedure accounts for the favourable effects of the confined state that can be developed within the hoops, the results become more consistent and without any trend with respect to the main mechanical parameters investigated (average 1.04, coefficient of variation 11.5 %). The simplicity of the method and the accuracy of the prediction for high-strength columns confirm the pertinence of considering the η_{cc} factor in the procedure.

3.6. Design values and partial safety factor for concrete

As already described in Section 3.2, the partial safety factor for concrete γ_C in Equation (3.1) is calibrated to account for uncertainties related to the material strength, to the resistance models and to the geometry of the structural member to be verified. This factor is normally calibrated for the case of members under pure compression [1] as the columns described in Section 3.4 (uncertainties related to the reinforcement are covered by its own partial safety factor γ_S).

For calibration of the partial safety factor of concrete, the principles of the First Order Reliability Methods (FORM) can be applied, whose implementation to columns in compression is thoroughly detailed in Annex B of this paper. In this case, the limit state function (considered here as the complete performance function) defining the structural strength (and whose reliability is to be calibrated) results:

$$R = \eta_{cc} \cdot k_t \cdot \eta_{is} \cdot f_{c,cyl} \cdot A_c \tag{3.12}$$

Where the different terms have already been introduced in the previous sections. In this expression, it can be noted the presence of the parameter η_{is}, that accounts for the difference between in-situ concrete strength and cylinder concrete strength ($\eta_{is} = f_{c,is}/f_{c,cyl}$). This parameter accounts for effects like bleeding and concrete settlement during pouring (leading to systematic differences between bottom and top parts of the member [16]), but also for other effects as differences of curing conditions between control specimens and structural member or variabilities of pouring conditions on the construction site. As shown in [16], the effect of bleeding and settlement is attenuated by the presence of confinement reinforcement, but, nevertheless, a certain effect can still be observed in the laboratory tests as shown in Figure 3.6 and can be incorporated in the calibration of the partial safety factor for design purposes.

With respect to the limit state function, it can be noted that for low values of the concrete strength (refer to $f_{c,cyl} \leq 30$ MPa in previous sections), the brittleness factor has a negligible influence on the structural response and can thus be assumed to be $\eta_{cc} = 1$. In such case, the structural strength depends linearly on the compressive material strength and the design resistance of the structural member can be written as:

$$R_d = \eta_{cc} \cdot k_t \cdot \frac{f_{ck}}{\gamma_C} \cdot A_c \tag{3.13}$$

where the in-situ concrete strength factor η_{is} and other neglected effects are thus considered implicitly in the partial safety factor γ_C [1]. As shown in Annex B according to the principles of FORM and by providing suitable values for the mean value and coefficient of variation of the different variables, it can be demonstrated in this case that a value $\gamma_C = 1.5$ ensures a sufficient level of reliability for design (corresponding to a target reliability index $\beta_{tgt} = 3.8$).

For higher concrete strengths ($f_{c,cyl} > 30$ MPa in previous sections), the influence of the brittleness factor η_{cc} in the structural resistance becomes noticeable and modifies the limit state function as follows:

$$R = \eta_{cc,1} \cdot \left(k_t \cdot \eta_{is} \cdot f_{c,cyl}\right)^{2/3} \cdot A_c \tag{3.14}$$

while the design value of the structural resistance results thus:

$$R_d = \eta_{cc,1} \cdot \frac{\left(k_t \cdot f_{ck}\right)^{2/3}}{\gamma_{C,1}} \cdot A_c \tag{3.15}$$

where $\eta_{cc,1}$ = (30 MPa)$^{1/3}$ and $\gamma_{C,1}$ is the partial safety factor for higher concrete strength.

In this latter case, the influence of the concrete strength on the resistance of an element is not linear, but depends upon an exponent 2/3. As a consequence, the effect of the concrete strength variability on the reliability of the resistance is attenuated, and the value of the partial safety factor $\gamma_{C,1}$ can be reduced. As demonstrated in Annex B by means of the FORM principles, the resulting value of the concrete partial safety factor can in this case be lowered to a value γ_{C1} = 1.37 while ensuring the same target reliability index.

It shall be noted that, for design purposes, having different values of the partial safety factor (γ_C = 1.50 for low values of concrete strength and γ_{C1} = 1.37 for high values of concrete strength) is not convenient. As an alternative approach for design, the brittleness factor used for design purposes (η_{cc}) can be corrected while keeping a constant value for γ_C. To do so, γ_C can be set to 1.5 and the reference concrete strength in Eq. (3.2) modified accordingly to 40 MPa ($\approx 30\cdot(1.5/1.37)^3$). Thus, the equation for the brittleness factor to be used for design (keeping a constant value γ_C = 1.5 independently of the concrete strength) results:

$$\eta_{cc} = \left(\frac{40}{f_{ck}}\right)^{1/3} \leq 1 \tag{3.16}$$

This is for instance the approach proposed in [7], see also [69].

3.7. Conclusions

This paper investigates the differences between the material strength of concrete and that developed within structural elements, with a particular focus on the influence of the material brittleness and its consideration within typical design idealizations. The main findings of the paper are summarized below:

1. The concrete compressive resistance in a structure can be significantly different to the material strength. Its value is influenced by a number of phenomena such as material brittleness, concrete cracking, loading rates, presence of disturbances or casting position. Such influences can be considered by means of strength reduction factors, usually considered in a multiplicative manner as a simplification of reality.

2. The consideration of the material brittleness is instrumental in cases when stress redistributions occur within a concrete element (some regions are in compression softening while others attain their peak strength) and to cover idealizations of design models (idealised distributions of stresses). This can be performed by reducing the material strength by means of a brittleness factor (η_{cc}).

3. The strength reduction factor η_{cc} according to *fib* MC 2010 [9] for the case of compression fields subjected to shear and strut-and-tie models provides a consistent manner to assess the

compressive strength of structural elements accounting for the brittle response of concrete. It should thus be included for design of reinforced compression members, particularly for columns in pure compression or with load eccentricity and for the compression zone related to bending. This conclusion has been confirmed with an extensive comparison to more than 400 tests gathered from the scientific literature and including high-strength concrete specimens.

4. The consideration of a parabola-rectangle diagram for the stress distribution of the compression zone of members in bending (with or without axial force) is observed to be theoretically consistent due to the internal redistributions of stresses occurring in this region at ultimate state. Such distribution of stresses can be used for design of members in bending and axial compression provided that the brittleness of concrete is accounted for (by means for instance of coefficient η_{cc}). Similar conclusions apply also to a simplified stress block distribution of stresses in the compression zone.

5. Due to the fact that for f_c > 30 MPa the influence of the concrete strength on the element resistance is not linear (but depends upon an exponent 2/3), the effect of the concrete strength variability on the reliability of the resistance is attenuated. For this reason, the value of the partial safety factor γ_C could be reduced with respect to cases where this influence is linear ($f_c \leq 30$ MPa). Alternatively, to keep a constant value of the partial safety factor of concrete, the strength reduction factor accounting for concrete brittleness (η_{cc}) can be adapted at design level accordingly.

3.8. References

[1] European Concrete Platform, "Eurocode 2 Commentary," European Committee for Standardization (CEN), Brussels, Belgium, 168 p., 2008.

[2] GB 50010-2010, "Code for Design of Concrete Structures," Ministry of Housing and Urban-Rural Development of the People's Republic of China, Beijing, 427 p., 2010.

[3] ABNT NBR 6118:2014, "Projeto de Estruturas de Concrete - Procedimento," Associação Brasileira de Normas Técnicas, Rio de Janeiro, Brazil, 238 p., 2014.

[4] ACI Committee 318, "Building Code Requirements for Structural Concrete (ACI 318-19) and Commentary," American Concrete Institute, Farmington Hills, USA, 624 p., 2019.

[5] Canadian Standards Association, "CSA A23.3 2014: Design of Concrete Structures," CSA Group, Mississauga, ON, Canada, 295 p., 2014.

[6] Standards Australia, "AS 3600:2018 : Concrete Structures," Standards Australia Limited, Sydney, Australia, 264 p., 2018.

[7] prEN 1992-1-1:2018, "Eurocode 2: Design of concrete structures - Part 1-1: General rules, rules for buildings, bridges and civil engineering structures," European Committee for Standardization (CEN), Brussels, Belgium, 293 p., 2018.

[8] EN 1992-1-1:2004, "Eurocode 2: Design of Concrete Structures - Part 1: General Rules and Rules for Buildings," European Committee for Standardization (CEN), Brussels, Belgium, 225 p., 2004.

[9] International Federation for Structural Concrete, “fib Model Code for Concrete Structures 2010,” Ernst & Sohn, Berlin, Germany, 434 p., 2013.

[10] H. Exner, “On the effectiveness factor in plastic analysis of concrete,” *IABSE reports of the working commissions*, pp. 35–42, 1979.

[11] E. Thorenfeldt, “Design Properties for High-Strength Concrete,” *Nordisk Betong, No. 1-2*, pp. 71–73, 1986.

[12] A. Muttoni, “The applicability of the theory of plasticity in the design of reinforced concrete (‘Die Andwendbarkeit der Plastizitätstheorie in der Bemessung von Stahlbeton’),” PhD thesis, ETH, Zürich, 164 p., 1990.

[13] F. Moccia, M. Fernández, and A. Muttoni, “Efficiency Factors for Plastic Design in Concrete: Influence of Brittleness in Compression,” *High Tech Concrete: Where Technology and Engineering Meet*, pp. 1234–1242, 2018.

[14] S. J. Foster and M. M. Attard, “Experimental Tests on Eccentrically Loaded High-Strength Concrete Columns,” *ACI Structural Journal*, vol. 94, no. 3, pp. 295–303, 1997.

[15] F. J. Vecchio and M. P. Collins, “The Modified Compression-Field Theory for Reinforced Concrete Elements Subjected to Shear,” *ACI journal*, vol. 83, no. 2, pp. 219–231, 1986.

[16] F. Moccia, X. Kubski, M. Fernández Ruiz, and A. Muttoni, “The influence of casting position and disturbance induced by reinforcement on the structural concrete strength,” *Structural Concrete*, vol. In press, pp. 1–28, 2020.

[17] H. Rüsch, “Researches Toward a General Flexural Theory for Structural Concrete,” Journal of the American Concrete Institute, 28 p., 1960.

[18] D. Tasevski, M. Fernández Ruiz, and A. Muttoni, “Assessing the compressive strength of concrete under sustained actions: From refined models to simple design expressions,” *Structural Concrete*, vol. 20, no. 3, pp. 971–985, 2019.

[19] A. Muttoni, O. L. Burdet, and E. Hars, “Effect of Duct Type on Shear Strength of Thin Webs,” *ACI Structural Journal*, vol. 103, no. 5, pp. 729–735, 2006.

[20] D. M. Wald, A. Moore, O. Bayrak, and J. O. Jirsa, “Compressive Behavior of Concrete Panels Containing Steel and Plastic Ducts,” *ACI Structural Journal*, vol. 114, no. 5, pp. 1167–1176, 2017.

[21] H. R. Ganz, A. Ahmad, and H. Hitz, “Load Transfer Through Concrete Sections with Grouted Ducts,” Report 242e, VSL, Bern, 32 p., 1992.

[22] N. Kostic, “Topologie des champs de contraintes pour le dimensionnement des structures en béton armé,” PhD Thesis, EPFL, Lausanne, 235 p., 2009.

[23] Z. B. Li, J. Song, X. L. Du, and X. G. Yang, “Size effect of confined concrete subjected to axial compression,” *Journal of Central South University*, vol. 21, no. 3, pp. 1217–1226, 2014.

[24] M. Fernández Ruiz and A. Muttoni, “On Development of Suitable Stress Fields for Structural Concrete,” *ACI Structural Journal*, vol. 104, no. 4, pp. 495–502, 2007.

[25] A. Muttoni, M. F. Ruiz, and F. Niketic, “Design versus assessment of concrete structures using stress fields and strut-and-tie models,” *ACI Structural Journal*, vol. 112, no. 5, pp. 605–615,

2015.

[26] S. J. Foster, J. Liu, and S. A. Sheikh, "Cover Spalling in HSC Columns Loaded in Concentric Compression," *Journal of Structural Engineering*, vol. 124, no. 12, pp. 1431–1437, 1998.

[27] S. J. Foster, "On Behavior of High-Strength Concrete Columns : Cover Spalling, Steel Fibers, and Ductility," *ACI Structural Journal*, vol. 98, no. 4, pp. 583–589, 2001.

[28] H. Kupfer, H. K. Hilsdorf, and H. Rüsch, "Behavior of Concrete Under Biaxial Stresses," *ACI Journal*, vol. 66, no. 52, pp. 656–666, 1969.

[29] D. Tasevski, M. F. Ruiz, and A. Muttoni, "Compressive Strength and Deformation Capacity of Concrete under Sustained Loading and Low Stress Rates," *Journal of Advanced Concrete Technology*, vol. 16, no. 8, pp. 396–415, 2018.

[30] S. J. Pantazopoulou and R. H. Mills, "Microstructural Aspects of the Mechanical Response of Plain Concrete," *ACI Materials Journal*, vol. 92, no. 6, pp. 605–616, 1995.

[31] D. Cusson and P. Paultre, "High-strength Concrete Columns Confined by Rectangular Ties," *Journal of Structural Engineering*, vol. 120, no. 3, pp. 783–804, 1994.

[32] EN 1998-1:2005, "Eurocode 8: Design of structures for earthquake resistance - Part 1: general rules, seismic actions and rules for buildings," European Committee for Standardization (CEN), Brussels, Belgium, 242 p., 2005.

[33] J. Einpaul, A. Muttoni, and O. Burdet, "Ultimate load capacity of prefabricated concrete column elements," Mandate SACAC prefabricated columns 11.21, EPFL, Lausanne, Switzerland, 19 p., 2011.

[34] J. Liu, S. J. Foster, and M. M. Attard, "Strength of Tied High-Strength Concrete Columns Loaded in Concentric Compression," *ACI Structural Journal*, vol. 97, no. 1, pp. 149–157, 2000.

[35] H.-O. Shin, Y.-S. Yoon, W. D. Cook, and D. Mitchell, "Axial Load Response of Ultra-High-Strength Concrete Columns and High-Strength Reinforcement," *ACI Structural Journal*, vol. 113, no. 2, pp. 325–336, 2016.

[36] H.-O. Shin, Y.-S. Yoon, W. D. Cook, and D. Mitchell, "Effect of Confinement on the Axial Load Response of Ultrahigh-Strength Concrete Columns," Journal of Structural Engineering, 12 p., 2015.

[37] S. R. Razvi and M. Saatcioglu, "Circular High-Strength Concrete Columns under Concentric Compression," *ACI Structural Journal*, vol. 96, no. 5, pp. 817–825, 1999.

[38] M. Saatcioglu and S. R. Razvi, "High-Strength Concrete Columns with Square Sections under Concentric Compression," *Journal of Structural Engineering*, vol. 124, no. 12, pp. 1438–1447, 1998.

[39] B. Li, "Strength and Ductility of Reinforced Concrete Members and Frames Constructed Using High Strength Concrete," Christchurch, New Zealand, 411 p., 1994.

[40] U. K. Sharma, P. Bhargava, and S. K. Kaushik, "Behavior of Confined High Strength Concrete Columns under Axial Compression," *Journal of Advanced Concrete Technology*, vol. 3, no. 2, pp. 267–281, 2005.

[41] J. B. Mander, M. J. N. Priestley, and R. Park, "Observed Stress-Strain Behavior of Confined

Concrete,” *Journal of structural engineering*, vol. 114, no. 8, pp. 1827–1849, 1988.

[42] B. D. Scott, R. Park, and M. J. N. Priestley, “Stress-Strain Behavior of Concrete Confined by Overlapping Hoops at Low and High Strain Rates,” *ACI Journal*, vol. 79, no. 1, pp. 13–27, 1982.

[43] Y. P. Sun, T. Oba, F. S. Tian, and T. Ikeda, “Confinement effects of transverse hoops in high-strength concrete,” Proceedings of the 11th World conference on Earthquake Engineering, Elsevier Science Ltd, Amsterdam, 8 p., 1996.

[44] P. Da Silva, “Effect of Concrete Strength on Axial Load Response of Circular Columns,” Department of Civil Engineering and Applied Mechanics, McGill University, Montréal, Canada, 105 p., 2000.

[45] Y. S. Hwee and B. V. Rangan, “Studies on Commercial High-Strength Concretes,” *ACI Materials Journal*, vol. 87, no. 5, pp. 440–445, 1990.

[46] B. V. Rangan, P. Saunders, and E. J. Seng, “Design of High-Strength Concrete Columns,” *Special Publication 128-52*, vol. 128, pp. 851–862, 1991.

[47] A. Parvez, S. J. Foster, H. Valipour, and G. Mcgregor, “Strength and Ductility of High-Strength Concrete Columns Confined with High-Strength Steel Ties,” 28th Biennial National Conference of the Concrete Institute of Australia, Adelaide, Australia, 13 p., 2017.

[48] M. K. Khalajestani, A. Parvez, S. J. Foster, H. Valipour, and G. McGregor, “Strength and ductility of high-strength concrete columns reinforced with high-strength steel,” The International Federation for Structural Concrete 5th International fib Congres, Melbourne, Australia, 8 p., 2017.

[49] A. Al-Hussaini, P. E. Regan, H.-Y. Xue, and K.-E. Ramdane, “The behaviour of HSC columns under axial load,” *High-Strength Concrete, Proceeding 1*, pp. 83–89, 1993.

[50] I. K. Fang, K. C. Hong, and J. Y. Wu, “Strength and ductility of high strength tied columns,” *Proceedings of the National Science Council, Republic of China*, vol. 18, no. 1, pp. 63–74, 1994.

[51] J. H. Sørensen, L. C. Hoang, and A. Muttoni, “Validation of expressions for calculation of the strength of confined concrete,” *Background document to prEN 1992-1-1:2018*, pp. 27–32, 2018.

[52] M. Fernández Ruiz and A. Muttoni, “Shear Strength of Thin-Webbed Post-Tensioned Beams,” *ACI Structural Journal*, vol. 105, no. 3, pp. 308–317, 2008.

[53] M. Rupf, M. Fernández Ruiz, and A. Muttoni, “Post-tensioned girders with low amounts of shear reinforcement: Shear strength and influence of flanges,” *Engineering Structures*, vol. 56, pp. 357–371, 2013.

[54] M. Iqbal and D. S. Hatcher, “Post-crushing behavior of unbound concrete beams,” *Journal of the Structural Division*, vol. 101, no. 11, pp. 2303–2316, 1975.

[55] A. Kanellopoulos, “Zum unelastischen Verhalten und Bruch von Stahlbeton,” PhD Thesis, Institut für Baustatik und Konstruktion, ETH, Zürich, 86 p., 1986.

[56] E. Hognestad, “A study of combined bending and axial load in reinforced concrete members,” University of Illinois at Urbana Champaign, College of Engineering, 128 p., 1951.

[57] E. Hognestad, “Inelastic Behavior in Tests of Eccentrically Loaded Short Reinforced Concrete Columns,” *Journal of the American Concrete Institute*, vol. 49, no. 10, pp. 117–139, 1952.

[58] E. Hognestad, N. W. Hanson, and D. McHenry, “Concrete Stress Distribution in Ultimate Strengh Design,” *Journal of the American Concrete Institute*, vol. 52, no. 12, pp. 455–480, 1955.

[59] A. H. Mattock, L. B. Kriz, and E. Hognestad, “Rectangular Concrete Stress Distribution in Ultimate Strength Design,” *Journal of the American Concrete Institute*, vol. 57, no. 2, pp. 875–928, 1961.

[60] H. H. H. Ibrahim and J. G. MacGregor, “Tests of Eccentrically Loaded High-Strength Concrete Columns,” *ACI Structural Journal*, vol. 93, no. 5, pp. 585–593, 1996.

[61] S. J. Foster, M. M. Attard, and N. Kokolis, “Tie confinement in eccentrically loaded high strength concrete columns,” UNICIV Report No. R-363, The University of New South Wales, Sydney, Australia, 41 p., 1997.

[62] M. M. Attard and S. J. Foster, “Ductility of High Strength Concrete Columns,” UNICIV Report No. R-344, The University of New South Wales, Sydney, Australia, 88 p., 1995.

[63] M. Husem, S. Pul, S. E. Gorkem, and S. Demir, “The behaviour of high-strength reinforced concrete columns under low eccentric loading,” *European Journal of Environmental and Civil Engineering*, vol. 20, no. 4, pp. 486–502, 2015.

[64] E. Canbay, G. Ozcebe, and U. Ersoy, “High-Strength Concrete Columns under Eccentric Load,” *Journal of Structural Engineering*, vol. 132, no. 7, pp. 1052–1060, 2006.

[65] M. Saatcioglu, A. H. Salamat, and S. R. Razvi, “Confined Columns under Eccentric Loading,” *Journal of Structural Engineering*, vol. 121, no. 11, pp. 1547–1556, 1995.

[66] T.-H. Tan and N.-B. Nguyen, “Flexural Behavior of Confined High-Strength Concrete Columns,” *ACI Structural Journal*, vol. 102, no. 2, pp. 198–205, 2005.

[67] M. Ghazi, “Behaviour of Eccentrically Loaded Concrete Columns under Confinement,” PhD Thesis, The University of New South Wales, Sydney, Australia, 567 p., 2001.

[68] Comité Euro-International du Béton (CEB), “CEB-FIP Model Code 1990,” Thomas Telford Publishing, London, 460 p., 1993.

[69] A. Muttoni, M. Fernández Ruiz, and F. Moccia, “Strength reduction factor for concrete in compression,” *Background document to prEN 1992-1-1:2018*, pp. 9–26, 2018.

[70] EN 1990:2002, “Eurocode - Basis of structural design,” European Committee for Standardization (CEN), Brussels, Belgium, 87 p., 2002.

3.9. Annexes

3.9.1. Annex A: Structural strength reductions for material resistance accounted in codes of practice

In this annex, a number of formulations presented in codes of practice to reduce the material compressive resistance as a function of the material strength are reviewed.

3.9.1.1. European standard EN 1992-1-1:2004

The EN 1992-1-1:2004 [8] proposes a strength reduction factor η to be applied in compression zones or for axially loaded members, which consist of reducing the stress block distribution for compressive strengths larger than 50 MPa. It is defined as follows:

$$\begin{aligned} &\eta = 1.0 && \text{for } f_{ck} \leq 50 \text{ MPa} \\ &\eta = 1 - (f_{ck} - 50)/200 && \text{for } 50 \text{ MPa} < f_{ck} \leq 90 \text{ MPa} \end{aligned} \tag{3.17}$$

With respect to shear, the design concrete strength of the compression field is corrected with a global efficiency factor ν:

$$\nu = 0.6 \cdot \left(1 - f_{ck}/250\right) \tag{3.18}$$

Considering that the value 0.6 accounts for the transverse strains imposed by the lateral reinforcement [52], it results that the material strength influences the response according to the following expression:

$$\eta_{cc} = 1 - f_{ck}/250 \tag{3.19}$$

The limit of applicability of these factors is defined for characteristic compressive strengths f_{ck} between 12 MPa and 90 MPa.

3.9.1.2. Fib Model Code 2010

The *fib* MC 2010 [9] considers the same strength reduction as EN 1992-1-1:2004 [8] for compression and bending to reduce the stress block. With respect to the assessment of the strength of the compression field related to shear, the brittleness factor as presented by Muttoni [12] is applied:

$$\eta_{fc} = \left(\frac{30}{f_{ck}}\right)^{1/3} \leq 1.0 \tag{3.20}$$

This factor is applicable for characteristic compressive strengths f_{ck} between 12 MPa and 120 MPa.

3.9.1.3. ACI 318-19

The ACI 318-19 [4] proposes an equivalent rectangular compressive stress distribution (stress block method) for compression zones and it defines the concrete compressive strength as follows:

$$0.85 \cdot f_c' \tag{3.21}$$

As it can be noted, no strength reduction factor directly accounts for the increased brittleness for higher concrete strength. The ACI 318-19 [4] formulation is valid for specific concrete compressive strength f_c' above 17.2 MPa (no upper limit is defined).

3.9.1.4. Australian standard AS 3600-2018

The Australian standard for concrete structures AS 3600-2018 [6] applies a strength reduction of the concrete compressive strength in the stress block procedure as follows:

- For compression zones:

$$\alpha_2 \cdot f_c^{'} \qquad \text{with } 0.67 \le \alpha_2 = 1 - 0.003 \cdot f_c^{'} \le 0.85 \tag{3.22}$$

- For axially loaded columns:

$$\alpha_1 \cdot f_c^{'} \qquad \text{with } 0.72 \le \alpha_1 = 1 - 0.003 \cdot f_c^{'} \le 0.85 \tag{3.23}$$

These procedures are applicable for characteristic compressive strengths between 20 MPa and 100 MPa.

3.9.1.5. Chinese standard GB 50010-2010

The Chinese Code for design of concrete structures GB 50010-2010 [2] defines a strength reduction factor α_1 to be applied in the stress block method. It is defined in the following manner:

$$\begin{aligned} &\alpha_1 = 1.0 && \text{for } f_{ck} \le 32.4 \text{ MPa} \\ &\alpha_1 = 1 + 0.06 \cdot \frac{32.4 - f_{ck}}{17.8} && \text{for } 32.4 < f_{ck} \le 50.2 \text{ MPa} \end{aligned} \tag{3.24}$$

The GB 50010-2010 also considers concrete brittleness by means of the α_{c2} factor for high strength concrete. It is accounted for in f_{ck} and is defined as follows:

$$\alpha_{c2} = 1.15 - 0.0055 \cdot f_{ck} \qquad \text{for } 26.8 \text{ MPa} \le f_{ck} \le 50.2 \text{ MPa} \tag{3.25}$$

The procedures outlined are valid for characteristic compressive strengths f_{ck} between 10 MPa and 50.2 MPa.

3.9.2. Annex B: Determination of the partial safety factor of concrete for members in compression

In this annex, the justification of γ_C = 1.50 in EN 1992-1-1:2004 [8] is presented and discussed with respect to the consequences of the nonlinear relationship of the brittleness factor η_{cc} (a slightly different justification of the same partial safety factor is presented in *fib* MC 2010 [9]). The analyses and derivations presented in this Annex are based on the principles of First Order Reliability Methods (FORM) for reliability analysis.

3.9.2.1. Design resistance and limit state function

According to EN 1990:2002 [70], for a lognormal distribution of the resistance, a design value R_d can be calculated as:

$$R_d = R_m \cdot \mu_R \cdot \exp\left(-\alpha_R \cdot \beta_{tgt} \cdot V_R\right) \tag{3.26}$$

where R_m is the mean value of the resistance, calculated with mean values of the basic variables, μ_R is the bias of the resistance (average of the ratio between the actual resistance and the resistance calculated using the design equation with the assumed variables, including the model bias), α_R is the sensitivity factor for resistance (typically 0.8 [70]), β_{tgt} is the target value of the reliability index defining the required safety level (usually assumed = 3.8 for persistent and transient design situations [70]) and V_R is the coefficient of variation of the resistance.

For members in compression, according to Eq. (3.2), and accounting for the piecewise response of η_{cc}

(for values lower or higher than f_c = 30 MPa), the limit state function is defined in a piecewise manner as:

$$R = \eta_{cc} \cdot k_t \cdot \eta_{is} \cdot f_{c,cyl} \cdot A_c \qquad \text{for } k_t \cdot \eta_{is} \cdot f_{c,cyl} \leq 30 \text{ MPa} \tag{3.27a}$$

$$R = \eta_{cc,1} \cdot \left(k_t \cdot \eta_{is} \cdot f_{c,cyl}\right)^{2/3} \cdot A_c \qquad \text{for } k_t \cdot \eta_{is} \cdot f_{c,cyl} > 30 \text{ MPa} \tag{3.27b}$$

with $\eta_{cc,1}$ = (30 MPa)$^{1/3}$.

Due to the piecewise form of the limit state function, the FORM design points can locate on two different regimes and result in different formulations of the design resistance values. The design values corresponding to the two regimes of the limit state function can thus be established as:

$$R_d = \eta_{cc} \cdot k_t \cdot \frac{f_{ck}}{\gamma_C} \cdot A_c \tag{3.28a}$$

$$R_d = \eta_{cc,1} \cdot \frac{\left(k_t \cdot f_{ck}\right)^{2/3}}{\gamma_{C,1}} \cdot A_c \tag{3.28b}$$

where the in-situ concrete strength factor η_{is} and other effects not explicit in the resistance functions are implicitly considered in the partial safety factors γ_C and γ_{C1} [1].

3.9.2.2. Partial safety factor for low values of concrete strength

For low values of concrete strength, the resistance is dominated by the first regime of the limit state function (Eq. (3.27a)) and consequently the FORM design point also locates on this regime. The partial safety factor can be calculated based on equations (3.26) and (3.28a) as:

$$\gamma_C = \frac{f_{ck}}{\eta_{is} \cdot f_{c,cyl,m}} \cdot \frac{\exp\left(\alpha_R \cdot \beta_{tgt} \cdot V_R\right)}{\mu_R} \tag{3.29}$$

where the mean value of the cylinder concrete strength $f_{c,cyl,m}$ can be calculated on the basis of its coefficient of variation $V_{fc,cyl}$ and by assuming that the characteristic value (5% quantile) corresponds to the specified value (potential overstrength neglected):

$$f_{c,cyl,m} = f_{ck} \cdot \exp\left(1.645 \cdot V_{fc,cyl}\right) \tag{3.30}$$

And the bias factor μ_R results:

$$\mu_R = \mu_{\eta cc} \cdot \mu_{kt} \cdot \mu_{\eta is} \cdot \mu_{Ac} \tag{3.31}$$

Assuming that all variables in the resistance function (Eq. (3.27a)) are independent, and that their distribution is lognormal and that their coefficient of variations are small, since their influence on the resistance is linear, the coefficient of variation V_R results:

$$V_R = \sqrt{V_{\eta cc}^2 + V_{kt}^2 + V_{\eta is}^2 + V_{fc,cyl}^2 + V_{Ac}^2} \tag{3.32}$$

It has to be noted that in Eq. (3.32), the material uncertainties are covered by $V_{\eta is}$ and $V_{fc,cyl}$, the model uncertainties by $V_{\eta cc}$ and V_{kt} and the geometric uncertainties by V_{Ac}. With respect to EN 1992-1-1:2004, according to [1], the partial factor γ_C = 1.50 is justified on the basis of the following assumptions: η_{is} = 0.85, all bias factors appearing in Eq. (3.31) equal to 1.0 (μ_R = 1.0), $V_{\eta cc}$ = 0.05, V_{kt} = 0, $V_{\eta is}$ = 0, $V_{fc,cyl}$ = 0.15 and V_{Ac} = 0.05, leading to $f_{c,cyl,m}$ / f_{ck} = 1.28 and V_R = 0.166.

3.9.2.3. Partial safety factor for high values of concrete strength

For high values of concrete strength, the resistance is dominated by the second regime of the limit state function (Eq. (3.27b)). Consequently, the FORM design point also locates on this regime. Thus, the partial safety factor $\gamma_{C,1}$ in this case results:

$$\gamma_{C,1} = \left(\frac{f_{ck}}{\eta_{is} \cdot f_{c,cyl,m}} \right)^{2/3} \cdot \frac{\exp\left(\alpha_R \cdot \beta_{tgt} \cdot V_R\right)}{\mu_R} \tag{3.33}$$

With the nonlinear relationship of η_{cc}, the bias factor and the coefficient of variation of the resistance become:

$$\mu_R = \mu_{\eta cc} \cdot \left(\mu_{kt} \cdot \mu_{\eta is}\right)^{2/3} \cdot \mu_{Ac} \tag{3.34}$$

and:

$$V_R = \sqrt{V_{\eta cc}^2 + \left(\frac{2}{3}\right)^2 \cdot V_{kt}^2 + \left(\frac{2}{3}\right)^2 \cdot V_{\eta is}^2 + \left(\frac{2}{3}\right)^2 \cdot V_{fc,cyl}^2 + V_{Ac}^2} \tag{3.35}$$

Since the contribution of the coefficients of variation of the material strength is attenuated by the squared value of the exponent 2/3, the coefficient of variation of the resistance V_R is also reduced (0.122 instead of 0.166) leading of a lowered partial safety factor $\gamma_{C,1}$ = 1.37 (instead of 1.50).

3.9.3. Annex C: Database on column tests without eccentricity

The complete database on column tests under pure compression is presented in the Appendix A of this thesis.

3.9.4. Annex D: Database on column tests with load eccentricity

For the complete database on column tests with load eccentricity, refer to the Appendix B of this thesis.

3.9.5. Annex E: confinement effect in reinforced concrete columns

For the calculations presented in this paper, the contribution of the confined core on the strength of reinforced columns is assessed with the guidelines of *fib* MC 2010 [9]. In this procedure, the effective lateral compressive stress σ_{c2} is defined according to the following expressions:

- For circular cross sections confined by spiral reinforcement (Figure 3.11a):

$$\sigma_{c2} = \omega_c \cdot f_{cd} \cdot \left(1 - \frac{s}{b_c}\right) \tag{3.36}$$

- For circular cross sections confined by circular hoops (Figure 3.11b):

$$\sigma_{c2} = \omega_c \cdot f_{cd} \cdot \left(1 - \frac{s}{b_c}\right)^2 \tag{3.37}$$

- For square cross sections confined by square stirrups (Figure 3.11c):

$$\sigma_{c2} = \omega_c \cdot f_{cd} \cdot \left(1 - \frac{s}{b_c}\right)^2 \cdot \frac{1}{3} \tag{3.38}$$

- For square cross sections confined by multiple stirrups with the layout presented in Figure 3.11d:

$$\sigma_{c2} = \omega_c \cdot f_{cd} \cdot \left(1 - \frac{s}{b_c}\right)^2 \cdot \left(1 - \frac{\sum b_i^2 / 6}{b_c^2}\right) = \omega_c \cdot f_{cd} \cdot \left(1 - \frac{s}{b_c}\right)^2 \cdot \frac{2}{3} \tag{3.39}$$

- For square cross sections confined by multiple stirrups with the layout shown in Figure 3.11e:

$$\sigma_{c2} = \omega_c \cdot f_{cd} \cdot \left(1 - \frac{s}{b_c}\right)^2 \cdot \left(1 - \frac{\sum b_i^2 / 6}{b_c^2}\right) = \omega_c \cdot f_{cd} \cdot \left(1 - \frac{s}{b_c}\right)^2 \cdot \frac{7}{9} \tag{3.40}$$

Where b_c represents the width of the external stirrup measured at its centreline and b_i is the distance between longitudinal bars engaged by a stirrup corner or a cross-tie. The ω_c coefficient defined in the previous expressions is computed as follows:

$$\omega_c = \frac{A_{ss} \cdot f_{yd}}{s \cdot b_c \cdot f_{cd}} \tag{3.41}$$

Where A_{ss} represents the total cross-sectional area of the stirrups.

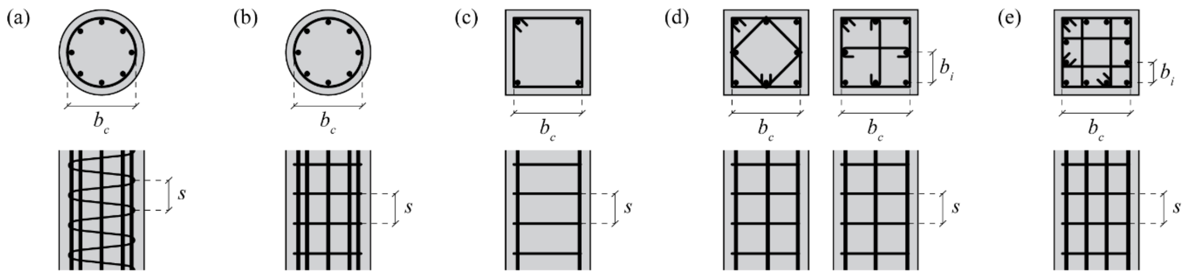

Figure 3.11: Frequent types of columns cross sections and confining reinforcement layouts: (a) circular cross section confined by spiral reinforcement; (b) circular cross section confined by circular hoops; (c) square cross section confined by square stirrups; and (d-e) square cross sections confined by multiple stirrups.

3.10. Notation

A_c : cross-sectional area of concrete

A_{cs} : cross-sectional area of concrete within the confinement reinforcement

A_g : gross cross-sectional area

A_s : cross-sectional area of the longitudinal reinforcement

E_s : modulus of elasticity of steel

F : applied force

F_c : force sustained by the concrete

F_s : force sustained by the steel reinforcement

N : axial load

N_{calc} : calculated axial load

N_{core} : axial force sustained by the concrete core

N_{cover} : axial force sustained by the concrete cover

N_s : axial force sustained by the steel reinforcement

N_{test} : measured failure load

N_{tot} : total axial force sustained by the structural member

N_u : ultimate axial force

M : moment

M_u : ultimate moment

V_R : coefficient of variation of the resistance

e : eccentricity

f_c : uniaxial compressive strength of concrete

f_c' : specific compressive strength of concrete

$f_{c,cyl}$: compressive strength of concrete cylinder

$\Delta f_{c,cyl}$: confinement contribution provided by the hoops

f_{cd} : design value of the compressive strength of concrete

f_{ck} : characteristic value of the compressive strength of concrete

f_{ct} : axial tensile strength of concrete

f_R : structural compressive resistance

f_y : mean value of the yield strength of reinforcement

$f_{y,conf}$: yield strength of confinement reinforcement

f_{yd} : design value of the yield strength of reinforcement

f_{yk} : characteristic value of the yield strength of reinforcement

$f_{y,long}$: yield strength of longitudinal reinforcement

h : depth of the cross section

k_t : strength reduction factor accounting for loading rate

x : depth of the compression zone

α_1, α_2 : strength reduction factors

α_R : sensitivity factor for resistance

β_{tgt} : target reliability index

γ_C : partial safety factor for concrete material

γ_S : partial safety factor for reinforcement

ε : strain

ε_c : concrete strain

ε_{c2} : strain at reaching the maximum compressive strength

ε_{cu2} : ultimate compressive strain in concrete

ε_{long} : strain in the longitudinal direction

ε_1 : maximum principal strain

ε_3 : minimum principal strain

η : strength reduction factor for stress block procedure

η_{cc} : strength reduction factor to account for concrete brittleness

η_D : strength reduction factor to account for reinforcement disturbances

η_i : strength reduction or enhancement factor

η_{is} : strength reduction factor to account for the difference between in-situ and control specimen compressive strength

η_t : strength reduction factor to account for time-dependent effects

η_ε : strength reduction factor to account for transverse strains

μ_R : bias factor

ν : strength reduction factor for compression field

$\rho_{s,conf}$: confinement reinforcement ratio

$\rho_{s,long}$: longitudinal reinforcement ratio

σ : stress

σ_c : concrete stress

σ_s : steel stress

σ_{c2} : effective lateral compressive stress due to confinement

ϕ : strength reduction factor

φ : concrete friction angle

ψ : rotation

Chapter 4.
Casting position effects on bond performance of reinforcement bars

This chapter is the preprint version of the article *Casting position effects on bond performance of reinforcement bars* submitted to the journal *Structural Concrete* in September 2020. The authors of this publication are Francesco Moccia (PhD Candidate), Miguel Fernández Ruiz (Senior lecturer and thesis co-director), Giovanni Metelli (Professor), Aurelio Muttoni (Professor and thesis director) and Giovanni Plizzari (Professor). The provisional reference is the following:

> F. Moccia, M. Fernández Ruiz, G. Metelli, A. Muttoni, G. Plizzari, *Casting position effects on bond performance of reinforcement bars,* Structural Concrete.

This article is the result of a collaboration between the Ecole Polytechnique Fédérale of Lausanne and The University of Brescia. It is the outcome of several joint discussions between all the authors of the paper. The work presented in this article was performed by Francesco Moccia with the exception of the sections describing the experimental program performed at The University of Brescia, written by Giovanni Metelli and Giovanni Plizzari (parts of sections 4.4 and 4.5.1). Also, Miguel Fernández Ruiz, Aurelio Muttoni, Giovanni Metelli and Giovanni Plizzari supervised the entire work, providing valuable feedback and performing several proof readings of the manuscript.

The main contributions of Francesco Moccia can be resumed as follows:

- Review of the state-of-the-art related to the effects of casting position on the bond strength.
- Casting and pull-out testing of 56 horizontal reinforcing bars with variable embedded length, concrete cover and casting height (test series ML10 and ML20).
- Development of specific loading setup for pull-out tests representative of actual bond conditions.
- Measurements of bond response using Digital Image Correlation. The measurements are resumed in the Appendix C of this thesis.
- Analysis and discussion of the test results.
- Discussion on the implications of concrete bleeding and plastic settlement on pull-out and spalling failures of horizontal and vertical reinforcement.
- Evaluation of the bond strength reductions for poor bond conditions as indicated in EN 1992-1-1:2004, *fib* MC 2010 and ACI 318-19.
- Design recommendations for the evaluation of casting position effects on bond performance.
- Evaluation of a mechanical approach for the consideration of casting condition effects on pull-out resistance.
- Production of the figures included in the article.
- Writing of the manuscript of the article, except from parts of sections 4.4 and 4.5.1 (test series BL5 described by Giovanni Metelli and Giovanni Plizzari).

4.1. Abstract

The phenomena associated with the consolidation of fresh concrete (bleeding and plastic settlement) are commonly agreed to be significant for the bond performance of reinforcement. However, rules to consider such influence for design are not consistent amongst design recommendations and may lead to notable differences. With this respect, two failure modes generally govern the bond failure, namely the spalling of the concrete cover (also called splitting failure) and the pull-out of the reinforcement. In this paper, a detailed investigation is presented on the influence of bleeding and plastic settlement on both failures modes, in an effort to understand their conceptual differences and to clarify how shall consistent design recommendations be formulated. Such investigation is based on a comprehensive experimental programme, comprising 137 pull-out tests on specimens with different casting conditions, embedment lengths, loading arrangements and concrete covers. On the basis of the test results, the phenomenological differences between pull-out and spalling failures are clarified, as well as the main influencing phenomena (particularly the potential presence of cracks and voids under the reinforcement and the mechanical properties of concrete). On that basis, a physically-consistent approach is presented to consider the casting conditions on the bond performance and failure modes.

4.2. Introduction

The structural behaviour of reinforced concrete members strongly depends on the interaction between the reinforcing bars and the surrounding concrete, which is generally referred to as rebar-to-concrete bond. Under service conditions, bond governs the deformability of structural concrete as well as the cracking development. At Ultimate Limit State, bond governs also a number of phenomena, such as anchorage, lap splices and the structural ductility.

Despite the large research efforts performed on bond-related topics, several fundamental questions still remain open. Amongst these, it can be highlighted the transfer of forces occurring at the interface between deformed reinforcement and concrete due to their contact and mechanical engagement. Such contacts are largely influenced by a series of phenomena associated with the consolidation of fresh concrete before hardening. The first effect is related to the upward flow of water during hardening (the so-called bleeding) [1] which is at the source of an enhanced porosity of the concrete located at the upper layer and of its weaker mechanical properties (Figure 4.1a). In addition, when the reinforcing bars are restrained from vertical movement, the concrete consolidation leads to the development of voids and a weaker concrete layer below top bars [2], [3], which can cause the development of internal and surface cracks at early age [4], [5] (plastic settlement phenomenon, Figure 4.1b). Therefore, the element depth, the position of the reinforcing bars, the rib orientation as well as the composition and consistency of concrete are governing factors of the concrete strength [6] and the interface properties with the reinforcement (influencing bond performance). In addition, the phenomena of bleeding and plastic settlement could affect in different manners the failure mechanisms of bond (pull-out, splitting or spalling; see Figure 4.1c-e).

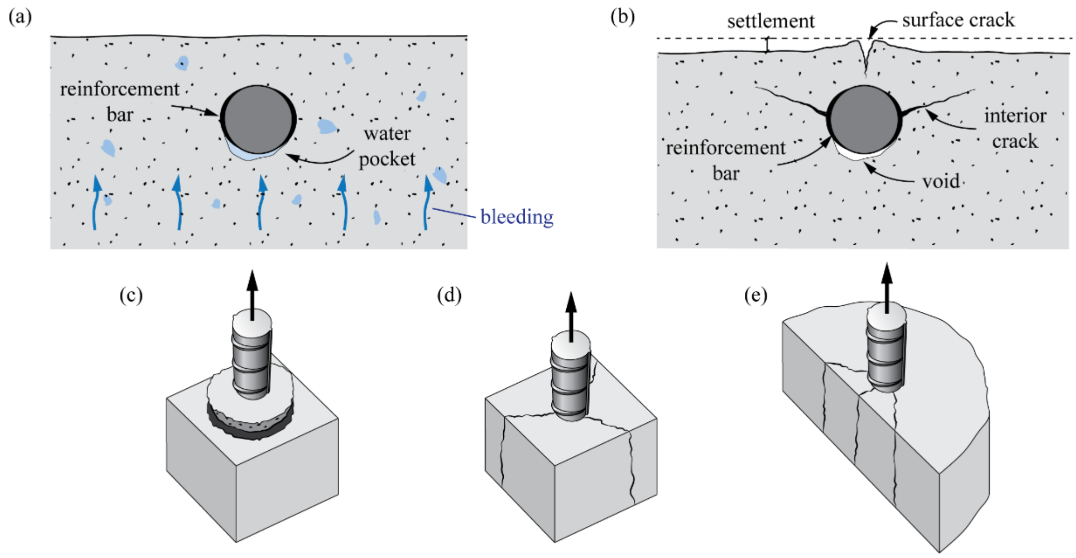

Figure 4.1: Fresh concrete behaviour during casting: (a) bleeding phenomenon; (b) effects of plastic settlement. Bond induced failure modes: (c) pull-out failure; (d) splitting failure; and (e) spalling failure.

The influence of the casting position on bond strength was already investigated in 1913 by Abrams [7], who performed pull-out tests on plain and deformed bars and observed that bars located close to the top surface exhibited lower bond resistances than those of bottom bars. In 1939, Menzel [8] investigated the influence of bar orientation and casting direction, showing that horizontal top bars presented the lowest bond strength and that vertical bars pulled-out in the opposite direction of the casting performed the best. These findings were already associated to the potential effects of bleeding and plastic settlement phenomena on bond of reinforcing bars. Similar tests were also performed by Clark [9], [10] by using both beam and pull-out specimens. His experimental programme showed that bars located in a top casting position were about two-thirds as effective as bottom reinforcement with respect to bond strength. Based on these findings, the top bar effect was first introduced in the ACI 318 building code in 1951 [11]. These observations on casting position and reinforcement orientation were later validated in Europe by Rehm [12].

The relationship between concrete consistency and casting position has also been thoroughly investigated in the past century. For instance, Welch and Patten [13] measured the settlement of mixes having different consistencies and established a correlation between increasing settlement and reduced bond strength. Additional studies (refer for instance to Jirsa and Breen [14], Zekany et al. [15], Donahey and Darwin [16]) highlighted that increased concrete consistency (high slumps) had a negative effect on the bond strength of top-cast bars. Also, Brettmann and co-authors [17] observed that the longer the concrete remained plastic (for instance due to low temperatures), the lower the bond strength of reinforcement located near the free surface during casting.

More recent studies focused on the role of casting position effects in the case of self-compacting concrete (SSC) and high-strength concrete (HSC). These studies have shown a less marked top-bar effect for SCC when compared to conventionally-vibrated concrete, which has been attributed to the better stability and cohesion of the paste [2], [18]–[21]. With respect to HSC, several researchers have noticed that higher strength concrete tend to show a lower top-cast effect due to the reduced water content and presence of admixtures [22]–[25]. Recently, a detailed and extensive review of studies investigating the effects of casting position on lap and anchorage strength was performed by Cairns [6].

In design codes, the top-bar effect is considered in most cases for calculation of the bond strength of embedded reinforcement [26]–[28]. This is typically performed by defining regions of good or poor bond conditions. For instance, EN 1992-1-1:2004 [26] considers good bond conditions those of a reinforcement having an inclination between 45°-90° with respect to the horizontal surface or bars inclined less than 45° which are up to 250 mm above the formwork or at least 300 mm below the free-surface during casting (Figure 4.2a). All other locations are considered as having poor bond conditions and the bond strength is reduced by 30%, thus causing an increase of the anchorage length of 43% with respect to the bottom bars. A similar recommendation is also proposed in *fib* MC 2010 [27]. The top-bar effect is also considered in the provisions of ACI 318 [28] which defines as poor bond condition those of horizontal reinforcing bars or laps having more than 305 mm (12 inches) of fresh concrete beneath them (Figure 4.2b). In this case, ACI 318-19 [28] proposes an increase of the development length of 30%.

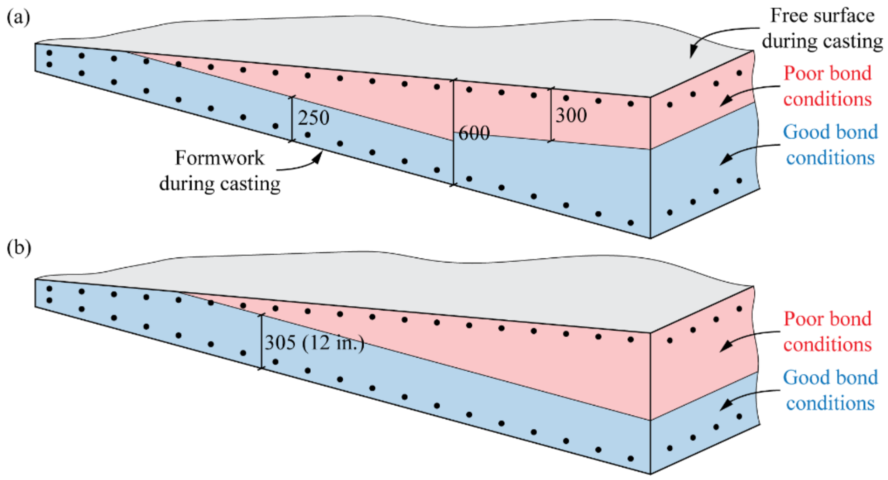

Figure 4.2: Definition of locations with good and poor bond conditions as function of the member's depth according to: (a) EN 1992-1-1:2004 [26] and *fib* MC 2010 [27]; and (b) ACI 314-19 [28] (dimensions in [mm]).

Looking at the state-of-the-art literature and at design recommendations, it can be noted that no apparent distinction is performed on the influence of casting effects on the various potential failure modes due to bond, such as pull-out (Figure 4.1c) and splitting or spalling (Figure 4.1d-e respectively) [29]–[31]. This may however be relevant, as the failure modes are potentially sensitive in a different manner to the effects of bleeding (associated mostly to a reduction of mechanical properties of concrete and the presence of pores under the bar) and plastic settlement (associated mostly to the presence of voids under the reinforcement and inclined cracks). In order to provide an answer to this question and to define more comprehensive rules for the influence of casting conditions on bond, a joint research programme has been carried out by the Ecole Polytechnique Fédérale de Lausanne (Switzerland) and the University of Brescia (Italy). This research comprises an experimental campaign on 137 specimens tested using different loading setups, embedment lengths and values of the concrete cover. On the basis of these tests, a number of phenomenological conclusions are derived, leading eventually to define a set of practical and simplified design rules.

4.3. Influence of casting position on bond response

4.3.1. Phenomena before concrete hardening

As previously described, two phenomena developing in fresh concrete can potentially influence the interface between concrete and reinforcement bars as well as concrete properties and local development of cracking. These phenomena refer to the migration of water to the top surface (bleeding, Figure 4.1a) as well as to the plastic settlement of fresh concrete (Figure 4.1b).

With respect to concrete bleeding, cavities or voids form under solid bodies (like coarse aggregates and bars) [3], reducing the mechanical properties of concrete (Figure 4.3a, [32]). In particular, the reduction of tensile strength is relevant for the bond strength of reinforcement, notably with reference to the splitting or spalling resistance of the concrete cover. Regarding plastic settlement, it is also a result of the consolidation process of fresh concrete which behaves as a saturated soil [1] and is normally estimated as some millimetres per meter of depth [3], [33], [34]. Concrete settlement does not have any significant influence on the properties of fresh concrete provided that its movement is unrestrained. This is however not the case in regions near longitudinal reinforcement bars, that are normally fixed to the stirrups or supported by spacers, leading to continuous voids below the reinforcement [2], [3] (progressing also in a sub-horizontal manner in the form of inner cracks at the sides of the bar [4] and also of surface cracks, see Figure 4.1b). It can be noted that the size of the void below the bar is generally smaller than the total settlement [3], as the concrete viscosity is low right after pouring of the concrete and this prevents the development of voids at early stages. With respect to bond, the presence of cavities under the bars reduces the bar-to-concrete contact area and, thus, their potential mechanical engagement (limiting the transfer of forces [2]).

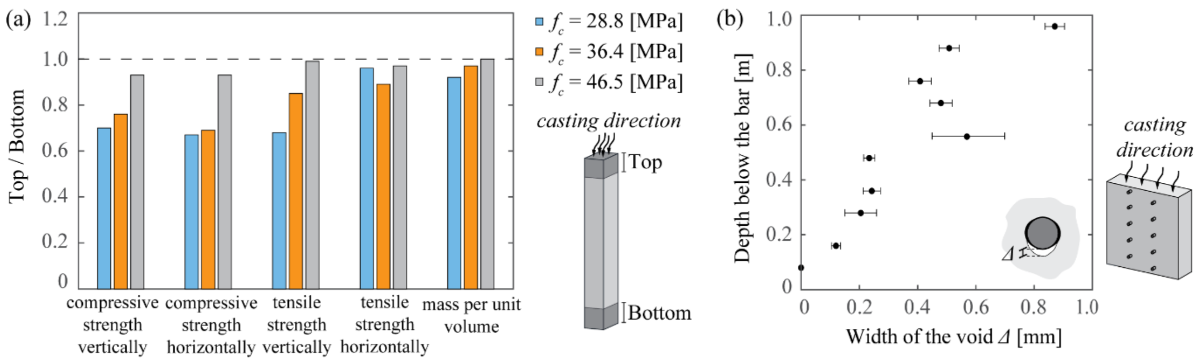

Figure 4.3: Effects of fresh concrete behaviour on performance of hardened concrete: (a) ratios between the measured properties at top and bottom of columns for different concrete mixes (adapted from Giaccio and Giovambattista [32]); (b) average thickness of the void under bars placed at different depths in a wall (adapted from Moccia et al. [3]).

4.3.2. Implications of casting conditions on pull-out resistance

The presence of voids (associated to bleeding and plastic settlement) developing under horizontally-oriented bars due to the reduction of potential contacts between ribs and the surrounding concrete [30] may favour bar pull-out (Figure 4.4a-c). Detailed measurements of the size of such voids have been performed by different researchers by means of tomography [3] or video-microscope [2], with sizes increasing almost linearly with respect to the depth of concrete under the reinforcement (with values up to 1.0 mm for depths of 1 m under the bar, see Figure 4.3b and Figure 4.5b). The pull-out strength, as experimentally observed by Castel et al. [2], is influenced by the presence of such voids, with decreasing values of the pull-out strength for increasing size of the voids (Figure 4.5; prisms tested according to Rilem recommendations [35]).

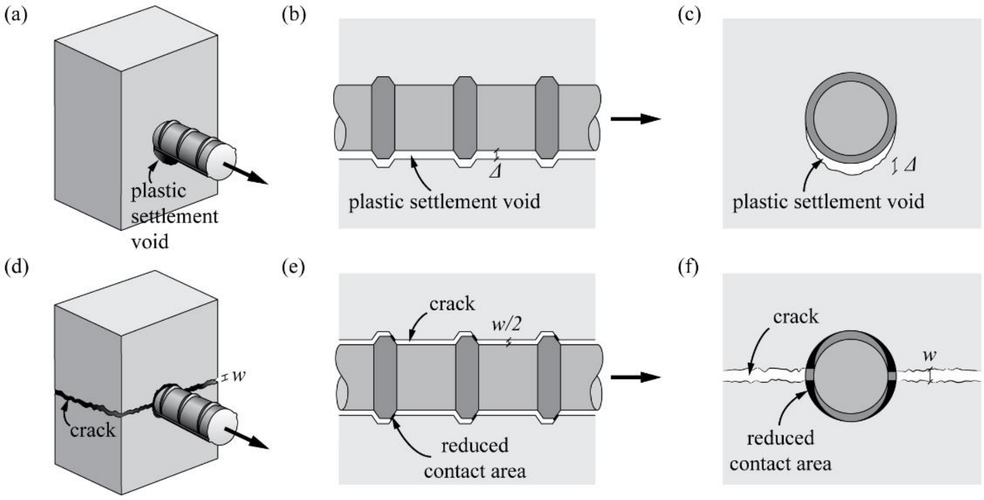

Figure 4.4: Bond behaviour in disturbed conditions: (a) pull-out test in presence of plastic settlement void; (b) reduced contact area due to the void underneath the reinforcement; (c) cross-sectional view of the bond conditions in case of plastic settlement voids; (d) pull-out test in cracked concrete; (e) reduced contact area in presence of a crack parallel to the reinforcement; (f) cross-sectional view of the bond interfaces in cracked conditions.

Based on these observations, the influence of voids under the reinforcement on the bond response can be assumed to be analogous to the influence of cracks developing parallel to the reinforcement (Figure 4.4d). As presented in Figure 4.4e-f (refer to Brantschen et al. [36]), for increasing openings of cracks parallel to the bars, the contacts between the ribs and the surrounding concrete are reduced and, therefore, forces that can be transferred by bond are limited. Despite the differences between the two cases (shape of the void due to settlement or crack), both phenomena present a similar disturbance in the bar-to-concrete contact.

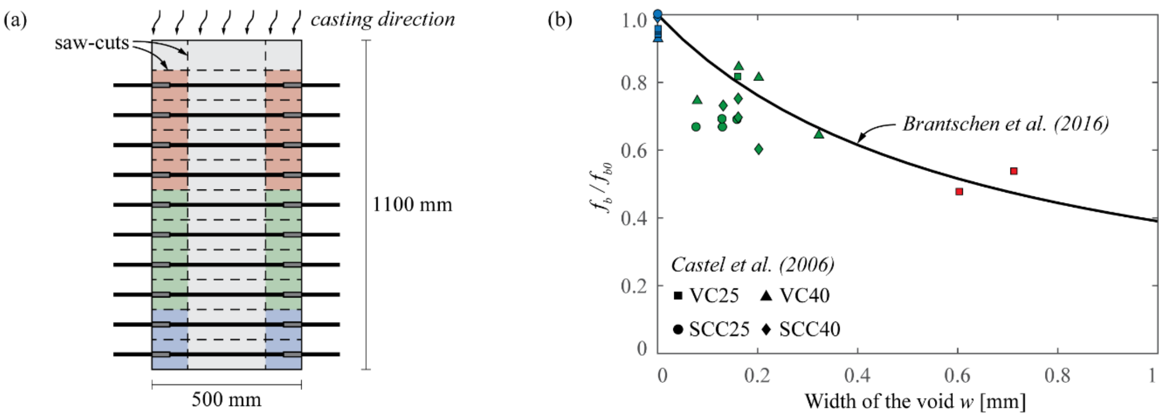

Figure 4.5: Influence of casting position effects on bond strength, pull-out tests from Castel et al. [2]: (a) specimens' geometry; (b) relative bond strength as function of the width of the voids under the bars and their location within the structural member (red: top region; green: middle region; blue: bottom region) and model according to Brantschen et al. [36].

A detailed analysis of the influence of longitudinal cracking on the bond strength was performed by Brantschen et al. [36]. By means of a simple mechanical model, it was shown that the reduction on the bond strength was dependent on the width of cracks parallel to the bars [36] and also associated to the depth of the ribs and their geometry (characterized by the bond index of the bar, f_R, and a parameter, κ_f, depending on the number of lugs per rib and geometry properties). This dependency can be expressed in terms of the following expression [36]:

$$\frac{f_b}{f_{b0}} = \frac{1}{1 + \frac{\kappa_f}{f_R} \cdot \frac{w}{\phi}} \tag{4.1}$$

where f_b refers to the bond strength, f_{b0} to the bond strength under uncracked condition, w to the crack opening and ϕ to the bar diameter. Such approach, applied to the tests of Castel et al. [2], shows consistent results, see Figure 4.5b. In this Figure, the measured depth of the voids under the bars are assumed to be equal to the crack width and f_{b0} refers to the bond strength without voids. In addition, the recommended value $\kappa_f = 1.5$ is adopted for a typical rib geometry [36] and a bond index (f_R) equal to 0.08 (usual value for a bar diameter of 12 mm [5], as also measured in tests presented later in this manuscript).

A similar study to that of Castel et al. was also performed by Parra [37] who carried out pull-out tests on horizontal bars located at different depths, with cubic prisms saw-cut from a 1.2 m-high columns (Figure 4.6a). In this study, the top-bar effect was studied for both conventional concrete (NC, Figure 4.6b) and self-compacting concrete (SCC, Figure 4.6c).

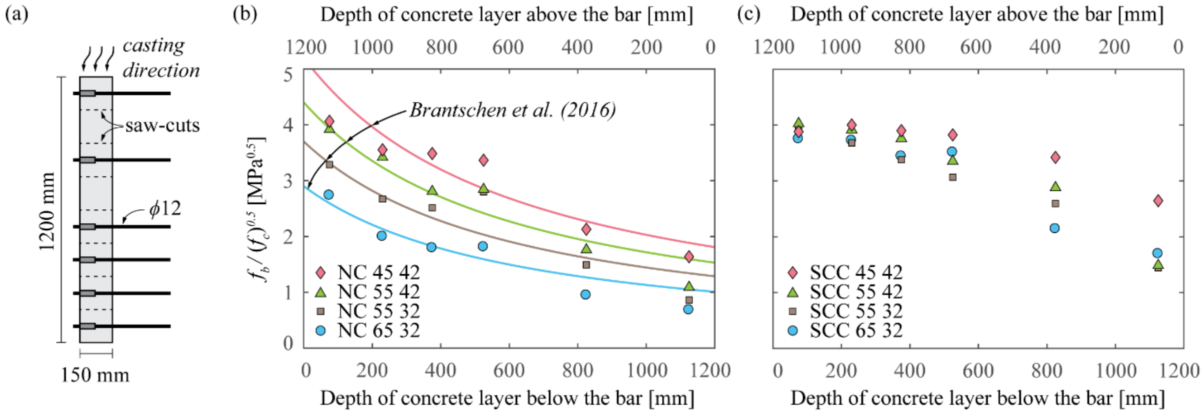

Figure 4.6: Normalized bond strength as function of the concrete depth above and below the bars, results from Parra [37] and model according to Brantschen et al. [36]: (a) specimens' geometry; (b) results of conventional concrete prisms; and (c) results of prisms with self-compacting concrete.

As shown in Figure 4.6b, conventional concrete exhibits a gradual reduction of the bond strength with increasing depth below the reinforcing bars (as for Castel et al. [2]). Also in this case, the model proposed by Brantschen et al. [36] provides good agreement with the experimental results, assuming a settlement of 1 mm/m for the calculation of the width of the void ($\kappa_f = 1.5$ and $f_R = 0.08$ for 12 mm bar diameter). On the other hand, the SCC specimens (Figure 4.6c) do not exhibit any strength reduction for small depth of concrete below the bars (h < 300 mm). Such conclusion is in agreement with the literature indicating a less marked top-bar effect for SCC ([2], [18]–[21]). This can be justified by a reduction of voids under the bars for moderate concrete depths (and higher hydrostatic pressure generated by the concrete above the bar) when a SCC is used, and shows that the calculation of the void depth (w) to be used in Eq. (4.1) is not straightforward. Beside the settlement gradient, also the diameter of the bar and the concrete rheology, which depends on pressure and viscosity before hardening, can play a major role.

The previous considerations on the disturbance introduced by voids under the bars are also in agreement with respect to the response of vertically-oriented bars, which show a milder effect associated to the casting position [2]. This is due to the fact that, for vertically-oriented bars, the voids can only be created under the ribs, which also explains the enhanced resistance of vertical bars pulled-out upwards and a softer behaviour for bars pulled downwards [5], [8], [12].

4.3.3. Implications of casting conditions on spalling failure

Concerning the spalling phenomenon, governing bond behaviour of bars near to the surface (refer to the failure mode of Figure 4.1e), its response is strongly dependent on the tensile strength of concrete. With this respect, bars located near to the top surface may exhibit a poorer performance as the voids under the coarse aggregates originated by bleeding (more porous matrix) have a detrimental influence on the concrete mechanical properties in the upper layers of the concrete [32]. In addition to this phenomenon, the plastic settlement may also have a detrimental influence on the spalling resistance. This is justified by the internal cracks developing at the sides of the bar (Figure 4.1b), which can be considered as crack initiators for a spalling failure mechanism (Figure 4.1e).

4.4. Experimental programme

The effects of bleeding and plastic settlement on the bond strength are investigated in this section within an experimental programme comprising two types of tests. The first type corresponds to pull-out tests performed with a short embedded length ($l_b = 5\phi$). These tests are addressed at the effect of the casting position on the local bond behaviour. The second type consists of pull-out tests on bars near horizontal surfaces and having an anchorage length longer than 10 times the bar diameter, aimed at investigating spalling failures and their transition to pull-out failures.

4.4.1. General overview

A number of parameters were varied in the different tests performed: the casting height, the bond length, the bar diameter, the cover of the bars and the concrete consistency. For this purpose, three different series of specimens were cast:

1. Series BL5 (Figure 4.7a) consisted of nine sets of pull-out tests performed on concrete prisms with three different bars diameters (12, 16 and 20 mm). In order to reproduce standard Rilem test conditions [35], the columns had a square section with the side and the height equal to 10ϕ and 30ϕ, respectively (see Figure 4.7a). In each column, three embedded bars were accommodated having a bond length $l_b = 5\phi$ and an increasing depth of concrete below the bar axis equal to 5ϕ, 15ϕ and 25ϕ, respectively. In order to ensure an embedded length equal to 5ϕ, a plastic sleeve was placed around half of the length of the bar (Figure 4.7a). The resulting concrete cover (c) was kept constant and equal to 4.5ϕ, as in a standard Rilem pull-out test. Each of the nine sets of tests consisted of three columns, leading to a total number of nine pull-out tests for each bar diameter (81 tests in total). All tests were performed with normal strength concrete, but the consistency class of the concrete was varied from S3 to S5 [38]. All columns were cast vertically with the bars in a horizontal position (perpendicularly to the casting direction).
2. Series ML10 (Figure 4.7b-c) consisted of two concrete specimens with straight transverse steel bars. Both specimens were 0.3 m-deep and their width corresponded to the bond length of the bars, which was set to 10ϕ. The first specimen (Figure 4.7b) contained ϕ20 bars while the second one (Figure 4.7c) accommodated ϕ14 bars. The bars for the pull-out tests were arranged in two horizontal layers, one near the top surface while the second near to the bottom surface. In addition, the concrete cover was varied from a case in which the reinforcement had no concrete cover ($c = 0$) to a case in which the cover corresponded to 2ϕ. The spacing between the bars was kept constant and equal to 15ϕ. Finally, both specimens contained one longitudinal reinforcement bar (ϕ14 mm or ϕ20 mm) placed at the axis of the girders (identical diameter as

the other bars) in order to control potential vertical cracking.

3. Series ML20 (Figure 4.7d-e) consisted of two tapered specimens with variable depth, ranging from 0.15 m to 0.4 m high. Both specimens had straight reinforcing bars that were placed near the upper and bottom surface. Similar to series ML10, the first specimen (Figure 4.7d) contained ϕ20 bars while the second one (Figure 4.7e) accommodated ϕ14 bars. The ML20 series was characterized by a bond length of 20ϕ, which also defined the width of the specimen. The concrete cover was kept constant and equal to c/ϕ = 1.25 and the spacing of the bars was set to 20ϕ. Finally, six longitudinal bars (ϕ14 mm or ϕ20 mm) were arranged near to the top and bottom layers of tested bars to reproduce the transverse reinforcement commonly encountered in practice and, also, to avoid uncontrolled propagation of cracks.

In all series, the reinforcing bars were fixed to the vertical formwork to avoid their movement and settlement during casting and concrete consolidation. In all specimens, the bars were arranged with the ribs pointing towards the vertical direction. Detailed information on the geometry of each test is given in Table 4.1 (series BL5) and Table 4.2 (series ML10 and ML20). The name of each test is composed by the series name (BL or ML), followed by the bonded length of the bars (L5, L10, L20), by the diameter of the anchored bar (D12, D14, D16, D20) and the specimen number.

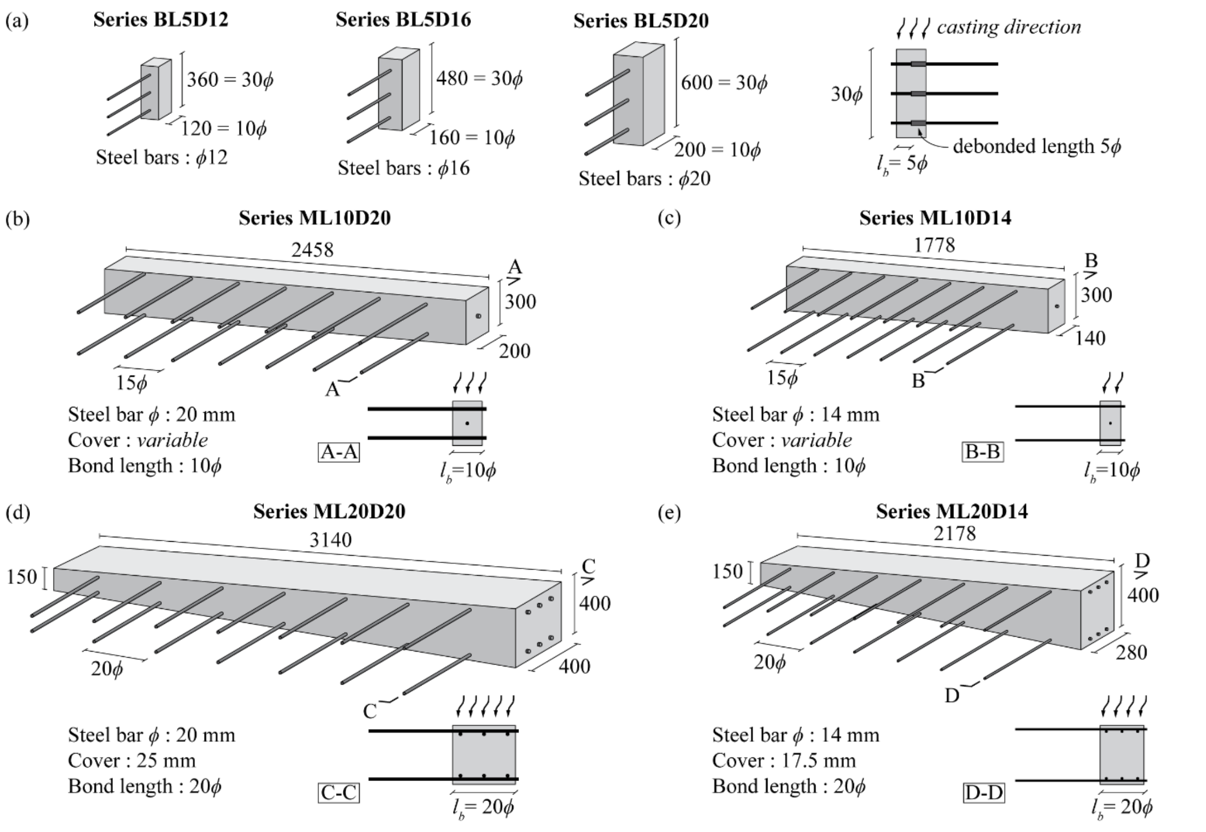

Figure 4.7: Geometry and reinforcement of the investigated series (dimensions in [mm], casting direction vertical): (a) prisms with ϕ12, ϕ16 and ϕ20 bars and short bond length of 5ϕ (series BL5); (b) beam with ϕ20 bars and variable concrete cover (series ML10D20); (c) beam with ϕ14 bars and varying concrete cover (series ML10D14); (d) tapered beam with ϕ20 bars (series ML20D20); and (e) tapered beam with ϕ14 bars (series ML20D14).

Table 4.1: Properties and main results of test series BL5 (D12 corresponds to a 12-mm diameter bar, D16 to a 16-mm diameter bar and D20 to a 20-mm diameter bar, *h*: depth of concrete beneath the bar, f_b: average bond strength for three samples, values in brackets refer to the coefficient of variation, cover for all specimens equal to 4.5 bar diameters, 1) one specimen with results having a relative deviation greater than 30% within the same series was neglected).

Series	Specimen	Position	*h* [mm]	f_b [MPa]					
				S3		S4		S5	
BL5D12	1-27	bottom	60	24.13	(2.3%)	21.81	(11.6%)	20.9	(7.2%)
		middle	180	16.26	(3.6%)	15.74	(17.0%)	12.90	(10.4%)
		top	300	12.38	(5.4%)	12.49 1)	(9.0%)	8.16 1)	(8.4%)
BL5D16	27-54	bottom	80	23.28	(4.2%)	23.85	(1.8%)	19.28	(7.3%)
		middle	240	15.90	(11.7%)	15.03	(5.9%)	14.11	(6.9%)
		top	400	12.47	(14.9%)	12.14	(1.5%)	9.93	(9.9%)
BL5D20	55-81	bottom	100	20.22	(2.5%)	21.01	(6.8%)	17.68	(8.5%)
		middle	300	14.31	(11.5%)	13.89	(10.9%)	11.39	(2.9%)
		top	500	8.94	(5.7%)	9.32	(10.1%)	7.07	(2.7%)

Table 4.2: Properties and main results of test series ML10 and ML20 (D20 corresponds to a 20-mm diameter bar and D14 to a 14-mm diameter bar, *c*: concrete cover, *h*: depth of concrete under the bar, f_b: bond strength, *S*: spalling failure mode, *P*: pull-out failure mode).

Series	l_b / ϕ	ϕ [mm]	*c* [mm]	c/ϕ	Top bars				Bottom bars			
					#	*h* [mm]	f_b [MPa]	Failure mode	#	*h* [mm]	f_b [MPa]	Failure mode
ML10D20	10	20	0	0	1	290	1.69	*S*	8	10	3.14	*S*
			5	0.25	2	285	2.09	*S*	9	15	3.13	*S*
			10	0.50	3	280	3.18	*S*	10	20	3.86	*S*
			15	0.75	4	275	3.31	*S*	11	25	4.82	*S*
			20	1.00	5	270	4.37	*S*	12	30	4.96	*S*
			30	1.50	6	260	4.90	*S*	13	40	5.96	*S*
			40	2.00	7	250	5.72	*P*	14	50	-	-
ML10D14	10	14	0	0	15	293	-	-	22	7	4.35	*S*
			3.5	0.25	16	290	3.72	*S*	23	11	4.80	*S*
			7	0.50	17	286	4.17	*S*	24	14	5.16	*S*
			10.5	0.75	18	283	5.46	*S*	25	18	5.59	*S*
			14	1.00	19	279	5.42	*S*	26	21	6.29	*P*
			21	1.50	20	272	4.45	*P*	27	28	8.06	*P*
			28	2.00	21	265	5.28	*P*	28	35	7.57	*P*
ML20D20	20	20	25	1.25	1	140	4.22	*S*	8	35	5.57	*S*
					2	173	3.93	*S*	9		6.11	*S*
					3	207	3.94	*S*	10		5.82	*S*
					4	240	4.27	*S*	11		5.58	*S*
					5	273	4.04	*S*	12		5.88	*S*
					6	307	4.36	*S*	13		6.86	*S*
					7	340	4.16	*S*	14		6.25	*S*
ML20D14	20	14	17.5	1.25	15	149	5.09	*S*	22	25	7.25	*S*
					16	183	5.14	*S*	23		7.24	*S*
					17	217	5.03	*S*	24		7.15	*S*
					18	251	5.78	*S*	25		7.16	*S*
					19	284	5.90	*S*	26		6.99	*S*
					20	318	5.64	*S*	27		7.34	*S*
					21	352	5.65	*S*	28		7.22	*S*

The dimensions of the specimens (in particular their height) and the position of the tested bars (with respect to the casting direction) were selected to cover a large range of practical situations. Figure 4.8 provides an overview of the tests and compares them to the poor or good bond conditions defined by EN 1992-1-1:2004 [26] and *fib* MC 2010 [27]. It can be noted that series BL5 contains specimens with clear poor and good bond conditions as well as specimens in the region of transition between these conditions. Furthermore, the top bars of series ML10 and ML20 can be in good or poor bond conditions as well as in the transition region between them (all bottom bars of series ML10 and ML20 correspond to good bond conditions).

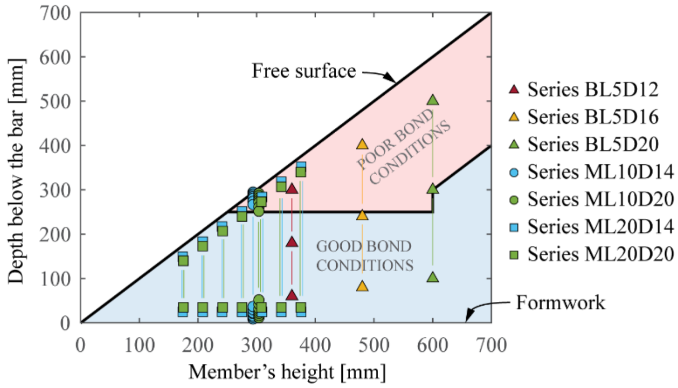

Figure 4.8: Casting positions of the experimental programme with respect to the good and poor bond conditions as defined in EN 1992-1-1:2004 [26] and *fib* MC 2010 [27].

4.4.2. Materials

The specimens of series BL5 were cast in groups of nine for each consistency class with concrete mixed on-site. Each mixture had a constant water-to-cement ratio and the same percentage of aggregates (with a maximum aggregate size of 20 mm). The consistency of fresh concrete was varied by modifying the amount of superplasticizer, leading to three levels of slump (140 mm, 190 mm and 235 mm), corresponding to the consistency classes S3, S4 and S5 [38]. With respect to series ML10 and ML20, they were cast each one with the same batch of concrete, by using standard ready-mix concrete provided by a local supplier. For these series, the maximum aggregate size was 16 mm and cement CEM II/B-M (T-LL) 42,5N was used (in compliance with [39]). In all cases, the concrete was manually poured and vibrated in two consecutive layers (according to [40]). Slumps tests were carried out at each casting and additional flow tests were also done for series ML10 and ML20, following the recommendations of [38], [41]. Concrete composition and consistency are listed in Table 4.3. Once the casting was completed, plastic sheets were placed on the upper surface of the specimens to provide appropriate curing conditions for at least two weeks [40] and were kept under standard laboratory conditions thereafter (approximately temperature of 21°C and relative humidity of 50%).

Table 4.3: Concrete properties.

Series	*c* [kg/m³]	*W/C* [-]	Aggregates [kg/m³] 0/4	4/8	8/16	8/20	Retarder [kg/m³]	Superpl. [kg/m³]	Slump [mm]	Flow [mm]	$f_{c,cyl}$ [MPa]	CoV [%]
BL5	350	0.51	1002	183	-	640	-	-	142 (S3)	-	33.9	7.0
							-	0.042	190 (S4)	-	32.2	2.9
							-	0.065	235 (S5)	-	29.0	2.2
ML10	344	0.53	830	380	671	-	0.95	1.30	200 (S4)	515 (F4)	41.1	2.9
ML20	340	0.57	819	375	674	-	1.02	1.36	120 (S3)	440 (F3)	35.7	3.7

Control specimens were also cast from the same batches of the specimens. For series BL5, cubes were used as control specimens (150 mm side), while cylinders (160 mm diameter and 320 mm high) were used for series ML10 and ML20. The control specimens were stored under identical ambient conditions and were tested in compression during the experimental programme. With respect to series BL5, the cylinder strength estimated on the basis of the control specimens ($f_{cm,cyl} = 0.83 \cdot f_{cm,cube}$) varied between 29 to 34 MPa at the day of testing of the pull-out specimens. For series ML10 and ML20, the concrete cylinder strength ($f_{c,cyl}$) at the day of testing (of the different specimens) varied between 36 and 41 MPa (see details in Table 4.3).

In addition, tensile tests were performed on the steel bars to characterize their response (in accordance with [42]). The ϕ12 and ϕ14 bars were made with cold-worked steel, while the ϕ16 and ϕ20 bars were made with hot-rolled steel. The average values of the yield strength (f_y), the ultimate strength (f_u) and the strain at maximum stress (A_{gt}) are summarized in Table 4.4. The surface of the bars was also laser-scanned to obtain a precise measurement of their profile in order to determine their relative rib area (f_R in Table 4.4).

Table 4.4: Reinforcing steel properties.

Series	Bar diameter [mm]	f_y [MPa]	f_u [MPa]	f_R	A_{gt} [%]
BL5	12	519	627	0.081	16
	16	530	654	0.081	12
	20	507	611	0.072	15
ML10 / ML20	14	518	554	0.062	7
	20	519	628	0.072	12

4.4.3. Instrumentation and setup

Two different test setups were designed to perform the pull-out tests. The setup shown in Figure 4.9a was used for the test series BL5, similar to the arrangement proposed by Rilem [35] for pull-out tests of short embedded length bars (5ϕ). The load was applied to the bar by means of a hydraulic jack pushing against a mechanical socket fixed to the bar end with a set of screws. A 2 mm-thick teflon sheet was placed between the bearing surface of the prism and the load cell to reduce friction between the surfaces. During the test, a Linear Variable Differential Transformer (LVDT) was fixed to the unloaded-end to measure its slip (δ_u), while the load was recorded by means of a load-cell placed between the jack and the bearing surface of the prism.

An adjustable steel frame (Figure 4.9b) was built to perform the pull-out tests of series ML10 and ML20. The frame was designed to be adapted to the different spacing between bars (15ϕ in series ML10, and 20ϕ in series ML20) and its supports were placed at a certain distance from the pulled bar (sufficiently spaced in order not the interfere with potential conical cracks due to bond according to Goto [43]). In addition, a hinge was placed near the retaining wedge to avoid transferring flexural moments in the bar. A loading cell and a LVDT were arranged in order to record the load-displacement curve of each specimen. The LVDT was placed at the unloaded-end of the bar, as shown in Figure 4.9b. All tests (BL5, ML10, ML20) were displacement-controlled, with a typical duration up to maximum load of approximately 3 min.

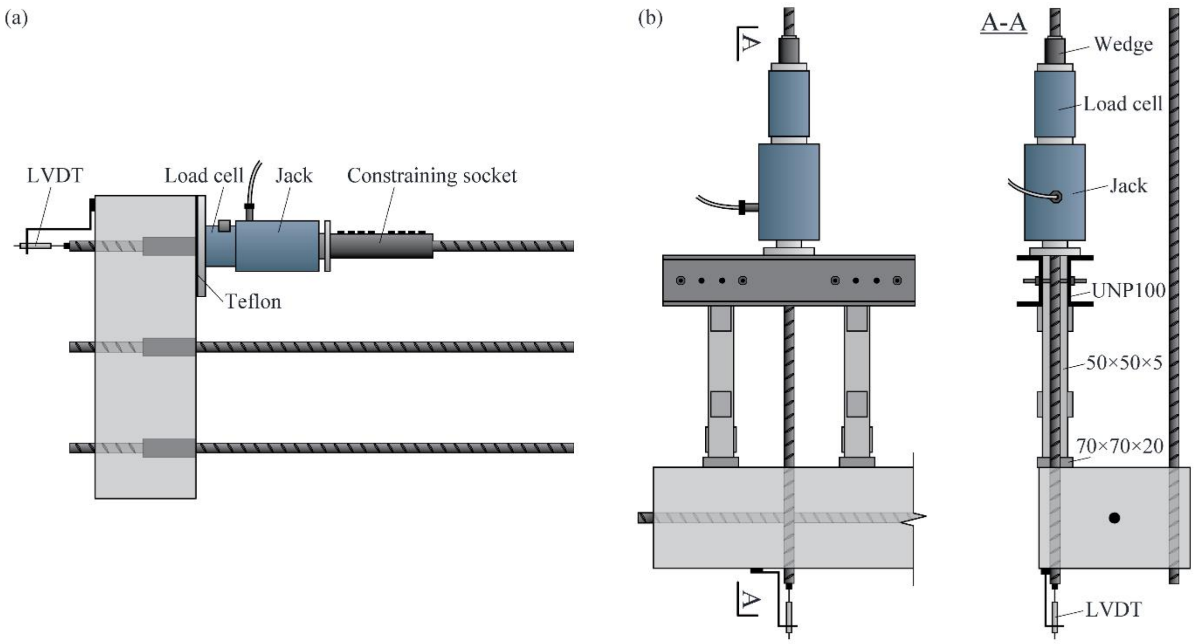

Figure 4.9: Testing and measuring devices for the pull-out tests: (a) setup for series BL5; and (b) setup for series ML10 and ML20.

4.5. Experimental results

A summary of the measured bond strength (f_b) and of the observed failure mode for each test is presented in Table 4.1 and Table 4.2. The results are discussed in detail in this section.

4.5.1. Short pull-out tests

The test on specimens with short embedded length (BL5, bonded length equal to 5 times the diameter of the bar) are aimed at characterizing the effect of the casting position on the local bond response of the bars. Since short anchorages (nominal bonded length = 5ϕ) are considered, the bond stress (τ) can be assumed to be uniformly distributed along the surface of the rebar in contact with concrete, according to the following equation:

$$\tau = \frac{P}{\pi \cdot \phi \cdot l_b} \tag{4.2}$$

where P refers to the applied load, ϕ to the nominal bar diameter and l_b to the nominal bonded length (equal to 5ϕ).

Most of the specimens failed by pull-out with the exception of some specimen at the bottom layer, which showed a splitting failure developing a horizontal crack on a longitudinal plane including the bar axis (refer to Figure 4.10b). Table 4.1 presents the average bond strength (f_b) for each series, defined as the maximum average bond stress (τ) recorded during the test. This value varied from 24 MPa (for the smallest bar diameter equal to 12 mm, bottom position during casting and a concrete consistency class S3) to 7 MPa (for the largest bar diameter equal to 20 mm, top position during casting and a concrete consistency class S5).

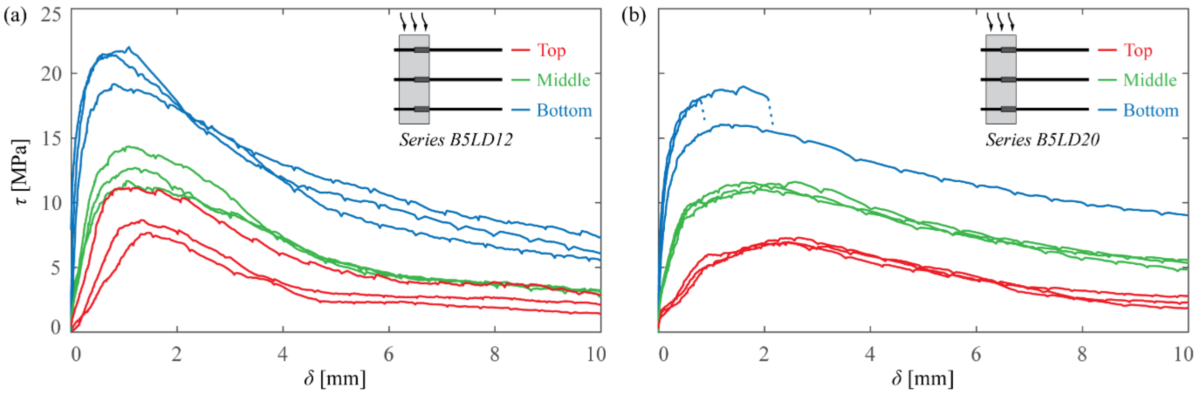

Figure 4.10: Bond-slip relationship of: (a) series BL5D12; and (b) BL5D20 with concrete consistency S5.

A comparison of the bond-slip response (where the slip δ is measured at the unloaded end) for the consistency class S5 is shown in Figure 4.10. As it can be observed, the overall strength and response are significantly influenced by the casting position, with higher strength and stiffness associated to higher distances from the top surface during casting. Also, a size effect on the strength is observed, with higher bond strength for lower bar diameters [44].

The bond strength (f_b) is also plotted in Figure 4.11a versus the depth (h) of concrete below the bar axis (for comparison purposes, test results are normalized by the square root of the compressive strength, $f_b / f_{cm}^{0.5}$). The results show a consistent reduction of bond strength of the top bars (poor bond condition) up to 60% with respect to the bottom bars (good bond condition). Such bond decrease is similar for all consistency classes and bar diameters, as shown in Figure 4.11b.

Referring to the bond stiffness, Figure 4.11c shows the bond stress ($\tau_{0.1}$) measured at an unloaded end slip of 0.1 mm (this bond stress can be considered as an indication of bond stiffness and is relevant for the serviceability limit state, since a crack width of about 0.2 mm is typically considered as a representative value). The average experimental results of each series are plotted against the depth of concrete below the bar (h) for all consistency classes (S3, S4 and S5). As for the bond strength, the bond stiffness reduces significantly when the bars are closer to the top surface (increasing depth h below the bar). Such reduction can be up to 90% for a bar diameter of 12 mm in specimens having S5 consistency class (Figure 4.11c). In general, it is observed that the reduction of the bond stiffness is higher for smaller bar diameters and higher workability of fresh concrete. This result is consistent with the presence of voids under the rebars which mainly influences bars with smaller diameter and, consequently, smaller ribs.

Finally, in Figure 4.11d the unloaded end slip at the peak bond stress (δ_{peak}) is plotted as a function of the concrete depth (h). These results may provide information on the secant stiffness at the peak stress of the bond-slip curve and, thus, on the capability of the bar to redistribute stresses over the bond length at ultimate limit state. It should be observed a trend of the slip to increase linearly from 1.0 mm up to 2.2 mm for a depth of concrete below the bar varying from 60 mm to 500 mm, respectively. Bars having larger diameter showed greater slip at the peak bond strength while no clear influence of consistency class is evident.

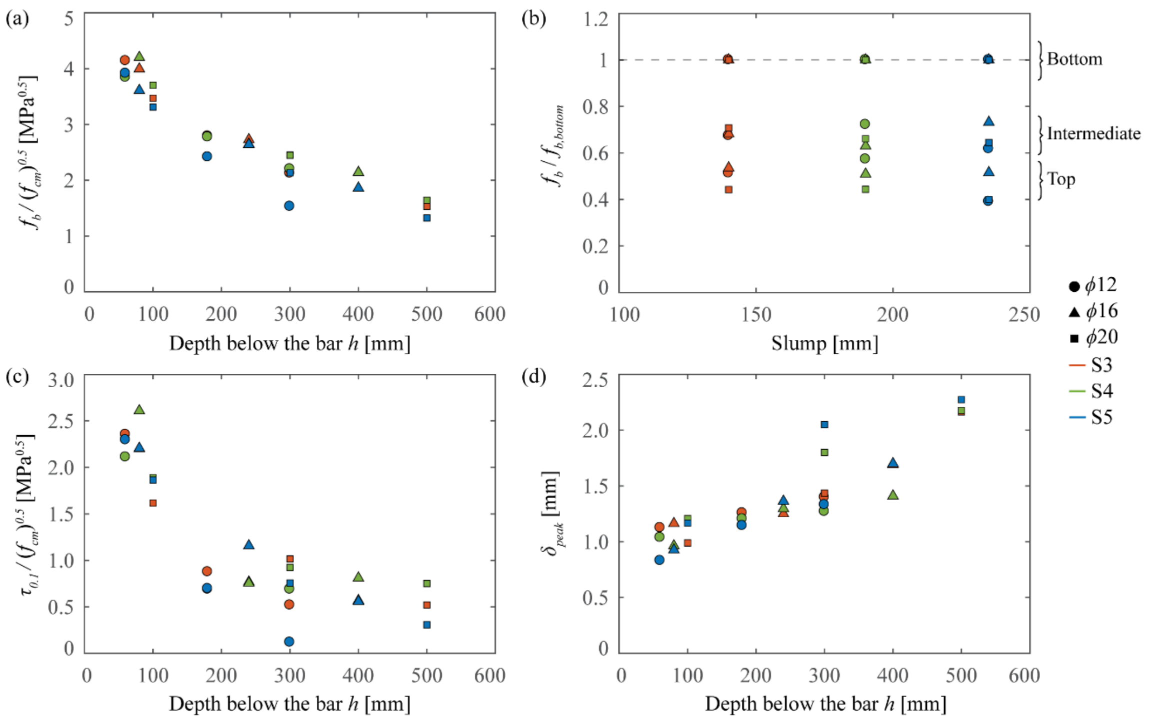

Figure 4.11: Test results on short anchorages: (a) effect of the depth (*h*) of concrete below the bar on the normalized bond strength; (b) top cast ratio against the concrete consistency class; (c) effect of the depth (*h*) of concrete below the bar on the normalized bond stress at an unloaded end slip of 0.1 mm; and (d) slip measured at the peak bond strength as function of the depth below the bar.

4.5.2. Tests with anchorage length 10ϕ

Figure 4.12 depicts the bond-slip behaviour of bars with identical c/ϕ ratio but different casting position (top and bottom reinforcement) of series ML10. This figure compares the response of specimens with small concrete cover (Figure 4.12a,d) to specimens with larger cover (Figure 4.12b,c,e,f), both for ϕ = 14 mm and ϕ = 20 mm bars. The specimens of Figure 4.12a,b,d,e had spalling failures while the specimens with higher concrete cover (c = 2.0ϕ, Figure 4.12c,f) developed pull-out failures.

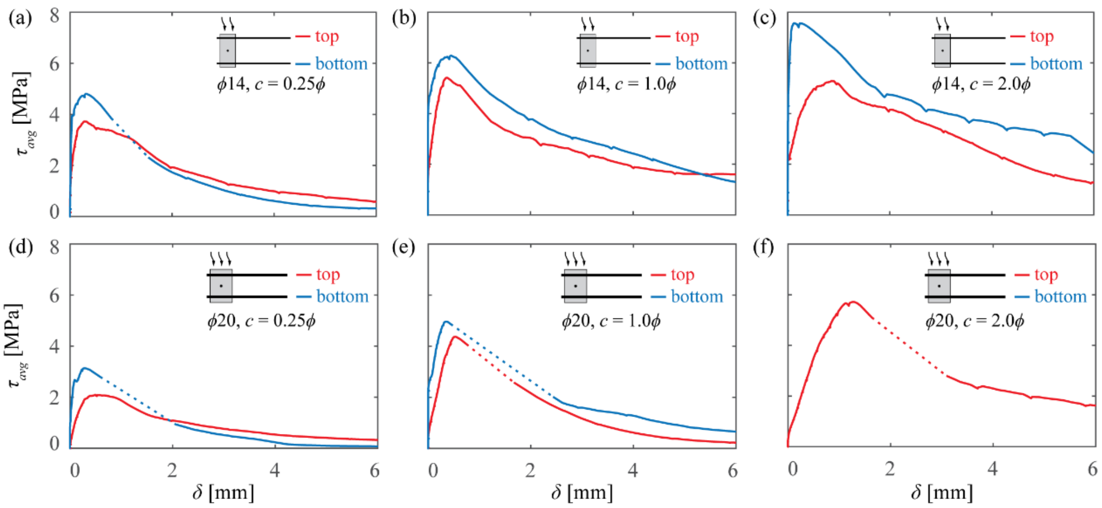

Figure 4.12: Bond-slip relationship of top and bottom reinforcement with an anchorage length 10ϕ and a concrete cover ranging from 0.25 to 2.0ϕ (dotted lines: no recording available): (a) specimens ML10D14-16 and MLD10D14-23; (b) specimens ML10D14-19 and ML10D14-26 (c) specimens ML10D14-21 and ML10D14-28; (d) specimens ML10D20-2 and ML10D20-9; (e) specimens ML10D20-5 and ML10D20-12; and (f) specimen ML10D20-7.

As shown in Figure 4.12, the bars placed in the top layers exhibit larger values for the slip for the same values of applied load. This can be related to the presence of the voids under the bars originated by plastic settlement (Figure 4.1b). These voids reduce the contact area between the bar and the surrounding concrete, requiring thus some level of slip to centre the bar and to engage mechanical contacts. With respect to the reinforcement of the bottom layer (Figure 4.12), the void associated to concrete settlement is negligible and the response is much stiffer at low load levels. It can also be observed that bottom bars exhibited a more brittle response, with a sudden drop of resistance after the peak load (this caused some difficulties in recording the complete post-peak behaviour of some specimens, evidenced by dotted lines in Figure 4.12). In addition, large concrete covers (c = 2.0ϕ) were also observed to provide a tougher residual response (Figure 4.12c,f).

The bond strength of the bars with an anchorage length of 10ϕ is presented as a function of the c/ϕ ratio in Figure 4.13a (for ϕ = 20 mm) and in Figure 4.13b (for ϕ = 14 mm). In addition, it is also depicted for each specimen the top cast ratio (Figure 4.13c-d) and the slip measured at peak bond strength (Figure 4.13e-f). These figures also show the location of the bars with respect to the casting direction (top position in red and bottom position in blue) as well as their failure mode (triangle for spalling or circle for pull-out).

As shown in Figure 4.13a-b, the bond strength increases for increasing values of the concrete cover. Such increase follows an almost linear trend until the cover-to-bar diameter reaches a ratio of approximately 1.0-1.5 and is governed by spalling failures (Figure 4.13). Thereafter, the bond strength remains roughly constant and the strength is controlled by pull-out failures.

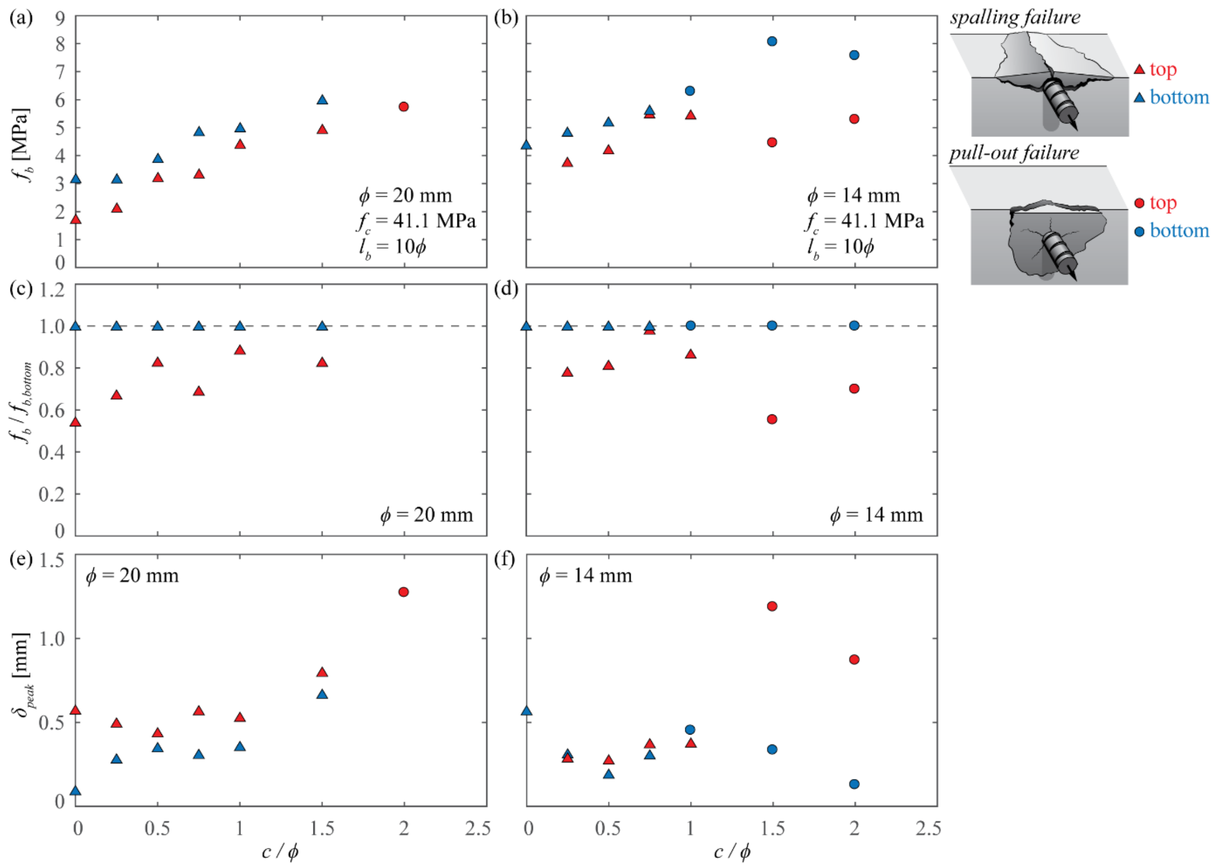

Figure 4.13: Bond strength averaged over the anchorage length as function of the concrete cover and bar position (top or bottom layer): (a) series ML10D20; (b) ML10D14. Top cast ratio as function of the cover-to-diameter ratio: (c) series ML10D20; and (d) ML10D14. Slip measured at the peak bond strength as function of the concrete cover and bar position: (e) series ML10D20; and (f) ML10D14.

Figure 4.13a-b shows a clear difference in the bond strength depending on the location of the bars, even if specimens mainly had a spalling failure. In fact, the top bars presented lower resistances in the majority of tests, corresponding to a situation of poor bond conditions (according to EN 1992-1-1:2004 [26] and *fib* MC 2010 [27], as shown in Figure 4.2a and Figure 4.8), which can be related to the reduction of the concrete tensile strength near the top surface (Figure 4.3a). In addition, inclined settlement cracks were visible around the top bars (as shown in Figure 4.1b) once the formwork was removed. As explained in Section 4.3, these cracks could also act as crack initiators for development of spalling failures (see Figure 4.1b).

As far as size effect is concerned, Figure 4.13a-b shows that the 14-mm diameter bars presented higher bond strengths than those of 20-mm diameter bars, both for the top and bottom reinforcement. This effect was systematically observed with respect to failures by cover spalling. For failures related to pull-out of the reinforcement, fewer and more scattered tests are available to lead to a clear conclusion (although a reduction of strength due to size effect can be observed for bars in good bond conditions).

The top cast ratio shown in Figure 4.13c-d corresponds on average to a value of 0.74 for ϕ20 bars and to 0.78 for ϕ14 bars. This result indicates that the proposed value $\eta_1 = 0.70$ as suggested in EN 1992-1-1:2004 [26] for the top-bar effect of anchorages is a reasonable (and generally safe) estimate of the investigated tests. With respect to the slip measured at peak bond stress (Figure 4.13e-f), it can be noted that it tends to increase with increasing values of the concrete cover (despite the recorded scatter for the ϕ14 bars). It should be noted that the top layer of reinforcement exhibits larger slips at peak as compared to the corresponding bottom layer.

4.5.3. Tests with anchorage length 20ϕ

A comparison of the bond-slip response of the bars of series ML20 is shown in Figure 4.14a-d for different specimen depths, by considering different bar diameters (ϕ14 and ϕ20) and positions during casting (top or bottom layer). As for test series ML10, the top bars develop larger slips at early loading stages. This effect seems more pronounced for bars having a larger concrete depth under them. In addition, the bottom reinforcement presented a more brittle response, which did not allow to record the post-peak phase of the test, as also observed in prisms with short anchorages experiencing splitting failures.

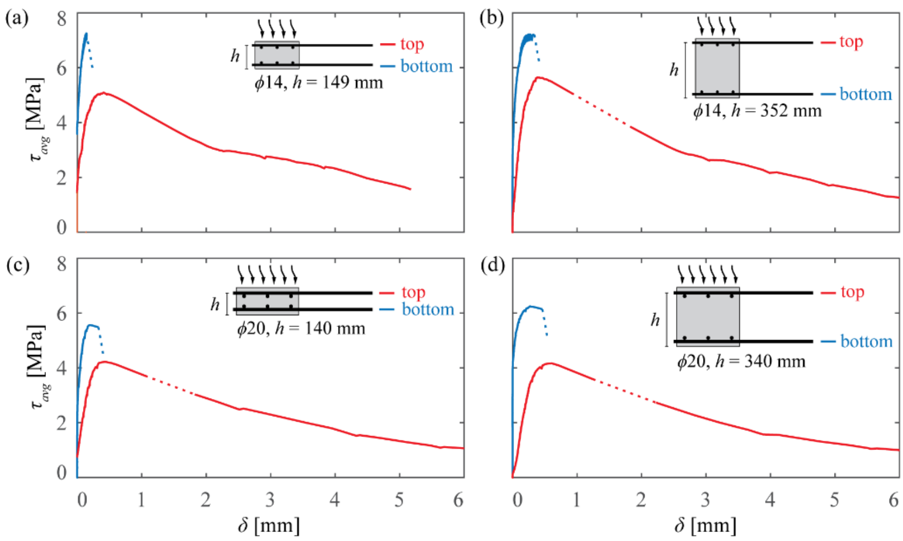

Figure 4.14: Bond-slip relationship of top and bottom reinforcement (dotted lines: no recording available): (a) specimens ML20D14-15 and ML20D14-22; (b) specimens ML20D14-21 and ML20D14-28; (c) specimens ML20D20-1 and ML20D20-8; and (d) specimens ML20D20-7 and ML20D20-14.

The bond strength of the bars of series ML20, with an anchorage length of 20ϕ (all tests with c = 1.25ϕ), is presented as function of their position (top or bottom layer) and bottom-concrete depth in Figure 4.15a (ϕ = 20 mm bars) and in Figure 4.15b (ϕ = 14 mm bars). The corresponding top cast ratio is shown in Figure 4.15c-d, while the slip measured at the peak bond strength is depicted in Figure 4.15e-f.

According to Figure 4.15a-b, the entire series was characterized by spalling failures, consistently with the observations of series ML10 with concrete cover-bar diameter ratio lower than 1.5. In most cases, spalling was reached before yielding of the bars while, in some cases, it happened after bar yielding (during the strain-hardening phase), particularly for ϕ14 bars in good bond conditions. The recorded bond strength for the different tests of a given layer and specimen appears to be roughly constant independently of the depth of concrete under the bar.

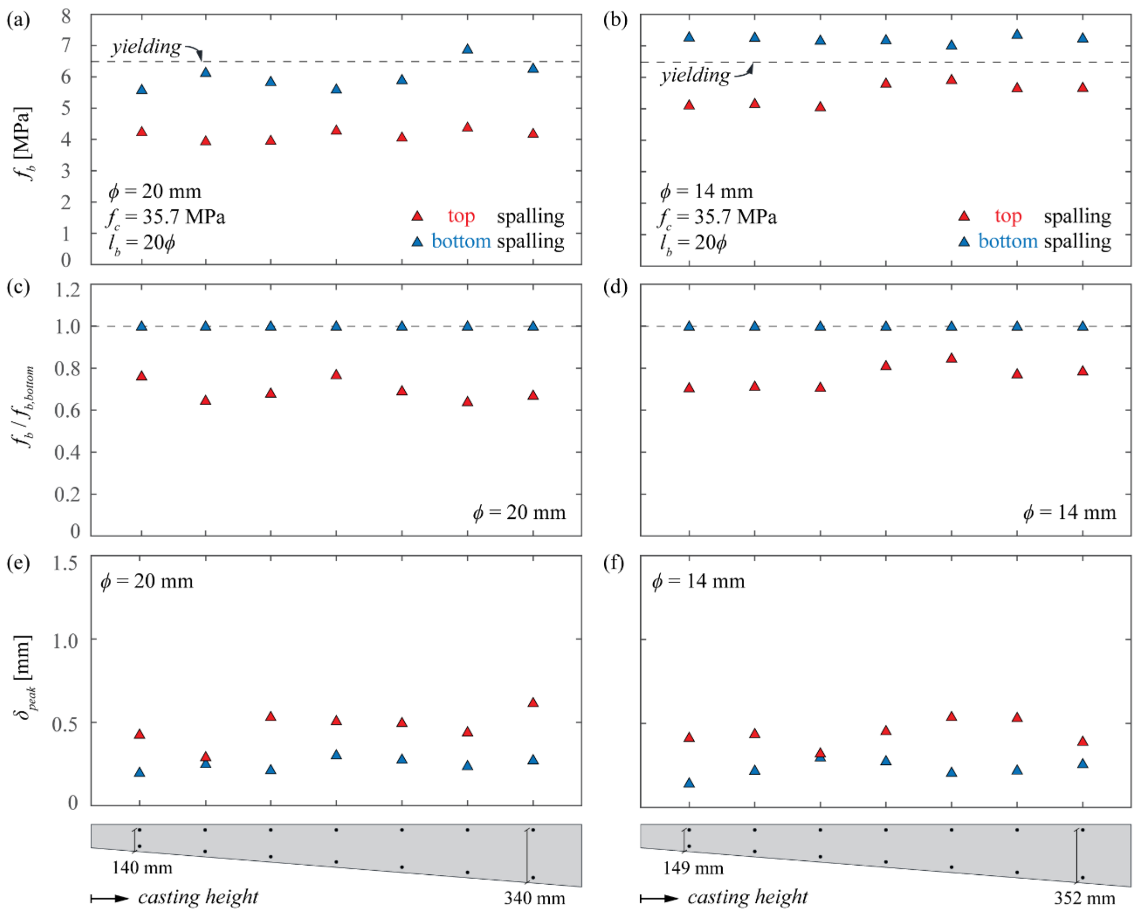

Figure 4.15: Bond strength averaged over the anchorage length as a function of the bar position and concrete height under the bar: (a) series ML20D20; and (b) ML20D14. Top cast ratio as function of concrete height under the bar: (c) series ML20D20; and (d) ML20D14. Slip measured at the peak bond strength as function of the bar position and concrete height under the bar: (e) series ML20D20; and (f) ML20D14.

As expected, due to the effects of bleeding and plastic settlement, the top bars presented lower resistances than the bottom bars (Figure 4.15a-b). This effect was consistently observed, despite the relatively low depth of some tests (as ML20D20-1 or ML20D14-15, which could be considered as good bond conditions according to EN 1992-1-1:2004 [26] or *fib* MC 2010 [27]). Size effect is also visible in this series, with bond resistance of the 14-mm diameter bars being higher than that of the 20-mm diameter bars.

The top cast ratio of series ML20 (Figure 4.15c-d) is on average equal to 0.69 for ϕ20 bars and to 0.76 for ϕ14 bars (where, for the ϕ14 bars, the ratio could be affected by plastic strains in the reinforcement). Once again, the proposed valued η_1 = 0.70 suggested by EN 1992-1-1:2004 [26] is in good agreement with the tests results. With respect to the slip measured at the peak bond strength (Figure 4.15e-f), it can be noted that it is more pronounced for the bars of the top layer as compared to the corresponding test of the bottom layer, as observed in the previous series of tests (BL5 and ML10). In addition, the slip at peak seems to be approximately constant for the different casting depths.

4.6. Discussion of results

4.6.1. Role of the void under the bar on pull-out and spalling failures

The normalized bond strength of the different series of the experimental programme are plotted in Figure 4.16 as a function of the concrete depth under the bar and by separating pull-out and spalling failures.

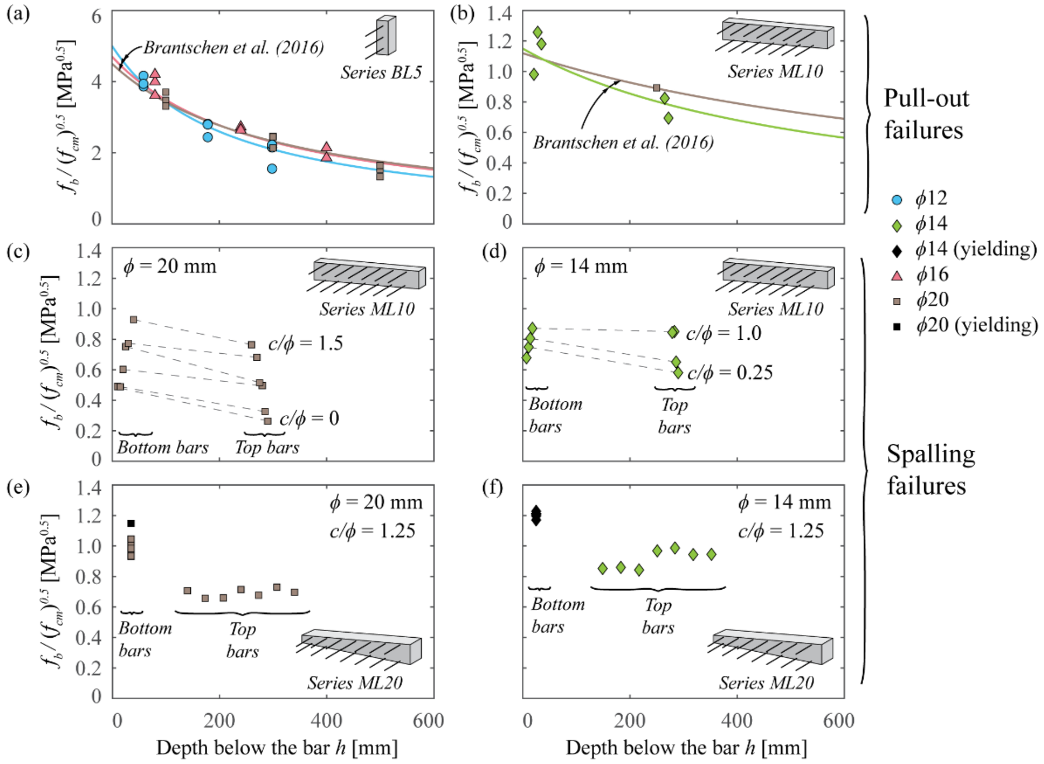

Figure 4.16: Effect of depth below the bar on the normalized bond strength for pull-out and spalling failures: (a) pull-out tests of series BL5 and model of Brantschen et al. [36]; (b) pull-out tests of series ML10 and model of Brantschen et al. [36]; (c) spalling tests of 20 mm bars, series ML10; (d) spalling tests of 14 mm bars, series ML10; (e) spalling tests of 20 mm bars, series ML20; and (f) spalling tests of 14 mm bars, series ML20.

For pull-out failures (Figure 4.16a,b for series BL5 and ML10, respectively), the bond strength gradually reduces with increasing depth of concrete under the reinforcing bars. By considering the bond strength to be influenced by a void depth under the bar, calculations performed by using the approach proposed by Brantschen et al. [36] are in good agreement with the test results, see Figure 4.16a-b (calculations performed by using the approach of Brantschen et al. [36] and considering a settlement strain of 3.0 mm/m for series BL5 and of 1.0 mm/m for series ML10). As it can be noted, the reduction of the bond performance is gradual and follows a hyperbolic trend (see Eq. (4.1)); this confirms the good agreement obtained with previous tests results [2], [37] (Figure 4.5 and Figure 4.6). Based on Eq. (4.1), the bond strength reduction due to concrete settlement depends on: (i) the settlement gradient and the rheology of fresh concrete, (ii) the bar diameter (with smaller bars more affected by bond reduction), (iii) the bond index f_R (with bars with smaller ribs more sensitive) and (iv) the rib geometry through coefficient k_f [36].

On the other hand, spalling failures do not show the same trend (Figure 4.16c-f) since there is a marked difference between bars near to the top or the bottom surface (Figure 4.16c-f). In fact, the spalling strength does not seem to be influenced by the concrete depth under the bar, since a rather constant bond strength was observed. Therefore, the spalling failures seem less affected by the size of the voids developing under the bars. A physical explanation for this behaviour can be found on the different mechanism triggering failure. Spalling failures are mainly governed by the tensile strength of concrete (affected by the bleeding phenomenon; see Figure 4.17a) and by crack development. The latter strongly depends on the presence of pre-existing cracks due to plastic settlement (acting as initiators of the spalling cracks). The size of the voids is potentially influencing the size of the cracks due to plastic settlement but with a reduced influence on the spalling resistance. A strength reduction factor $\eta_1 = 0.70$, as suggested by EN 1992-1-1:2004 [26], seems to provide a safe estimate of the top-bar effect and can be adopted for design purposes in case of spalling failures (Figure 4.13c-d and Figure 4.15c-d).

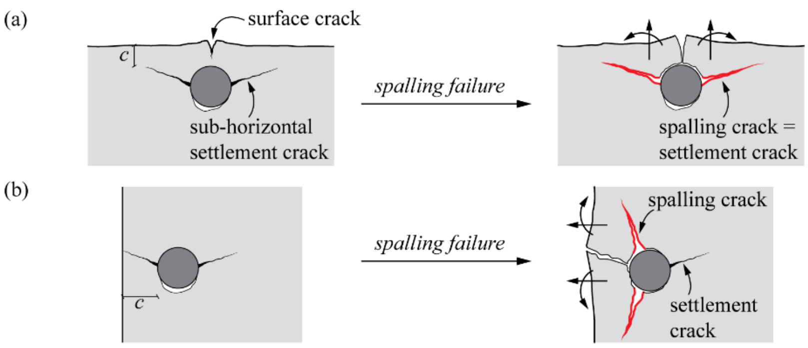

Figure 4.17: Influence of casting position effects on spalling mechanisms: (a) influence of interior cracks related to plastic settlement on the spalling failure of top bars; and (b) influence of interior cracks due to plastic settlement on cover spalling of bars near the side surface of a member.

Based on these observations, the behaviour of horizontal bars close to the vertical side surface of a concrete element (as a wall or girder's web), where a bond splitting-failure may occur, are expected to have a less pronounced effect of casting position on the spalling resistance. As shown in Figure 4.17b, the spalling cracks may not coincide with the settlement cracks (only the sub-horizontal branch of the settlement crack toward the free surface presents some similarities with the longitudinal crack, which appears on the surface along bars due to high bond stresses). In addition, the horizontal tensile strength of concrete governing the spalling strength seems less influenced by the phenomenon of bleeding than its vertical strength (refer to Figure 4.3a).

4.6.2. Design implications

The previous observations lead to a series of practical conclusions:

- For failures governed by pull-out of horizontal reinforcement, the concept of a clear difference between good and poor bond conditions does not seem to be physically sound. Instead, a gradual reduction of the bond strength as a function of the void depth developing under the bars shows a consistent agreement to test results and the physics of the phenomenon (Figure 4.18a). The size of such void can be estimated on the basis of the depth of concrete under the bars, the consistency and the rheology of fresh concrete. The reduction of bond performance as a function of the size of the voids under the bars can be suitably reproduced by means of bond engagement models [36], accounting for the reduction of the contact surface in presence of disturbances. According to the model used to predict the bond reduction due to settlement [36], also the bar diameter and the bond index of the deformed bar can play a major role.

- When the bond strength of a horizontal rebar is governed by spalling (i.e. a bar close to top or bottom surfaces), the concept of good and poor bond conditions as a function of the location of the bar seems valid (Figure 4.18b). This is mainly related to the presence of pre-existing cracks due to plastic settlement, acting as crack initiators, as well as to the lower tensile strength of concrete due to bleeding. With this respect a distinction of poor and good bond conditions can be established for the top and bottom bars respectively, by considering a bond strength reduction factor η_1 = 0.70 for the top bars (as proposed in codes of practice [26]).
- In case of horizontal bars close to the vertical side surface in walls and webs potentially affected by spalling failures, according to the considerations described in previous subsection, the casting positions plays potentially a smaller role.

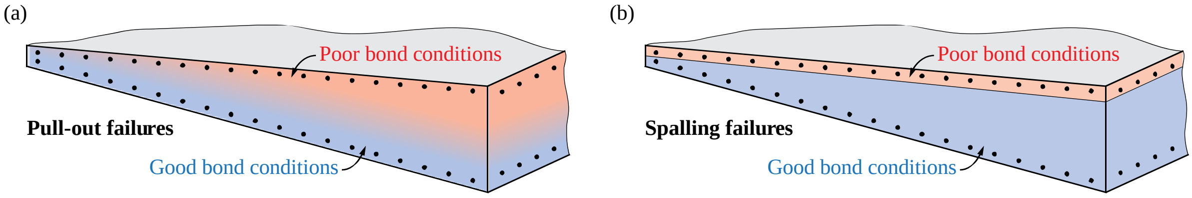

Figure 4.18: Potential implications of failure mechanism on the definition of poor bond condition as function of member's depth: (a) case of pull-out failures; and (b) case of spalling failures.

4.7. Conclusions

The influence of the casting position on the anchorage of reinforcement bars is investigated in the current paper by means of a comprehensive experimental programme. The main findings of the paper are the following:

1. There is a significant phenomenological difference of the casting position on bond performance for failures occurring by rebar pull-out or by spalling of the concrete cover.
2. Reductions on the bond performance (strength and stiffness) in pull-out failures of horizontal reinforcement are governed by the size of the voids originated under the bars due to plastic settlement. This phenomenon is analogous to the influence of cracks developing through a bar (plane of the crack containing the reinforcement) and shows a gradual reduction of the bond performance for increasing depths of the voids under the bars. A consistent mechanical description and agreement with the test results is obtained by using such approach.
3. The reduction of the pull-out strength due to the casting position is thus not suitably reproduced by considering regions with poor and good bond conditions, but with a gradual reduction as a function of the thickness of the voids under the bars, depending on the concrete depth under the bar, the rheology of fresh concrete, the bar diameter and the bond index of the bar (with small bars and/or bars with small bond indexes more affected by a bond strength reduction).
4. For spalling failures of horizontal reinforcement close to horizontal free surfaces, the concept of regions with good and poor bond conditions (as most codes of practice propose) is more suitable, but the spalling strength does not seem to be influenced by the depth of concrete under the bar. Spalling failures are mostly affected by the vertical tensile strength reduction near the top surface due to bleeding and by the presence of internal cracks at the sides of the bars induced by plastic settlement. The strength reduction factor η_1 = 0.70, as suggested in EN 1992-1-1:2004 [26], is shown to provide safe estimates of spalling failures for the case of top bars.

5. For bars close to the vertical side surface of a concrete member, a less pronounced effect of casting position can be expected on the spalling resistance. This can be explained by the fact that the tensile strength of concrete in the horizontal direction, which governs the spalling strength, is less influenced by the phenomenon of bleeding than in the vertical direction. In addition, plastic settlement cracks (roughly perpendicular to the free surface) are less prone to develop and to initiate spalling of the cover. This conclusion, based on qualitative considerations, should be verified experimentally with additional tests.

4.8. References

[1] T. C. Powers, "The properties of fresh concrete," John Wiley & Sons, Hoboken, NJ, United States, 664 p., 1968.

[2] A. Castel, T. Vidal, K. Viriyametanont, and R. François, "Effect of reinforcing bar orientation and location on bond with self-consolidating concrete," *ACI Structural Journal*, vol. 103, no. 4, pp. 559–567, 2006.

[3] F. Moccia, X. Kubski, M. Fernández Ruiz, and A. Muttoni, "The influence of casting position and disturbance induced by reinforcement on the structural concrete strength," *Structural Concrete*, pp. 1–28, 2020.

[4] R. Combrinck, L. Steyl, and W. P. Boshoff, "Interaction between settlement and shrinkage cracking in plastic concrete," *Construction and Building Materials*, vol. 185, pp. 1–11, 2018.

[5] International Federation for Structural Concrete, "fib Bulletin 10: Bond of reinforcement in concrete," State-of-art report prepared by Task Group Bond Models, Lausanne, Switzerland, 439 p., 2000.

[6] J. Cairns, "Influence of casting position on lap and anchorage strength," Heriot Watt University, Edinburgh, UK, 40 p., 2018.

[7] D. A. Abrams, "Tests of bond between concrete and steel," University of Illinois Bulletin No. 71, University of Illinois at Urbana-Champaign, Urbana, IL, USA, 240 p., 1913.

[8] C. A. Menzel, "Some Factors Influencing Results Of Pull-Out Bond Tests," *Journal of the American Concrete Institute, Journal Proceedings*, vol. 35, no. 6, pp. 517–542, 1939.

[9] A. P. Clark, "Comparative bond efficiency of deformed concrete reinforcing bars," *Journal of Research of the National Bureau of Standards*, vol. 37, pp. 399–407, 1946.

[10] A. P. Clark, "Bond of concrete reinforcing bars," *Journal of the American Concrete Institute*, vol. 46, no. 11, pp. 161–184, 1949.

[11] ACI Committee 318, "Building Code Requirements for Reinforced Concrete (ACI 318-51)," American Concrete Institute, Farmington Hills, USA, 1951.

[12] G. Rehm, "Über die Grundlagen des Verbunds zwischen Stahl und Beton," *Deutscher Ausschuss für Stahlbeton*, vol. 138, pp. 1–59, 1961.

[13] G. B. Welch and B. J. F. Patten, "Bond Strength of Reinforcement Affected by Concrete Sedimentation," *Journal Of The American Concrete Institute*, vol. 62, no. 2, pp. 251–264, 1965.

[14] J. O. Jirsa and J. E. Breen, "Influence of Casting position and shear on development and splice length - design reccomendations," Report No. 242-3F, Centre for Transportation Research, The University of Texas at Austin, Austin, TX, USA, 45 p., 1981.

[15] A. Zekany, S. Neumann, J. Jirsa, and J. Breen, "The Influence of Shear on Lapped Splices in Reinforced Concrete," Report No. 242-2, Center for Transportation Research, Bureau of Engineering Research, University of Texas at Austin, Austin, TX, USA, 88 p., 1981.

[16] R. C. Donahey and D. Darwin, “Bond of Top-Cast Bars in Bridge Decks,” *ACI Journal*, vol. 82, no. 5, pp. 57–66, 1985.

[17] B. B. Brettmann, D. Darwin, and R. C. Donahey, “Bond of Reinforcement To Superplasticized Concrete,” *ACI journal*, vol. 83, no. 12. pp. 98–107, 1986.

[18] M. Valcuende and C. Parra, “Bond behaviour of reinforcement in self-compacting concretes,” *Construction and Building Materials*, vol. 23, no. 1, pp. 162–170, 2009.

[19] K. H. Khayat, K. Manai, and A. Trudel, “In Situ Mechanical Properties of Wall Elements Cast Using Self-Consolidating Concrete,” *ACI Materials Journal*, vol. 94, no. 6, pp. 491–500, 1997.

[20] A. A. A. Hassan, K. M. A. Hossain, and M. Lachemi, “Bond strength of deformed bars in large reinforced concrete members cast with industrial self-consolidating concrete mixture,” *Construction and Building Materials*, vol. 24, no. 4, pp. 520–530, 2010.

[21] K. M. A. Hossain and M. Lachemi, “Bond Behavior of Self-Consolidating Concrete with Mineral and Chemical Admixtures,” *Journal of materials in Civil Engineering*, vol. 20, no. 9, pp. 608–616, 2008.

[22] B. S. Hamad and M. S. Itani, “Bond strength of reinforcement in high-performance concrete: The role of silica fume, casting position, and superplasticizer dosage,” *ACI Materials Journal*, vol. 95, no. 5, pp. 499–511, 1998.

[23] T. A. Soylev and R. François, “Quality of steel-concrete interface and corrosion of reinforcing steel,” *Cement and Concrete Research*, vol. 33, no. 9, pp. 1407–1415, 2003.

[24] O. E. Gjorv, P. J. M. Monteiro, and P. K. Mehta, “Effect of condensed silica fume on the steel-concrete bond,” *ACI Materials Journal*, vol. 87, no. 6, pp. 573–580, 1990.

[25] A. Azizinamini, M. Stark, J. J. Roller, and S. K. Ghosh, “Bond performance of reinforcing bars embedded in high-strength concrete,” *ACI Structural Journal*, vol. 90, no. 5, pp. 554–561, 1993.

[26] EN 1992-1-1:2004, “Eurocode 2: Design of Concrete Structures - Part 1: General Rules and Rules for Buildings,” European Committee for Standardization (CEN), Brussels, Belgium, 225 p., 2004.

[27] International Federation for Structural Concrete, “fib Model Code for Concrete Structures 2010,” Ernst & Sohn, Berlin, Germany, 434 p., 2013.

[28] ACI Committee 318, “Building Code Requirements for Structural Concrete (ACI 318-19) and Commentary,” American Concrete Institute, Farmington Hills, USA, 624 p., 2019.

[29] R. Tepfers, “A theory of bond applied to overlapped tensile reinforcement splices for deformed bars,” PhD Thesis, Division of Concrete Structures, Chalmers University of Technology, Göteborg, Sweden, 328 p., 1973.

[30] E. Giuriani, G. Plizzari, and C. Schumm, “Role of stirrups and residual tensile strength of cracked concrete on bond,” *Journal of Structural Engineering*, vol. 117, no. 1, pp. 1–18, 1991.

[31] J. Cairns and K. Jones, “The splitting forces generated by bond,” *Magazine of Concrete Research*, vol. 47, no. 171, pp. 153–165, 1995.

[32] G. Giaccio and A. Giovambattista, “Bleeding: Evaluation of its effects on concrete behaviour,” *Materials and Structures*, vol. 19, no. 4, pp. 265–271, 1986.

[33] L. Josserand, O. Coussy, and F. de Larrard, “Bleeding of concrete as an ageing consolidation process,” *Cement and Concrete Research*, vol. 36, no. 9, pp. 1603–1608, 2006.

[34] H. J. Yim, J. H. Kim, H. G. Kwak, and J. K. Kim, “Evaluation of internal bleeding in concrete using a self-weight bleeding test,” *Cement and Concrete Research*, vol. 53, pp. 18–24, 2013.

[35] RILEM TC, “RILEM Recommendations for the Testing and Use of Constructions Materials,” Springer, Berlin, Germany, 618 p., 1994.

[36] F. Brantschen, D. M. V. Faria, M. Fernández Ruiz, and A. Muttoni, “Bond behaviour of straight, hooked, U-shaped and headed bars in cracked concrete,” *Structural Concrete*, vol. 17, no. 5, pp. 799–810, 2016.

[37] C. J. Parra, “Experimental study of self-compacted concrete in hardened state (‘Estudio experimental de los hormigones autocompactables en estado endurecido’),” PhD thesis, Polytechnic University of Valencia, Valencia, Spain, 337 p., 2005.

[38] EN 12350-2:2019, “Testing fresh concrete - Part 2: Slump test,” European Committee for Standardization (CEN), Brussels, Belgium, 8 p., 2019.

[39] EN 197-1:2011, “Cement - Part 1: Composition, specifications and conformity criteria for common cements,” European Committee for Standardization (CEN), Brussels, Belgium, 38 p., 2011.

[40] EN 13670:2013, “Execution of concrete structures,” European Committee for Standardization (CEN), Brussels, Belgium, 66 p., 2013.

[41] EN 12350-5:2019, “Testing fresh concrete - Part 5: Flow table test,” European Committee for Standardization (CEN), Brussels, Belgium, 12 p., 2019.

[42] EN ISO 6892-1:2016, “Metallic materials - Tensile testing - Part 1: Method of test at room temperature,” European Committee for Standardization (CEN), Brussels, Belgium, 79 p., 2016.

[43] Y. Goto, “Cracks Formed in Concrete Around Deformed Tension Bars,” *ACI Journal*, vol. 68, no. 4, pp. 244–251, 1971.

[44] G. Metelli and G. A. Plizzari, “Influence of the relative rib area on bond behaviour,” *Magazine of Concrete Research*, vol. 66, no. 6, pp. 277–294, 2014.

4.9. Annexes

4.9.1. Annex A: Evaluation of spalling strength

In the following chapter (Chapter 5), it is presented an extensive investigation on cover spalling induced by reinforcement, in which it is proposed a model assessing the spalling strength of pull-out bars. The latter model is applied in this Annex to evaluate the resistance of the tested bars that failed due to cover spalling (for more details on the model, refer to Chapter 5).

It should be noted that this Annex was not published in the article “Casting position effects on bond performance of reinforcement bars”, but it is a complement of this thesis.

Succinctly, the proposed approach of Chapter 5 defines the bond strength in case of spalling failures in the following manner:

$$f_b = \left(\lambda \cdot p_\perp + (1-\lambda)\cdot p_{//}\right)\cdot \cot\theta \tag{4.3}$$

where :

- λ : is a coefficient defining the contribution of the splitting components and is set equal to 0.5
- $p_\perp$: is the pressure perpendicular to the cover and is defined as follows:
    - case where the angle ψ is optimized:

$$p_\perp = \frac{\eta_{is}\cdot\eta_{ct}\cdot f_{ct}}{\tan\gamma}\cdot 2\cdot\sqrt{\frac{c_y}{\phi}+\left(\frac{c_y}{\phi}\right)^2}\cdot\left(\frac{d_{dg}}{1.6\phi}\right)^{1/3} \tag{4.4}$$

- case where the angle $\psi = 0°$:

$$p_{\perp} = \frac{\eta_{is} \cdot \eta_{ct} \cdot f_{ct}}{\tan\gamma} \cdot \left(1 + \frac{2c_y}{\phi}\right) \cdot \left(\frac{d_{dg}}{1.6\phi}\right)^{1/3} \tag{4.5}$$

- $p_{//}$: is the pressure parallel to the cover and is defined as follows (situation in which the ribs are oriented towards the free surface):

$$\begin{aligned} p_{//,top} &= \eta_{is} \cdot p_{//,bot} \\ p_{//,bottom} &= 6.0 \text{ MPa} \end{aligned} \tag{4.6}$$

- θ : is the inclination of compressive struts with respect to bar axis and is defined as follows:
  - case with a constant angle:

$$\begin{aligned} \theta &= 50° \qquad \text{(top bars)} \\ \theta &= 55° \qquad \text{(bottom bars)} \end{aligned} \tag{4.7}$$

  - case with variable angle:

$$\begin{aligned} \theta &= 40° + 20 \cdot \ln\left(1 + \frac{c}{\phi}\right) \le 50° \qquad \text{(top bars)} \\ \theta &= 45° + 20 \cdot \ln\left(1 + \frac{c}{\phi}\right) \le 55° \qquad \text{(bottom bars)} \end{aligned} \tag{4.8}$$

In addition, since the mean tensile strength is not measured in current experimental programme, the concrete tensile stress f_{ct} is approximated on the basis of f_c using the formulation suggested in *fib* MC 2010 [27] ($f_{ct} = 0.3 \cdot f_c^{2/3}$ for $f_c < 50$ MPa).

<u>Tests with anchorage length 10ϕ</u>

The approach presented in Chapter 5 is compared in Figure 4.19 to the results of the experimental programme of series ML10. In general, the different predictions show consistent agreement with the observed trends for the case of spalling failures (pull-out failures are not assessed with this model).

It should be pointed out that the formulation defining the pressure parallel to the cover $p_{//}$ had to be adapted in the following manner:

- for bars with ϕ = 20 mm (specimens ML10D20):

$$\begin{aligned} p_{//,top} &= \eta_{is} \cdot p_{//,bot} \\ p_{//,bottom} &= 4.0 \text{ MPa} \end{aligned} \tag{4.9}$$

  The reason for this change could be related to the fact that the specimens did not experience a cure in the first 24 hours after casting due to DIC measurements on the top surface. Additional experimental data is however needed for a more suitable definition of $p_{//}$.

- for bars with ϕ = 14 mm (specimens ML10D14), the formulation of Eq. (4.6) is corrected to account for size effect in the following manner:

$$\begin{aligned} p_{//,top} &= \eta_{is} \cdot p_{//,bot} \\ p_{//,bottom} &= 6.0 \cdot \left(\frac{d_{dg}}{1.6\phi}\right)^{1/3} = 6.76 \text{ MPa} \end{aligned} \tag{4.10}$$

Table 4.5 resumes the average of the measured-to-calculated strength as well as the Coefficient of

Variation for each investigated approach (only the specimens failing by cover spalling are considered).

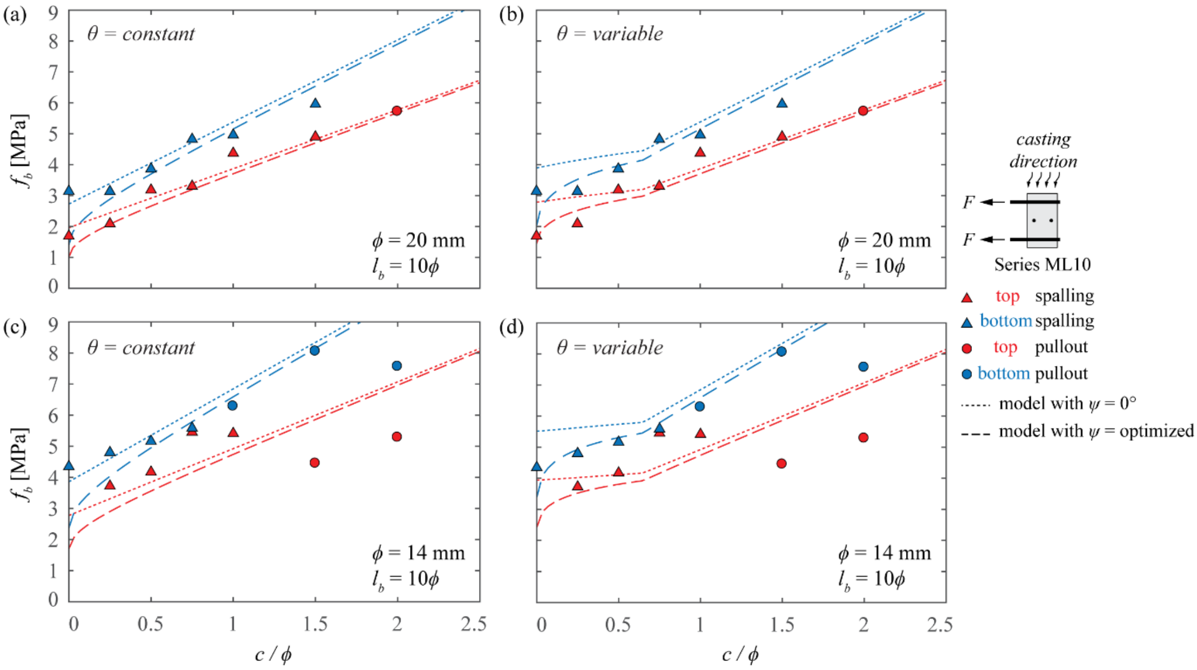

Figure 4.19: Main results of the proposed models (dotted lines) and comparison to the pull-out tests performed in current study (triangles and circle markers, series ML10): (a) series ML10D20, case with angle of the struts θ constant; (b) series ML10D20, case with θ variable; (c) series ML10D14, case with θ constant; and (d) series ML10D14, case with θ variable.

As noted in Table 4.5, the bond strength calculated with the formulation of $p_{\perp}$ from Eq. (4.5) and with the angle θ constant provides the most accurate results with the lowest scatter. Further experimental evidence should however be considered to validate this statement.

Table 4.5: Main results of the proposed models with respect to the tests failing by cover spalling: ratio between the measured bond strength (series ML10) and the calculated bond strength (proposed models).

Test series			θ constant		θ variable	
			Eq. (4.5)	Eq. (4.4)	Eq. (4.5)	Eq. (4.4)
ML10D20	$f_{b,meas}$ / $f_{b,calc}$	Average	0.98	1.21	0.89	1.06
		CoV [%]	10.3	31.6	17.0	18.3
ML10D14	$f_{b,meas}$ / $f_{b,calc}$	Average	1.07	1.24	0.97	1.10
		CoV [%]	9.5	21.4	15.1	12.6

Tests with anchorage length 20ϕ

The estimates of the model presented in Chapter 5 are compared in Figure 4.20 to the test series ML20.

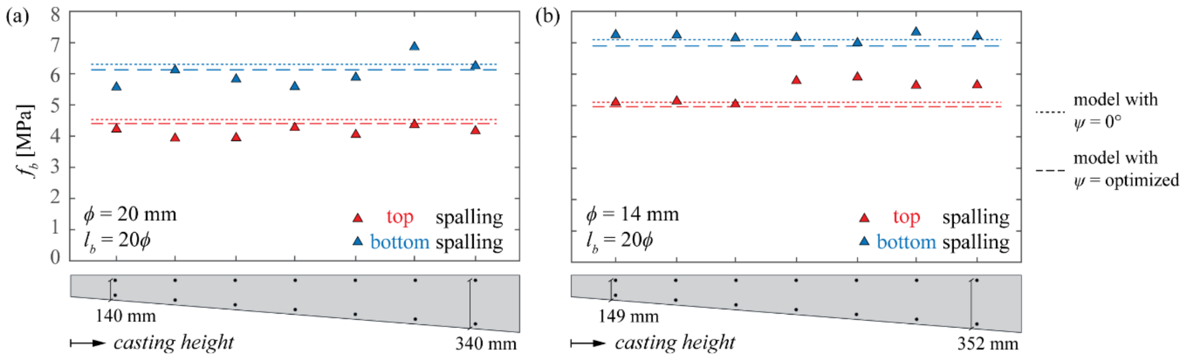

Figure 4.20: Main results of the proposed models (dotted lines) with respect to the results of the experimental programme (triangles and circle markers, series ML20): (a) series ML20D20; and (b) series ML20D14.

As shown in Figure 4.20, the predictions are in good agreement with the experimental results. In this case as well, the size effect was considered in the definition of $p_{//}$ for reinforcing bars of ϕ = 14 mm. Despite this change, the other formulations were not modified as they were shown to provide accurate predictions of the bond strength in case of spalling failures. It should be noted that only the formulation with the angle θ constant is considered (the Eq. (4.8) also provides constant values of θ).

In Table 4.6 it is outlined the average of the measured-to-calculated strength as well as the Coefficient of Variation for each investigated approach (only the specimens failing by cover spalling are considered).

Table 4.6: Main results of the proposed models with respect to the tests failing by cover spalling: ratio between the measured bond strength (series ML20) and the calculated bond strength (proposed models).

Test series			**Eq. (4.5)**	**Eq. (4.4)**
ML20D20	$f_{b,meas}$ / $f_{b,calc}$	Average	0.93	0.96
		CoV [%]	6.3	6.3
ML20D14	$f_{b,meas}$ / $f_{b,calc}$	Average	1.04	1.07
		CoV [%]	5.5	5.5

As shown in Table 4.6, the calculated bond strength provides accurate estimates of the tests results with a small Coefficient of Variation for both formulations of $p_{\perp}$ (Eq. (4.4) and Eq. (4.5)).

4.10. Notation

A_{gt} : reinforcement strain at maximum stress

P : applied load

W/C : water / cement ratio

c : concrete cover

d_{dg} : average roughness

f_b : bond strength

f_{b0} : bond strength in uncracked concrete

$f_{c,cube}$: compressive strength of concrete cube

$f_{c,cyl}$: compressive strength of concrete cylinder

f_R : bond index (relative rib area)

f_u : mean value of tensile strength of reinforcement

f_y : mean value of yield strength of reinforcement

h : depth of concrete

k_f : factor for rib geometry

l_b : anchorage length

$p_{\perp}$: pressure perpendicular to the cover

$p_{//}$: pressure parallel to the cover

w : crack or void thickness

Δ : width of void

δ : relative displacement between steel and concrete (slip)

δ_{peak} : slip at peak bond stress

η_1 : bond strength reduction factor related to bond condition and casting position

η_{ct} : strength reduction factor accounting for concrete brittleness in tension

η_{is} : strength reduction factor accounting for casting position effects

θ : inclination of compressive strut to bar axis

λ : coefficient defining the contribution of the splitting components

τ : bond stress

$\tau_{0.1}$: bond stress for 0.1 mm slip

ϕ : nominal diameter of reinforcing bar

ψ : angle defining the crack geometry

Chapter 5.
Spalling of concrete cover induced by reinforcement

This chapter is the preprint version of the article *Spalling of concrete cover induced by reinforcement* submitted to the journal *Engineering Structures* in October 2020. The authors of this publication are Francesco Moccia (PhD Candidate), Miguel Fernández Ruiz (Senior lecturer and thesis co-director) and Aurelio Muttoni (Professor and thesis director). The provisional reference is the following:

> F. Moccia, M. Fernández Ruiz, A. Muttoni, *Spalling of concrete cover induced by reinforcement*, Engineering Structures.

The work presented in this article was performed by Francesco Moccia under the supervision of Miguel Fernández Ruiz and Aurelio Muttoni, who provided valuable suggestions and expertise as well as proof-read the manuscript several times.

The main contributions of Francesco Moccia are the following:

- Review of studies focusing on spalling failures of concrete due to engagement of bond or by application of internal radial pressure.
- Casting of 44 specimens and testing using hydraulic inflator devices (test series CM11, CM12 and CM13).
- Casting and pull-out testing of 12 horizontal reinforcing bars with variable concrete cover (test series CM11).
- Production of custom-made hydraulic inflator devices following the design of Prof. Muttoni and the expertise of laboratory technicians (Serge Despont, Gérald Rouge).
- Analysis and discussion of the test results.
- Detailed measurements of cover spalling and crack propagation by means of Digital Image Correlation.
- Assessment of the influence of casting position, size effect and group effect on the resistance to cover spalling.
- Proposal for a mechanical approach assessing the spalling strength against an internal radial pressure, accounting for casting position, size and group effects.
- Proposal for an approach assessing the spalling strength of pull-out bars.
- Validation of proposed models based on experimental results.
- Production of the figures included in the article.
- Writing of the manuscript of the article.

5.1. Abstract

This paper investigates the phenomenon of cover spalling in reinforced concrete induced by bond or by the action of an inner pressure. This research is based on an experimental programme comprising a series of bond tests and a series of tests with inner-pressure on cylindrical openings. The inner-pressure test series (aimed at representing the conditions occurring for instance due to corrosion of reinforcement) was performed with hydraulic inflator devices embedded within concrete openings near to the free concrete surface. By means of detailed surface measurements performed with Digital Image Correlation, the mechanisms triggering spalling failures and the associated resistance are discussed and analysed thoroughly. This series investigates in addition a number of phenomena relevant to spalling failures, such as the influence of the casting position, group and size effects. The observed response, analysed by means of a mechanical analogy, is later used to investigate a series of structural tests performed on pull-out specimens. This analysis highlights the analogies and differences between the two types of tests (subjected to an imposed pressure or to bond stresses). On that basis, a comprehensive approach for treatment of bond-related cases failing by cover spalling is proposed, showing consistent agreement to the experimental evidence.

5.2. Introduction

Spalling of the concrete cover is a complex phenomenon that influences not only the ultimate limit state of a concrete member, but also its serviceability response and its durability. Spalling failures originate when a transverse force acting near to the concrete surface (originated by the presence of the reinforcement in the investigated cases) equals the tensile resistance of the concrete cover. The actions originating spalling failures can have different sources, as stresses associated to bond between reinforcing bars and surrounding concrete (Figure 5.1a) [1]–[3], the volume expansion due to corrosion of the steel reinforcement (Figure 5.1b) [4]–[8], deviation forces related to detailing with reinforcement bent in parallel to the surface (Figure 5.1c) [9]–[11] or in curved members (Figure 5.1d) [12]–[16], dowel action (Figure 5.1e) [17]–[21] or vapour-pressure under fire conditions [22], [23]. The spalling resistance depends in these cases upon a number of factors [3], such as the layout and dimensions of the reinforcing bars, the concrete cover and its strength or the casting position.

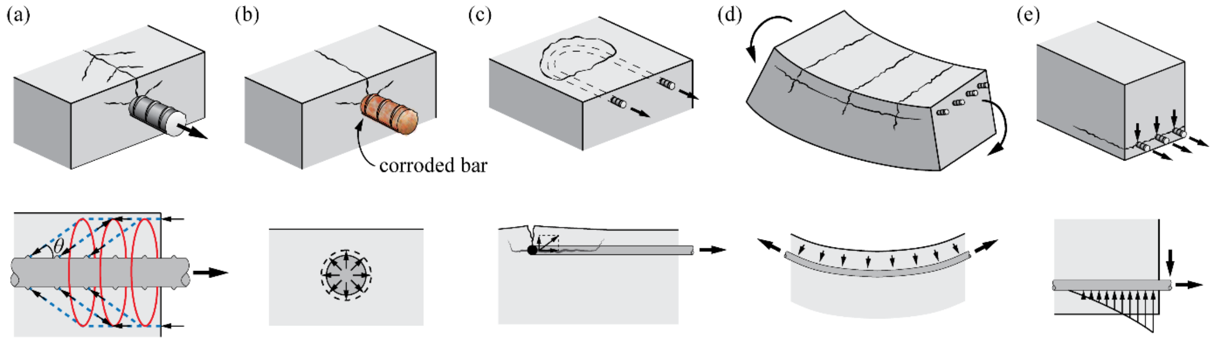

Figure 5.1: Potential causes of spalling of the concrete cover related to steel reinforcement: (a) bond-induced spalling; (b) corrosion-induced spalling; (c) spalling related to bent reinforcement; (d) spalling induced by deviation forces on curved members; and (e) spalling induced by dowel action.

In this paper, the phenomenon of spalling in structural concrete is investigated with reference to the action of a radial transverse pressure (as that originated by bond between reinforcement and concrete, Figure 5.1a, or associated to volumetric expansion of corroded reinforcement, Figure 5.1b). First, an extensive review of the state-of-the-art is presented, followed by a specific testing programme. The experiments were performed both on specimens subjected to inner-pressure acting on cylindrical opening (44 tests) as well as on anchorages (12 pull-out tests). With this programme, a special focus is set on the analysis of the relationship between pull-out failures and the applied transverse pressure, on the influence of the cover thickness and casting position as well as on the size and group effects. This programme was in addition instrumented with Digital Image Correlation, allowing to track in a detailed manner the development of surface cracking and to investigate on the associated load-carrying actions. On the basis of these results, a design approach is proposed based on a simple mechanical model. The consistency of such approach is validated with the test results of this paper as well as with others gathered from the scientific literature.

5.3. Review of the state-of-the-art

A large number of studies have been performed in the past with reference to spalling failures of concrete. In this section, the most relevant works concerning spalling due to engagement of bond stresses or by application of internal pressures inside concrete will be reviewed. The aim will be to clarify the phenomena triggering spalling failures and to relate them to the experimental programme presented in the next section. Other specific cases related to spalling issues (deviation forces of curved reinforcement or dowel action, Figure 5.1c-e) will not be reviewed in detail in this section.

5.3.1. Influence of internal pressures inside concrete

The application of internal pressures inside openings has been a manner to traditionally investigate the resistance to cover spalling, see Figure 5.2. Such approach is in addition suitable to investigate the potential response of corroded reinforcement, where the volumetric expansion of rust acts as an imposed radial displacement generating internal pressures [6]–[8], [24], [25].

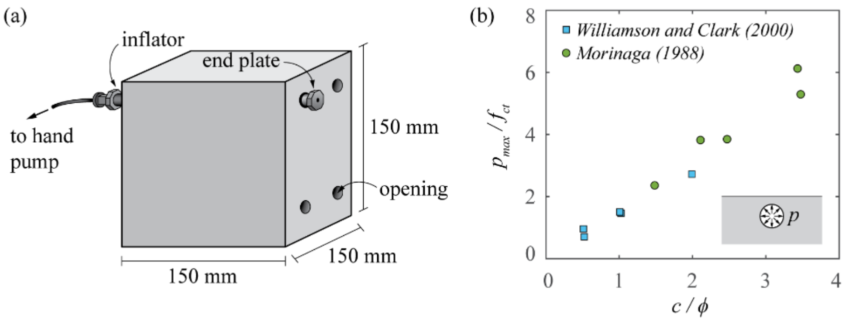

Figure 5.2: Uniform internal pressure applied with hydraulic inflator devices: (a) instance of test setup, as described by Williamson and Clark [26]; and (b) normalized maximum pressure applied with inflator devices as function of the cover-to-diameter ratio, adapted from [26].

For instance, Williamson and Clark [26] inserted hydraulic inflator devices within openings located in 150 mm concrete cubes and used a manual pump to pressurize the system (Figure 5.2a). The authors varied both the concrete cover and the diameter of the openings (8 mm and 16 mm). A similar study was performed by Morinaga [27] where a uniform pressure was applied within hollow concrete cylinders with variable external diameter (100, 150, 200 mm) and opening diameter (9, 19, 25 mm). Figure 5.2b presents the results of the two testing programmes [26], [27]. As it can be observed, both programmes have consistently shown an increase on the resistance to internal pressures with increasing values of the concrete cover. In addition, it was noted that for equal thickness of the cover, the maximum pressure reduced with increasing diameter of the openings, indicating the significance of size effect.

In addition, Allan and Cherry [28] simulated local corrosion by injecting oil at the interface between the bar and concrete. It should also be mentioned the work of Noghabai [29], in which pressure was exerted by an inflator placed within concrete cylinders having variable compressive strength and containing in some cases spiral reinforcement.

No specific researches have however been performed so far with such devices on the influence of the casting position, which has been identified as a relevant parameter for the concrete tensile strength and bond [3]. In addition, the outlined experimental programmes were all using pressure-controlled hydraulic pumps (load-controlled tests) and the post-peak behaviour of the cover was thus not recorded in detail. Such response can however be instrumental in cases where potential redistributions of stresses can occur, as in bond failures.

5.3.2. Spalling induced by bond

Spalling of the concrete cover has been thoroughly investigated in the frame of bond resistance and particularly for the performance of lap joints. Bond stresses are initially developed by the chemical adhesion between steel and hardened concrete. Such adhesion is however relatively low and vanishes at the onset of a relatively small bar slippage. At that moment, the transfer of forces by bond is ensured in ribbed reinforcement by the mechanical engagement between the ribs and the surrounding concrete (Figure 5.1a). In assessing the resistance of anchored bars and lap splices, Tepfers [1], [30], [31] observed that longitudinal cracks appeared in the cover near failure and that these cracks were caused by the tensile stresses related to bond (in accordance to the tension ring shown in Figure 5.1a). Longitudinal splitting cracks appear once the stresses reach the concrete tensile strength, which can be governing for the bond strength particularly for bars located near to the concrete surface (where the splitting cracks can lead to spalling of the cover). Following the approach of Tepfers, an analogy can be made between the bond stresses and a radial pressure generated by the rib action (Figure 5.1a) according to the following relationship:

$$f_b = f_{sp} \cdot \cot\theta \qquad (5.1)$$

Where f_b refers to the bond strength, f_{sp} to the internal radial pressure and θ to the angle of the struts with respect to the bar axis (refer to Figure 5.1a). Tepfers proposed that an internal angle $\theta = 45°$ could be assumed, although this value has been shown later not to be constant and to depend on the surface roughness (bond index) and considered kinematics [32].

The work of other researchers showed, however, that considering the bond strength is not only dependent on the development of inclined (conical) struts. For instance, Cairns [2], [33] observed that the bond strength should be regarded as the sum of two components, one related to the conical struts (associated to the splitting stresses) and a cohesive component depending on the concrete strength. Based on a Mohr-Coulomb failure criterion, the bond resistance was eventually determined as:

$$f_b = f_{sp} \cdot \cot\theta + f_{nsp} \qquad (5.2)$$

Where f_{nsp} refers to the bond strength related to the cohesive component and thus not related to the internal radial pressure leading to splitting stresses. It is also interesting to note that, following these researches, it was also established the dependence of the bond strength with respect to the orientation of the ribs in relation to the concrete surface where spalling can potentially occur. These researches showed in addition that spalling failures occurred when the concrete cover is smaller than three times the bar diameter, while pull-out failures are governing for higher values of the cover.

Similar results have been obtained recently by Tirassa et al. [32] by using a special test equipment which allows measuring directly the internal radial pressure f_{sp} and with a refined mechanical model which allows calculating the engaged stresses f_{sp} and f_b as a function of the rib geometry and the relative displacement between bar and concrete interface (slip δ and radial displacement w). Both experimental and theoretical results (which are in fine agreement) show that the cohesive component f_{nsp} decreases rapidly with an increase of both displacements (δ and w) and that the angle θ decreases from approximately 50° for small radial displacements to $\theta \approx 15°$ for large radial displacements w. In addition, since the ribs of actual reinforcement bars are not symmetrical with respect to the bar axis, all parameters can depend significantly on the bar orientation. Further studies on the interaction between bond and splitting stresses were also conducted by Giuriani et al. [34] (refer also to [35], [36]) who developed a model taking into account the confining actions of both the transverse reinforcement and concrete cover. These conclusions were also confirmed by Darwin et al. [37] and were followed by a general approach based on limit analysis and considering the influence of concrete cover and transverse pressures formulated by Gambarova et al. [38] (refer also to [39]–[41]), as shown in Figure 5.3a. According to this approach, the application of confining pressures reduces the influence of the concrete cover on the bond strength (as the pressure limits both the crack widths and their extension). In addition, as shown in Figure 5.3a, the bond strength exhibits an upper bound related to development of pull-out failures, as well as a shape of the resulting law in agreement to the cohesive component suggested by Cairns [2], [33] and later by Malvar [42].

Within the frame of limit analysis, the works of Nielsen and Hoang [43] on spalling failure mechanisms shall also be acknowledged, as well as the considerations of Schenkel [44], accounting for the cracked response of concrete. Schenkel [45] performed in addition a comprehensive experimental programme on pull-out specimens (Figure 5.3b), confirming the trends of the previous approaches, notably a potential cohesive component and the transition to pull-out failures.

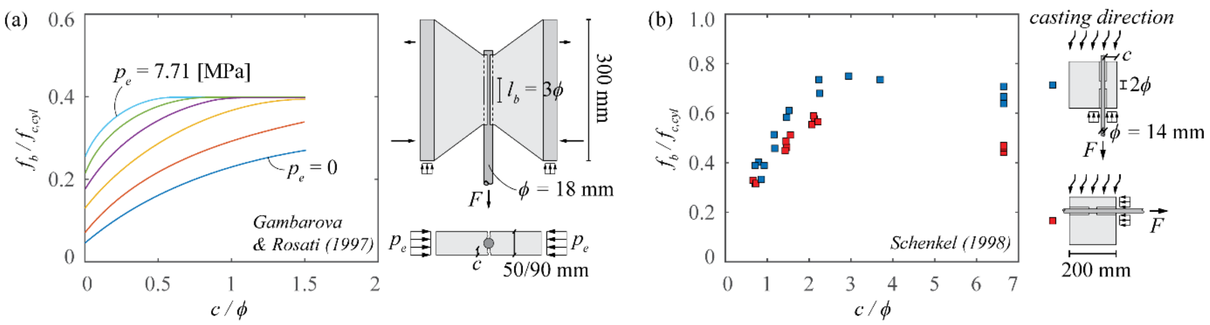

Figure 5.3: Influence of cover-to-diameter ratio on the spalling resistance: (a) normalized bond strength as function of the cover-to-diameter ratio and for different values of external pressure (p_e), calculations according to an elastic-cracked-cohesive model, adapted from [38]; and (b) short pull-out tests: normalized bond strength as function of the cover-to-diameter ratio and the casting direction, adapted from [44].

It is also interesting to note from the tests of Schenkel the significant differences observed depending on the casting direction of pull-out specimens (Figure 5.3b). Such effect has also been reported consistently by other researches as [46]–[50] (an extensive review of this topic can be consulted elsewhere [51]).

5.4. Experimental programme

An experimental programme was performed at Ecole Polytechnique Fédérale de Lausanne (Switzerland) to investigate on the effects of radial inner pressure on the spalling resistance of concrete. This programme consisted of both inner-pressure tests (where a controlled radial pressure was applied on cylindrical openings within concrete prisms) and structural tests consisting of pull-out tests on embedded reinforcement. The tests were addressed at completing current experimental state-of-the-art and were performed with refined measurements tracking the surface development of cracking. The tests allowed in particular for a detailed analysis of the relationship between failures originated by bond and transverse pressure, the influence of cover and casting conditions as well as the role of size and group effects.

5.4.1. Description of test series

Three different test series were performed within this programme:

1. Series CM11 (Figure 5.4a-d). This series was addressed at the effect of the concrete cover on the spalling resistance under various conditions. In this series, two prismatic specimens were cast with a cross section 0.2×0.4 m and a length of 3.7 m. The first specimen (Figure 5.4a) presented cylindrical 20-mm openings placed near to the top and bottom surfaces with variable concrete covers (clear cover *c* varying from 0.25ϕ to 3ϕ). The openings were created by placing plastic tubes fixed to the formwork during concreting and removing them after hardening of the concrete. These openings were used to apply a radial pressure by means of a hydraulic inflator device later described. The second specimen (Figure 5.4b) was nominally identical to the first one, but was cast with two layers of 20-mm steel bars that were tested under pull-out conditions. The bars were fixed to the formwork during casting and had a bond length equal to 10ϕ. All reinforcing bars presented two lugs at opposed sides and the ribs of all bars were aligned perpendicular to the direction of the cover (see Figure 5.4d) to ensure uniform conditions amongst them.
2. Series CM12 (Figure 5.4e-f). This series was aimed at investigating the influence of the size of the openings on the spalling resistance and was performed on specimens cast with openings (as in Figure 5.4a). It consisted of two specimens with identical cross section as series CM11 and a length of 3.2 m. Both specimens presented openings of variable diameter (from 10 mm to 40 mm) arranged near the top and bottom surface. The openings of the first specimen had a constant cover-to-bar diameter ratio (c_y / ϕ) equal to 1.25, while for the second specimen, this ratio was kept constant and equal to 2.0.
3. Series CM13 (Figure 5.4g). This series was aimed at the influence of the group effect on the spalling resistance. It consisted of a 4.08 m-long specimens with identical cross section as the previous series. The specimen had 20-mm openings placed in two layers located near to the top and bottom surfaces with constant concrete cover (c = 1.25ϕ). Isolated top and bottom openings were used as reference tests, while the rest of the openings were arranged in groups of three with variable clear spacing c_s between them (c_s / c_y ratio from 0 to 9, see Figure 5.4g).

Casting of the specimens was consistently performed over the 400-mm height, see Figure 5.4. As comparable tests were performed near to the top and bottom surface, the effects of the casting position on the spalling strength [52] could be investigated systematically. In addition to the described openings and bars, all specimens had two 16-mm bars placed longitudinally at mid-height of the cross section to control potential transverse cracks. A summary of the main properties is given in Table 5.1.

Table 5.1: Properties and tests results of series CM11, CM12 and CM13 (ϕ: opening or bar diameter; c_y: concrete cover; c_s / c_y: ratio between the clear spacing between multiple openings with respect to their cover; p_{max}: pressure at peak; f_b: bond strength).

Series	ϕ [mm]	c_s / c_y	Top layer				Bottom layer			
			#	c_y / ϕ	p_{max} [MPa]	f_b [MPa]	#	c_y / ϕ	p_{max} [MPa]	f_b [MPa]
		-	1	0.25	2.1	-	9	0.25	2.4	-
		-	2	0.50	2.7	-	10	0.50	5.2	-
		-	3	0.75	4.1	-	11	0.75	6.4	-
		-	4	1.0	4.7	-	12	1.0	7.8	-
		-	5	1.5	6.5	-	13	1.5	10.4	-
		-	6	2.0	8.4	-	14	2.0	13.9	-
		-	7	2.5	9.1	-	15	2.5	17.2	-
		-	8	3.0	-	-	16	3.0	19.2	-
CM11	20	-	17	0.25	-	3.1	25	0.25	-	4.7
		-	18	0.50	-	3.1	26	0.50	-	4.9
		-	19	0.75	-	3.6	27	0.75	-	5.0
		-	20	1.0	-	5.1	28	1.0	-	5.6
		-	21	1.5	-	-	29	1.5	-	6.3
		-	22	2.0	-	5.6	30	2.0	-	-
		-	23	2.5	-	-	31	2.5	-	8.1
		-	24	3.0	-	7.5	32	3.0	-	-
	10	-	1		-	-	6		11.4	-
	14	-	2		7.0	-	7		-	-
	20	-	3	1.25	6.2	-	8	1.25	9.5	-
	28	-	4		6.5	-	9		10.8	-
	40	-	5		6.1	-	10		8.3	-
CM12	10	-	11		11.1	-	16		-	-
	14	-	12		9.2	-	17		16.5	-
	20	-	13	2.0	9.5	-	18	2.0	15.3	-
	28	-	14		7.9	-	19		13.1	-
	40	-	15		8.6	-	20		-	-
		-	1		6.9	-	8		9.6	-
		0	2		1.9	-	9		2.2	-
		1	3		-	-	10		4.1	-
CM13	20	3	4	1.25	5.2	-	11	1.25	9.1	-
		4	5		5.9	-	12		9.7	-
		6.5	6		5.7	-	13		9.8	-
		9	7		5.9	-	14		9.5	-

Table 5.2: Concrete properties and strength ($f_{c,cyl}$ and f_{ct} given at the days of test).

Series	Test type	Cement [kg/m³]	*W/C* [-]	Aggregates [kg/m³]			Retarder [kg/m³]	Superpl. [kg/m³]	Age at testing [days]	$f_{c,cyl}$ [MPa]	CoV [%]	f_{ct} [MPa]	CoV [%]
				0/4	4/8	8/16							
CM11	Inflator								37-44	39.7	1.6	2.49	3.4
CM11	Pull-out	342	0.57	893	394	687	1.35	1.70	84-91	42.3	3.9	3.45	4.2
CM12	Inflator								47-54	40.5	2.5	2.78	-
CM13	Inflator								54-62	41.0	2.9	2.90	-

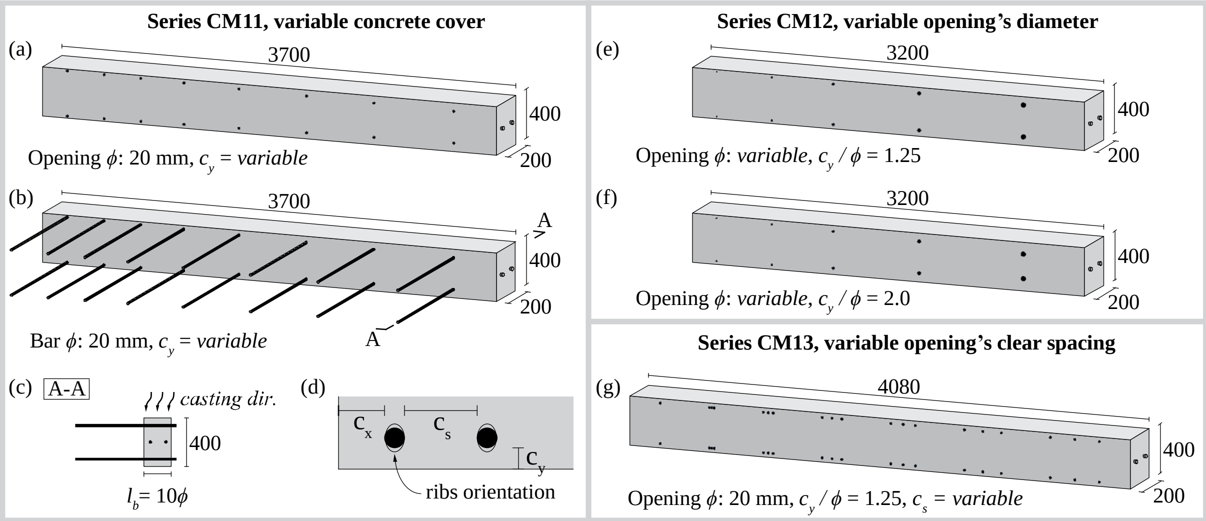

Figure 5.4: Geometry and reinforcement of the investigated series (dimensions in [mm], casting direction vertical): (a) specimen with 20 mm openings with variable concrete cover (series CM11); (b) specimen with 20 mm bars with variable concrete cover (series CM11); (c) cross section of prismatic specimen with reinforcing bars of series CM11; (d) definition of clear spacing c_s and concrete cover c_x, c_y in horizontal and vertical direction; (e) specimen with variable opening diameter and ratio c_y / ϕ = 1.25 (series CM12); (f) specimen with variable opening diameter and ratio c_y / ϕ = 2.0 (series CM12); and (g) specimen with variable clear spacing between the openings and constant opening diameter and c_y / ϕ ratio (series CM13).

5.4.2. Materials

The specimens were cast with ordinary ready-mix concrete provided by a local supplier. The cement was CEM II/B-LL 32.5R [53] and the maximum aggregate size was 16 mm. The concrete was poured in two layers of approximately 200 mm, with vibration of the first layer prior to pouring of the second one (casting and vibration conditions according to [54]). During casting, slump and flow tests were performed, ensuring the conditions of [55]–[57]. A slump of 140 mm was measured (corresponding to class S3) as well as a flow of 480 mm (F3 class). Details on the composition of the concrete are summarized in Table 5.2.

The concrete compressive strength was assessed by means of 30 concrete cylinders (160-mm diameter with a height of 320 mm) cast with the same batch of the girders. The cylinders were later sealed and cured during 14 days [54], being unmoulded and stored thereafter under the same standard laboratory conditions as for the prismatic specimens (average temperature of 21°C and average relative humidity of 50%). The cylinders were tested during the complete experimental programme under rapid loading conditions (with failure within approximately 2 minutes [58]), comprising also tests performed at reference ages (7, 14, 21 and 28 days). In addition, two direct tension tests were carried out on cylinders (identical dimensions as for compression tests) at 28 days and two additional tension tests were performed at the end of the experimental campaign. The compressive and tensile strength at the day of testing for each series was estimated on the basis of the strength development curve of the concrete (using the expressions provided in [59], with coefficients resulting from best-fit of the test results). Details for each specimen are provided in Table 5.2.

The reinforcement steel of the pull-out tests consisted of ϕ20 hot-rolled ribbed bars with a yield strength f_y = 521 MPa (standard deviation equal to 0.7 MPa) and a tensile strength f_t = 620 MPa (standard deviation equal to 1.2 MPa), tested according to [60]. The surface of the bars was laser-scanned to obtain accurate measurements of their rib area and bond index (f_R = 0.072 calculated according to [3]). No tests were performed on the 16-mm bars placed to control transverse cracking (f_{yk} = 500 MPa) as they did not reach characteristic yield strength.

5.4.3. Instrumentation and setup

5.4.3.1. Tests with hydraulic inflator devices

Custom-made hydraulic inflator devices of variable diameters (10, 14, 20, 28, 40 mm) were produced to introduce a controlled radial pressure inside of a circular opening (Figure 5.5a-c). The devices were inserted into openings located within concrete specimens and were gradually filled with water by means of a pump, providing a uniform radial pressure on the surface of the openings. The inflator has been designed to minimise the volume of introduced water in the device in order to reduce the amount of stored energy during loading (thus allowing for a lower energy release at failure and thus for a stiffer response of the device). Consequently, the hydraulic inflator device was designed with an inner stainless steel tube and an outer membrane, with water only filling their gap (see Figure 5.5b).

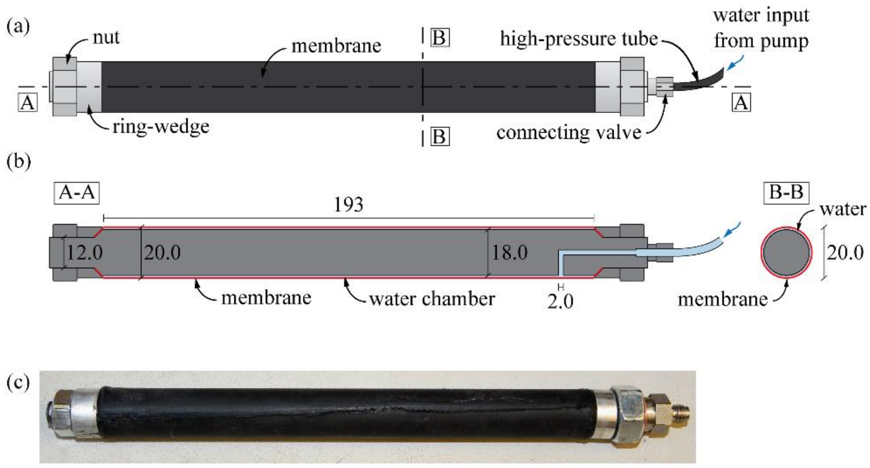

Figure 5.5: Testing arrangement (dimensions [mm]): (a) longitudinal view of ϕ20 hydraulic inflator device; (b) longitudinal and cross-sectional view of the hydraulic inflator; and (c) photo of an actual hydraulic inflator device.

The external membrane was made of a heat-shrink tube with a nominal thickness of 1 mm that was mechanically processed to obtain the required external diameter. In general, the external diameter was set 0.4 mm smaller than the diameter of the openings to ease their installation. The length of the membrane (193 mm) was slightly shorter than the total length of the openings (200 mm) to avoid development of bumps at their ends. The membrane water-tightness was ensured by two external steel rings tightened by two nuts (Figure 5.5a). Tests on water-tightness showed that the device could resist 32 MPa of pressure (maximum capacity of the water pump) without any leakage or degradation. Prior to testing, air has been removed completely from the system.

The pressure in the device was tracked by means of a pressure gauge. Tests performed on air with the device showed that inflating the membrane required approximately 0.3 MPa for a dilatation of the diameter equal to 1 mm. This pressure shows that the stiffness of the membrane is very low and will thus be neglected in the following. Pumping was performed by means of an electronic water pump (GDS ADVDPC 32 MPa [61]) with the following sequence: initial water flow of 8 mm^3/s until a pressure of 0.3 MPa; reduced water flow of 3 mm^3/s between 0.3 and 1 MPa; and finally 1.5 mm^3/s until failure of the concrete cover (tests with a typical duration of 30 minutes).

5.4.3.2. Pull-out tests

With respect to the pull-out tests of reinforcement, an adjustable steel frame was used (Figure 5.6). Before testing, the frame was centred to the actual location of the bar and the load was introduced by means of a mechanical hinge (ensuring no transferred bending moment to the bar). The tests were displacement-controlled, with a duration until maximum load of approximately 5 min. The pull-out specimens were instrumented with a linear variable displacement transformer (LVDT) placed at the unloaded-end of the bar (refer to Figure 5.6).

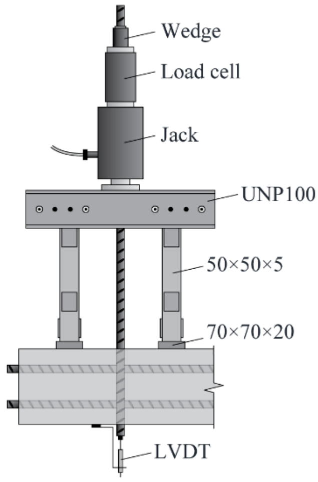

Figure 5.6: Pull-out setup (dimensions [mm]).

5.4.3.3. DIC measurements

All tests were monitored with Digital Image Correlation (DIC) using two pairs of high-resolution cameras (Manta G1235B with a resolution of 12.3 Mpix and Manta G419B with 4 Mpix) tracking the surface displacements. The DIC measurements were performed at a frequency of 0.1 Hz at low load levels and were ultimately increased to 2 Hz near failure. The software VIC-3D [62] was used to post-process the data, with a maximum error of approximately 1/25 of a pixel (93×93 μm^2 pixel dimension of Manta G1235B, and 116×116 μm^2 for Manta G419B).

5.5. Experimental results

A summary of the measured peak pressure (p_{max}) and bond strength (f_b) are presented in Table 5.1 for the entire experimental programme. As shown in Table 5.1, for the tests performed with the hydraulic inflator devices, it was not possible to reach spalling of the cover for six specimens due to the premature failure of the inflator’s membrane. These tests will thus not be considered in the following. With respect to the pull-out tests, four bars could not be tested due to the presence of a pre-existing crack originated by a test previously performed on the opposite layer.

5.5.1. Inner-pressure tests with the hydraulic inflator device

5.5.1.1. Influence of cover

Series CM11 aimed at investigating the effect of concrete cover and casting position on the spalling resistance. Figure 5.7 shows the maximum pressure recorded for this series providing also a detailed overview of the out-of-plane displacements measured with DIC on the top and bottom surfaces.

All tests failed by spalling of the concrete cover. As shown in Figure 5.7a, the maximum recorded pressure increases almost linearly with increasing concrete cover and was consistently higher for the bottom position than for the top one. This latter fact indicates that the casting position plays a major role in the spalling resistance of the cover. Such effect can be explained by the reduced concrete tensile strength near to the top surface due to bleeding (in particular in the vertical direction, refer to [63]) as well as by the presence of pre-existing cracks and voids around the openings related to the plastic settlement of fresh concrete [46], [52]. More details on this aspect will be discussed later. Also, the trends observed in Figure 5.7a are in agreement with those obtained by other authors with similar testing devices [26], [27], as shown in Figure 5.2b.

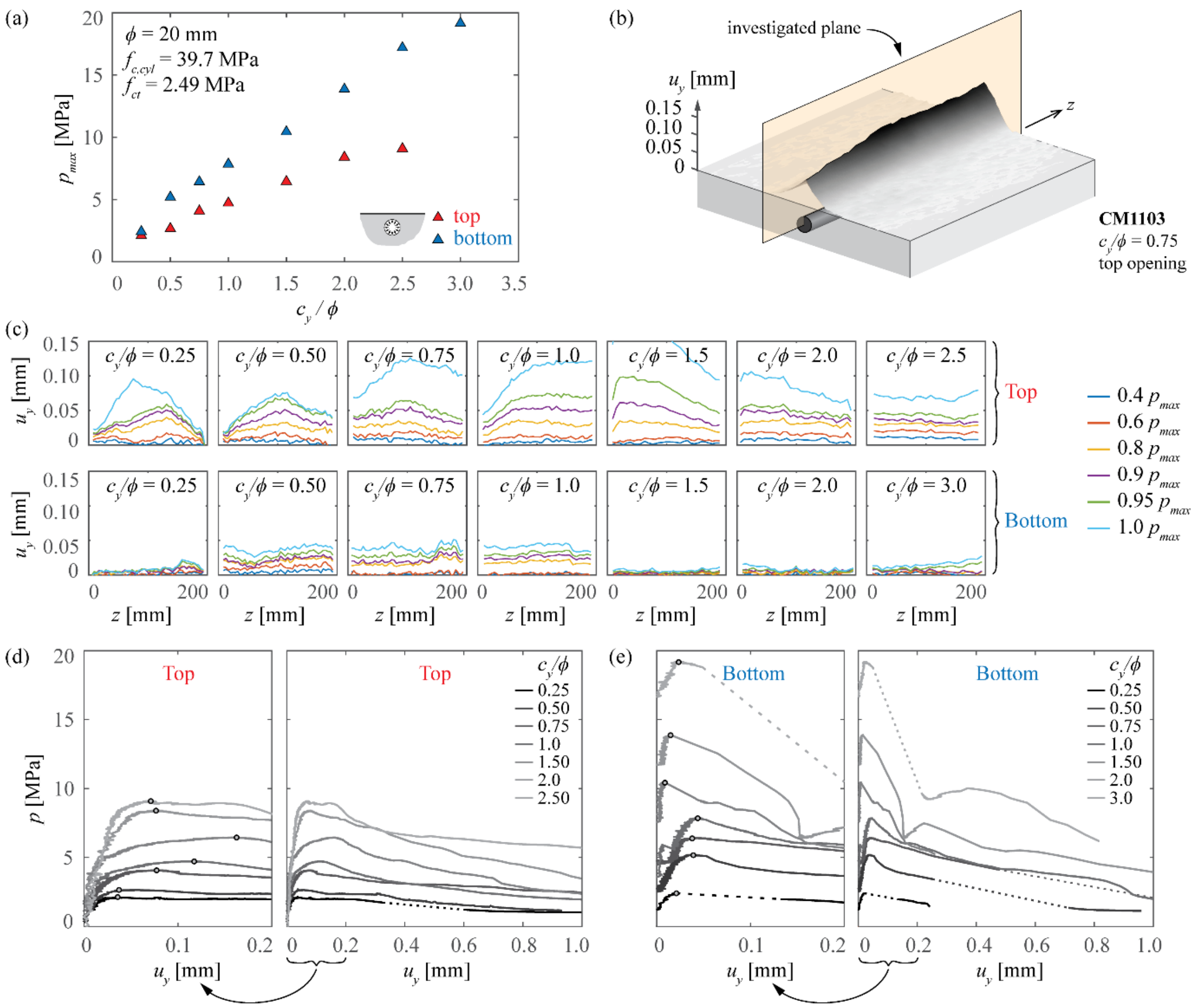

Figure 5.7: Main results of test series CM11 with hydraulic inflator devices: (a) maximum pressure reached within the openings as a function of the concrete cover and position (top or bottom layer); (b) instance of the out-of-plane displacement (u_y) measured on the surface; (c) longitudinal distribution of the out-of-plane displacement for several load steps; (d-e) pressure as a function of the maximum out-of-plane displacement recorded on the surface (dotted lines: no recording available; plots to the left correspond to a zoom of the first loading stages with indication of maximum pressure).

Figure 5.7b shows the out-of-plane displacements of the free surface for an illustrative test. From such measurements, the profile of out-of-plane displacements along the inflator axis can be determined as depicted in Figure 5.7c. This figure shows that the out-of-plane displacements for tests near to the top surface are significantly higher than the corresponding of the bottom layer. In general, out-of-plane maximum displacements of about 0.05-0.15 mm were recorded at peak load on the top surface, while these values were generally smaller than 0.05 mm on the bottom surface.

The recorded pressure as a function of the maximum out-of-plane displacement is also plotted in Figure 5.7d-e for the top and bottom surfaces and different cover-to-diameter ratios. As depicted in Figure 5.7d, the tests on the top openings showed a relatively tough post-peak behaviour, particularly in case of low concrete covers. On the other hand, the tests on the openings of the bottom layer presented a significantly brittle post-peak behaviour, with a large decrease of the residual capacity for increasing concrete covers (Figure 5.7e). In some cases, the increase of out-of-plane displacements was sudden and, despite the high frequency of measurements, it was not possible to follow the entire post-peak response (indicated with dotted lines in Figure 5.7d-e). Interestingly, the residual capacity of the bottom openings seems to stabilize to values similar to the ones observed in the post-peak response of the top openings.

A closer look at the evolution of the horizontal and vertical displacements at the sides of the openings (instrumented with DIC) can be seen in Figure 5.8 for some selected specimens. According to this Figure, the relative horizontal displacement near top openings appears to have a stiffer response compared to the vertical one (perpendicular to the free surface). The softer response in the vertical direction could be explained by the gradual opening with increasing inner pressure of pre-existing plastic settlement cracks. On the contrary, for bottom openings (in which casting position effects are not relevant), the relative displacement in the vertical and horizontal direction are virtually identical. It can also be noted that the out-of-plane displacement measured on the surface (refer to Figure 5.7d-e) corresponds to the relative vertical displacement u_y measured at the side of the elements (Figure 5.8).

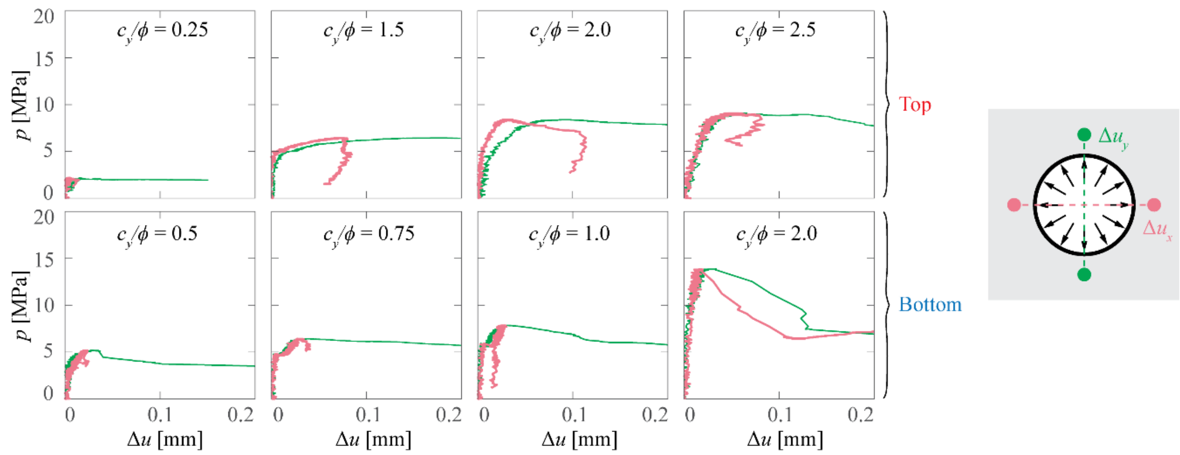

Figure 5.8: Vertical and horizontal relative displacements measured with DIC around the openings as a function of the applied pressure for specimens with different concrete cover (green: vertical measurement perpendicular to the free surface, orange: horizontal measurement parallel to the free surface).

The DIC measurements performed at the sides of the elements allowed in addition for detailed analyses on the crack patterns and their evolution. Figure 5.9 shows for some selected locations the measured crack opening (w) as a function of the applied pressure. The response observed is very different for top and bottom openings. Two representative cases of the top layer are shown in Figure 5.9a-b. For these specimens, the cracks developed gradually, with larger crack widths near the circular openings. The spalling failure mechanism was characterized by the development of two concrete wedges formed at each side of the bar. With respect to the cracks, an opening was recorded even at low pressures (refer to graphs of points A, B, C). This implies that the cracks already existed prior to testing, which can be attributed to the plastic settlement of fresh concrete [52], [64]. The phenomenon of plastic settlement has thus a direct impact on the position and shape of the cracks and, eventually, also on the failure mechanism of the investigated specimens.

With respect to the openings of the bottom layer (Figure 5.9c-d), the crack development was significantly different. In fact, prior to failure, only the vertical crack towards the surface developed, a phenomenon that occurred at approximately 70-80% of the maximum pressure (refer to graphs of point B in Figure 5.9c-d). All other cracks developed suddenly at the peak value of the pressure. The crack propagation was thus unstable, showing a very brittle behaviour. It should also be pointed out that, for both top and bottom openings, the inclination and shape of the cracks was different for each test, implying a variety of potential failure mechanisms.

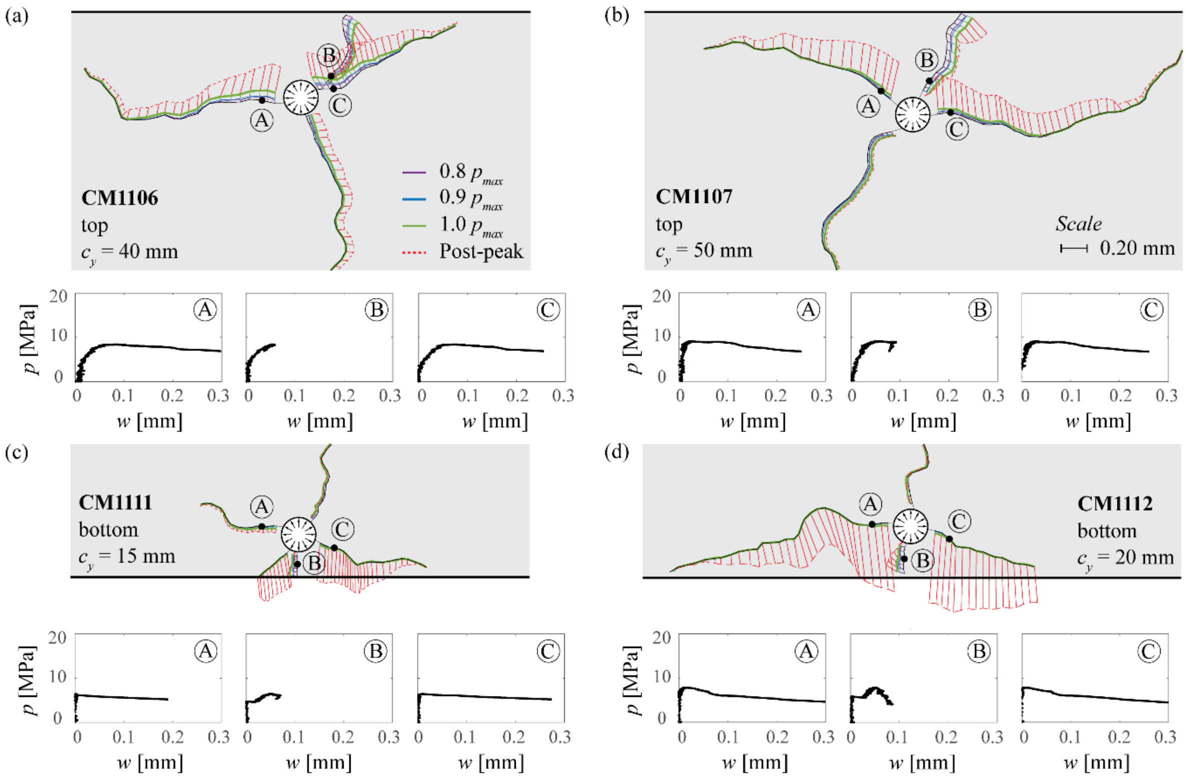

Figure 5.9: Crack development and relative crack displacements at selected load steps and crack opening as a function of the applied pressure at selected crack locations (A, B, C): (a) specimen CM1106; (b) specimen CM1107; (c) specimen CM1111; and (d) specimen CM1112.

5.5.1.2. Influence of size of the opening (size effect)

Series CM12 was aimed at investigating the influence of the size of the openings on the spalling resistance. Figure 5.10a-b depicts the peak value of the pressure as a function of the diameter and position of the openings as well as their representation in double-log scale. The out-of-plane displacements (based on DIC measurements) are also plotted in Figure 5.10c-f as a function of the applied radial pressure.

As shown in Figure 5.10a-b, the maximum pressure recorded appears to decrease with increasing diameter of the openings. This result is consistent both for the top and bottom layers as well as for cover-to-diameter ratios of 1.25 and 2.0. In addition, it can be noted that the strength decrease with increasing size is more pronounced for larger cover dimensions (Figure 5.10b). These observations give evidence of the significance of size effect when dealing with spalling failures. The measured slopes of the size effect in double-log scale for the specimens with small cover (c / ϕ = 1.25) leads to an approximate slope of -1:5 for bottom openings and to a slope of -1:10 for top openings. This is in accordance with a significantly more brittle response for bottom openings. These slopes are in any case clearly milder than the one corresponding to a behaviour governed by linear-elastic fracture mechanics (-1:2) according to the size-effect law for bond [65]. They indicate thus that nonlinear fracture mechanics is governing for the response in the range of parameters investigated and that some level of redistribution of internal stresses is potentially possible (as for shear-related failures [66], [67]). Insufficient experimental data is however available for a complete analysis of the associated size-effect law [65]. With respect to the tests with larger cover (c / ϕ = 2.0), the measured slopes are higher, -1:3 for bottom openings and -1:5 for top openings, corresponding to a more brittle response (this is also consistent with the more brittle behaviour shown in Figure 5.7d-e). As for the low concrete cover specimens, the response of openings located at the bottom is observed again to be more brittle (associated to higher slopes of the size effect in double-log scale).

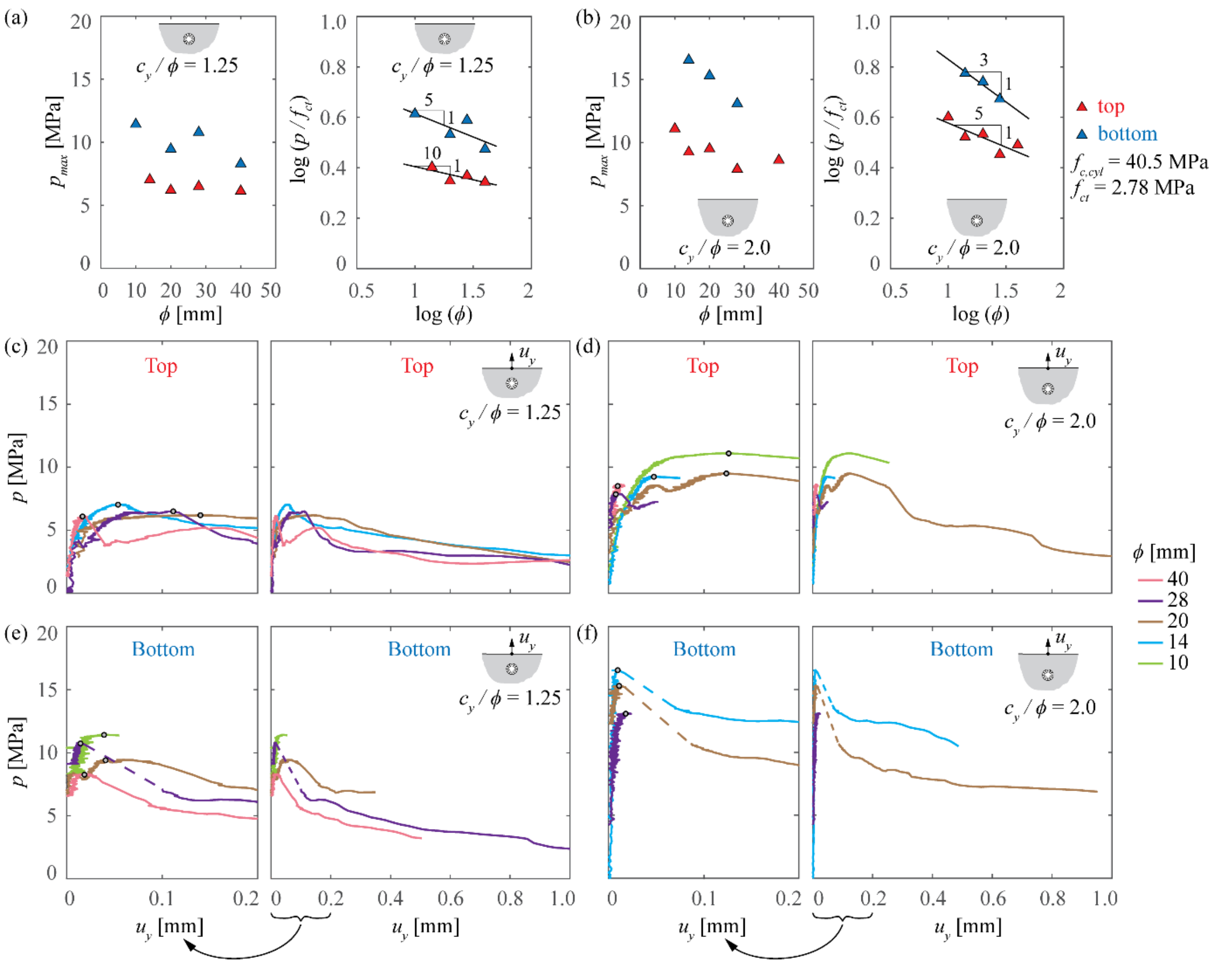

Figure 5.10: Main results of test series CM12: (a-b) maximum pressure as a function of their diameter and position (top or bottom layer) for c_y / ϕ = 1.25 and c_y / ϕ = 2.0 as well as representation in double-log scale; (c-f) applied pressure as a function of the maximum out-of-plane displacement recorded on the surface (top or bottom layer) for a cover-to-diameter ratio of 1.25 and 2.0.

In a similar manner as for series CM11, the openings located near to the top surface exhibited in all cases smaller peak pressures compared to the openings of the bottom layer. This observation shows again the significance of the casting position effects on the spalling resistance.

Figure 5.10c-f presents the load - out-of-plane displacement relationships at the location where the peak value of such displacement was reached. Here again, the tests on the top openings showed a higher out-of-plane displacement at peak pressure and a more ductile behaviour compared to the openings of the bottom layer. However, it seems that larger opening diameters (for instance ϕ = 40 mm) were associated in almost all cases to lower out-of-plane displacements at failure and to a more brittle post-peak response for both the top and bottom position. With this respect, it has to be observed that the enhanced brittleness could however be also partly attributed to the energy stored in the larger volume of water stored in the inflator device.

5.5.1.3. Influence of disturbance spacing (group effect)

Series CM13 was addressed at investigating the influence of the group effect on the spalling resistance of the cover. Figure 5.11a displays the maximum pressure recorded for different values of the clear spacing c_s when compared to a reference (isolated) opening (shown with dashed lines). A representative cracking pattern with the associated displacements is also shown in Figure 5.11b.

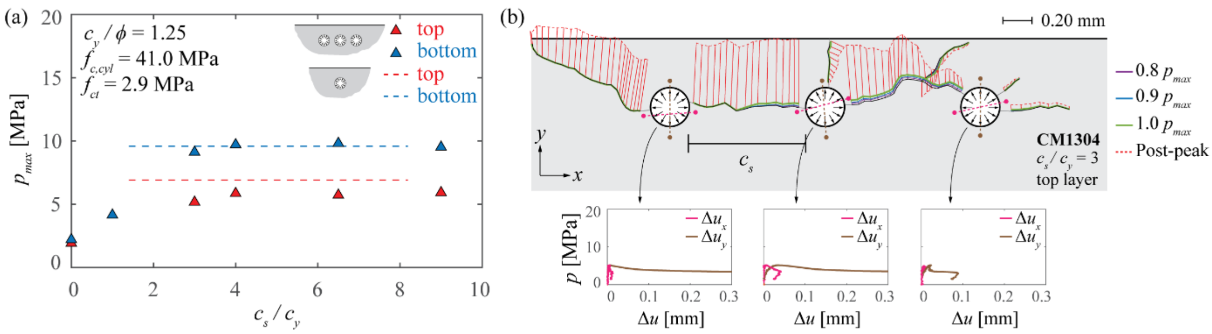

Figure 5.11: Main results of test series CM13: (a) maximum pressure as a function of their clear spacing and opening position (top or bottom layer); and (b) specimen CM1304: crack development and relative crack displacements at selected load steps and vertical (Δu_y) and horizontal (Δu_x) relative displacement at each opening.

As depicted in Figure 5.11a, for groups of widely spaced openings (c_s / c_y > 3), the peak strength reaches similar values as the one of the references with single openings both for top and bottom casting positions (represented with horizontal dashed lines in the Figure). For lower values of the opening spacing (c_s / c_y < 3), the resistance is however reduced. This result clearly indicates that the group effect has an influence on the spalling resistance of the cover.

With respect to the detailed cracking pattern shown in Figure 5.11b for a specimen influenced by the group interaction (specimen CM1304 with c_s / c_y = 3), the crack development differs significantly from that of isolated openings (see for instance Figure 5.9). The failure surface develops with a horizontal crack between the different openings and two inclined cracks at the sides plus a quasi-vertical crack (Figure 5.11b). As for isolated disturbances, for group of bars, a clear difference is also observed in terms of strength for top and bottom openings, with lower spalling resistances associated to the top position.

5.5.2. Pull-out tests

With respect to the pull-out tests with embedded length 10ϕ, Figure 5.12 depicts the bond strength f_b averaged over the anchorage length and the corresponding slip at peak load δ_{peak} (measured at the unloaded end of the bars) as a function of the cover-to-diameter ratio. The location of the bars with respect to the casting direction (top or bottom layer) as well as the observed failure mode (spalling or pull-out) are also indicated with different colours and symbols.

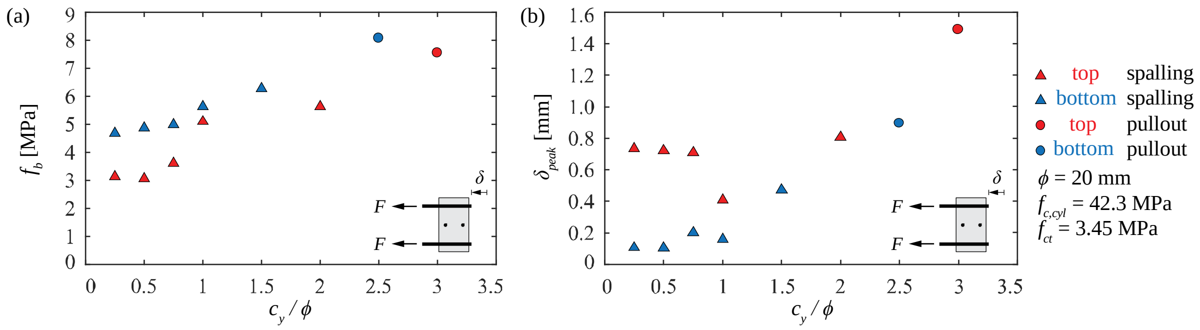

Figure 5.12: Main results of the pull-out tests of series CM11: (a) bond strength averaged over the anchorage length as a function of the concrete cover and bar position (top or bottom layer); (b) slip measured at the peak bond strength as a function of the concrete cover and bar position.

As shown in Figure 5.12a, the bond strength increases for increasing cover of the bars. Such increase seems to follow an almost linear trend, both for the top and bottom reinforcing bars. It can be noted that, even for low values of the concrete cover, a significant bond strength is observed, in accordance to the observations of Cairns and Jones [2]. Spalling failures occurred for cover-to-diameter ratios lower than approximately 1.5-2.0. For higher values, pull-out failures were observed (as also reported by Schenkel [44], [45] on short pull-out specimens, refer to Figure 5.3b).

With respect to the influence of casting conditions, top bars were observed to provide lower bond strength than the corresponding bottom bars, indicating poorer bond conditions. This response can be attributed to the phenomena of bleeding and plastic settlement [52]. The latter (plastic settlement) is responsible for creating continuous voids under the reinforcement [46], [52] as well as inclined cracks reaching the surface [68]. The former (bleeding) influences mostly the tensile resistance of concrete in the top region and can also create large pores under bars or aggregates [63].

With respect to the slip measured at peak load (Figure 5.12b), it can be noted that it tends to increase for increasing values of the concrete cover. The phenomenon is however somewhat scattered. Also, the top layer of reinforcement presents larger slips at peak compared to the corresponding bottom layer. This observation can be related to the presence of voids under the bars originated by plastic settlement that requires some slip of the bar to engage the ribs, as discussed more in detail in the following.

Figure 5.13 relates the average bond stress, the slip recorded at the unloaded end of the bars and the out-of-plane displacement of the surface (measured with the DIC at the centre of the bond length). Both results for the top layer (Figure 5.13a) and bottom layer (Figure 5.13b) are presented. It should be noted that it was not possible to record the complete post-peak behaviour at the surface (measured with DIC) due to the significant spalling of the cover once the peak bond strength is reached. On the contrary, the LVDT (placed at the unloaded end of the bar) recorded the slip for the entire post-peak response of most of the bars (refer to Figure 5.13).

As shown in Figure 5.13a, bars placed in the top layer start to slip at low values of the applied load. This occurs in addition for an almost negligible out-of-plane displacement (particularly for low values of concrete cover), implying that early slip of the bar can occur without developing significant transverse pressures. Such observation can be justified, as previously discussed, by the presence of voids originated by plastic settlement and located under the bars (reducing the contact area between the bar and the surrounding concrete and requiring some level of slip to centre the bar and to engage mechanical contacts [69]). With respect to the bottom reinforcement (Figure 5.13b), the voids associated to plastic settlement are negligible and the response is much stiffer, with low slip at early loading stages. In addition, small slips of these bars are accompanied by an out-of-plane displacement on the surface, indicating an almost perfect engagement between the bar and the surrounding concrete.

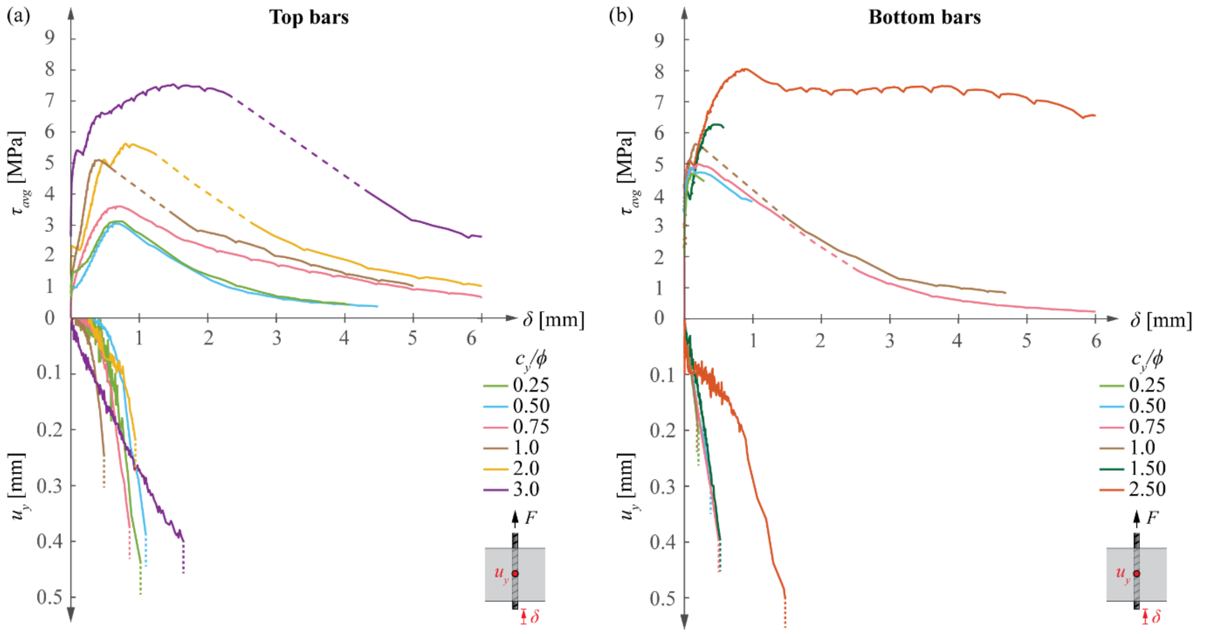

Figure 5.13: Bond response and out-of-plane displacement as function of the slip at the unloaded end of the bars (dotted lines: no recording available): (a) top layer; (b) bottom layer.

With respect to the post-peak response, the bottom bars showed a relatively brittle response, Figure 5.13b, with a sudden drop of resistance once the maximum load was reached. Also, it can be noted that the tests characterized by pull-out failures ($c_y / \phi \geq 3.0$ in the top layer, $c_y / \phi \geq 2.5$ in the bottom layer) exhibit a less brittle behaviour and a larger residual strength compared to test failing by spalling of the concrete cover.

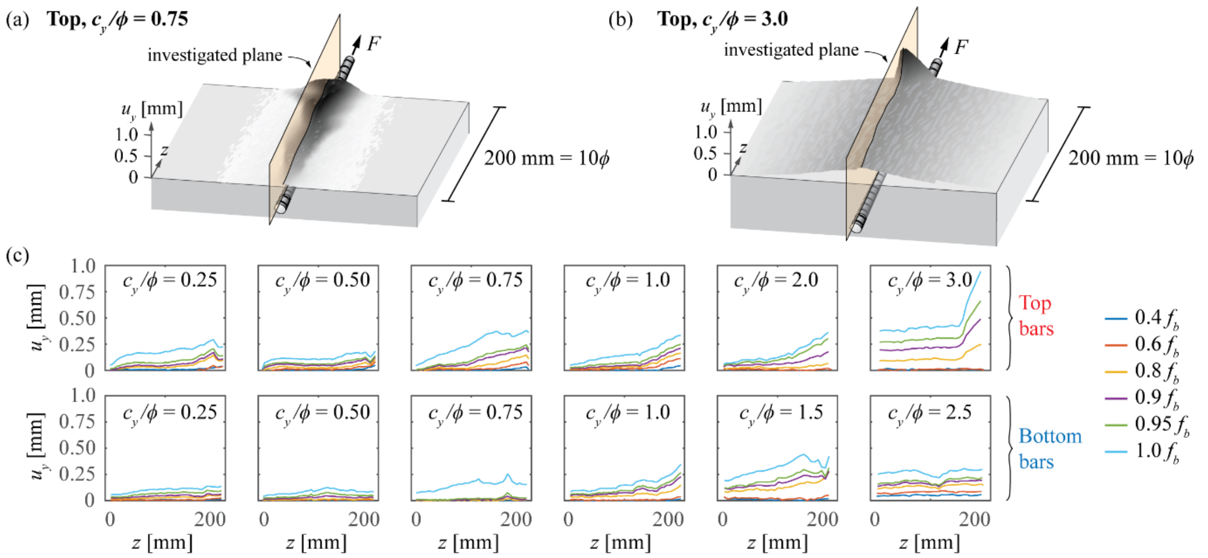

Figure 5.14: Out-of-plane displacement (u_y) at failure measured on the surface: (a) specimen CM1119 at peak load; (b) specimen CM1124 at peak load; and (c) longitudinal distribution of the out-of-plane displacement for several load steps and for all pull-out tests.

The measured out-of-plane displacements are presented in Figure 5.14. The observed profiles are relatively different to those of inner-pressure tests, with maximum values concentrated at the loaded end of the bar, which can be explained by the higher slips in this region. Figure 5.14c shows the distribution of the out-of-plane displacements measured on the surface along the reinforcing bars for selected load steps. The overall out-of-plane displacements seem to increase with increasing concrete cover, both for top and bottom bars. Just before failure, near to the loaded end, large values of the out-of-plane displacement were recorded (u_y above 0.2 mm) indicating that concrete in tension was in its softening regime and that stress redistributions potentially occurred. In addition, some discontinuities can be observed near to the loaded ends (probably related to the development of conical cracks around the bar and reaching the surface, as observed by Goto [70]). Differently to the tests with the hydraulic inflator device, the out-of-plane displacements were similar for top and bottom bars.

5.6. Analysis of spalling failures based on detailed measurements of crack development

The use of DIC measurement techniques allowed for accurate observations of the behaviour of the concrete cover and crack propagation at the sides of the members. With respect to tests performed with the hydraulic inflator device, the crack propagation occurred in a stable manner for most of the tests in the top casting position (except for large diameters of openings). However, the propagation was unstable and very brittle for bottom bars (and large diameters openings). In this section, the recorded crack openings and kinematics of the tests performed with the inflator device are used to investigate on the state of stresses developed in the failure region (information later used to develop a design model).

5.6.1. Tests with stable crack propagation

As previously discussed (refer to Figure 5.9), different types of cracks leading to spalling failures were observed: i) cracks inclined towards the free surface, ii) quasi-vertical cracks connecting to the free surface and iii) sub-vertical cracks opposed to the free surface. When the openings are located near to the top surface, cracks of the first two types were already present after casting due to plastic settlement (Figure 5.15a) [46], [52], [68]. Similar patterns were also observed when the disturbances were located near the bottom surfaces, but the cracks did not open until some level of internal pressure was reached (Figure 5.9c-d). In fact, in the region near the bottom formwork, the concrete surrounding the opening was not influenced by any previous cracking or reduction of the tensile strength related to bleeding and plastic settlement (Figure 5.15b).

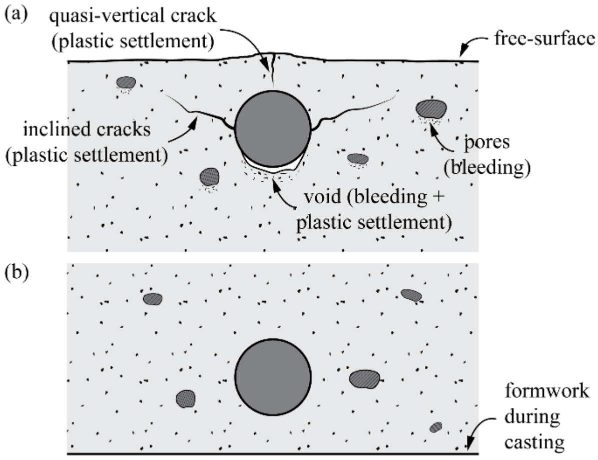

Figure 5.15: Influence of casting position effects on the spalling resistance, adapted from [52]: (a) observed cracks types in the region near the top surface (free surface during casting), cracks related to plastic settlement and reduction of the concrete tensile strength due to bleeding; and (b) region near the bottom formwork without cracks due to settlement and without major pores due to bleeding.

On the basis of the crack shape and kinematics, an estimate of the stresses transferred through the cracked surfaces can be obtained. This will be performed following the methodology presented by Cavagnis et al. [71] (refer also to Campana et al. [72]) for shear cracks. This approach [71] accounts for the recorded crack opening (w_n) and sliding (w_t) at every point of a crack. On this basis, the residual tensile strength (depending on w_n) and the contact stresses associated to aggregate interlocking (depending on w_n and w_t) can be determined by means of suitable constitutive laws (Reinhart for the residual tensile strength [73] and expressions consistent with the Two-Phase Model by Walraven [74] for the interlock contribution). By integration of such stresses, the transferred forces across the crack can eventually be determined. Figure 5.16a-b shows an instance for two representative cases (specimens CM1105 and CM1106) analysed with this methodology.

As shown in Figure 5.16, different responses can be observed depending on the shape and kinematics of the cracks, with contributions to the spalling resistance both of shear (associated to crack sliding) and normal stresses (associated to crack opening). In addition, it can be noted that the cracks are not fully developed at peak load until the free surface, implying the presence of an uncracked concrete region potentially contributing to the spalling resistance (but whose contribution cannot be determined since the measurement of the strains in the uncracked zone was not sufficiently accurate). With respect to the distribution of the vertical stresses resulting from the normal and tangential stresses acting on the crack surface at failure, it appears that the ratio f_v/f_{ct} varies around a value of approximately 0.5 (despite some level of scatter, see Figure 5.16). This indicates that a reduced strength should be considered when assessing the spalling resistance of openings near the top surface. In addition, the horizontal position of the resultant of stresses varies between values of approximately 0.8-1.2 × c_y.

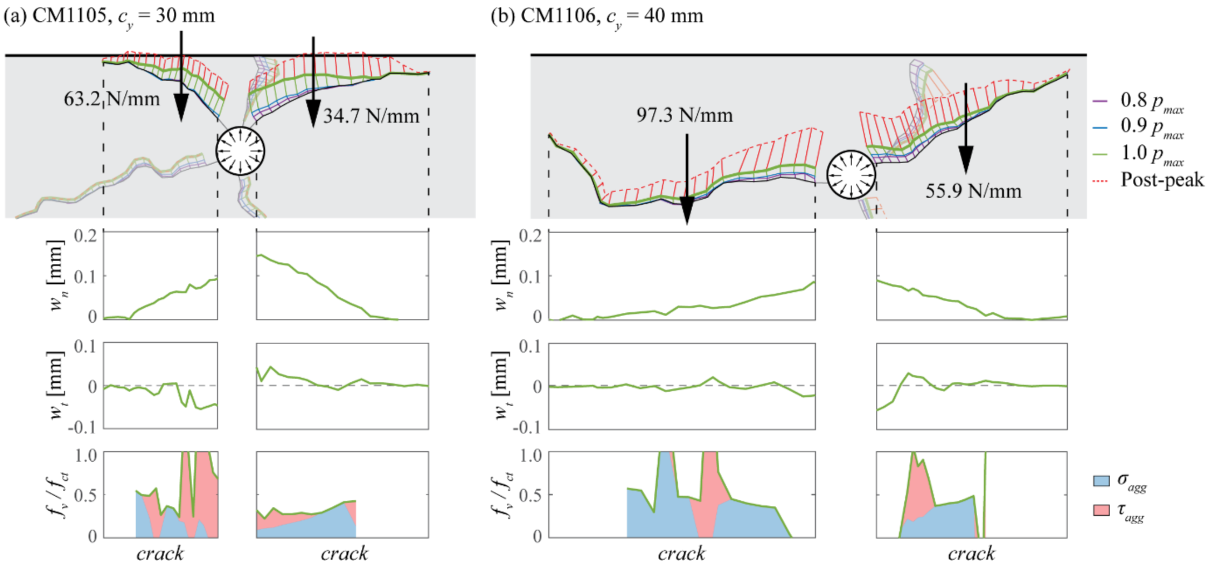

Figure 5.16: Resultant of the integration of the shear and normal stresses along the crack at failure according to Cavagnis [71] (w_n: crack opening, w_t: crack sliding, τ_{agg}: shear stresses, σ_{agg}: normal stresses, f_v: vertical force per unit length): (a) specimen CM1105; and (b) specimen CM1106.

It should be pointed out that the analyses have been performed on the basis of measurements on one side of the member and a potential variation through the thickness of the element is possible. However, Cavagnis et al. [75] noticed that this effect leads in general to limited variations of the strength in the case of beams in shear (within the experimental scatter).

5.6.2. Tests with unstable crack propagation

For the tests performed near to the bottom surface, the observed shapes of the cracks were comparable to those performed near to the top surface. However, except for the quasi-vertical crack, all cracks presented almost negligible opening before the peak pressure was attained, when they followed a sudden and unstable propagation (Figure 5.9c-d). In this case, the response can be assumed to be governed fundamentally by fracture mechanics considerations (although the asymptotic size effect of linear-elastic fracture mechanics does not apply for the investigated cases as previously discussed) and no conclusions can be drawn on the analysis of the crack surfaces. It is yet interesting to note that, despite the relatively different phenomenon triggering failure, comparable trends to those of tests failing with stable crack propagation were observed. This can for instance be seen in Figure 5.10 for the large bar diameter in top position (failing by unstable propagation but with a trend comparable to the other tests on top position failing with stable crack propagation).

5.7. Design approach for spalling failures due to the application of an internal pressure

On the basis of the previous considerations, a simplified approach can be proposed to assess the spalling strength of bars located near the concrete cover. This approach is consistent with previous simplified models [16], [43], [44], assuming a given geometry for the crack surface and an average strength of the concrete cover in tension.

5.7.1. Geometrical parameters

Based on the observations of the crack development and kinematics, the spalling failure mechanism is assumed to be characterized by two concrete wedges developing a translation movement and a rotation due to the pressure applied, refer to Figure 5.17a.

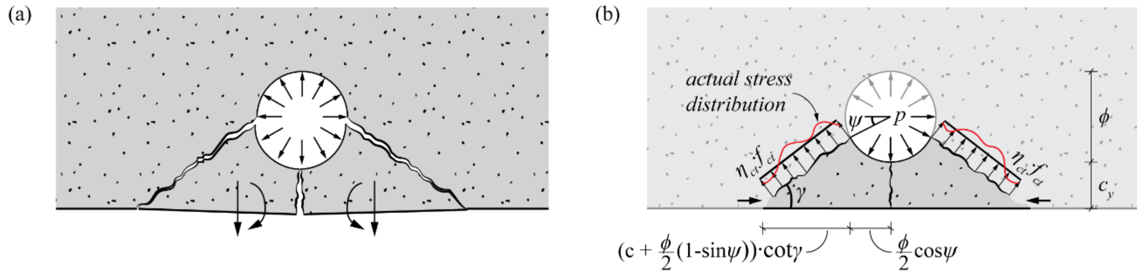

Figure 5.17: Idealized model for radial pressure: (a) idealized cover spalling mechanism; and (b) assumed stress distribution along the cracks.

In this approach, it is assumed that cracks develop from a point located at an angle ψ with respect to the mid-height of the openings and have a linear shape characterized by an inclination γ. As previously shown in Figure 5.9, the angle at which these cracks develop is highly variable, both for top and bottom openings. As a simplification of all these cases, the γ angle is set to a constant value assumed such that $\sin\gamma = 0.60$ ($\gamma \approx 37°$).

5.7.2. Stress distribution and equilibrium of forces

The potentially variable distribution of the tensile stresses along a crack (Figure 5.17b) is simplified in the following by assuming an average value of the tensile stress equal to $\sigma_t = \eta_{ct} \cdot f_{ct}$, where η_{ct} accounts for the concrete brittleness in tension and is taken equal to 0.8 (expression considered valid for concrete strengths up to 50 MPa according to [16]). In the following calculations, the mean tensile strength measured in the experimental programme is considered for the definition of f_{ct} (values outlined in Table 5.2). As shown in Figure 5.17b, the vertical component of the concrete tensile stresses is given by:

$$\eta_{ct} \cdot f_{ct} \cdot \cos\gamma \tag{5.3}$$

and the length over which it develops corresponds to:

$$\left(c_y + \phi/2 \cdot (1-\sin\psi)\right) \Big/ \sin\gamma \tag{5.4}$$

The equilibrium condition of the forces acting in the vertical direction leads to:

$$p \cdot \frac{\phi}{2} \cdot \cos\psi = \frac{\eta_{ct} \cdot f_{ct}}{\tan\gamma} \cdot \left(c_y + \frac{\phi}{2} \cdot (1-\sin\psi) \right) \tag{5.5}$$

so that:

$$p = \frac{\eta_{ct} \cdot f_{ct}}{\tan\gamma} \cdot \frac{2c_y/\phi + (1-\sin\psi)}{\cos\psi} \tag{5.6}$$

According to limit analysis, the governing failure mechanism can be obtained by minimizing:

$$F(\psi) = \frac{2c_y/\phi + (1-\sin\psi)}{\cos\psi} \tag{5.7}$$

so that:

$$\sin\psi = \frac{1}{1+\dfrac{2c_y}{\phi}} \tag{5.8}$$

which allows determining the load carrying capacity as:

$$p = \frac{\eta_{ct} \cdot f_{ct}}{\tan\gamma} \cdot 2 \cdot \sqrt{\frac{c_y}{\phi} + \left(\frac{c_y}{\phi}\right)^2} \tag{5.9}$$

It can be noted that when c_y/ϕ is large, the optimum value is obtained with $\psi \approx 0°$, which corresponds to:

$$p = \frac{\eta_{ct} \cdot f_{ct}}{\tan\gamma} \cdot \left(1 + \frac{2c_y}{\phi}\right) \tag{5.10}$$

Such response is relevant when concrete covers are large, but could also be governing in case pre-existing cracks are present (for instance due to plastic settlement near top bars, Figure 5.15a) and govern the shape of the failure surface. In the following, the formulation of Eq. (5.9), in which the angle ψ is optimized, is further developed, but considerations will also be performed on the case of $\psi = 0°$.

5.7.3. Consideration of size effect

The experimental programme has confirmed that peak pressures decrease with increasing size of the openings (refer to Figure 5.10), giving evidence of the significance of size effect for spalling failures. This effect is related to the tensile strength of the cover, but also to the opening of the cracks in cases of stable crack opening [66], [67] (where larger sizes are associated to larger crack openings and thus to a lower residual tensile strength of concrete). On this basis, Eq. (5.9) is corrected to account for this effect, adopting the same parameter as for shear-related cases according to prEN 1992-1-1:2018 [76]:

$$p = \frac{\eta_{ct} \cdot f_{ct}}{\tan\gamma} \cdot 2 \cdot \sqrt{\frac{c_y}{\phi} + \left(\frac{c_y}{\phi}\right)^2} \cdot \left(\frac{d_{dg}}{d_{dg0}} \cdot \frac{\phi_0}{\phi}\right)^{1/m} \tag{5.11}$$

Where d_{dg0} = 32 mm and ϕ_0 = 20 mm (reference sizes). It can be noted that the size effect factor accounts for the maximum aggregate size and the bar diameter [76]. This dependence is a simplified approach, as other potentially influencing parameters (for instance the concrete cover) are not explicitly considered. By simplifying the reference sizes, the previous equation becomes:

$$p = \frac{\eta_{ct} \cdot f_{ct}}{\tan\gamma} \cdot 2 \cdot \sqrt{\frac{c_y}{\phi} + \left(\frac{c_y}{\phi}\right)^2} \cdot \left(\frac{d_{dg}}{1.6\phi}\right)^{1/m} \tag{5.12}$$

Where the d_{dg} parameter is an average roughness whose value can be calculated as [71]:

$$d_{dg} = \min(40 \text{ mm}; 16 + d_g) \qquad \text{for } f_c \le 60 \text{ MPa} \tag{5.13}$$

where d_g corresponds to the maximum aggregate size. The value of exponent m corresponds to the slope of the size effect law observed in the double-log scale diagram of Figure 5.10. Its value is assumed in the following equal to 3 according to prEN 1992-1-1:2018 [76] for similar problems. This leads to a constant slope of the size effect in double-log scale equal to -1:3, which was observed to be a safe estimate of the results shown in Figure 5.10 for the range of typical dimensions related to the bond phenomenon.

5.7.4. Considerations on casting position and tensile strength

Consistently to the experimental results by other authors [44], [47], it has been observed in this testing programme that the casting position had a significant influence on the spalling resistance. As previously discussed, this influence can be attributed to the phenomena of bleeding and plastic settlement. Bleeding reduces mostly the concrete tensile strength (especially in the vertical direction due to the presence of pores under coarse aggregates [63]), while the plastic settlement is associated to the initiation of cracks around the bar (Figure 5.15a). For design purposes, it is suggested to account for them by means of an additional strength reduction factor (η_{is}):

$$p = \frac{\eta_{is} \cdot \eta_{ct} \cdot f_{ct}}{\tan\gamma} \cdot 2 \cdot \sqrt{\frac{c_y}{\phi} + \left(\frac{c_y}{\phi}\right)^2} \cdot \left(\frac{d_{dg}}{1.6\phi}\right)^{1/m} \tag{5.14}$$

On the basis of the test results presented in this paper, it will be adopted in the following a constant reduction factor η_{is} = 0.6 when the disturbances are located in the top layer. As it can be noted, the consideration of both η_{is} and η_{ct} reduces the concrete tensile strength to a value of approximately $0.5f_{ct}$ (as $\eta_{is}\times\eta_{ct} = 0.48 \approx 0.5$), in accordance with the measured distribution of f_v / f_{ct} along the cracks shown in Figure 5.16. Although some future work would be required to lead to a more comprehensive definition of this parameter, such approach gives consistent agreement to the different cases, as it will later be shown.

5.7.5. Consideration of multiple disturbances

The experimental programme has also shown the detrimental effect of groups of narrow-spaced disturbances (Figure 5.11b). In these cases, the failure surface of one disturbance can intersects those of the surrounding elements, resulting in the development of horizontal cracks amongst them. Therefore, the spalling failure mechanism presented in Figure 5.17 is adapted to account for the group effect, as illustrated in Figure 5.18.

In this case, it can be noted that the governing solution is close to $\psi \approx 0°$ as the interaction between the failure surfaces of the individual bars takes place for sufficient depth of the concrete cover. In the following, Eq. (5.10) will thus be adopted for consideration of multiple disturbances.

Based on geometrical considerations of Figure 5.18, one can compute the spacing leading to a group effect as:

$$c_{s,\lim} = 2 \cdot \frac{c_y + \phi / 2}{\sin\gamma} \cdot \cos\gamma = \frac{2c_y + \phi}{\tan\gamma} \tag{5.15}$$

Considering a number of n disturbances at a spacing lower than $c_{s,lim}$, the resistance will result:

$$n \cdot p \cdot \phi = \frac{2 \cdot \eta_{is} \cdot \eta_{ct} \cdot f_{ct}}{\tan\gamma} \cdot \left(c_y + \frac{\phi}{2} \right) \cdot \left(\frac{d_{dg}}{1.6\phi} \right)^{1/m} + (n-1) \cdot \eta_{is} \cdot \eta_{ct} \cdot f_{ct} \cdot c_s \cdot \left(\frac{d_{dg}}{1.6\phi} \right)^{1/m} \tag{5.16}$$

$$p = \frac{\eta_{is} \cdot \eta_{ct} \cdot f_{ct}}{n \cdot \phi} \cdot \left(\frac{2c_y + \phi}{\tan\gamma} + (n-1) \cdot c_s \right) \cdot \left(\frac{d_{dg}}{1.6\phi} \right)^{1/m} \tag{5.17}$$

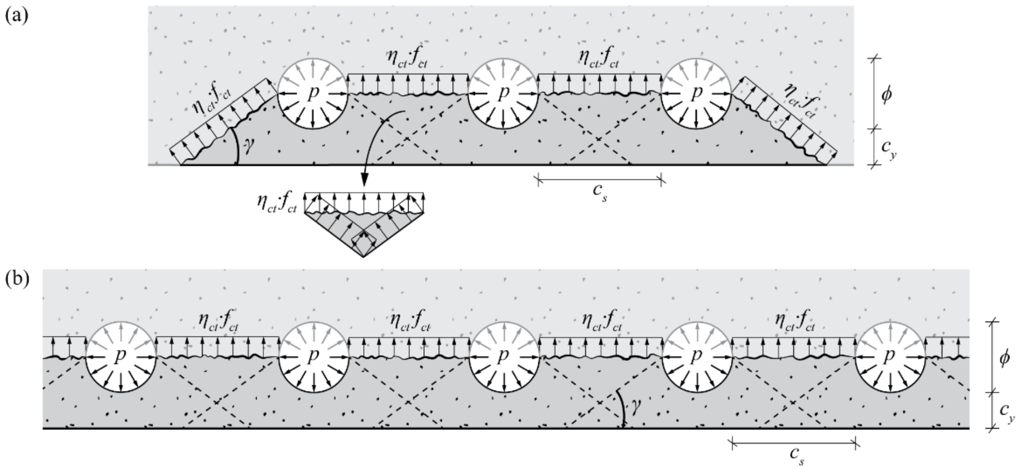

Figure 5.18: Spalling failure mechanism in case of multiple openings closely spaced: (a) case with three openings; and (b) case with large number of openings.

5.7.6. Comparison to test results

The results of the experimental programme are compared in Figure 5.19 to the spalling resistance calculated on the basis of the proposed approach for single openings (Eq. (5.14)) and for multiple openings (Eq. (5.17)). The results show sound agreement with an average of measured-to-calculated strength of 1.02 and a Coefficient of Variation of 12.3 %. If a constant value ψ = 0° were adopted, the overall average becomes 0.98 and the Coefficient of Variation is 12.7 %. In general, significant differences between both approaches are only notable for low values of c / ϕ (< 1.0), refer to Figure 5.19a.

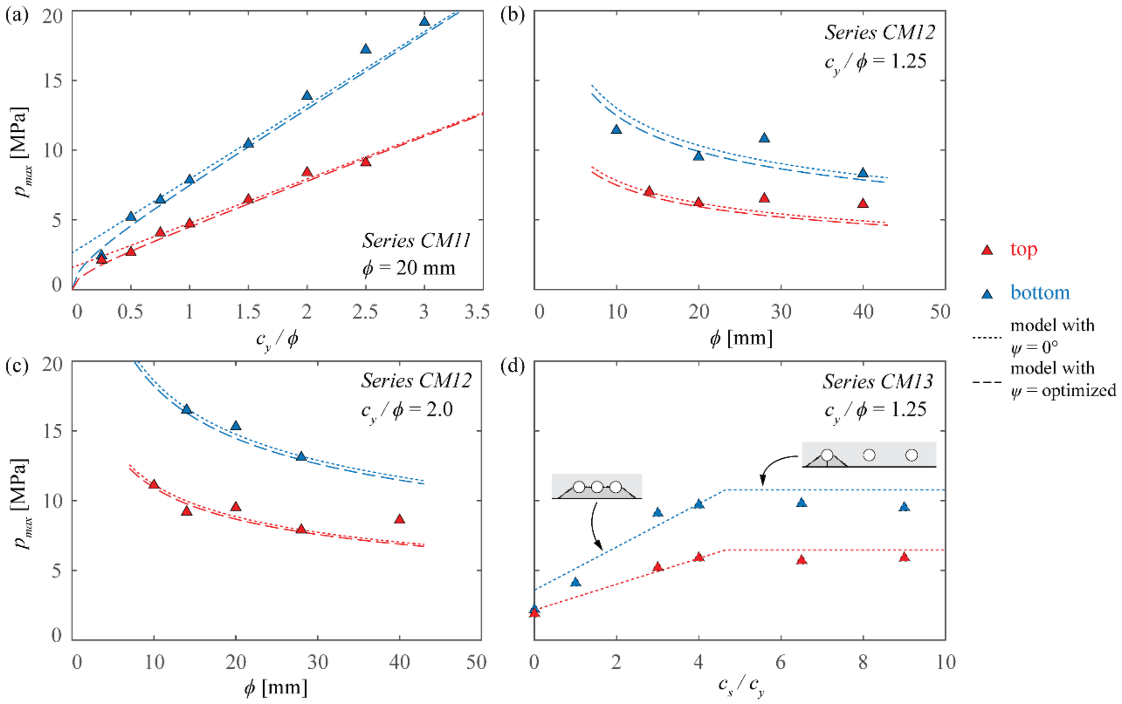

Figure 5.19: Main results of the proposed models (refer to Eqs. (5.10, 5.14, 5.17)) for the entire results of the experimental programme (triangle markers): (a) model for top and bottom openings with variable concrete cover (series CM11); (b) model for top and bottom openings with variable diameter (series CM12, c/ϕ = 1.25); (c) model for top and bottom openings with variable diameter (series CM12, c/ϕ = 2.0); and (d) model for top and bottom openings with variable spacing (series CM13).

In addition, the results of the test series CM11 (variable cover-to-diameter ratio) are compared to the experimental findings of Williamson and Clark [26] and Morinaga [27]. As shown in Figure 5.20, the results of the latter authors follow a similar trend as for the top openings of series CM11 (despite the differences in the diameter of the openings, the dimensions of the specimens, loading rates and that the casting position and direction are not specified). With this respect, the series of Williamson and Clark and of Morinaga were performed on specimens with small dimensions (150-200 mm), leading to comparable conditions as for openings in the upper part of series CM11.

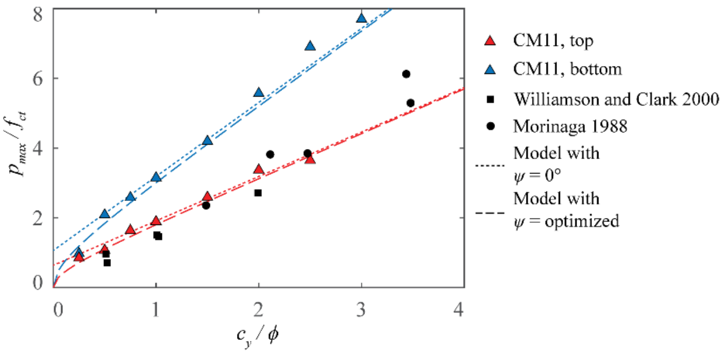

Figure 5.20: Comparison of test series CM11 and proposed models with available tests performed with hydraulic inflator devices taken from the literature [26], [27].

5.8. Design proposal for pull-out spalling failures

The tests on pull-out specimens showed a complex response in which, just before failure, the out-of-plane displacements were highly variable. According to the performed measurements (refer to Figure 5.14), some regions presented out-of-plane displacements larger than those developed at peak strength for tests performed with inflator devices while other regions showed relatively low values. Based on these observations, indicating potential stress redistributions between different regions, the phenomenon of cover spalling due to bond engagement is investigated in this section on the basis of a simple mechanical approach. The approach integrates the information on the response of openings subjected to an internal pressure (as presented in the previous section) by accounting for the observed out-of-plane displacements in pull-out tests.

Following the idealization by Tepfers, it is assumed in the following that the response of a bar being pulled-out is governed by two components, one depending on the pressure developing perpendicular to the cover ($p_\perp$) and another depending on a pressure acting parallel to the cover ($p_{//}$), see Figure 5.21a. According to this consideration, equation (5.1) proposed by Tepfers [1], [30], [31] can be rewritten as follows:

$$f_b = \lambda \cdot p_\perp \cdot \cot\theta_\perp + (1-\lambda) \cdot p_{//} \cdot \cot\theta_{//} \tag{5.18}$$

where coefficient λ denotes the part of bar perimeter associated to each component, that will be set in the following equal to 0.5 for simplicity purposes (future work on this value is however advised to address in a consistent manner the influence of rib orientation and shape).

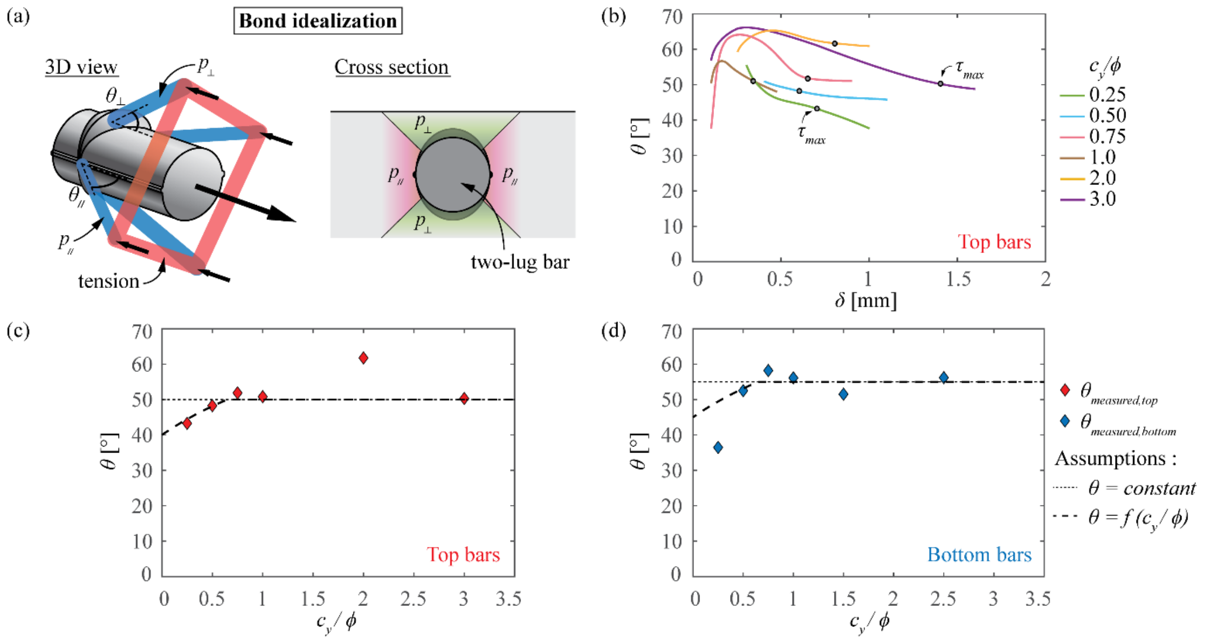

Figure 5.21: (a) Idealization of bond strength by means of splitting components $p_\perp$ and $p_{//}$; (b) measured average angle of the struts θ as function of the slip δ; (c) measured angle θ at peak bond strength for the top bars of series CM11 and comparison to assumed values of θ; and (d) measured angle θ at peak bond strength for the bottom bars of series CM11 and comparison to assumed values of θ.

In absence of specific measurements, it will also be assumed in a simplified manner that $\cot\theta_\perp = \cot\theta_{//} = \cot\theta$, leading to:

$$f_b = \left(\lambda \cdot p_\perp + (1-\lambda) \cdot p_{//}\right) \cdot \cot\theta \tag{5.19}$$

The values of the angle θ (angle between the compressive struts and the bar axis, refer to Figure 5.1a) can be obtained from the measurements performed in the experimental programme. To do so, the measured out-of-plane displacements u_y are used to compute the corresponding radial pressure p (which is assumed to account for its two components, i.e. $p = \lambda \cdot p_{\perp} + (1-\lambda) \cdot p_{//}$). This is performed by using the p-u_y measurements obtained with the inflator devices shown in Figure 5.7d-e and considering the difference on the tensile strengths for the two series (refer to values in Table 5.2). Such value can be eventually associated to a given bond stress (Figure 5.13) allowing to determine the $\tau - p$ relationship and consequently the values of θ (by using Eq. (5.1)). Instances of the calculated angle θ as a function of the slip of the bars δ are shown in Figure 5.21b for the complete loading process (case of top bars). From these measurements, it is also possible to select the value of θ at maximum bond strength for each investigated specimen (indicated as bullets in Figure 5.21b).

The results referring to the angle θ at maximum bond strength obtained following this procedure are depicted in Figure 5.21c-d for top and bottom bars, respectively. As it can be noted, the angle θ is relatively constant for the different c_y/ϕ ratios (except for low values of this ratio). Also, a difference between top and bottom bars can be observed, with higher values at failure for bottom bars. As a first estimate of θ, a simplified (constant) value of the angle θ can thus be adopted based on the measurements (Figure 5.21c-d) as follows:

$$\begin{aligned} &\theta = 50° &&\text{(top bars)} \\ &\theta = 55° &&\text{(bottom bars)} \end{aligned} \tag{5.20}$$

For a more accurate evaluation of this angle, is it also possible to consider the influence of the ratio c_y/ϕ (Figure 5.21c-d):

$$\begin{aligned} &\theta = 40° + 20 \cdot \ln\left(1 + \frac{c}{\phi}\right) \leq 50° &&\text{(top bars)} \\ &\theta = 45° + 20 \cdot \ln\left(1 + \frac{c}{\phi}\right) \leq 55° &&\text{(bottom bars)} \end{aligned} \tag{5.21}$$

For evaluation of Eq. (5.19), the pressure acting perpendicular to the cover $p_{\perp}$ (related to the radial pressure induced by the wedging action of the ribs) can be estimated on the basis of the pressure p determined with the formulations derived for the case of the application of an internal pressure (refer to Eqs. (5.14) and (5.17) for an optimized value of ψ or to Eq. (5.10) for ψ = 0°). With respect to the pressure acting parallel to the concrete cover ($p_{//}$), it is likely to be dependent on the geometry and spacing of the ribs, as well as the state of cracking surrounding the bar. The measurements performed in the experimental programme did not allow for an accurate estimate of this parameter. In the following, for the case investigated experimentally (ribs oriented toward the free surface), a simplified value will be assumed:

$$\begin{aligned} p_{//,top} &= \eta_{is} \cdot p_{//,bot} \\ p_{//,bottom} &= 6.0 \text{ MPa} \end{aligned} \tag{5.22}$$

Where a distinction is made between top and bottom bars, by considering the casting position effects η_{is} = 0.6.

Based on these considerations, the bond strength at failure can be computed in a simple manner. To do so, Eq. (5.19) can be used with either constant (Eq. (5.20)) or variable (Eq. (5.21)) angles of the struts and the formulations presented in Eqs. (5.10), (5.14) and (5.17) for the radial pressure $p_{\perp}$ as well as Eq. (5.22) for the pressure $p_{//}$. This approach is compared in Figure 5.22 to the results of current experimental programme. The predictions show consistent agreement with the observed trends of the spalling failures in pull-out conditions. With respect to the formulation with constant values of θ (Figure 5.22a), the average of the measured-to-calculated strength results 1.07 with a Coefficient of Variation equal to 14.0 % when the angle ψ is optimized. If the angle $\psi = 0°$ is used (Eq. (5.10)), the average becomes 1.0 and the scatter is lower (Coefficient of Variation of 11.2 %).

When the angle θ is considered as variable (see Eq. (5.21) and Figure 5.22b), the formulation of Eq. (5.19) gives an average of measured-to-calculated strength of 1.01 and Coefficient of variation of 9.9 % for an optimized value of ψ. In this case, if $\psi = 0°$ is adopted, the average becomes 0.95 and the Coefficient of Variation is equal to 10.0 %. As it can be noted, the trends are suitably reproduced in all cases. Additional experimental evidence should however be considered for a more comprehensive definition of the angle θ and the component $p_{//}$.

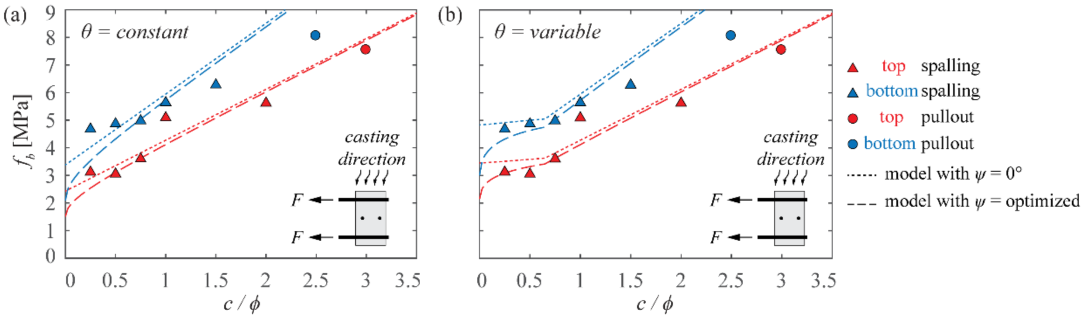

Figure 5.22: Main results of the proposed models (dotted lines) and comparison to the pull-out tests performed in current study (triangles and circle markers, series CM11): (a) case with angle of the struts θ constant; and (b) case with θ variable.

5.9. Conclusions

This paper presents the results of an investigation on the spalling of concrete cover induced by an internal radial pressure (as can be generated for instance by expansion of rust due to bar corrosion) or by bond in reinforced concrete. The phenomenon is investigated by means of detailed measurements on a series of tests performed with hydraulic inflator devices as well as on pull-out tests of embedded reinforcement. On that basis, the mechanisms triggering failure are identified and reproduced by means of simple mechanical models. The main findings of the paper are summarized below:

1. The spalling response is observed to be relatively different for elements cast in the top and bottom layers due to the phenomena of bleeding and plastic settlement of fresh concrete. Plastic settlement generates cracks radiating from top bars to the surface, which can progress when an internal pressure is applied and eventually become part of a spalling mechanism. Such cracks do not exist on the contrary for bars located near a bottom surface. Bleeding is also associated to a lower tensile strength of the concrete near to the top casting surface, reducing the spalling strength with respect to bars located near to the bottom surface.

2. An analysis of the crack propagation leading to spalling failures shows a more brittle response for elements in the bottom layer when a pressure is applied inside an opening. In this case, failure occurs by a sudden development and propagation of cracks (only quasi-vertical cracks can develop in a stable manner). On the contrary, for elements in the top layer, the presence of existing cracks due to plastic settlement allows for their controlled propagation until failure. This is associated to a less brittle response.

3. The difference of the response of top and bottom layers in terms of brittleness is also confirmed by means of an analysis of the size effect significance when an internal pressure is applied in

the openings. For bottom bars, the observed slopes of the size effect in double-log scale for the cases investigated (in the range corresponding to practical design situations) reach values ranging between -1/5 and -1/3, while the slopes range between -1/10 and -1/5 for top bars. These values are in any case milder than the asymptotic slope corresponding to linear-elastic fracture mechanics (-1/2) and confirm that for practical design purposes, adopting a constant slope equal to -1/3 (as performed by prEN1992-1-1:2018 for similar cases) is a reasonable and safe choice.

4. The group effect has an influence on the spalling strength of the cover. For low values of the clear spacing, the cracks of neighbouring bars intersect and generate a more unfavourable failure surface (associated to a lower length where tensile stresses oppose the spalling forces).
5. A model to assess the spalling resistance against a uniform radial pressure is proposed and validated on the basis of the results and observations of the experimental programme. The model is based on a simplified geometry and stress profile of the failure surface, consistently with the analysis performed on actual cracking patterns, and accounts as well for the casting position, size and group effects.
6. Differently to tests subjected to a uniform radial pressure (showing a rather constant out-of-plane displacement along the location where the pressure is applied), pull-out tests show a non-uniform profile of out-of-plane displacements along the bar. Just before failure, some regions display relatively high out-of-plane displacements (associated to regions in softening) while others have low values. This indicates that stress redistributions can potentially occur.
7. The analysis of the out-of-plane displacements of pull-out tests and its comparison to inner-pressure tests allows estimating the angle of the compression struts transferring forces by bond. Based on these measurements together with an estimate of the acting pressures, a simple approach can be proposed to assess the spalling strength of pull-out bars. Such approach shows consistent agreement to experimental evidence and opens a field for future modelling of bond.

5.10. References

[1] R. Tepfers, "A theory of bond applied to overlapped tensile reinforcement splices for deformed bars," PhD Thesis, Division of Concrete Structures, Chalmers University of Technology, Göteborg, Sweden, 328 p., 1973.

[2] J. Cairns and K. Jones, "The splitting forces generated by bond," *Magazine of Concrete Research*, vol. 47, no. 171, pp. 153–165, 1995.

[3] International Federation for Structural Concrete, "fib Bulletin 10: Bond of reinforcement in concrete," State-of-art report prepared by Task Group Bond Models, Lausanne, Switzerland, 439 p., 2000.

[4] P. D. Cady and R. E. Weyers, "Deterioration rates of concrete bridge decks," *Journal of Transportation Engineering*, vol. 110, no. 1, pp. 34–44, 1984.

[5] M. Prieto, P. Tanner, and C. Andrade, "Bond Response in Structural Concrete with Corroded Steel Bars. Experimental Results," *Modelling of Corroding Concrete Structures, RILEM Bookseries 5, Springer Netherlands, Dordrecht*, pp. 231–241, 2011.

[6] I. Balafas and C. J. Burgoyne, "Modeling the Structural Effects of Rust in Concrete Cover," *Journal of Engineering Mechanics*, vol. 137, no. 3, pp. 175–185, 2011.

[7] S. J. Pantazopoulou and K. D. Papoulia, "Modeling Cover-Cracking due to Reinforcement Corrosion in RC Structures," *Journal of Engineering Mechanics*, vol. 127, no. 4, pp. 342–351,

2001.

[8] K. Bhargava, A. K. Ghosh, Y. Mori, and S. Ramanujam, “Analytical model for time to cover cracking in RC structures due to rebar corrosion,” *Nuclear Engineering and Design*, vol. 236, no. 11, pp. 1123–1139, 2006.

[9] O. Graf, “Versuche über die Widerstandsfähigkeit des Betons an den Abbiegestellen der schief abgebogenen Eisen in Eisenbetonbalken,” *Deutscher Ausschuss für Eisenbeton, Heft 94, Berlin-München, Germany*, pp. 1–55, 1940.

[10] F. Leonhardt, R. Walther, and H. Dieterle, “Versuche zur Ermittlung der Tragfähigkeit von Zugschlaufenstössen,” *Deutscher Ausschuss für Stahlbeton, Heft 226, Berlin-München, Germany*, pp. 1–22, 1973.

[11] D. Stucki and B. Thürlimann, “Versuche an Eckverbindungen aus Stahlbeton,” *Institut für Baustatik und Konstruktion, ETH Zürich, Switzerland, Nr. 8701-1*, pp. 1–68, 1990.

[12] G. Franz and H. D. Fein, “Tests on R/C Culvert and Tunnel Lining, 2nd test series (‘Betonversuche mit Baustahlgewebe-Bewehrungen für Rohre und Tunnelverkleidungen, Versuchsreihe 2’),” Baustahlgewebe Berichte aus Forschung und Technik, Heft 8, Düsseldorf-Oberkassel, Germany, 52 p., 1971.

[13] H. D. Fein and U. Zwissler, “Accomodating Deviation Forces of Curved Reinforcing Bars with Concrete (‘Aufnahme von Umlenkkräften aus stetig gekrümmten Bewehrungsstäben durch den Beton’),” *Die Bautechnik*, vol. 51, no. 2, pp. 58–61, 1974.

[14] J. Neuner and S. Stöckl, “Research on Accommodating Deviation Forces of Curved Reinforcing Bars with Concrete Cover and Stirrups (‘Versuche zur Aufnahme der Umlenkkräfte von gekrümmten Bewehrungsstäben durch Betondeckung und Bügel’),” *Deutscher Ausschuss für Stahlbeton, Heft 322, Berlin-München, Germany*, pp. 71–106, 1981.

[15] M. Intichar, “Investigation on the Interaction between Bond Stresses and Deviation Stresses (Untersuchung der Interaktion zwischen Verbundspannungen und Umlenkspannungen),” Technische Universität Graz, Insitut für Betonbau, Graz, Austria, 95 p., 2002.

[16] M. Fernández Ruiz, S. Plumey, and A. Muttoni, “Interaction between bond and deviation forces in spalling failures of arch-shaped members without transverse reinforcement,” *ACI Structural Journal*, vol. 107, no. 3, pp. 346–354, 2010.

[17] W. Krefeld and C. W. Thurston, “Contribution of Longitudinal Steel to Shear Resistance of Reinforced Concrete Beams,” *ACI Journal Proceedings*, vol. 63, no. 3, pp. 325–344, 1966.

[18] T. Baumann, “Versuche zum Studium der Verdübelungswirkung der Biegezugbewehrung eines Stahlbetonbalken,” *Deutscher Ausschuss für Stahlbeton, Heft 210, Berlin-München, Germany*, pp. 43–83, 1970.

[19] P. Soroushian, K. Obaseki, M. Rojas, and H. S. Najm, “Behavoir of Bars in Dowel Action against Concrete Cover,” *ACI Journal*, vol. 84, no. 2, pp. 170–176, 1987.

[20] E. N. Vintzēleou and T. P. Tassios, “Mathematical models for dowel action under monotonic and cyclic conditions,” *Magazine of Concrete Research*, vol. 38, no. 134, pp. 13–22, 1986.

[21] S. Dei Poli, M. Di Prisco, and P. G. Gambarova, “Cover and Stirrup Effects on the Shear Response of Dowel Bar Embedded in Concrete,” *ACI Structural Journal*, vol. 90, no. 4, pp. 441–450, 1993.

[22] E. W. H. Klingsch, “Explosive spalling of concrete in fire,” Institut für Baustatik und Konstruktion, Bericht Nr. 356, ETH, Zürich, Switzerland, 251 p., 2014.

[23] International Federation for Structural Concrete, “fib Bulletin 38: Fire design of concrete structures,” State-of-art report, Lausanne, Switzerland, 106 p., 2007.

[24] Z. Bažant, “Physical model for steel corrosion in concrete sea structures — application,” *Journal*

of the Structural Division, Proceedings of the American Society of Civil Engineers, vol. 105, no. 6, pp. 1155–1166, 1979.

[25] Z. Bažant, “Physical model for steel corrosion in concrete sea structures — theory,” *Journal of the Structural Division, Proceedings of the American Society of Civil Engineers*, vol. 105, no. 6, pp. 1137–1153, 1979.

[26] S. J. Williamson and L. A. Clark, “Pressure required to cause cover cracking of concrete due to reinforcement corrosion,” *Magazine of Concrete Research*, vol. 52, no. 6, pp. 455–467, 2000.

[27] S. Morinaga, “Prediction of service lives of reinforced concrete buildings based on the rate of corrosion,” Special Report No. 23, Institute of Technology, Shimuzu Corporation, 1988.

[28] M. L. Allan and B. W. Cherry, “Factors controlling the amount of corrosion for cracking in reinforced concrete,” *Corrosion*, vol. 48, no. 5, pp. 426–430, 1992.

[29] K. Noghabai, “Splitting of concrete covers - a fracture mechanics approach,” Fracture Mechanics of Concrete Structures, Proceedings FRAMCOS-2, Aedificatio Publishers, Freiburg, Germany, 1575-1584, 1995.

[30] R. Tepfers, “Cracking Of Concrete Cover Along Anchored Deformed Reinforcing Bars,” *Magazine of Concrete Research*, vol. 31, no. 106, pp. 3–12, 1979.

[31] R. Tepfers, “Lapped Tensile Reinforcement Splices,” *ASCE Journal of the Structural Division*, vol. 108, no. 1, pp. 283–301, 1982.

[32] M. Tirassa, M. Fernández Ruiz, and A. Muttoni, “An interlocking approach for the rebar-to-concrete contact in bond,” *Magazine of Concrete Research*, pp. 1–15, 2020, doi: https://doi.org/10.1680/jmacr.20.00209.

[33] J. Cairns, “An Analysis of The Ultimate Strength Of Lapped Joints Of Compression Reinforcement,” *Magazine of Concrete Research*, vol. 31, no. 106, pp. 19–27, 1979.

[34] E. Giuriani, G. Plizzari, and C. Schumm, “Role of stirrups and residual tensile strength of cracked concrete on bond,” *Journal of Structural Engineering*, vol. 117, no. 1, pp. 1–18, 1991.

[35] E. Giuriani and G. A. Plizzari, “Local bond-slip law after splitting of concrete (‘Legami locali dell’aderenza in presenza di fessure di splitting’),” *Studi e Ricerche, School for the Design of R/C Structures, Milan University of Technology*, vol. 7, pp. 57–118, 1985.

[36] E. Giuriani and G. P. Rosati, “Behaviour of concrete elements under tension after cracking (‘Comportamento di elementi tesi di calcestruzzo in fase fessurata’),” *Studi e Ricerche, School for the Design of R/C Structures, Milan University ofTechnology*, vol. 8, pp. 65–82, 1986.

[37] D. Darwin, S. McCabe, E. Idun, and S. Schoenekase, “Development Length Criteria: Bars not confined by Transverse Reinforcement,” *ACI Structural Journal*, vol. 89, no. 6, pp. 709–720, 1992.

[38] P. G. Gambarova and G. P. Rosati, “Bond and splitting in bar pull-out: Behavioural laws and concrete cover role,” *Magazine of Concrete Research*, vol. 49, no. 179, pp. 99–110, 1997.

[39] P. G. Gambarova, G. P. Rosati, and B. Zasso, “Steel-to-concrete bond after concrete splitting: test results,” *Materials and Structures*, vol. 22, no. 1, pp. 35–47, 1989.

[40] P. G. Gambarova, G. P. Rosati, and B. Zasso, “Steel-to-concrete bond after concrete splitting: constitutive laws and interface deterioration,” *Materials and Structures*, vol. 22, no. 5, pp. 347–356, 1989.

[41] P. G. Gambarova and G. P. Rosati, “Bond and splitting in reinforced concrete : Test results on bar pull-out,” *Materials and Structures/Materiaux et Constructions*, vol. 29, no. 5, pp. 267–276, 1996.

[42] L. J. Malvar, “Bond of reinforcement under controlled confinement,” Technical Report N-1833,

Naval Civil Engineering Laboratory, Port Hueneme, California, USA, 40 p., 1991.

[43] M. P. Nielsen and L. C. Hoang, "Limit Analysis and Concrete Plasticity," Third Edition, CRC Press, Taylor & Francis Group, Boca Raton, FL, USA, 788 p., 2011.

[44] M. Schenkel, "Zum Verbundverhalten von Bewehrung bei kleiner Betondeckung," PhD Thesis, Institut für Baustatik und Konstruktion, ETH, Zürich, Switzerland, 162 p., 1998.

[45] M. Schenkel and T. Vogel, "Versuche zum Verbundverhalten von Bewehrung bei mangelhafter Betondeckung," Institut für Baustatik und Konstruktion, ETH, Zürich, Switzerland, 92 p., 1997.

[46] A. Castel, T. Vidal, K. Viriyametanont, and R. François, "Effect of reinforcing bar orientation and location on bond with self-consolidating concrete," *ACI Structural Journal*, vol. 103, no. 4, pp. 559–567, 2006.

[47] J. O. Jirsa and J. E. Breen, "Influence of Casting position and shear on development and splice length - design reccomendations," Report No. 242-3F, Centre for Transportation Research, The University of Texas at Austin, Austin, TX, USA, 45 p., 1981.

[48] G. B. Welch and B. J. F. Patten, "Bond Strength of Reinforcement Affected by Concrete Sedimentation," *Journal Of The American Concrete Institute*, vol. 62, no. 2, pp. 251–264, 1965.

[49] B. B. Brettmann, D. Darwin, and R. C. Donahey, "Bond of Reinforcement To Superplasticized Concrete," *ACI journal*, vol. 83, no. 12. pp. 98–107, 1986.

[50] P. Dybel, D. Walach, and K. Ostrowski, "The Top-Bar Effect in Specimens with a Single Casting Point at One Edge in High-Performance Self-Compacting Concrete," *Journal of Advanced Concrete Technology*, vol. 16, no. 7, pp. 282–292, 2018.

[51] J. Cairns, "Influence of casting position on lap and anchorage strength," Heriot Watt University, Edinburgh, UK, 40 p., 2018.

[52] F. Moccia, X. Kubski, M. Fernández Ruiz, and A. Muttoni, "The influence of casting position and disturbance induced by reinforcement on the structural concrete strength," *Structural Concrete*, pp. 1–28, 2020.

[53] EN 197-1:2011, "Cement - Part 1: Composition, specifications and conformity criteria for common cements," European Committee for Standardization (CEN), Brussels, Belgium, 38 p., 2011.

[54] EN 13670:2013, "Execution of concrete structures," European Committee for Standardization (CEN), Brussels, Belgium, 66 p., 2013.

[55] EN 206+A1:2016-11, "Concrete - Specification, performance, production and conformity," European Committee for Standardization (CEN), Brussels, Belgium, 102 p., 2016.

[56] EN 12350-2:2019, "Testing fresh concrete - Part 2: Slump test," European Committee for Standardization (CEN), Brussels, Belgium, 8 p., 2019.

[57] EN 12350-5:2019, "Testing fresh concrete - Part 5: Flow table test," European Committee for Standardization (CEN), Brussels, Belgium, 12 p., 2019.

[58] D. Tasevski, M. Fernández Ruiz, and A. Muttoni, "Assessing the compressive strength of concrete under sustained actions: From refined models to simple design expressions," *Structural Concrete*, vol. 20, no. 3, pp. 971–985, 2019.

[59] International Federation for Structural Concrete, "fib Model Code for Concrete Structures 2010," Ernst & Sohn, Berlin, Germany, 434 p., 2013.

[60] EN ISO 6892-1:2016, "Metallic materials - Tensile testing - Part 1: Method of test at room temperature," European Committee for Standardization (CEN), Brussels, Belgium, 79 p., 2016.

[61] GDS Instruments, "Copyright," 2020.

[62] Correlated Solutions, “VIC-3D Digital Image Correlation.” Copyright 1998-2018 Correlated Solutions, Inc.

[63] G. Giaccio and A. Giovambattista, “Bleeding: Evaluation of its effects on concrete behaviour,” *Materials and Structures*, vol. 19, no. 4, pp. 265–271, 1986.

[64] F. Moccia, Q. Yu, M. Fernández Ruiz, and A. Muttoni, “Concrete compressive strength: From material characterization to a structural value,” *Structural Concrete*, pp. 1–21, 2020.

[65] Z. P. Bažant and S. Sener, “Size Effect in Pullout Tests,” *ACI Materials Journal*, vol. 85, no. 5, pp. 347–351, 1988.

[66] M. Fernández Ruiz, A. Muttoni, and J. Sagaseta, “Shear strength of concrete members without transverse reinforcement : A mechanical approach to consistently account for size and strain effects,” *Engineering Structures, Elsevier*, vol. 99, pp. 360–372, 2015.

[67] M. Fernández Ruiz and A. Muttoni, “Size effect in shear and punching shear failures of concrete members without transverse reinforcement: Differences between statically determinate members and redundant structures,” *Structural Concrete*, vol. 19, no. 1, pp. 65–75, 2018.

[68] R. Combrinck, L. Steyl, and W. P. Boshoff, “Interaction between settlement and shrinkage cracking in plastic concrete,” *Construction and Building Materials*, vol. 185, pp. 1–11, 2018.

[69] F. Brantschen, D. M. V. Faria, M. Fernández Ruiz, and A. Muttoni, “Bond behaviour of straight, hooked, U-shaped and headed bars in cracked concrete,” *Structural Concrete*, vol. 17, no. 5, pp. 799–810, 2016.

[70] Y. Goto, “Cracks Formed in Concrete Around Deformed Tension Bars,” *ACI Journal*, vol. 68, no. 4, pp. 244–251, 1971.

[71] F. Cavagnis, M. Fernández Ruiz, and A. Muttoni, “A mechanical model for failures in shear of members without transverse reinforcement based on development of a critical shear crack,” *Engineering Structures*, vol. 157, pp. 300–315, 2018.

[72] S. Campana, M. Fernández Ruiz, A. Anastasi, and A. Muttoni, “Analysis of shear-transfer actions on one-way RC members based on measured cracking pattern and failure kinematics,” *Magazine of Concrete Research*, vol. 56, no. 6, pp. 386–404, 2013.

[73] H. W. Reinhardt, “Fracture Mechanics of an Elastic Softening Material Like Concrete,” *Heron*, vol. 29, no. 2, pp. 1–42, 1984.

[74] J. C. Walraven, “Fundamental Analysis of Aggregate Interlock,” *Journal of the Structural Division*, vol. 107, no. 11, pp. 2245–2270, 1981.

[75] F. Cavagnis, M. Fernández Ruiz, and A. Muttoni, “An analysis of the shear-transfer actions in reinforced concrete members without transverse reinforcement based on refined experimental measurements,” *Structural Concrete*, vol. 19, no. 1, pp. 49–64, 2018.

[76] prEN 1992-1-1:2018, “Eurocode 2: Design of concrete structures - Part 1-1: General rules, rules for buildings, bridges and civil engineering structures,” European Committee for Standardization (CEN), Brussels, Belgium, 293 p., 2018.

5.11. Notation

c_x, c_y : cover thickness in x, y direction

c_s : clear spacing

d_g : maximum aggregate size

d_{dg} : average roughness

f_b : bond strength

$f_{c,cyl}$: compressive strength of concrete cylinder

f_{ct} : tensile strength of concrete

f_R : bond index

f_{sp} : radial splitting stress

f_t : reinforcement tensile strength

f_v : vertical force per unit length

f_y : mean value of the yield strength of reinforcement

l_b : anchorage length

n : number of disturbances

m : slope

p : pressure

p_e : external pressure

p_{max} : pressure at peak

$p_{\perp}$: pressure perpendicular to the cover

$p_{//}$: pressure parallel to the cover

u_x, u_y, u_z : displacements in x, y, z direction

w_n : crack opening

w_t : crack sliding

W/C : water-to-cement ratio

γ : crack inclination

δ : relative displacement between steel and concrete (slip)

η_{ct} : strength reduction factor to account for concrete brittleness in tension

η_{is} : strength reduction factor to account for casting position effects

θ : inclination of compressive strut to bar axis

λ : coefficient defining the contribution of the splitting components

σ_{agg} : normal stress

σ_{sp} : confining stress

τ_{agg} : shear stress

τ_{avg} : bond stress averaged along anchorage length

ϕ : diameter

ψ : angle defining the crack geometry

Chapter 6.
Conclusions and outlook

6.1. General conclusions

The structural response of reinforced concrete members can be complex, with internal stress redistributions, the development of different load-carrying actions and the interaction between reinforcement and concrete. Despite this complexity, a number of idealizations and simplifications are often performed in their design. Nevertheless, it is of paramount importance to improve the understanding of the phenomena that may have a detrimental effect on the concrete resistance. In this regard, the aim of this thesis was to investigate the structural properties of the compressive and bond strength, providing both experimental and theoretical contributions.

An in-depth investigation was performed on the phenomena occurring during the consolidation process of concrete. The plastic settlement was measured and quantified in the minutes and hours after concrete pouring using Digital Image Correlation (DIC). In addition, the effects of concrete bleeding and plastic settlement on horizontal bars were evaluated using tomography. The latter measurement technique evaluated with high accuracy the magnitude of the voids and cracks developing around bars restrained from any vertical movement during casting.

The influence of bleeding and plastic settlement was further observed at the structural level both in the compressive and bond response. For compression members, the influence of casting position, loading direction and presence of transverse reinforcement were investigated. The significance of casting position effects was outlined for unconfined columns or elements without suitable crack control. In this regard, DIC measurements displayed the disturbances on the compression field due to the voids originated from bleeding and plastic settlement and located under horizontal bars. Such disturbances lead to regions with stress concentrations, affecting the concrete compressive resistance.

The experiments also showed that casting position effects are relatively negligible in case structural elements accommodate confining reinforcement. In fact, hoops or ties allows for the redistribution of internal forces, compensating the disturbances related to voids and internal cracks. Nevertheless, for the design of such members, it was demonstrated the necessity of considering for material brittleness in compression by means of a specific strength reduction factor. The latter accounts for the softening response of concrete once its peak strength is reached and covers for idealized distribution of stresses assumed in design. In particular, the pertinence of this factor was demonstrated for reinforced concrete columns under pure compression and for compression zones of members in bending.

In addition, the detailed measurements of bleeding and plastic settlement allowed for new contributions in the understanding of the top bar effect, phenomenon acknowledged since decades in the literature and design codes. In this regard, the implications of concrete consolidation on bond-related failure mechanisms were assessed. Pull-out failures were shown to be mainly governed by the size of the voids originated from plastic settlement and located under horizontal bars. As a result, a mechanical approach was proposed for the determination of the pull-out strength based on the size of these voids as well as on the characteristics of reinforcing bars. With respect to spalling failures, they were shown to be mainly affected by the tensile strength reductions near the casting surface due to bleeding and by the presence of internal cracks at the sides of the bars due to plastic settlement.

The spalling failure mechanism was further investigated by means of specific tests performed with hydraulic inflator devices. By means of DIC measurements, the effects of plastic settlement cracks on the failure mechanism were established and the stresses transferred along the failures surfaces were determined. Consequently, a mechanical approach was proposed for the assessment of the spalling strength against an internal radial pressure. The latter is suited for the evaluation of the pressure induced by the bond action or by corrosion products and takes into account for the failure kinematic, the material properties, the geometrical dimensions and the casting position. Finally, the model was further developed to assess the spalling strength of pull-out bars.

More detailed findings and contributions of this thesis are summarized in the next section, followed by an outlook on research topics that could be addressed in future work.

6.2. Detailed findings

This thesis comprises a series of scientific publications [1]–[4] that are presented in Chapters 2-5 and each focuses on different aspects of the concrete structural resistance. In Chapter 2, it is outlined the investigations on the influence of casting position and disturbance of embedded reinforcement on the concrete compressive resistance. The main conclusions of this study are the following [1]:

1. Casting position effects can be significant for concrete members without confinement reinforcement, with lower resistances near the casting surface. For consistent design, a strength reduction factor is proposed for members located in top regions.
2. The compressive resistance of members with confinement reinforcement is potentially not affected by casting position nor casting direction. This behaviour resulted from the favourable action of hoops and ties compensating the detrimental effects related to bleeding and plastic settlement. A strength reduction factor should however be considered in the design of such elements to account for the potential development of internal stress redistributions and the material brittleness.
3. DIC measurements on fresh concrete and tomography scanning of embedded bars greatly improved the phenomenological understanding of bleeding and plastic settlement. These phenomena were quantified and their effects at the structural level evaluated.
4. The size of the voids developing under horizontal reinforcement (due to bleeding and plastic settlement) were shown to be dependent on the distance from the free surface and the effective casting height under the bars. These voids perturb the compression field and can lead to stress concentrations and eventually concrete crushing. In case crack propagation is not suitably controlled, the compressive resistance is affected by the direction of casting, as the latter governs the location of the voids with respect to the loading direction. To account for this type of disturbances, a specific strength reduction factor was proposed.

The role of concrete brittleness and internal stress redistributions was discussed in Chapter 2 in the design of columns with hoops. This topic was further investigated in Chapter 3 with respect to reinforced concrete columns and compression zones of beams in bending. The main findings can be summarized as follows [2]:

1. Based on theoretical considerations and experimental evidence, the pertinence of considering a brittleness factor in the calculation of reinforced concrete columns and compression zones of beams was demonstrated. This strength reduction factor accounts for the development of potential stress redistributions related to material brittleness and covers for design idealizations.

2. The strength reduction factor η_{cc} presented in *fib* MC 2010 [5] for strut-and-tie models and for compression fields subjected to shear is shown to provide suitable consideration of material brittleness and should be included in the design of columns and compression zones of beams.
3. Investigations were performed on the evaluation of the stress distributions occurring within the compression region of beams and columns with bending moments. These regions display a complex response, in which redistribution of stresses take place at ultimate limit state. In this regard, the parabola-rectangle diagram represents a suitable stress distribution for the compression zone of members in bending, provided that the material brittleness is accounted for in the calculation (for instance by means of the η_{cc} factor). Similar validation was performed with respect to the simplified stress block distribution.
4. The analysis of the test results showed the potential influence of casting direction on the resistance of the investigated members, with safer calculations for specimens cast horizontally compared to vertically-cast members. Based on the finding of Chapter 2 (refer also to [1]), the observed difference is attributed to the location of plastic settlement voids with respect to the loading direction.

The findings of these investigations were eventually used for validation of formulations proposed for the future revision of EN 1992-1-1:2004 [6].

Based on the detailed measurements of concrete bleeding and plastic settlement performed in Chapter 2, the effects of casting position on the bond performance were assessed in Chapter 4 by means of a comprehensive experimental programme. The main findings of these investigations are the following [3]:

1. Concrete bleeding and plastic settlement affect in different manners the bond-related failure mechanisms (pull-out, splitting or spalling).
2. Failures occurring by bar pull-out are mainly affected by the size of the void developing under the horizontal reinforcement and originated from plastic settlement and bleeding (as measured in Chapter 2). The pull-out resistance is thus influenced by structural properties such as the concrete depth under the bar, the concrete consistency and bar characteristics (diameter and bond index).
3. The detrimental effect of casting position on the pull-out resistance is shown analogous to the bond strength reductions observed when a crack longitudinally crosses a reinforcing bar. As a result, a physically-consistent approach previously derived for bond in cracked concrete is proposed and validated based on the experimental evidence.
4. The pull-out strength gradually decreases with the increase of the size of the voids located under the bars. Therefore, the recommendations of distinct regions with poor or good bond conditions, as presented in design codes, do not suitably represent the actual behaviour observed in the experiments.
5. Failures by cover spalling are influenced by the reduced tensile strength near the top surface due to bleeding and by the presence of inclined cracks at the sides of the bars resulting from plastic settlement.
6. Casting position effects are potentially less significant for spalling failures of horizontal bars located near the side surface of a structural member. In these cases, plastic settlement cracks do not match with the failure surfaces and the horizontal tensile strength of concrete is less affected by bleeding compared to the vertical direction.

The findings on the spalling failure mechanism of Chapter 4 were further evaluated in Chapter 5 by means of refined measurements (Digital Image Correlation) and by manufacturing specific hydraulic inflator devices that reproduce the radial pressure induced by the bond action or corrosion. The main findings of this study are the following [4]:

1. The spalling resistance is lower for specimens of top layers with respect to those of the bottom layers due to the effects of bleeding and plastic settlement (confirming the findings of Chapter 4).
2. Casting position effects are shown to induce different spalling responses depending on the location of the investigated specimen. The elements located near the top surface experience a gradual and controlled propagation of plastic settlement cracks until spalling of the concrete cover. The geometry of the failure mechanism is thus partially defined by plastic settlement cracks. On the other hand, specimens of the bottom layers experience a brittle failure with a sudden development and propagation of cracks.
3. The experimental programme outlined the significance of size and group effects on the crack pattern and on the resistance to cover spalling.
4. A mechanical model assessing the spalling resistance against an internal radial pressure is proposed and validated based on the results of the experimental programme and on tests gathered from the literature. The model considers for simplified stress profiles along the failure surfaces and accounts for casting position, size and group effects.
5. For inner-pressure tests, the DIC measurements showed rather constant out-of-plane displacements along the axis of the hydraulic inflator devices. On the other hand, the DIC measurements along pulled-out bars displayed non-uniform out-of-plane displacements, indicating potential stress redistributions. Based on these measurements and combined with an estimate of the acting pressures obtained in inner-pressure tests, a simple approach is proposed to assess the spalling strength of pull-out bars.

6.3. Outlook and future work

The findings of this research represent a step forward in the comprehension of reinforced concrete structures, in particular with respect to the bond and compressive response. Nevertheless, some questions remain open. In the following, it is presented a list of topics that would be interesting to investigate in future works.

<u>Phenomena of bleeding and plastic settlement (subject treated in Chapters 2, 3, 4, 5)</u>

- Systematic investigations should be performed to assess the influence of concrete consistency and presence of admixtures on bleeding and plastic settlement. For different concrete mixes, the plastic settlement of the top surface and the thickness of the voids situated under horizontal bars should be measured with DIC and tomography, respectively. As a result, a relationship among the surface settlement, the size of the voids and the casting height could be proposed for each concrete mix and consistency. The relevance of these properties should also be assessed with respect to surface cracking due to plastic settlement.
- In Chapters 4 and 5, the implications of bleeding on the tensile strength of concrete and the spalling resistance are discussed. Some of the assumptions were based on the work of Giaccio and Giovambattista [7], in which it was shown that near the top surface bleeding affected the concrete tensile strength mainly in the vertical direction. Additional phenomenological tests should however be provided to validate these findings. For instance, concrete cores should be extracted from tall concrete members at different depths and orientations and subsequently

scanned in a tomograph. The magnitude and shape of the pores developing under coarse aggregates could thus be measured and their influence on the tensile strength assessed. After scanning, the cores could also be tested to determine the concrete tensile strength.

- Several authors observed milder casting position effects for vertically oriented bars with respect to horizontal reinforcement, implying a lower impact of bleeding and plastic settlement on the steel-concrete interface. In this respect, tomography scanning could provide accurate measurements of the voids and porosity that develop under the ribs of vertically oriented bars.

<u>Concrete compressive resistance (topic covered in Chapters 2, 3):</u>

- As discussed in Chapters 2 and 3, the concrete brittleness in compression can lead to a limitation of stress redistributions within reinforced concrete members. In this respect, the new developments in fiber optic measurements could drastically improve the understanding of such stress redistributions. In the case of reinforced concrete columns, optical fibers could be glued on longitudinal bars and hoops or even placed in the concrete. As a result, the stress redistributions taking place between the reinforcement, the concrete cover and the core could be recorded throughout the entire loading process. In case of a positive outcome, similar investigations could additionally be performed on beams and walls under various loading conditions.
- Additional tests should be carried out to evaluate the effects of the loading rate on concrete brittleness and on internal stress redistributions for members under pure compression or subjected to compression and bending.
- The casting position effects and the disturbances of embedded bars were assessed in Chapter 2 for columns and prisms made of normal strength concrete. These investigations should be completed with additional tests on members made of high-strength concrete and self-compacting concrete.
- The characterization of the brittleness factor η_{cc} was based on the compressive strength of conventional concrete. However, with the development of new types of concretes (e.g. fiber-reinforced concrete or textile concrete), the definition of this coefficient should be generalized to account also for the material toughness. Additional investigations on this aspect should be performed in future works.
- For reinforced concrete columns, the role of the voids that may develop under hoops and ties due to casting position effects should be further assessed with respect to cover spalling. Tomography measurements should be performed to evaluate their size and shape, while optical fibers should be placed in the concrete to measure the crack propagation induced by such voids.
- Theoretical considerations and experimental evidence should be provided with respect to reinforced concrete columns experiencing an early brittle failure of the concrete cover. This behaviour is observed in conventional compression tests but also when concrete is subjected to high temperatures, as it occurs in a fire. The role of potential stress redistributions and concrete brittleness should be evaluated for this specific case.
- From the experimental programme presented in Chapter 2, it resulted that, whenever suitable confinement reinforcement is provided, the casting direction do not affect the compressive resistance of a concrete member. However, from the database of column tests collected from the literature (Chapter 3), it appeared that horizontally casted columns are slightly more resistant compared to those vertically casted. These differences should be clarified in future research.

Bond strength of reinforcing bars (subject treated in Chapters 4, 5)

- The use of fiber optic measurements should be implemented in the study of bond. Optical fibers should be glued on the reinforcement, providing for a direct and continuous recording of its deformation. From these measurements, the distribution of the bond stresses along the bar and the slip could be derived. Also, optical fibers should be placed in the concrete surrounding the tested bars to measure the development of conical cracks, as described by Goto [8]. These recordings should be coupled with surface measurements performed with DIC. Therefore, correlation could be established between the cracks measured on the surface using DIC and the stresses measured along the bars with optical fibers. These findings could eventually be extended for the assessment and retrofit of existing structures.
- Pull-out tests should be performed on the turning plate of a tomograph while scanning. These measurements could lead to a phenomenological and three-dimensional view of the crack propagation during a pull-out test.
- In Chapter 4, a mechanical approach is proposed to evaluate the casting condition effects on the pull-out resistance of steel bars. Its validity was confirmed based on test results, however additional experimental evidence should be considered for a suitable evaluation of the proposed coefficients of the model.
- The model presented in Chapter 5, assessing the pull-out strength in case of spalling failures, should be further developed into a general model for bond. Its coefficients should be validated and eventually defined in a more comprehensive manner based on additional experimental programmes. The influence of various parameters on the bond strength should also be evaluated, such as the presence of confinement (active or passive), the orientation of the bars, the presence of cracks, the concrete strength and consistency, the geometry and bond index of the reinforcement and the effects of steel fibers. In addition, the model should be based on detailed measurements performed with state-of-the-art techniques, such as DIC, optical fibers and tomography. Also, it should account for the observed transition from spalling to pull-out failures based on the cover dimensions but also on other parameters.

Spalling of the concrete cover (topic presented in Chapters 4, 5)

- Systematic series of experiments should be performed to evaluate the influence of the rib orientation, bond index and rib shape on the spalling strength and the spalling failure mechanism.
- Spalling failures were investigated in Chapters 4 and 5 for horizontal bars located near the top and bottom surfaces of prismatic concrete specimens. Additional phenomenological tests should thus be carried out on bars located near the side surfaces of concrete elements (for instance in walls or webs). Tomography should be used to identify voids and surface cracks surrounding lateral bars due to bleeding and plastic settlement. Thereafter, pull-out tests and inner-pressure tests should be performed. During the tests, the spalling of the cover should be monitored with DIC to assess the crack patterns and the kinematic of the failure mechanism.
- It is necessary to validate the proposed model assessing the spalling resistance against an internal radial pressure in the case of corrosion. In this regard, specific experimental tests should be carried out.
- Systematic tests should be performed using hydraulic inflator devices to validate the coefficients of the proposed model for spalling failures.
- In past decades, spalling of the concrete cover has been thoroughly investigated in the case of lap splices. However, complementary studies should be performed using state-of-the-art

measurement techniques (DIC, optical fibers, tomography), allowing for a more detailed and comprehensive description of the failure mechanism.

6.4. References

[1] F. Moccia, X. Kubski, M. Fernández Ruiz, and A. Muttoni, "The influence of casting position and disturbance induced by reinforcement on the structural concrete strength," *Structural Concrete*, pp. 1–28, 2020.

[2] F. Moccia, Q. Yu, M. Fernández Ruiz, and A. Muttoni, "Concrete compressive strength: From material characterization to a structural value," *Structural Concrete*, pp. 1–21, 2020.

[3] F. Moccia, M. Fernández Ruiz, G. Metelli, A. Muttoni, and G. Plizzari, "Casting position effects on bond performance of reinforcement bars," *Structural Concrete, Submitted for review*.

[4] F. Moccia, M. Fernández Ruiz, and A. Muttoni, "Spalling of concrete cover induced by reinforcement," *Engineering Structures, Submitted for review*.

[5] International Federation for Structural Concrete, "fib Model Code for Concrete Structures 2010," Ernst & Sohn, Berlin, Germany, 434 p., 2013.

[6] EN 1992-1-1:2004, "Eurocode 2: Design of Concrete Structures - Part 1: General Rules and Rules for Buildings," European Committee for Standardization (CEN), Brussels, Belgium, 225 p., 2004.

[7] G. Giaccio and A. Giovambattista, "Bleeding: Evaluation of its effects on concrete behaviour," *Materials and Structures*, vol. 19, no. 4, pp. 265–271, 1986.

[8] Y. Goto, "Cracks Formed in Concrete Around Deformed Tension Bars," *ACI Journal*, vol. 68, no. 4, pp. 244–251, 1971.

Appendices

Appendix A: Database on column tests without eccentricity

Annex C of "Concrete compressive strength: from material characterization to a structural value”.

Authors	Specimen	Cross section	$f_{cm,cyl}$ [MPa]	$Ø_{ext}$ [mm]	$Ø_{int}$ [mm]	A_c [mm^2]	c [mm]	$f_{y,long}$ [MPa]	$Ø_{long,1}$ [mm]	n°	$Ø_{long,2}$ [mm]	n°	$A_{s,long}$ [mm^2]	$\rho_{s,long}$ [%]	$f_{y,conf}$ [MPa]	$Ø_{conf}$ [mm]	Stirrup spacing [mm]	$A_{s,conf}$ [mm^2]	$\rho_{s,conf}$ [%]	Stirrup type	N_{test} [kN]
Liu, Foster, Attard, 2000	2C60-10S50-15	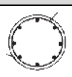	60	250	-	48167	15	430	12.1	8	0	0	920	1.9	470	10.0	50	157	1.5	circular	2970
	2C60-10S100-15	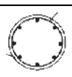	60	250	-	48167	15	430	12.1	8	0	0	920	1.9	470	10.0	100	157	0.7	circular	2460
	2C60-10S150-15	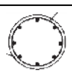	60	250	-	48167	15	430	12.1	8	0	0	920	1.9	470	10.0	150	157	0.5	circular	2300
	2C80-10S50-15	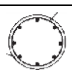	82	250	-	48167	15	430	12.1	8	0	0	920	1.9	660	10.3	50	167	1.6	spiral	3880
	2C80-6S50-15	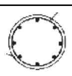	82	250	-	48167	15	430	12.1	8	0	0	920	1.9	620	7.1	50	79	0.7	spiral	3850
	2C80-6S100-15	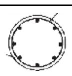	82	250	-	48167	15	430	12.1	8	0	0	920	1.9	620	7.1	100	79	0.4	spiral	3590
	2C90-10S100-25	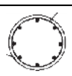	96	250	-	48167	25	430	12.1	8	0	0	920	1.9	560	9.2	100	133	0.7	spiral	3600
	2C90-6S50-25	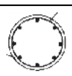	96	250	-	48167	25	430	12.1	8	0	0	920	1.9	600	5.7	50	51	0.5	spiral	3300
	2C90-6S100-25	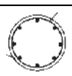	96	250	-	48167	25	430	12.1	8	0	0	920	1.9	600	5.7	100	51	0.3	spiral	3775
	2C90-10S50-0	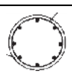	96	250	-	48167	0	430	12.1	8	0	0	920	1.9	560	9.2	50	133	1.1	spiral	5270
	2C90-10S100-0	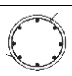	96	250	-	48167	0	430	12.1	8	0	0	920	1.9	560	9.2	100	133	0.6	spiral	4500
	2C90-6S50-0	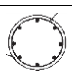	96	250	-	48167	5	430	12.1	8	0	0	920	1.9	600	5.7	50	51	0.4	spiral	4100
Shin, Yoon, Cook, Mitchell, 2016	C-NT-6.1		199.8	220	-	46812	15	497.5	15.9	8	0	0	1588	3.3	549.5	9.5	40	284	3.9	multiple	7610
	D-NT-6.1		199.8	220	-	46880	15	479.6	12.7	12	0	0	1520	3.1	549.5	9.5	47	284	3.3	multiple	7720
	C-HT-6.1		184.7	220	-	46812	15	497.5	15.9	8	0	0	1588	3.3	806.0	11	50	380	4.2	multiple	7544
	D-HT-6.1		184.7	220	-	46880	15	479.6	12.7	12	0	0	1520	3.1	786.9	9.2	42	266	3.5	multiple	7590
	C-HT-4.4		199.8	220	-	46812	15	497.5	15.9	8	0	0	1588	3.3	786.9	9.2	50	266	2.9	multiple	7637
	D-HT-4.4		199.8	220	-	46880	15	479.6	12.7	12	0	0	1520	3.1	786.9	9.2	58	266	2.5	multiple	6924
	C-NT-6.1-HL		199.8	220	-	46812	15	641.9	15.9	8	0	0	1588	3.3	549.5	9.5	40	284	3.9	multiple	8049

Authors	Specimen	Cross section	$f_{cm,cyl}$ [MPa]	$Ø_{ext}$ [mm]	$Ø_{int}$ [mm]	A_c [mm^2]	c [mm]	$f_{y,long}$ [MPa]	$Ø_{long,1}$ [mm]	n°	$Ø_{long,2}$ [mm]	n°	$A_{s,long}$ [mm^2]	$\rho_{s,long}$ [%]	$f_{y,conf}$ [MPa]	$Ø_{conf}$ [mm]	Stirrup spacing [mm]	$A_{s,conf}$ [mm^2]	$\rho_{s,conf}$ [%]	Stirrup type	N_{test} [kN]
	C-HT-4.4-HL		199.9	220	-	46812	15	641.9	15.9	8	0	0	1588	3.3	786.9	9.2	50	266	2.9	multiple	7198
Shin, Yoon, Cook, Mitchell, 2015	200-A1	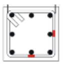	199.8	220	-	46812	15	497.5	15.9	8	0	0	1588	3.3	549.5	9.5	40	142	2.0	square	6898
	200-B1	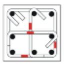	199.8	220	-	46812	15	497.5	15.9	8	0	0	1588	3.3	549.5	9.5	40	213	2.9	multiple	8009
	200-C1		199.8	220	-	46812	15	497.5	15.9	8	0	0	1588	3.3	549.5	9.5	35	284	4.5	multiple	7301
	200-D1		199.8	220	-	46880	15	479.6	12.7	12	0	0	1520	3.1	549.5	9.5	35	284	4.5	multiple	7503
	200-A2	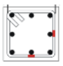	199.8	220	-	46812	15	497.5	15.9	8	0	0	1588	3.3	549.5	9.5	23	142	3.4	square	7231
	200-B2	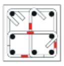	199.8	220	-	46812	15	497.5	15.9	8	0	0	1588	3.3	549.5	9.5	35	213	3.4	multiple	8002
	50-B1	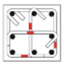	70.4	220	-	46812	15	497.5	15.9	8	0	0	1588	3.3	549.5	9.5	100	213	1.2	multiple	3634
	100-B1	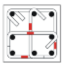	110.8	220	-	46812	15	497.5	15.9	8	0	0	1588	3.3	549.5	9.5	60	213	2.0	multiple	5531
	50-A1	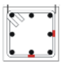	70.4	220	-	46812	15	497.5	15.9	8	0	0	1588	3.3	549.5	9.5	40	142	2.0	square	4182
	100-A1	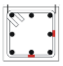	110.8	220	-	46812	15	497.5	15.9	8	0	0	1588	3.3	549.5	9.5	40	142	2.0	square	5402
Razvi, Saatcioglu 1999	CC-1		60	250	-	47479	10	450	16	8	0	0	1608	3.3	660	6.3	135	62	0.2	spiral	3499
	CC-2		60	250	-	47479	10	450	16	8	0	0	1608	3.3	400	11.3	135	201	0.7	spiral	3035
	CC-3		60	250	-	47479	10	450	16	8	0	0	1608	3.3	660	6.3	70	62	0.4	spiral	3483
	CC-4		60	250	-	47479	10	450	16	8	0	0	1608	3.3	660	6.3	70	62	0.4	circular	3402
	CC-8		124	250	-	47479	10	450	16	8	0	0	1608	3.3	660	6.3	70	62	0.4	spiral	5354
	CC-9		124	250	-	47479	10	450	16	8	0	0	1608	3.3	400	11.3	135	201	0.7	spiral	5564
	CC-10		124	250	-	47479	10	450	16	8	0	0	1608	3.3	400	11.3	60	201	1.5	spiral	5076
	CC-11		124	250	-	47479	10	450	16	8	0	0	1608	3.3	660	6.3	60	62	0.5	spiral	5424
	CC-12		124	250	-	47479	10	450	16	8	0	0	1608	3.3	1000	7.5	60	88	0.7	spiral	5482
	CC-14		92	250	-	47479	10	450	16	8	0	0	1608	3.3	1000	7.5	60	88	0.7	spiral	4590
	CC-15		92	250	-	47479	10	450	16	8	0	0	1608	3.3	400	11.3	60	201	1.5	spiral	4501

Authors	**Specimen**	**Cross section**	$f_{cm,cyl}$ **[MPa]**	$Ø_{ext}$ **[mm]**	$Ø_{int}$ **[mm]**	A_c **[mm^2]**	c **[mm]**	$f_{y,long}$ **[MPa]**	$Ø_{long,1}$ **[mm]**	**n°**	$Ø_{long,2}$ **[mm]**	**n°**	$A_{s,long}$ **[mm^2]**	$\rho_{s,long}$ **[%]**	$f_{y,conf}$ **[MPa]**	$Ø_{conf}$ **[mm]**	**Stirrup spacing [mm]**	$A_{s,conf}$ **[mm^2]**	$\rho_{s,conf}$ **[%]**	**Stirrup type**	N_{test} **[kN]**
	CC-16		92	250	-	47479	10	450	16	8	0	0	1608	3.3	1000	7.5	100	88	0.4	spiral	4266
	CC-19		92	250	-	47479	10	450	16	8	0	0	1608	3.3	400	11.3	100	201	0.9	spiral	4339
	CC-20		92	250	-	47479	10	450	16	8	0	0	1608	3.3	660	6.3	100	62	0.3	spiral	4172
	CC-21		92	250	-	47479	10	450	16	8	0	0	1608	3.3	660	6.3	70	62	0.4	spiral	4323
	CC-22		92	250	-	47479	10	450	16	8	0	0	1608	3.3	400	11.3	135	201	0.7	spiral	4237
Saatcioglu Razvi 1998	CS-1		124	250	-	61696	10	450	16	4	0	0	804	1.3	400	11.3	55	201	1.7	square	6040
	CS-2		124	250	-	60892	10	450	16	8	0	0	1608	2.6	570	6.5	55	100	0.8	multiple	6597
	CS-3		124	250	-	60087	10	450	16	12	0	0	2413	3.9	570	6.5	55	133	1.1	multiple	7402
	CS-4		124	250	-	60892	10	450	16	8	0	0	1608	2.6	1000	7.5	55	133	1.1	multiple	6631
	CS-5		124	250	-	60087	10	450	16	12	0	0	2413	3.9	1000	7.5	120	177	0.7	multiple	6849
	CS-6		124	250	-	60892	10	450	16	8	0	0	1608	2.6	400	6.5	85	100	0.5	multiple	6927
	CS-7		124	250	-	60087	10	450	16	12	0	0	2413	3.9	400	6.5	120	133	0.5	multiple	6910
	CS-8		124	250	-	60892	10	450	16	8	0	0	1608	2.6	400	11.3	85	301	1.6	multiple	6165
	CS-9		124	250	-	60087	10	450	16	12	0	0	2413	3.9	400	11.3	120	401	1.5	multiple	7177
	CS-11	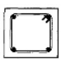	81	250	-	61696	10	450	16	4	0	0	804	1.3	400	11.3	40	201	2.3	square	4856
	CS-12	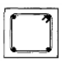	81	250	-	61696	10	450	16	4	0	0	804	1.3	400	11.3	55	201	1.7	square	4366
	CS-13		92	250	-	60892	10	450	16	8	0	0	1608	2.6	570	6.5	55	100	0.8	multiple	4874
	CS-14		92	250	-	60087	10	450	16	12	0	0	2413	3.9	570	6.5	55	133	1.1	multiple	5561
	CS-15		81	250	-	60892	10	450	16	8	0	0	1608	2.6	1000	7.5	55	133	1.1	multiple	5296
	CS-16		81	250	-	60087	10	450	16	12	0	0	2413	3.9	1000	7.5	85	177	0.9	multiple	5578
	CS-17		81	250	-	60892	10	450	16	8	0	0	1608	2.6	400	6.5	85	100	0.5	multiple	5242
	CS-18		81	250	-	60087	10	450	16	12	0	0	2413	3.9	400	6.5	85	133	0.7	multiple	5536

Authors	Specimen	Cross section	$f_{cm,cyl}$ [MPa]	$Ø_{ext}$ [mm]	$Ø_{int}$ [mm]	A_c [mm^2]	c [mm]	$f_{y,long}$ [MPa]	$Ø_{long,1}$ [mm]	n°	$Ø_{long,2}$ [mm]	n°	$A_{s,long}$ [mm^2]	$\rho_{s,long}$ [%]	$f_{y,conf}$ [MPa]	$Ø_{conf}$ [mm]	Stirrup spacing [mm]	$A_{s,conf}$ [mm^2]	$\rho_{s,conf}$ [%]	Stirrup type	N_{test} [kN]
	CS-19		92	250	-	60892	10	450	16	8	0	0	1608	2.6	400	11.3	85	301	1.6	multiple	5536
	CS-20		92	250	-	60087	10	450	16	12	0	0	2413	3.9	400	11.3	85	401	2.2	multiple	5911
	CS-22		60	250	-	60892	10	450	16	8	0	0	1608	2.6	1000	7.5	85	133	0.7	multiple	4322
	CS-23		60	250	-	60087	10	450	16	12	0	0	2413	3.9	1000	7.5	120	177	0.7	multiple	4790
	CS-24		60	250	-	60892	10	450	16	8	0	0	1608	2.6	400	11.3	85	301	1.6	multiple	4763
	CS-25		60	250	-	60087	10	450	16	12	0	0	2413	3.9	400	11.3	120	401	1.5	multiple	4996
	CS-26		60	250	-	60087	10	450	16	12	0	0	2413	3.9	570	6.5	55	133	1.1	multiple	5365
Li, 1994	1A		60	240	-	57148	12.5	443	12	4	0	0	452	0.8	445	6	20	57	1.4	square	3475
	2A		60	240	-	56695	12.5	443	12	8	0	0	905	1.6	445	6	20	113	2.7	multiple	4375
	4A		60	240	-	57148	12.5	443	12	4	0	0	452	0.8	445	6	35	57	0.8	square	3225
	5A		60	240	-	56695	12.5	443	12	8	0	0	905	1.6	445	6	35	113	1.5	multiple	3725
	7A		60	240	-	57148	12.5	443	12	4	0	0	452	0.8	445	6	50	57	0.5	square	3350
	8A		60	240	-	56695	12.5	443	12	8	0	0	905	1.6	445	6	50	113	1.1	multiple	3575
	10A	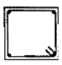	60	240	-	57148	12.5	443	12	4	0	0	452	0.8	445	6	65	57	0.4	square	3325
	11A		60	240	-	56695	12.5	443	12	8	0	0	905	1.6	445	6	65	113	0.8	multiple	3550
	1B		72.3	240	-	57148	12.5	443	12	4	0	0	452	0.8	445	6	20	57	1.4	square	3725
	2B		72.3	240	-	56695	12.5	443	12	8	0	0	905	1.6	445	6	20	113	2.7	multiple	5100
	4B		72.3	240	-	57148	12.5	443	12	4	0	0	452	0.8	445	6	35	57	0.8	square	3950
	5B		72.3	240	-	56695	12.5	443	12	8	0	0	905	1.6	445	6	35	113	1.5	multiple	4000
	7B	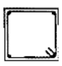	72.3	240	-	57148	12.5	443	12	4	0	0	452	0.8	445	6	50	57	0.5	square	4200
	8B		72.3	240	-	56695	12.5	443	12	8	0	0	905	1.6	445	6	50	113	1.1	multiple	4000
	10B	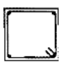	72.3	240	-	57148	12.5	443	12	4	0	0	452	0.8	445	6	65	57	0.4	square	4000

Authors	Specimen	Cross section	$f_{cm,cyl}$ [MPa]	$Ø_{ext}$ [mm]	$Ø_{int}$ [mm]	A_c [mm^2]	c [mm]	$f_{y,long}$ [MPa]	$Ø_{long,1}$ [mm]	n°	$Ø_{long,2}$ [mm]	n°	$A_{s,long}$ [mm^2]	$\rho_{s,long}$ [%]	$f_{y,conf}$ [MPa]	$Ø_{conf}$ [mm]	Stirrup spacing [mm]	$A_{s,conf}$ [mm^2]	$\rho_{s,conf}$ [%]	Stirrup type	N_{test} [kN]
	11B		72.3	240	-	56695	12.5	443	12	8	0	0	905	1.6	445	6	65	113	0.8	multiple	4150
	3A	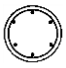	63	240	-	44560	15	443	12	6	0	0	679	1.5	445	6	20	57	1.4	spiral	3350
	6A	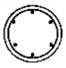	63	240	-	44560	15	443	12	6	0	0	679	1.5	445	6	35	57	0.8	spiral	2800
	9A	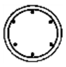	63	240	-	44560	15	443	12	6	0	0	679	1.5	445	6	50	57	0.6	spiral	2725
	12A	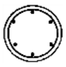	63	240	-	44560	15	443	12	6	0	0	679	1.5	445	6	65	57	0.4	spiral	2625
	3B	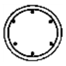	72.3	240	-	44560	15	443	12	6	0	0	679	1.5	445	6	20	57	1.4	spiral	3900
	6B	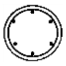	72.3	240	-	44560	15	443	12	6	0	0	679	1.5	445	6	35	57	0.8	spiral	3350
	9B	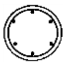	72.3	240	-	44560	15	443	12	6	0	0	679	1.5	445	6	50	57	0.6	spiral	3150
	12B	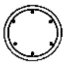	72.3	240	-	44560	15	443	12	6	0	0	679	1.5	445	6	65	57	0.4	spiral	3100
Cusson, Paultre 1994	1A	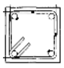	95.4	235	-	54030	15.3	406	19.5	4	0	0	1195	2.2	410	9.5	50	142	1.5	square	4244
	1B		95.4	235	-	54020	16.1	450	16	4	11.3	4	1205	2.2	392	7.9	50	196	2.0	multiple	4679
	1C	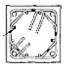	95.4	235	-	54022	16.1	450	11.3	12	0	0	1203	2.2	392	7.9	50	196	2.0	multiple	4716
	1D		100.4	235	-	54022	16.1	450	11.3	12	0	0	1203	2.2	392	7.9	50	196	2.0	multiple	5001
	2A	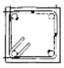	96.4	235	-	54030	16.1	406	19.5	4	0	0	1195	2.2	392	7.9	50	98	1.0	square	4657
	2B		96.4	235	-	54020	16.8	450	16	4	11.3	4	1205	2.2	414	6.4	50	129	1.3	multiple	4388
	2C	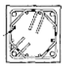	96.4	235	-	54022	16.8	450	11.3	12	0	0	1203	2.2	414	6.4	50	129	1.3	multiple	4525
	2D		96.4	235	-	54022	16.8	450	11.3	12	0	0	1203	2.2	414	6.4	50	129	1.3	multiple	4635
	3A	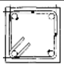	98.1	235	-	54030	15.3	406	19.5	4	0	0	1195	2.2	410	9.5	100	142	0.7	square	4371
	3B		98.1	235	-	54020	15.3	450	16	4	11.3	4	1205	2.2	410	9.5	100	284	1.5	multiple	4410
	3C	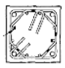	98.1	235	-	54022	15.3	450	11.3	12	0	0	1203	2.2	410	9.5	100	284	1.5	multiple	4499
	3D		98.1	235	-	54022	15.3	450	11.3	12	0	0	1203	2.2	410	9.5	100	284	1.5	multiple	4661
	4A	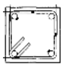	93.1	235	-	53230	15.3	420	25.2	4	0	0	1995	3.6	410	9.5	50	142	1.5	square	4606

Authors	Specimen	Cross section	$f_{cm,cyl}$ [MPa]	$Ø_{ext}$ [mm]	$Ø_{int}$ [mm]	A_c [mm^2]	c [mm]	$f_{y,long}$ [MPa]	$Ø_{long,1}$ [mm]	n°	$Ø_{long,2}$ [mm]	n°	$A_{s,long}$ [mm^2]	$\rho_{s,long}$ [%]	$f_{y,conf}$ [MPa]	$Ø_{conf}$ [mm]	Stirrup spacing [mm]	$A_{s,conf}$ [mm^2]	$\rho_{s,conf}$ [%]	Stirrup type	N_{test} [kN]
	4B		93.1	235	-	53226	16.1	406.5	19.5	4	16	4	1999	3.6	392	7.9	50	196	2.0	multiple	4882
	4C	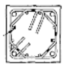	93.1	235	-	53228	16.1	406.5	19.5	4	11.3	8	1997	3.6	392	7.9	50	196	2.0	multiple	4864
	4D		93.1	235	-	53228	16.1	406.5	19.5	4	11.3	8	1997	3.6	392	7.9	50	196	2.0	multiple	4863
	5A	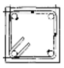	99.9	235	-	53230	15.3	420	25.2	4	0	0	1995	3.6	705	9.5	50	142	1.5	square	4728
	5B		99.9	235	-	53226	16.1	406.5	19.5	4	16	4	1999	3.6	770	7.9	50	196	2.0	multiple	5037
	5C	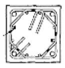	99.9	235	-	53228	16.1	406.5	19.5	4	11.3	8	1997	3.6	770	7.9	50	196	2.0	multiple	5214
	5D		99.9	235	-	53228	16.1	406.5	19.5	4	11.3	8	1997	3.6	770	7.9	50	196	2.0	multiple	5457
	6B		115.9	235	-	53226	15.3	482.4	19.5	4	16	4	1999	3.6	715	9.5	50	284	2.9	multiple	5395
	6D		113.6	235	-	53228	16.1	482.5	19.5	4	11.3	8	1997	3.6	680	7.9	50	196	2.0	multiple	5545
	7B		75.9	235	-	53226	15.3	482.4	19.5	4	16	4	1999	3.6	715	9.5	50	284	2.9	multiple	4954
	7D		67.9	235	-	53228	16.1	482.5	19.5	4	11.3	8	1997	3.6	680	7.9	50	196	2.0	multiple	4701
	8B		52.6	235	-	53226	15.3	482.4	19.5	4	16	4	1999	3.6	715	9.5	50	284	2.9	multiple	4530
	8D		55.6	235	-	53228	16.1	482.5	19.5	4	11.3	8	1997	3.6	680	7.9	50	196	2.0	multiple	4532
Sharma, Bhargava, Kaushik, 2005	CA	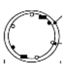	62.2	150	-	17370	10	412	8	6	0	0	302	1.7	412	8	50	101	1.6	spiral	1109
	CB	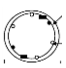	62.8	150	-	17370	10	412	8	6	0	0	302	1.7	412	8	75	101	1.1	spiral	1059
	CC	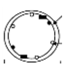	61.9	150	-	17370	10	412	8	6	0	0	302	1.7	520	8	50	101	1.6	spiral	1148
	CD	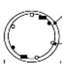	63.4	150	-	16993	10	395	12	6	0	0	679	3.8	412	8	50	101	1.6	spiral	1241
	CE	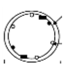	82.5	150	-	17370	10	412	8	6	0	0	302	1.7	412	8	30	101	2.7	spiral	1381
	CF	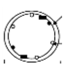	81.8	150	-	17370	10	412	8	6	0	0	302	1.7	412	8	50	101	1.6	spiral	1294
	CG	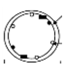	83.2	150	-	17370	10	412	8	6	0	0	302	1.7	412	8	75	101	1.1	spiral	1352
	CH	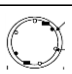	81.8	150	-	17370	10	412	8	6	0	0	302	1.7	520	8	50	101	1.6	spiral	1321
	CI	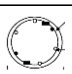	82.6	150	-	16993	10	395	12	6	0	0	679	3.8	412	8	50	101	1.6	spiral	1379

Authors	Specimen	Cross section	$f_{cm,cyl}$ [MPa]	$Ø_{ext}$ [mm]	$Ø_{int}$ [mm]	A_c [mm^2]	c [mm]	$f_{y,long}$ [MPa]	$Ø_{long,1}$ [mm]	n°	$Ø_{long,2}$ [mm]	n°	$A_{s,long}$ [mm^2]	$\rho_{s,long}$ [%]	$f_{y,conf}$ [MPa]	$Ø_{conf}$ [mm]	Stirrup spacing [mm]	$A_{s,conf}$ [mm^2]	$\rho_{s,conf}$ [%]	Stirrup type	N_{test} [kN]
	SA	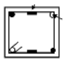	62.2	150	-	22048	10	395	12	4	0	0	452	2.0	412	8	50	101	1.6	square	1334
	SB	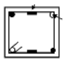	62.8	150	-	22048	10	395	12	4	0	0	452	2.0	412	8	75	101	1.1	square	1364
	SC	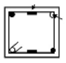	61.9	150	-	22048	10	395	12	4	0	0	452	2.0	520	8	50	101	1.6	square	1308
	SD	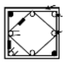	63.4	150	-	21595	10	395	12	8	0	0	905	4.0	412	8	50	201	3.3	multiple	1626
	SE	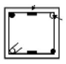	82.5	150	-	22048	10	395	12	4	0	0	452	2.0	412	8	30	101	2.7	square	1641
	SF	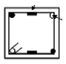	81.8	150	-	22048	10	395	12	4	0	0	452	2.0	412	8	50	101	1.6	square	1604
	SG	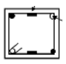	83.2	150	-	22048	10	395	12	4	0	0	452	2.0	412	8	75	101	1.1	square	1730
	SH	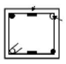	81.8	150	-	22048	10	395	12	4	0	0	452	2.0	520	8	50	101	1.6	square	1621
	SI	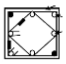	82.6	150	-	21595	10	395	12	8	0	0	905	4.0	412	8	50	201	3.3	multiple	1819
Mander, Priestley, Park, 1988	1	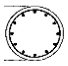	28	500	-	193937	25	295	16	12	0	0	2413	1.2	340	12	41	226	1.3	spiral	8300
	2	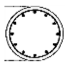	28	500	-	193937	25	295	16	12	0	0	2413	1.2	340	12	69	226	0.7	spiral	7800
	3	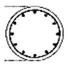	28	500	-	193937	25	295	16	12	0	0	2413	1.2	340	12	103	226	0.5	spiral	7150
	4	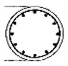	28	500	-	193937	25	295	16	12	0	0	2413	1.2	320	10	119	157	0.3	spiral	6750
	5	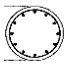	28	500	-	193937	25	295	16	12	0	0	2413	1.2	320	10	36	157	1.0	spiral	7800
	6	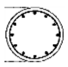	28	500	-	193937	25	295	16	12	0	0	2413	1.2	307	16	93	402	1.0	spiral	7500
	7	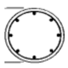	31	500	-	191424	25	296	28	8	0	0	4926	2.5	340	12	52	226	1.0	spiral	9100
	8	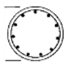	27	500	-	191373	25	260	24	11	0	0	4976	2.5	340	12	52	226	1.0	spiral	8400
	9		31	500	-	191323	25	286	20	16	0	0	5027	2.6	340	12	52	226	1.0	spiral	9000
	10	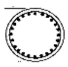	27	500	-	191524	25	295	16	24	0	0	4825	2.5	340	12	52	226	1.0	spiral	9100
	11		27	500	-	189111	25	295	16	36	0	0	7238	3.7	340	12	52	226	1.0	spiral	10000
	12	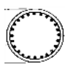	31	500	-	191524	25	360	16	24	0	0	4825	2.5	340	12	52	226	1.0	spiral	9400
Scott, Park, Priestley, 1982	2	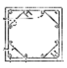	25.3	450	-	198730	20	434	20	12	0	0	3770	1.9	309	10	72	314	1.1	multiple	7070

Authors	Specimen	Cross section	$f_{cm,cyl}$ [MPa]	$Ø_{ext}$ [mm]	$Ø_{int}$ [mm]	A_c [mm^2]	c [mm]	$f_{y,long}$ [MPa]	$Ø_{long,1}$ [mm]	n°	$Ø_{long,2}$ [mm]	n°	$A_{s,long}$ [mm^2]	$\rho_{s,long}$ [%]	$f_{y,conf}$ [MPa]	$Ø_{conf}$ [mm]	Stirrup spacing [mm]	$A_{s,conf}$ [mm^2]	$\rho_{s,conf}$ [%]	Stirrup type	N_{test} [kN]
	3	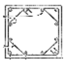	25.3	450	-	198730	20	434	20	12	0	0	3770	1.9	309	10	72	314	1.1	multiple	8410
	6	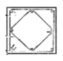	25.3	450	-	198881	20	394	24	8	0	0	3619	1.8	309	10	72	314	1.1	multiple	6720
	7	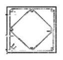	25.3	450	-	198881	20	394	24	8	0	0	3619	1.8	309	10	72	314	1.1	multiple	7850
	12	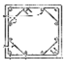	24.8	450	-	198730	20	434	20	12	0	0	3770	1.9	309	10	98	314	0.8	multiple	8500
	13	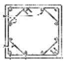	24.8	450	-	198730	20	434	20	12	0	0	3770	1.9	309	10	72	314	1.1	multiple	8650
	14	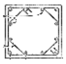	24.8	450	-	198730	20	434	20	12	0	0	3770	1.9	296	12	88	452	1.3	multiple	8800
	15	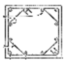	24.8	450	-	198730	20	434	20	12	0	0	3770	1.9	296	12	64	452	1.8	multiple	9400
	17		24.8	450	-	198881	20	394	24	8	0	0	3619	1.8	309	10	98	314	0.8	multiple	7900
	18		24.8	450	-	198881	20	394	24	8	0	0	3619	1.8	309	10	72	314	1.1	multiple	8500
	19		24.8	450	-	198881	20	394	24	8	0	0	3619	1.8	296	12	88	452	1.3	multiple	8400
	20		24.8	450	-	198881	20	394	24	8	0	0	3619	1.8	296	12	64	452	1.8	multiple	8800
	22	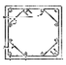	24.2	450	-	198730	20	272	20	12	0	0	3770	1.9	309	10	98	314	0.8	multiple	7300
	23	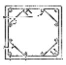	24.2	450	-	198730	20	272	20	12	0	0	3770	1.9	309	10	72	314	1.1	multiple	7450
	24	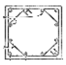	24.2	450	-	198730	20	272	20	12	0	0	3770	1.9	309	12	88	452	1.3	multiple	7800
	25	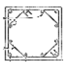	24.2	450	-	198730	20	272	20	12	0	0	3770	1.9	309	12	64	452	1.8	multiple	8500
Sun, Oba, Tian, Ikeda, 1996	NA6-20		52.9	200	-	38938	4.6	362	13	8	0	0	1062	2.7	342	6.4	20	64	1.7	square	2590
	NA6-30		52.9	200	-	38938	4.6	362	13	8	0	0	1062	2.7	342	6.4	30	64	1.2	square	2372
	NA10-47		52.9	200	-	38938	3.4	362	13	8	0	0	1062	2.7	344	9.6	47	145	1.7	square	2426
	NB6-35	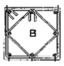	53.4	200	-	38938	4.6	362	13	8	0	0	1062	2.7	342	6.4	35	129	2.0	multiple	2519
	NB6-50		53.4	200	-	38938	4.6	362	13	8	0	0	1062	2.7	342	6.4	50	129	1.4	multiple	2430
	NB10-75	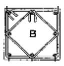	53.4	200	-	38938	2.9	362	13	8	0	0	1062	2.7	344	9.6	75	290	2.1	multiple	2514
	NC6-30	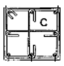	52.5	200	-	38938	4.6	362	13	8	0	0	1062	2.7	342	6.4	30	97	1.7	multiple	2489

Authors	Specimen	Cross section	$f_{cm,cyl}$ [MPa]	$Ø_{ext}$ [mm]	$Ø_{int}$ [mm]	A_c [mm^2]	c [mm]	$f_{y,long}$ [MPa]	$Ø_{long,1}$ [mm]	n°	$Ø_{long,2}$ [mm]	n°	$A_{s,long}$ [mm^2]	$\rho_{s,long}$ [%]	$f_{y,conf}$ [MPa]	$Ø_{conf}$ [mm]	Stirrup spacing [mm]	$A_{s,conf}$ [mm^2]	$\rho_{s,conf}$ [%]	Stirrup type	N_{test} [kN]
	NC6-43	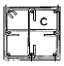	52.5	200	-	38938	4.6	362	13	8	0	0	1062	2.7	342	6.4	43	97	1.2	multiple	2421
	NC10-70		52.5	200	-	38938	2.9	362	13	8	0	0	1062	2.7	344	9.6	70	217	1.7	multiple	2421
	ND6-47		52.9	200	-	38407	4.6	362	13	12	0	0	1593	4.0	342	6.4	47	129	1.5	multiple	2671
	ND6-70		52.9	200	-	38407	4.6	362	13	12	0	0	1593	4.0	342	6.4	70	129	1.0	multiple	2543
	NE6-40	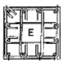	52.9	200	-	38407	4.6	362	13	12	0	0	1593	4.0	342	6.4	40	129	1.7	multiple	2680
	NE6-60	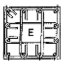	52.9	200	-	38407	4.6	362	13	12	0	0	1593	4.0	342	6.4	60	129	1.2	multiple	2666
	NBM-60	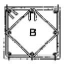	52.9	200	-	38938	1.4	362	13	8	0	0	1062	2.7	344	9.6	60	290	2.6	multiple	2571
	NBM-75	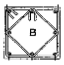	52.9	200	-	38938	1.4	362	13	8	0	0	1062	2.7	344	9.6	75	290	2.1	multiple	2377
	NCM-60	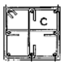	52.5	200	-	38938	1.4	362	13	8	0	0	1062	2.7	344	9.6	60	217	1.9	multiple	2435
	NCM-75	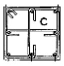	52.5	200	-	38938	1.4	362	13	8	0	0	1062	2.7	344	9.6	75	217	1.5	multiple	2391
Da Silva, 2000	C30-400		35.5	305	-	71270	15	402	19.5	6	0	0	1792	2.5	410	11.3	100	201	0.8	spiral	2789
	C30-500		35.5	305	-	71270	15	402	19.5	6	0	0	1792	2.5	510	9.5	100	142	0.5	spiral	2771
	C40-400		39.5	305	-	71270	15	402	19.5	6	0	0	1792	2.5	410	11.3	100	201	0.8	spiral	3893
	C40-500		39.5	305	-	71270	15	402	19.5	6	0	0	1792	2.5	510	9.5	100	142	0.5	spiral	3984
	C60-400		59.5	305	-	71270	15	402	19.5	6	0	0	1792	2.5	410	11.3	75	201	1.0	spiral	3982
	C60-500		59.5	305	-	71270	15	402	19.5	6	0	0	1792	2.5	510	9.5	80	142	0.7	spiral	4024
	C100-400		119.9	305	-	71270	15	402	19.5	6	0	0	1792	2.5	410	11.3	45	201	1.7	spiral	6222
	C100-500		119.9	305	-	71270	15	402	19.5	6	0	0	1792	2.5	510	9.5	50	142	1.1	spiral	6598
	C120-400		125.4	305	-	71270	15	402	19.5	6	0	0	1792	2.5	410	11.3	35	201	2.2	spiral	7303
	C120-500		125.4	305	-	71270	15	402	19.5	6	0	0	1792	2.5	510	9.5	40	142	1.3	spiral	7611
Hwee, Rangan, 1990	1	Square	59	150	-	22048	15	430	12	4	0	0	452	2.0	355	6	50	57	1.0	square	1250
	2	Square	61	150	-	22048	15	430	12	4	0	0	452	2.0	355	6	100	57	0.5	square	1253

Authors	Specimen	Cross section	$f_{cm,cyl}$ [MPa]	$Ø_{ext}$ [mm]	$Ø_{int}$ [mm]	A_c [mm^2]	c [mm]	$f_{y,long}$ [MPa]	$Ø_{long,1}$ [mm]	n°	$Ø_{long,2}$ [mm]	n°	$A_{s,long}$ [mm^2]	$\rho_{s,long}$ [%]	$f_{y,conf}$ [MPa]	$Ø_{conf}$ [mm]	Stirrup spacing [mm]	$A_{s,conf}$ [mm^2]	$\rho_{s,conf}$ [%]	Stirrup type	N_{test} [kN]
	3	Square	61	150	-	22048	15	430	12	4	0	0	452	2.0	355	6	150	57	0.3	square	1340
	4	Square	61	150	-	21696	15	440	16	4	0	0	804	3.6	355	6	50	57	1.0	square	1389
	5	Square	62	150	-	21696	15	440	16	4	0	0	804	3.6	355	6	100	57	0.5	square	1389
	6	Square	62	150	-	21696	15	440	16	4	0	0	804	3.6	355	6	150	57	0.3	square	1370
	7	Square	68	150	-	22048	15	430	12	4	0	0	452	2.0	355	6	50	57	1.0	square	1400
	8	Square	68	150	-	22048	15	430	12	4	0	0	452	2.0	355	6	100	57	0.5	square	1420
	9	Square	68	150	-	22048	15	430	12	4	0	0	452	2.0	355	6	150	57	0.3	square	1422
	10	Square	68	150	-	21696	15	440	16	4	0	0	804	3.6	355	6	50	57	1.0	square	1615
	11	Square	68	150	-	21696	15	440	16	4	0	0	804	3.6	355	6	100	57	0.5	square	1518
	12	Square	68	150	-	21696	15	440	16	4	0	0	804	3.6	355	6	150	57	0.3	square	1381
Rangan, Saunders, Seng, 1991	RC-1	Square	65	160	-	25148	15	430	12	4	0	0	452	1.8	450	4	100	25	0.2	square	1557
	RC-2	Square	65	160	-	25148	15	430	12	4	0	0	452	1.8	450	4	100	25	0.2	square	1495
	RC-4	Square	65	160	-	25148	15	430	12	4	0	0	452	1.8	450	5	200	39	0.2	square	1515
	RC-5	Square	65	160	-	25148	15	430	12	4	0	0	452	1.8	450	4	50	25	0.4	square	1453
	RC-7	Square	65	160	-	25148	15	430	12	4	0	0	452	1.8	450	6	200	57	0.2	square	1820
	RC-8	Square	65	160	-	25148	15	430	12	4	0	0	452	1.8	450	4	50	25	0.4	square	1620
	RC-9	Square	65	160	-	25148	15	430	12	4	0	0	452	1.8	450	5	100	39	0.3	square	1520
	RC-10	Square	65	160	-	25148	15	430	12	4	0	0	452	1.8	450	5	150	39	0.2	square	1595
Parvez, Foster, Valipour, McGregor 2017	2H0-70S-NS-1	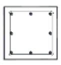	105	200	-	39095	15	520	12	8	0	0	905	2.3	810	5.5	70	48	0.4	square	3144
	2H0-70S-NS-2	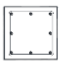	115	200	-	39095	15	520	12	8	0	0	905	2.3	810	5.5	70	48	0.4	square	4171
	2H0-120D-NS-1		105	200	-	39095	15	520	12	8	0	0	905	2.3	810	5.5	120	95	0.5	multiple	2826
	2H0-120D-NS-2		115	200	-	39095	15	520	12	8	0	0	905	2.3	810	5.5	120	95	0.5	multiple	3934

Authors	Specimen	Cross section	$f_{cm,cyl}$ [MPa]	$Ø_{ext}$ [mm]	$Ø_{int}$ [mm]	A_c [mm^2]	c [mm]	$f_{y,long}$ [MPa]	$Ø_{long,1}$ [mm]	n°	$Ø_{long,2}$ [mm]	n°	$A_{s,long}$ [mm^2]	$\rho_{s,long}$ [%]	$f_{y,conf}$ [MPa]	$Ø_{conf}$ [mm]	Stirrup spacing [mm]	$A_{s,conf}$ [mm^2]	$\rho_{s,conf}$ [%]	Stirrup type	N_{test} [kN]
	2H0-70S-HS		115	200	-	39281	15	650	10.7	8	0	0	719	1.8	810	5.5	70	48	0.4	square	4271
Khalajestani, Parvez, Foster, Valipour, McGregor 2018	1.8H0-70S-HS		110	200	-	39281	15	670	10.7	8	0	0	719	1.8	810	5.5	70	48	0.4	square	4271
Moccia, Kubski, Fernandez Muttoni 2020	CM1A0		35.2	250	-	62186	20	531	10	4	0	0	314	0.5	496	8	150	101	0.3	square	2282
	CM1A2	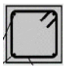	35.2	250	-	62186	20	531	10	4	0	0	314	0.5	496	8	150	101	0.3	square	2436
	CM1B0		35.2	250	-	62186	20	531	10	4	0	0	314	0.5	531	12	150	226	0.8	square	2353
	CM1B1		35.2	250	-	62186	20	531	10	4	0	0	314	0.5	531	12	150	226	0.8	square	2340
	CM1B2		35.2	250	-	62186	20	531	10	4	0	0	314	0.5	531	12	150	226	0.8	square	2581
	CM1B3		35.2	250	-	62186	20	531	10	4	0	0	314	0.5	531	12	150	226	0.8	square	2506
	CM1C0		35.2	250	-	62186	20	531	10	4	0	0	314	0.5	474	16	150	402	1.4	square	2410
	CM1C1		35.2	250	-	62186	20	531	10	4	0	0	314	0.5	474	16	150	402	1.4	square	2511
	CM1C2		35.2	250	-	62186	20	531	10	4	0	0	314	0.5	474	16	150	402	1.4	square	2723
	CM1C3		35.2	250	-	62186	20	531	10	4	0	0	314	0.5	474	16	150	402	1.4	square	2486
Al-Hussaini, Regan, Xue, Ramdane, 1993	C12		101	250	-	61243	20	549	20	4	0	0	1257	2.0	353	6	200	56.5	0.1	square	5500
	C13		100	250	-	60537	20	472	25	4	0	0	1963	3.1	318	8	250	100.5	0.2	square	5500
	C14		106	250	-	58573	20	472	25	8	0	0	3927	6.3	318	8	50	100.5	1.0	square	6616
	C21		89	250	-	62048	20	559	12	4	0	0	452	0.7	353	6	70	56.5	0.4	square	4625
	C22		98	250	-	61243	20	549	20	4	0	0	1257	2.0	318	8	50	100.5	1.0	square	5625
	C23		104	250	-	60892	20	514	16	8	0	0	1608	2.6	318	8	50	100.5	1.0	square	5500
	C24		89	250	-	60537	20	472	25	4	0	0	1963	3.1	318	8	50	100.5	1.0	square	4875
Fang, Hong, Wu 1994	HA1-1		72.93	250	-	61360	0	489	19.05	4	0	0	1140	1.8	310	9.5	50	141.8	1.2	square	4415
	HA1-2		78.69	250	-	61360	0	489	19.05	4	0	0	1140	1.8	310	9.5	50	141.8	1.2	square	4326
	HA2-1		76.35	250	-	61360	0	489	19.05	4	0	0	1140	1.8	310	9.5	62.5	141.8	0.9	square	4493

Authors	Specimen	Cross section	$f_{cm,cyl}$ [MPa]	$Ø_{ext}$ [mm]	$Ø_{int}$ [mm]	A_c [mm^2]	c [mm]	$f_{y,long}$ [MPa]	$Ø_{long,1}$ [mm]	n°	$Ø_{long,2}$ [mm]	n°	$A_{s,long}$ [mm^2]	$\rho_{s,long}$ [%]	$f_{y,conf}$ [MPa]	$Ø_{conf}$ [mm]	Stirrup spacing [mm]	$A_{s,conf}$ [mm^2]	$\rho_{s,conf}$ [%]	Stirrup type	N_{test} [kN]
	HA2-2		76.35	250	-	61360	0	489	19.05	4	0	0	1140	1.8	310	9.5	62.5	141.8	0.9	square	4331
	HA3-1		72.93	250	-	61360	0	489	19.05	4	0	0	1140	1.8	310	9.5	125	141.8	0.5	square	4150
	HA3-2		78.69	250	-	61360	0	489	19.05	4	0	0	1140	1.8	310	9.5	125	141.8	0.5	square	4047
	MA1-1		43.82	250	-	61360	0	489	19.05	4	0	0	1140	1.8	310	9.5	50	141.8	1.2	square	3567
	MA1-2		56.85	250	-	61360	0	489	19.05	4	0	0	1140	1.8	310	9.5	50	141.8	1.2	square	3836
	MA2-1		48.87	250	-	61360	0	489	19.05	4	0	0	1140	1.8	310	9.5	62.5	141.8	0.9	square	3983
	MA2-2		48.87	250	-	61360	0	489	19.05	4	0	0	1140	1.8	310	9.5	62.5	141.8	0.9	square	3934
	MA3-1		43.82	250	-	61360	0	489	19.05	4	0	0	1140	1.8	310	9.5	125	141.8	0.5	square	3488
	MA3-2		56.85	250	-	61360	0	489	19.05	4	0	0	1140	1.8	310	9.5	125	141.8	0.5	square	3782
	HB1-3		66.88	250	-	60912	0	476	15.9	8	0	0	1588	2.5	310	9.5	62.5	212.6	1.4	multiple	4694
	HB1-4		63.33	250	-	60912	0	476	15.9	8	0	0	1588	2.5	310	9.5	62.5	212.6	1.4	multiple	4522
	HB2-3		66.88	250	-	60912	0	476	15.9	8	0	0	1588	2.5	310	9.5	90	212.6	1.0	multiple	4493
	HB2-4		63.33	250	-	60912	0	476	15.9	8	0	0	1588	2.5	310	9.5	90	212.6	1.0	multiple	4209
	HB3-1		79.82	250	-	60220	0	489	19.05	8	0	0	2280	3.6	310	9.5	125	212.6	0.7	multiple	4797
	HB3-2		66.77	250	-	60220	0	489	19.05	8	0	0	2280	3.6	310	9.5	125	212.6	0.7	multiple	4655
	MB1-3		52.8	250	-	60912	0	476	15.9	8	0	0	1588	2.5	310	9.5	62.5	212.6	1.4	multiple	4287
	MB1-4		52.8	250	-	60912	0	476	15.9	8	0	0	1588	2.5	310	9.5	62.5	212.6	1.4	multiple	4052
	MB2-3		52.8	250	-	60912	0	476	15.9	8	0	0	1588	2.5	310	9.5	90	212.6	1.0	multiple	3944
	BM2-4		52.8	250	-	60912	0	476	15.9	8	0	0	1588	2.5	310	9.5	90	212.6	1.0	multiple	3934
	MB3-1		67.97	250	-	60220	0	489	19.05	8	0	0	2280	3.6	310	9.5	125	212.6	0.7	multiple	4513
	MB3-2		69.58	250	-	60220	0	489	19.05	8	0	0	2280	3.6	310	9.5	125	212.6	0.7	multiple	4542
Einpaul, Muttoni, Burdet, 2011	CCF1		118.9	300	100	58584	20	819	26	8	0	0	4247	6.8	560	6	70	57	0.3	spiral	7560

Authors	Specimen	Cross section	$f_{cm,cyl}$ [MPa]	$Ø_{ext}$ [mm]	$Ø_{int}$ [mm]	A_c [mm^2]	c [mm]	$f_{y,long}$ [MPa]	$Ø_{long,1}$ [mm]	n°	$Ø_{long,2}$ [mm]	n°	$A_{s,long}$ [mm^2]	$\rho_{s,long}$ [%]	$f_{y,conf}$ [MPa]	$Ø_{conf}$ [mm]	Stirrup spacing [mm]	$A_{s,conf}$ [mm^2]	$\rho_{s,conf}$ [%]	Stirrup type	N_{test} [kN]
	CCF2		106.2	300	100	58584	20	819	26	8	0	0	4247	6.8	560	6	70	57	0.3	spiral	7930
	CSF1	Circular	98.8	300	-	66438	20	819	26	8	0	0	4247	6.0	560	6	70	57	0.3	spiral	7880
	CSF2	Circular	87.8	300	-	66438	20	819	26	8	0	0	4247	6.0	560	6	70	57	0.3	spiral	7400

Appendix B: Database on column tests with load eccentricity

Annex D of "Concrete compressive strength: from material characterization to a structural value".

Authors	Specimen	Cross section	$f_{cm,cyl}$ [MPa]	Length [mm]	Width [mm]	A_c [mm²]	c [mm]	$f_{y,long}$ [MPa]	$Ø_{long,1}$ [mm]	n°	$A_{s,long}$ [mm²]	$\rho_{s,long.}$ [%]	$f_{y,conf}$ [MPa]	$Ø_{conf}$ [mm]	Stirrup spacing [mm]	$A_{s,conf}$ [mm²]	$\rho_{s,conf}$ [%]	e [mm]	N_{test} [kN]	M_{test} [kNm]
Ibrahim, MacGregor 1996	V1	rect.	71	300	200	59196	11	433	16.0	4	804	1.34	423	11.3	200	201	0.33	18.2	3203	58.4
	V7	rect.	85	300	200	59196	14	433	16.0	4	804	1.34	401	8.7	200	119	0.20	46.6	3013	140.3
	V8	rect.	129	300	200	59196	14	433	16.0	4	804	1.34	401	8.7	200	119	0.20	45.9	4422	203.0
	V11	rect.	128	300	200	59196	11	433	16.0	4	804	1.34	423	11.3	200	201	0.33	47.4	3743	177.6
	V12	rect.	121	300	200	59196	11	433	16.0	4	804	1.34	423	11.3	200	201	0.33	45.5	3960	180.2
	V13	rect.	73	300	200	59196	14	433	16.0	4	804	1.34	401	8.7	100	119	0.40	39.7	2718	108.0
	V15	rect.	125	300	200	59196	14	433	16.0	4	804	1.34	401	8.7	100	119	0.40	51.1	4424	226.0
	V16	rect.	59	300	200	59198	14	423	11.3	8	802	1.34	401	8.7	50	238	1.59	40.5	2729	110.6
	V17	rect.	128	300	200	59198	14	423	11.3	8	802	1.34	401	8.7	50	238	1.59	42.6	4218	179.8
Foster, Attard, 1997	2L8-30	square	43	150	150	22040	9	480	12.1	4	460	2.04	360	6.3	30	62	1.65	14.5	960	13.9
	2L8-60	square	43	150	150	22040	12	480	12.1	4	460	2.04	360	6.3	60	62	0.87	14.0	857	12.0
	2L8-120	square	43	150	150	22040	15	480	12.1	4	460	2.04	360	6.3	120	62	0.46	14.0	912	12.8
	2L20-30	square	40	150	150	22040	10	480	12.1	4	460	2.04	360	6.3	30	62	1.68	24.8	750	18.6
	2L20-60	square	43	150	150	22040	12	480	12.1	4	460	2.04	360	6.3	60	62	0.87	26.2	700	18.3
	2L20-120	square	43	150	150	22040	14	480	12.1	4	460	2.04	360	6.3	120	62	0.45	25.5	782	19.9
	2L50-30	square	40	150	150	22040	12	480	12.1	4	460	2.04	360	6.3	30	62	1.74	59.0	440	26.0
	2L50-60	square	43	150	150	22040	10	480	12.1	4	460	2.04	360	6.3	60	62	0.84	58.5	472	27.6
	2L50-120	square	40	150	150	22040	14	480	12.1	4	460	2.04	360	6.3	120	62	0.45	59.0	440	26.0
	4L8-30	square	43	150	150	21580	15	480	12.1	8	920	4.09	360	6.3	30	62	1.83	17.0	1100	18.7
	4L8-60	square	43	150	150	21580	9	480	12.1	8	920	4.09	360	6.3	60	62	0.83	14.0	1150	16.1
	4L8-120	square	43	150	150	21580	13	480	12.1	8	920	4.09	360	6.3	120	62	0.44	13.7	975	13.4
	4L20-30	square	40	150	150	21580	11	480	12.1	8	920	4.09	360	6.3	30	62	1.71	27.0	1020	27.5
	4L20-60	square	40	150	150	21580	15	480	12.1	8	920	4.09	360	6.3	60	62	0.91	23.5	968	22.7
	4L20-120	square	40	150	150	21580	13	480	12.1	8	920	4.09	360	6.3	120	62	0.44	24.0	900	21.6
	4L50-30	square	40	150	150	21580	17	480	12.1	8	920	4.09	360	6.3	30	62	1.89	68.5	517	33.0
	4L50-60	square	40	150	150	21580	9	480	12.1	8	920	4.09	360	6.3	60	62	0.83	58.0	550	31.9
	4L50-120	square	40	150	150	21580	13	480	12.1	8	920	4.09	360	6.3	120	62	0.44	58.0	525	30.5
	2M8-30	square	75	150	150	22040	11	480	12.1	4	460	2.04	360	6.3	30	62	1.71	13.0	1348	17.5
	2M8-60	square	75	150	150	22040	11	480	12.1	4	460	2.04	360	6.3	60	62	0.85	13.0	1432	18.6
	2M8-120	square	75	150	150	22040	14	480	12.1	4	460	2.04	360	6.3	120	62	0.45	12.0	1239	14.9
	2M20-30	square	74	150	150	22040	10	480	12.1	4	460	2.04	360	6.3	30	62	1.68	26.0	1160	30.2
	2M20-60	square	74	150	150	22040	12	480	12.1	4	460	2.04	360	6.3	60	62	0.87	26.0	1231	32.0
	2M20-120	square	74	150	150	22040	13	480	12.1	4	460	2.04	360	6.3	120	62	0.44	25.0	1067	26.7
	2M50-30	square	74	150	150	22040	11	480	12.1	4	460	2.04	360	6.3	30	62	1.71	59.5	630	37.5
	2M50-60	square	74	150	150	22040	15	480	12.1	4	460	2.04	360	6.3	60	62	0.91	61.5	747	45.9
	2M50-120	square	74	150	150	22040	9	480	12.1	4	460	2.04	360	6.3	120	62	0.41	61.5	652	40.1
	4M8-30	square	74	150	150	21580	17	480	12.1	8	920	4.09	460	6.3	30	62	1.89	11.0	1102	12.1
	4M8-60	square	75	150	150	21580	18	480	12.1	8	920	4.09	460	6.3	60	62	0.96	12.0	1404	16.8
	4M8-120	square	74	150	150	21580	12	480	12.1	8	920	4.09	460	6.3	120	62	0.43	11.5	1404	16.1
	4M20-30	square	75	150	150	21580	15	480	12.1	8	920	4.09	460	6.3	30	62	1.83	24.0	1052	25.2
	4M20-60	square	75	150	150	21580	19	480	12.1	8	920	4.09	460	6.3	60	62	0.98	25.0	1004	25.1

Authors	Specimen	Cross Section	$f_{cm,cyl}$ [MPa]	Length [mm]	Width [mm]	A_c [mm^2]	c [mm]	$f_{y,long}$ [MPa]	$Ø_{long,1}$ [mm]	n°	$A_{s,long}$ [mm^2]	$\rho_{s,long.}$ [%]	$f_{y,conf}$ [MPa]	$Ø_{conf}$ [mm]	Stirrup Spacing [mm]	$A_{s,conf}$ [mm^2]	$\rho_{s,conf}$ [%]	e [mm]	N_{test} [kN]	M_{test} [kNm]
	4M20-120	square	75	150	150	21580	15	480	12.1	8	920	4.09	460	6.3	120	62	0.46	25.0	1226	30.7
	4M50-30	square	74	150	150	21580	18	480	12.1	8	920	4.09	460	6.3	30	62	1.93	59.5	656	39.0
	4M50-60	square	75	150	150	21580	17	480	12.1	8	920	4.09	460	6.3	60	62	0.95	59.5	686	40.8
	4M50-120	square	74	150	150	21580	12	480	12.1	8	920	4.09	460	6.3	120	62	0.43	59.5	677	40.3
	4H8-30	square	91	150	150	21580	10	480	12.1	8	920	4.09	360	6.3	30	62	1.68	12.8	1601	20.5
	4H8-60	square	92	150	150	21580	12	480	12.1	8	920	4.09	360	6.3	60	62	0.87	13.5	1702	23.0
	4H8-120	square	92	150	150	21580	12	480	12.1	8	920	4.09	360	6.3	120	62	0.43	12.2	1654	20.2
	4H20-30	square	88	150	150	21580	11	480	12.1	8	920	4.09	360	6.3	30	62	1.71	27.0	1352	36.5
	4H20-60	square	88	150	150	21580	9	480	12.1	8	920	4.09	360	6.3	60	62	0.83	27.5	1358	37.3
	4H20-120	square	92	150	150	21580	12	480	12.1	8	920	4.09	360	6.3	120	62	0.43	27.0	1374	37.1
	4H50-30	square	88	150	150	21580	11	480	12.1	8	920	4.09	360	6.3	30	62	1.71	60.5	780	47.2
	4H50-60	square	88	150	150	21580	11	480	12.1	8	920	4.09	360	6.3	60	62	0.85	59.5	790	47.0
	4H50-120	square	92	150	150	21580	10	480	12.1	8	920	4.09	360	6.3	120	62	0.42	59.5	818	48.7
	2L8-120R	square	56	150	150	22040	15	480	12.1	4	460	2.04	460	6.3	120	62	0.46	12.5	1092	13.7
	2L20-120R	square	56	150	150	22040	13	480	12.1	4	460	2.04	460	6.3	120	62	0.44	25.0	897	22.4
	4L8-120R	square	56	150	150	21580	10	480	12.1	8	920	4.09	460	6.3	120	62	0.42	12.0	1247	15.0
	4L20-120R	square	53	150	150	21580	13	480	12.1	8	920	4.09	460	6.3	120	62	0.44	26.0	945	24.6
	4L50-30R	square	40	150	150	21580	14	480	12.1	8	920	4.09	460	6.3	30	62	1.80	60.0	546	32.8
	2M8-30R	square	68	150	150	22040	13	480	12.1	4	460	2.04	360	6.3	30	62	1.77	9.0	1326	11.9
	2M20-60R	square	73	150	150	22040	12	480	12.1	4	460	2.04	360	6.3	60	62	0.87	27.0	1203	32.5
	2M20-120R	square	73	150	150	22040	13	480	12.1	4	460	2.04	360	6.3	120	62	0.44	27.0	1180	31.9
	2M50-60R	square	67	150	150	22040	13	480	12.1	4	460	2.04	360	6.3	60	62	0.88	58.4	670	39.1
	2M50-120R	square	73	150	150	22040	10	480	12.1	4	460	2.04	360	6.3	120	62	0.42	63.2	672	42.5
	4M20-60R	square	68	150	150	21580	15	480	12.1	8	920	4.09	360	6.3	60	62	0.91	24.4	1198	29.2
	4M20-120R	square	73	150	150	21580	10	480	12.1	8	920	4.09	360	6.3	120	62	0.42	27.2	1105	30.1
	4M50-60R	square	73	150	150	21580	12	480	12.1	8	920	4.09	360	6.3	60	62	0.87	58.5	800	46.8
	4M50-120R	square	70	150	150	21580	13	480	12.1	8	920	4.09	360	6.3	120	62	0.44	59.5	633	37.7
Foster, Attard, Kokolis, 1997	2H8-30N	square	105	150	150	22040	12	420	12.1	4	460	2.04	355	6.3	30	62	1.74	11.8	1370	16.2
	2H8-60N	square	105	150	150	22040	13	420	12.1	4	460	2.04	355	6.3	60	62	0.88	12.5	1257	15.7
	2H8-120N	square	105	150	150	22040	14	420	12.1	4	460	2.04	355	6.3	120	62	0.45	11.6	1451	16.8
	2H20-30N	square	105	150	150	22040	13	420	12.1	4	460	2.04	355	6.3	30	62	1.77	24.3	1160	28.2
	2H20-60N	square	105	150	150	22040	13	420	12.1	4	460	2.04	355	6.3	60	62	0.88	24.2	1125	27.2
	2H20-120N	square	105	150	150	22040	12	420	12.1	4	460	2.04	355	6.3	120	62	0.43	24.8	964	23.9
	2H50-30N	square	105	150	150	22040	14	420	12.1	4	460	2.04	355	6.3	30	62	1.80	58.0	626	36.3
	2H50-60N	square	105	150	150	22040	16	420	12.1	4	460	2.04	355	6.3	60	62	0.93	57.6	636	36.6
	2H50-120N	square	105	150	150	22040	12	420	12.1	4	460	2.04	355	6.3	120	62	0.43	55.7	609	33.9
Husem, Pul, Gorkem, Demir, 2015	HSC-2	rect.	72	300	200	58768	15	562	14.0	8	1232	2.05	571	8.0	100	101	0.38	25.0	3847	105.8
	HSC-3	rect.	72	300	200	58768	15	562	14.0	8	1232	2.05	571	8.0	100	101	0.38	50.0	2915	157.1
	HSC-5	rect.	72	300	200	58768	15	562	14.0	8	1232	2.05	571	8.0	200	101	0.19	25.0	3469	97.2
	HSC-6	rect.	72	300	200	58768	15	562	14.0	8	1232	2.05	571	8.0	200	101	0.19	50.0	2640	139.6
	HSC-8	rect.	74	300	200	59076	15	562	14.0	6	924	1.54	571	8.0	100	101	0.38	25.0	3557	99.3
	HSC-9	rect.	74	300	200	59076	15	562	14.0	6	924	1.54	571	8.0	100	101	0.38	50.0	2770	153.7
	HSC-11	rect.	75	300	200	59076	15	562	14.0	6	924	1.54	571	8.0	200	101	0.19	25.0	3120	90.8
	HSC-12	rect.	75	300	200	59076	15	562	14.0	6	924	1.54	571	8.0	200	101	0.19	50.0	2441	136.6

Authors	Specimen	Cross Section	$f_{cm,cyl}$ [MPa]	Length [mm]	Width [mm]	A_c [mm²]	c [mm]	$f_{y,long}$ [MPa]	$Ø_{long,1}$ [mm]	n°	$A_{s,long}$ [mm²]	$\rho_{s,long.}$ [%]	$f_{y,conf}$ [MPa]	$Ø_{conf}$ [mm]	Stirrup Spacing [mm]	$A_{s,conf}$ [mm²]	$\rho_{s,conf}$ [%]	e [mm]	N_{test} [kN]	M_{test} [kNm]
	HSC-14	rect.	73	300	200	59384	15	562	14.0	4	616	1.03	571	8.0	100	101	0.38	25.0	3260	101.2
	HSC-15	rect.	73	300	200	59384	15	562	14.0	4	616	1.03	571	8.0	100	101	0.38	50.0	2518	135.2
	HSC-17	rect.	74	300	200	59384	15	562	14.0	4	616	1.03	571	8.0	200	101	0.19	25.0	3020	92.7
	HSC-18	rect.	74	300	200	59384	15	562	14.0	4	616	1.03	571	8.0	200	101	0.19	50.0	2342	130.6
Canbay, Ozcebe, Ersoy, 2006	D8-75	square	90	250	250	61268	10	410	14.0	8	1232	1.97	323	8.0	75	201	1.21	20.0	4500	92.4
	D10-135	square	92	250	250	61268	8	410	14.0	8	1232	1.97	400	10.0	135	314	1.04	20.0	4100	90.6
	L8-75	square	92	250	250	61268	10	410	14.0	8	1232	1.97	323	8.0	75	151	0.91	20.0	4500	92.0
	S8-75	square	92	250	250	61268	10	410	14.0	8	1232	1.97	323	8.0	75	151	0.91	20.0	4400	89.2
	D10-100	square	77	250	250	61268	8	410	14.0	8	1232	1.97	400	10.0	100	314	1.40	89.0	1600	142.4
	D10-60	square	75	250	250	61268	8	410	14.0	8	1232	1.97	400	10.0	60	314	2.34	88.9	1500	133.4
	D9-100	square	71	250	250	61268	9	410	14.0	8	1232	1.97	594	9.0	100	254	1.14	91.7	1500	137.5
	D9-60	square	73	250	250	61268	9	410	14.0	8	1232	1.97	594	9.0	60	254	1.90	89.9	1550	139.4
	D6-100	square	71	250	250	61268	12	410	14.0	8	1232	1.97	530	6.0	100	113	0.51	88.6	1550	137.4
	D6-60	square	66	250	250	61268	12	410	14.0	8	1232	1.97	530	6.0	60	113	0.86	91.5	1500	137.3
Saatcioglu, Salamat, Razvi, 1995	C1-1	square	34	210	210	43298	13	517	11.3	8	802	1.82	410	6.3	50	266	2.98	60.0	960	65.0
	C2-1	square	35	210	210	43298	13	517	11.3	8	802	1.82	410	6.3	50	227	2.54	60.0	930	68.0
	C3-1	square	34	210	210	42897	13	517	11.3	12	1203	2.73	410	6.3	50	240	2.69	60.0	1050	79.5
	C4-2	square	35	210	210	43298	13	517	11.3	8	802	1.82	410	6.3	50	266	2.98	75.0	720	66.0
	C5-2	square	35	210	210	43298	13	517	11.3	8	802	1.82	410	6.3	50	227	2.54	75.0	740	67.0
	C6-2	square	34	210	210	42897	13	517	11.3	12	1203	2.73	410	6.3	50	240	2.69	75.0	850	80.5
	C7-1	square	25	210	210	43298	13	517	11.3	8	802	1.82	410	6.3	100	266	1.49	60.0	750	50.5
	C8-1	square	25	210	210	43298	13	517	11.3	8	802	1.82	410	6.3	100	227	1.27	60.0	750	52.0
	C9-1	square	26	210	210	42897	13	517	11.3	12	1203	2.73	410	6.3	100	239	1.34	60.0	800	60.0
	C10-2	square	27	210	210	43298	13	517	11.3	8	802	1.82	410	6.3	100	266	1.49	75.0	590	58.0
	C11-2	square	26	210	210	43298	13	517	11.3	8	802	1.82	410	6.3	100	227	1.27	75.0	600	57.0
	C12-2	square	26	210	210	42897	13	517	11.3	12	1203	2.73	410	6.3	100	239	1.34	75.0	670	67.0
Scott, Park, Priestley, 1982	s-5	square	25	450	450	198730	20	434	20.0	12	3770	1.86	309	10.0	72	314	1.09	60.8	6250	380.0
	s-8	square	25	450	450	198881	20	394	24.0	8	3619	1.79	309	10.0	72	314	1.09	58.9	5600	330.0
	s-9	square	25	450	450	198881	20	394	24.0	8	3619	1.79	309	10.0	72	314	1.09	39.7	6550	260.0
Tan, Nguyen, 2005	S40-B-N3	square	48	200	200	39372	15	595	10.0	8	628	1.57	455	6.0	50	113	1.38	122.4	1666	204.0
	S40-B-N4	square	49	200	200	39372	15	595	10.0	8	628	1.57	455	6.0	50	113	1.38	121.6	1603	195.0
	S40-B-N5	square	49	200	200	39372	15	595	10.0	8	628	1.57	455	6.0	50	113	1.38	127.7	1644	210.0
	S40-C-N1	square	46	200	200	39372	15	595	10.0	8	628	1.57	455	6.0	100	113	0.69	118.1	1713	202.3
	S40-D-N2	square	48	200	200	39372	15	595	10.0	8	628	1.57	455	6.0	28	57	1.23	122.2	1736	212.1
	S70-B-N1	square	69	200	200	39372	15	595	10.0	8	628	1.57	455	6.0	50	113	1.38	123.5	1722	212.6
	S70-B-N2	square	76	200	200	39372	15	595	10.0	8	628	1.57	455	6.0	50	113	1.38	123.3	1987	245.0
	S70-C-N	square	69	200	200	39372	15	595	10.0	8	628	1.57	455	6.0	100	113	0.69	120.9	1805	218.3
	S90-B-N	square	90	200	200	39372	15	595	10.0	8	628	1.57	636	6.0	50	113	1.38	99.5	3107	309.0
	S90-E-N1	square	95	200	200	39372	15	595	10.0	8	628	1.57	636	6.0	100	57	0.34	126.6	2031	257.2
	S90-E-N2	square	92	200	200	39372	15	595	10.0	8	628	1.57	636	6.0	100	57	0.34	122.7	2192	268.9
	S90-E-N3	square	101	200	200	39372	15	595	10.0	8	628	1.57	636	6.0	100	57	0.34	132.6	2259	299.5
	S40-B-E20/2	square	49	200	200	39372	15	595	10.0	8	628	1.57	455	6.0	50	113	1.38	20.0	1709	34.2
	S40-B-E40/1	square	49	200	200	39372	15	595	10.0	8	628	1.57	455	6.0	50	113	1.38	40.0	1400	56.0
	S40-B-E40/2	square	49	200	200	39372	15	595	10.0	8	628	1.57	455	6.0	50	113	1.38	40.0	1392	55.7

Authors	Specimen	Cross Section	$f_{cm,cyl}$ [MPa]	Length [mm]	Width [mm]	A_c [mm^2]	c [mm]	$f_{y,long}$ [MPa]	$Ø_{long,1}$ [mm]	n°	$A_{s,long}$ [mm^2]	$\rho_{s,long.}$ [%]	$f_{y,conf}$ [MPa]	$Ø_{conf}$ [mm]	Stirrup Spacing [mm]	$A_{s,conf}$ [mm^2]	$\rho_{s,conf}$ [%]	e [mm]	N_{test} [kN]	M_{test} [kNm]
	S40-B-E60/1	square	49	200	200	39372	15	595	10.0	8	628	1.57	455	6.0	50	113	1.38	60.0	985	59.1
	S40-B-E60/2	square	49	200	200	39372	15	595	10.0	8	628	1.57	455	6.0	50	113	1.38	60.0	967	58.0
	S70-B-E20	square	76	200	200	39372	15	595	10.0	8	628	1.57	455	6.0	50	113	1.38	20.0	2075	41.5
	S70-B-E40	square	76	200	200	39372	15	595	10.0	8	628	1.57	455	6.0	50	113	1.38	40.0	1557	62.3
	S70-B-E60	square	76	200	200	39372	15	595	10.0	8	628	1.57	455	6.0	50	113	1.38	60.0	1075	64.5
Ghazi, 2001	4L0-30M	square	36	150	150	21595	10	430	12.0	8	905	4.02	580	4.0	30	25	0.66	7.0	844	7.8
	4L0-60M	square	36	150	150	21595	10	430	12.0	8	905	4.02	580	4.0	60	25	0.33	7.0	878	7.9
	4L0-120M	square	36	150	150	21595	10	430	12.0	8	905	4.02	580	4.0	120	25	0.17	0.0	998	1.6
	4L8-30M	square	36	150	150	21595	10	430	12.0	8	905	4.02	580	4.0	30	25	0.66	14.0	789	16.6
	4L8-60M	square	36	150	150	21595	10	430	12.0	8	905	4.02	580	4.0	60	25	0.33	17.0	751	17.6
	4L8-120M	square	36	150	150	21595	10	430	12.0	8	905	4.02	580	4.0	120	25	0.17	18.0	787	19.4
	4L20-30M	square	36	150	150	21595	10	430	12.0	8	905	4.02	580	4.0	30	25	0.66	20.0	747	19.5
	4L20-60M	square	36	150	150	21595	10	430	12.0	8	905	4.02	580	4.0	60	25	0.33	20.0	707	18.5
	4L20-120M	square	36	150	150	21595	10	430	12.0	8	905	4.02	580	4.0	120	25	0.17	20.0	681	17.8
	4L50-30M	square	36	150	150	21595	10	430	12.0	8	905	4.02	580	4.0	30	25	0.66	50.0	467	27.9
	4L50-60M	square	36	150	150	21595	10	430	12.0	8	905	4.02	580	4.0	60	25	0.33	50.0	431	26.2
	4L50-120M	square	36	150	150	21595	10	430	12.0	8	905	4.02	580	4.0	120	25	0.17	50.0	471	28.5
	4H0-30M	square	96	150	150	21595	10	430	12.0	8	905	4.02	580	4.0	30	25	0.66	0.0	1948	2.2
	4H8-30M	square	96	150	150	21595	10	430	12.0	8	905	4.02	580	4.0	30	25	0.66	8.0	1606	15.4
	4H8-60M	square	96	150	150	21595	10	430	12.0	8	905	4.02	580	4.0	60	25	0.33	8.0	1761	17.6
	4H8-120M	square	96	150	150	21595	10	430	12.0	8	905	4.02	580	4.0	120	25	0.17	8.0	1569	15.1
	4H20-30M	square	96	150	150	21595	10	430	12.0	8	905	4.02	580	4.0	30	25	0.66	20.0	1462	33.6
	4H20-60M	square	96	150	150	21595	10	430	12.0	8	905	4.02	580	4.0	60	25	0.33	20.0	1691	44.7
	4H20-120M	square	96	150	150	21595	10	430	12.0	8	905	4.02	580	4.0	120	25	0.17	20.0	1283	30.0
	4H50-30M	square	96	150	150	21595	10	430	12.0	8	905	4.02	580	4.0	30	25	0.66	50.0	993	59.9
	4H50-60M	square	96	150	150	21595	10	430	12.0	8	905	4.02	580	4.0	60	25	0.33	50.0	961	57.3
	4H50-120M	square	96	150	150	21595	10	430	12.0	8	905	4.02	580	4.0	120	25	0.17	50.0	855	50.2

Appendix C: DIC measurements of series ML10

The pull-out tests of series ML10 are presented in the paper “Casting position effects on spalling and bond performance of reinforcement bars”. This series was monitored with Digital Image Correlation (DIC) using two pairs of cameras (Manta G504B with a resolution of 5 Mpix and Sony XCG-5005E with 5 Mpix) that recorded the displacements of the top and bottom surfaces of the specimens as well as on their sides. However, these measurements were not shown in the article. The aim of this appendix is to summarize the measurements performed in order to give a phenomenological view of the behaviour of each specimen investigated. The output provides an insight on the development of cracking associated to spalling and pull-out failures on a qualitative basis (no detailed values provided).

The frequency of measurements was 0.1 Hz in the first stages of test and was gradually increased to 1 Hz near the failure of the specimen. The data were then post-processed by means of the software VIC-3D. The error of this procedure corresponded to approximately 1/30 of a pixel (66×66 μm^2 pixel dimension of Manta G504B, and 199×199 μm^2 for Sony XCG-5005E). The following tables depict for increasing loading (F_u corresponds to the ultimate load) the following measurements: the out-of-plane displacement (w) and the principal strain (ε_1).

ML10D20-1 (top bar, c = 0 mm, ϕ = 20 mm)

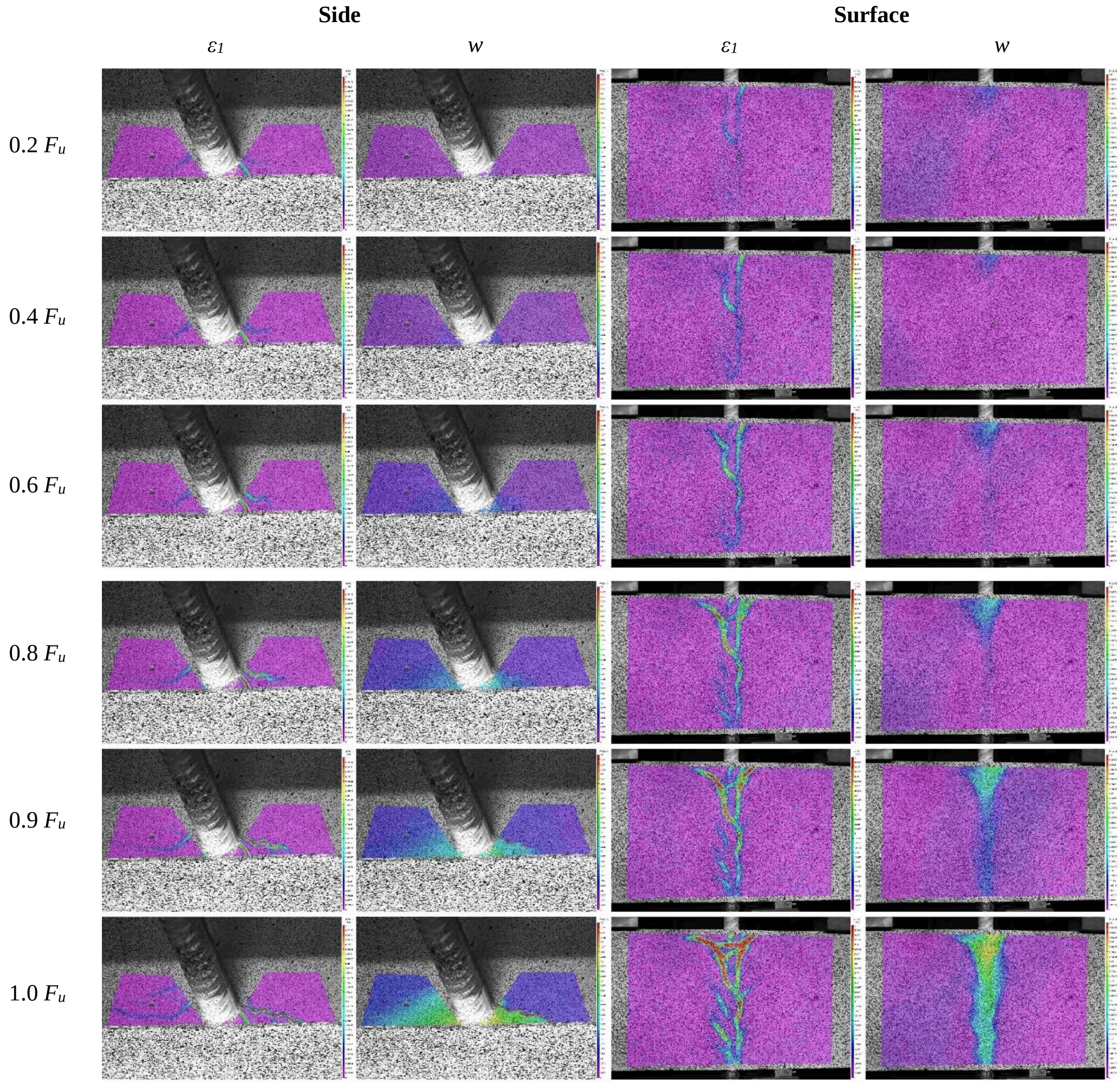

<u>ML10D20-2 (top bar, c = 5 mm, ϕ = 20 mm)</u>

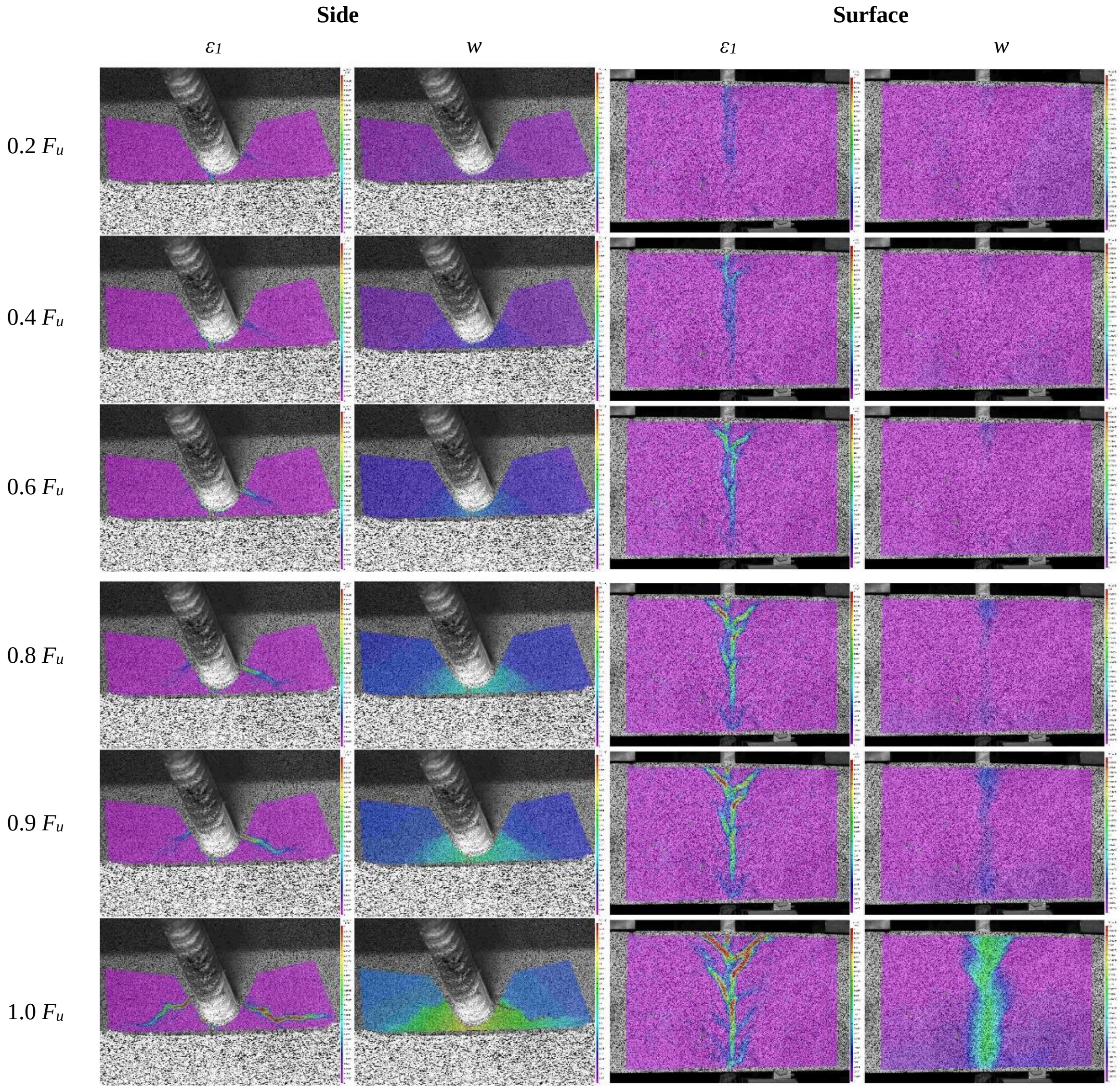

<u>ML10D20-3 (top bar, c = 10 mm, ϕ = 20 mm)</u>

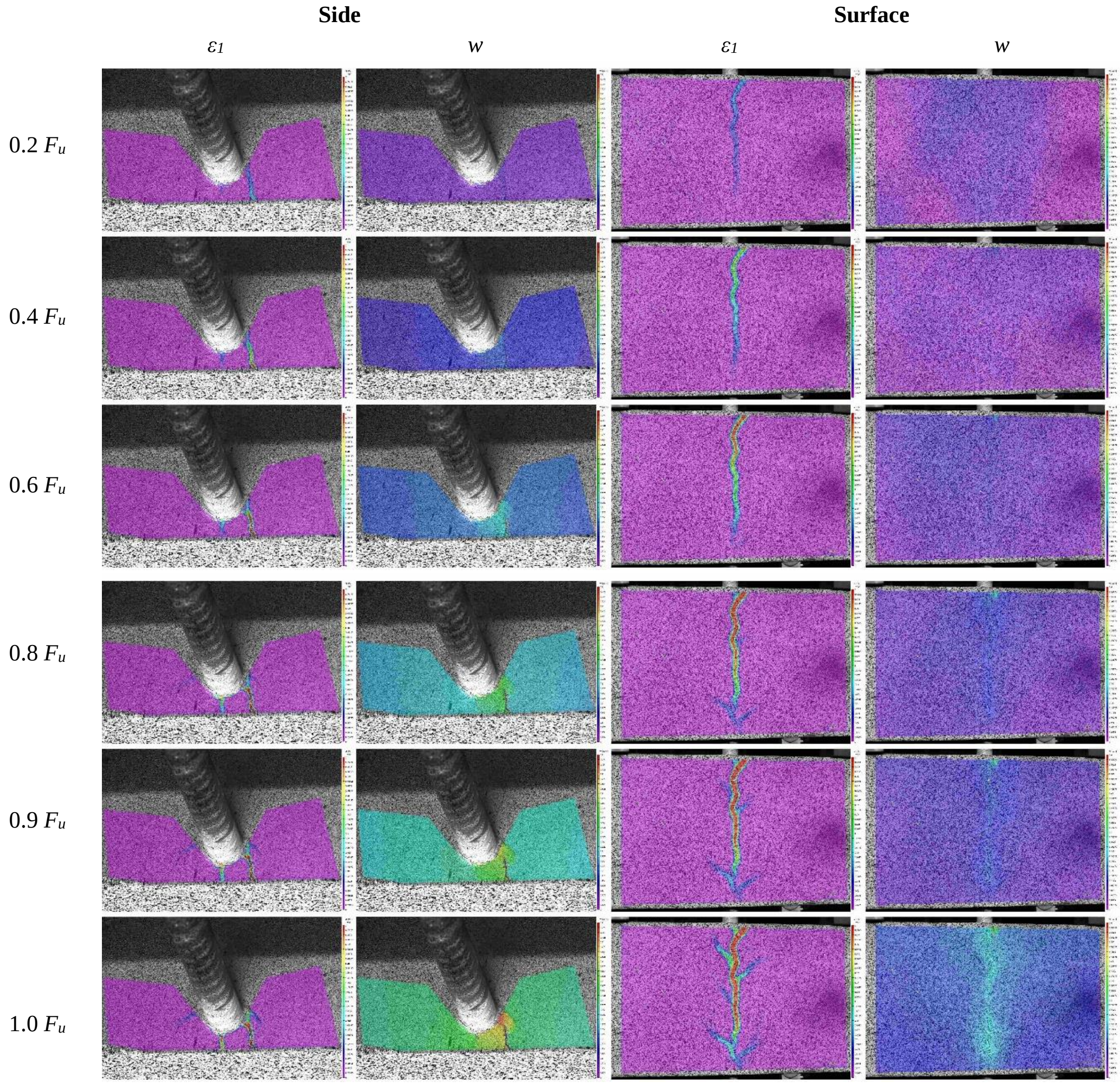

<u>ML10D20-4 (top bar, c = 15 mm, ϕ = 20 mm)</u>

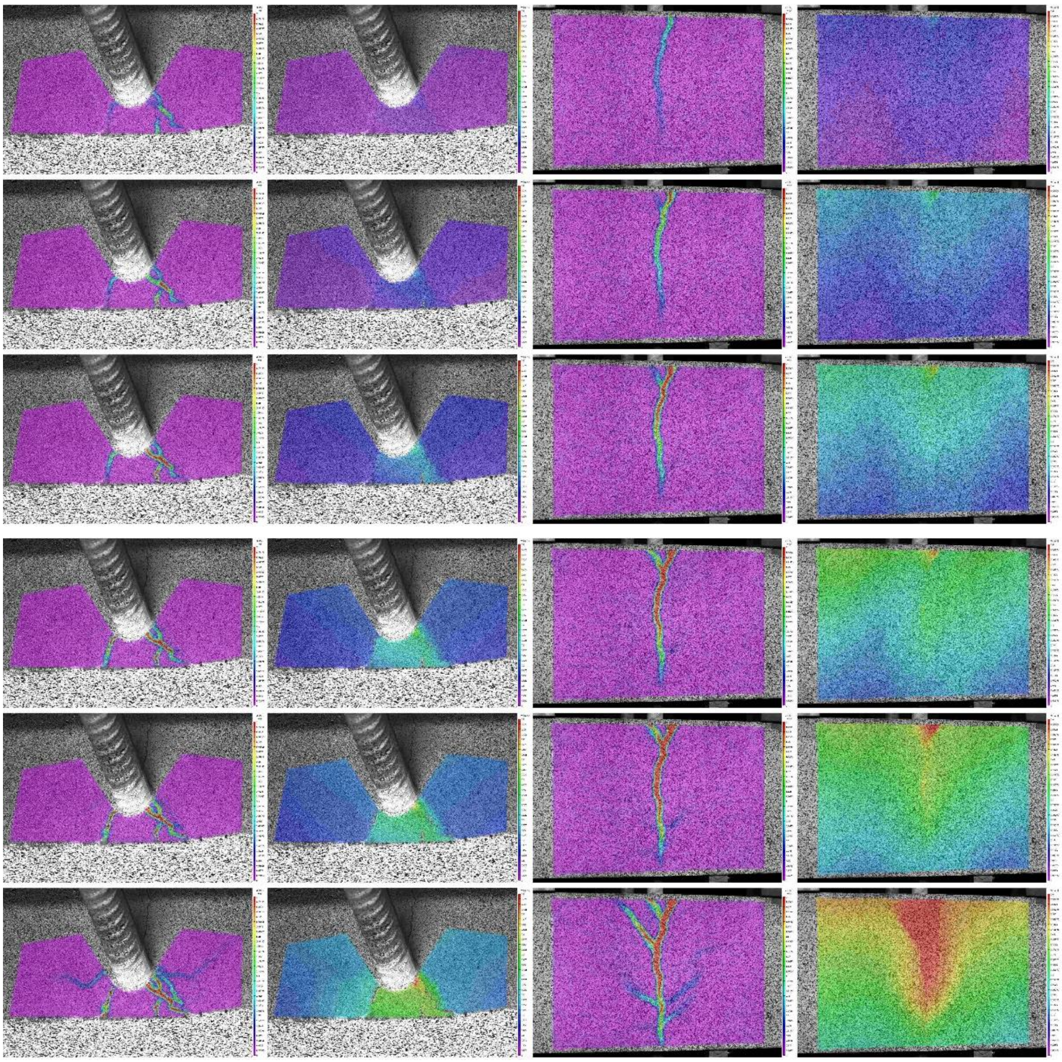

ML10D20-5 (top bar, c = 20 mm, ϕ = 20 mm)

Side | Surface

ε_1 | w | ε_1 | w

0.2 F_u

0.4 F_u

0.6 F_u

0.8 F_u

0.9 F_u

1.0 F_u

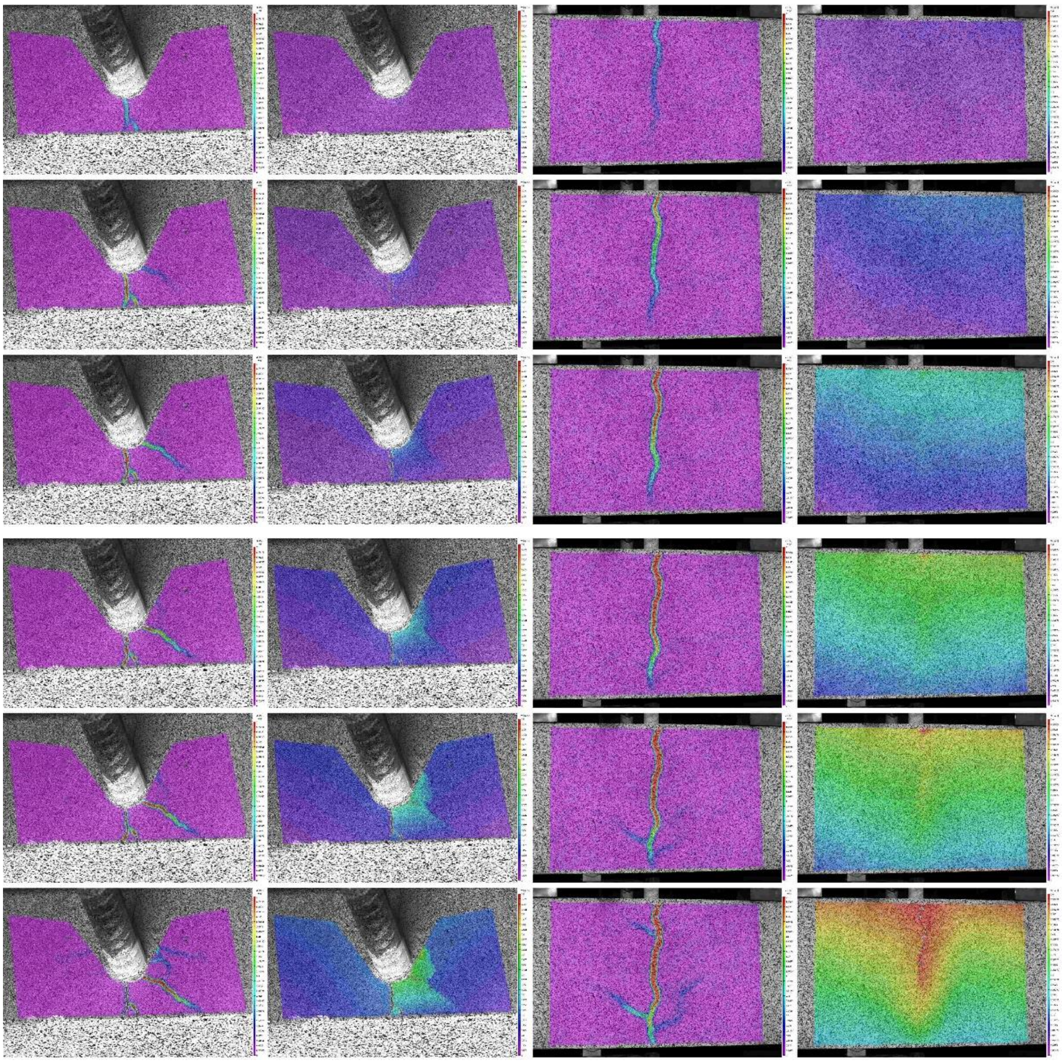

<u>ML10D20-6 (top bar, c = 30 mm, ϕ = 20 mm)</u>

	Side		Surface	
	ε_1	w	ε_1	w
0.2 F_u				
0.4 F_u				
0.6 F_u				
0.8 F_u				
0.9 F_u				
1.0 F_u				

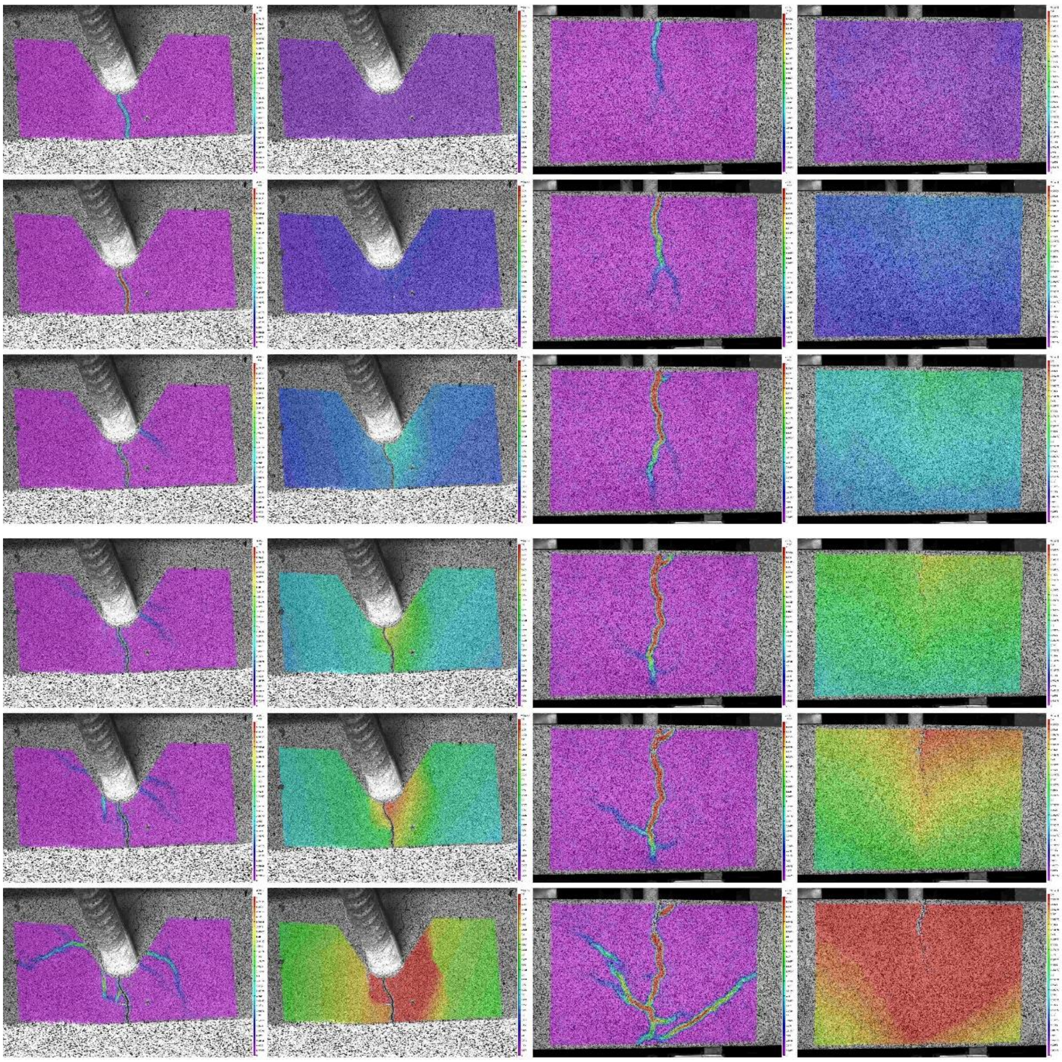

ML10D20-7 (top bar, c = 40 mm, ϕ = 20 mm)

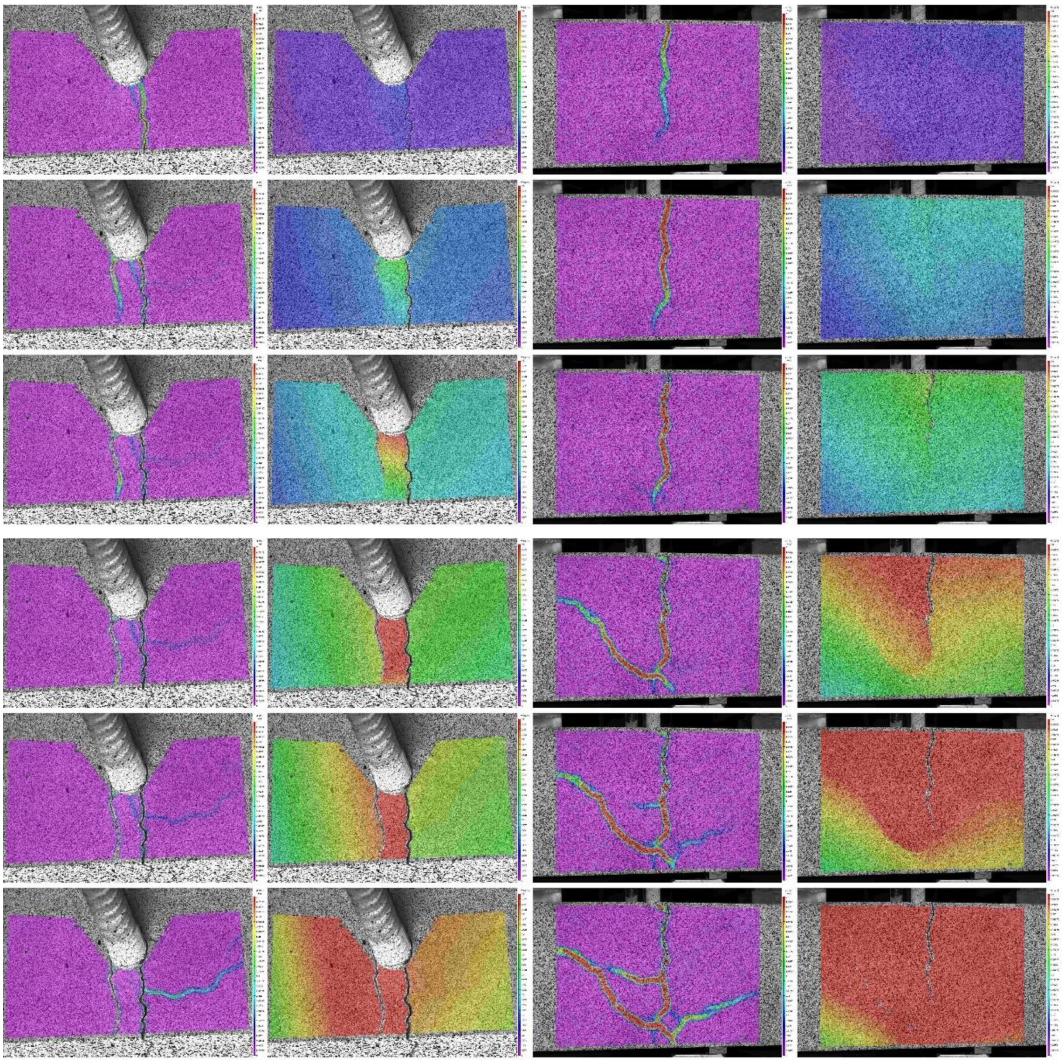

<u>ML10D20-8 (bottom bar, c = 0 mm, ϕ = 20 mm)</u>

	Side		Surface	
	ε_1	w	ε_1	w
0.2 F_u				
0.4 F_u				
0.6 F_u				
0.8 F_u				
0.9 F_u				
1.0 F_u				

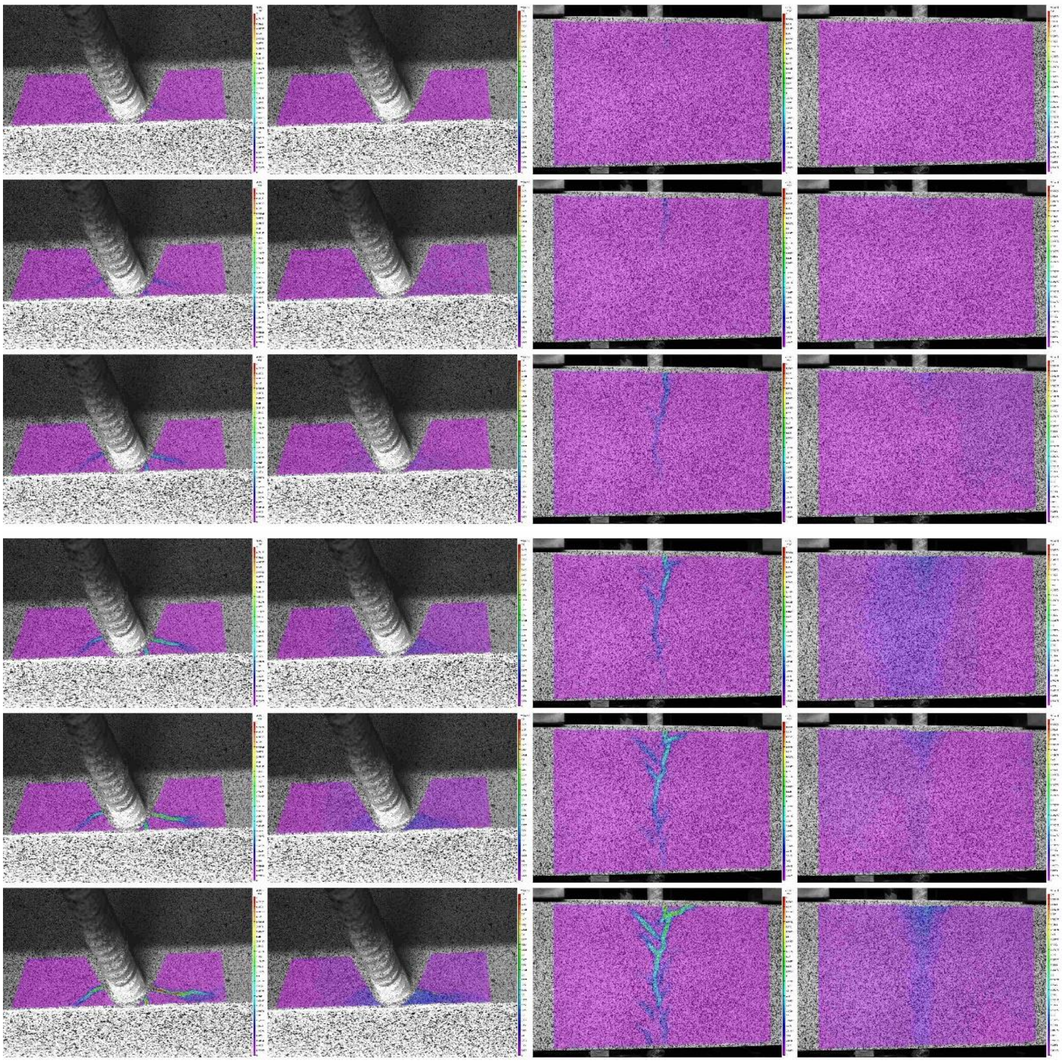

ML10D20-9 (bottom bar, c = 5 mm, ϕ = 20 mm)

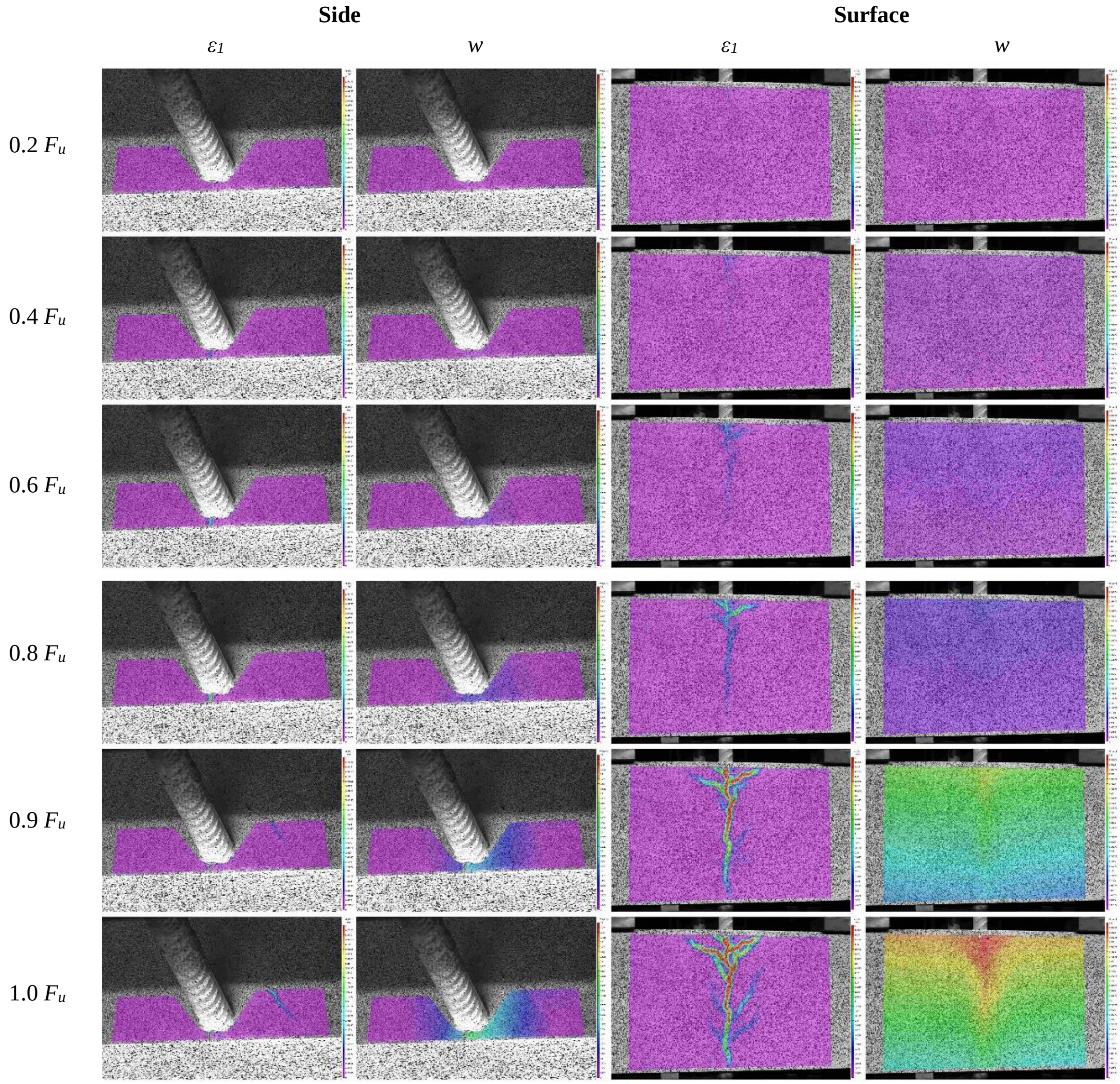

<u>ML10D20-10 (bottom bar, c = 10 mm, ϕ = 20 mm)</u>

	Side		Surface	
	ε_1	w	ε_1	w
0.2 F_u				
0.4 F_u				
0.6 F_u				
0.8 F_u				
0.9 F_u				
1.0 F_u				

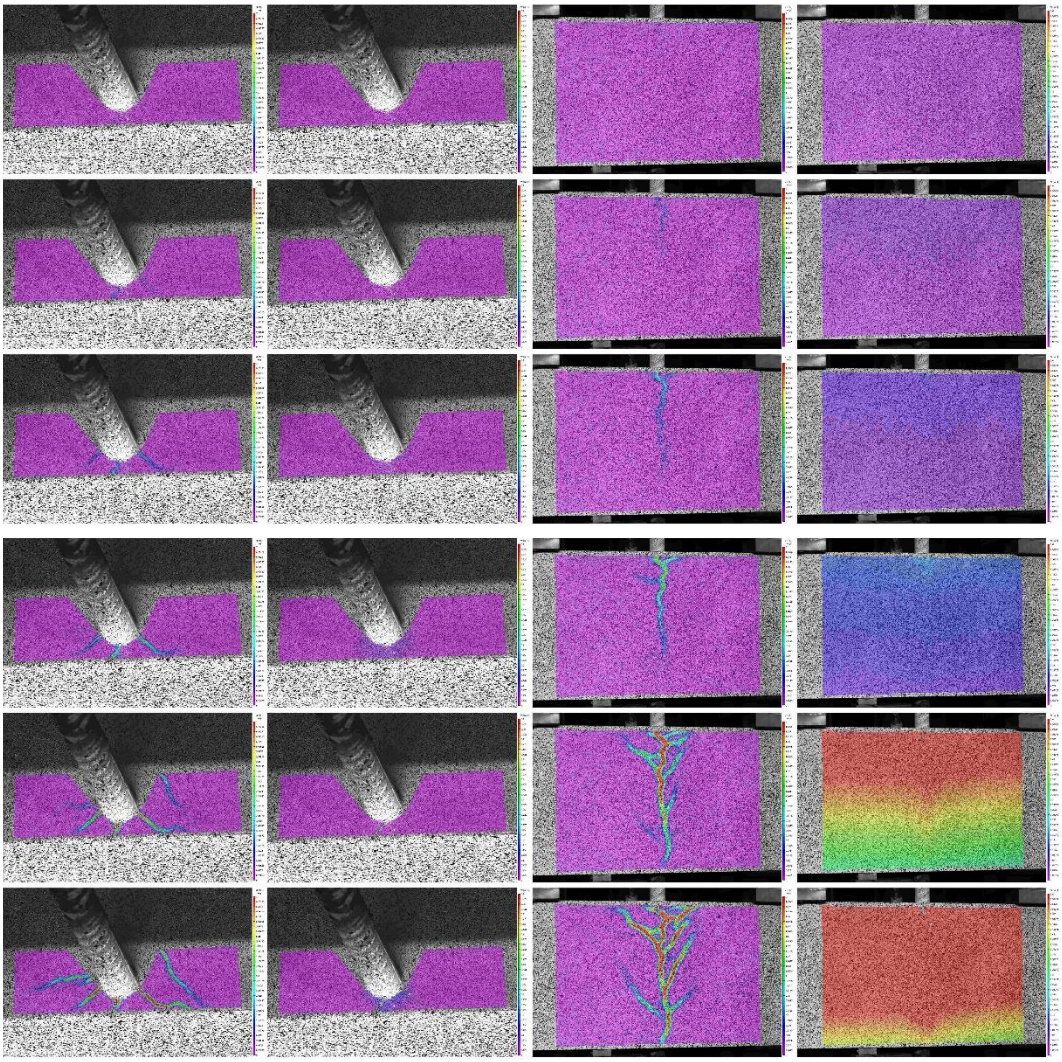

ML10D20-11 (bottom bar, c = 15 mm, ϕ = 20 mm)

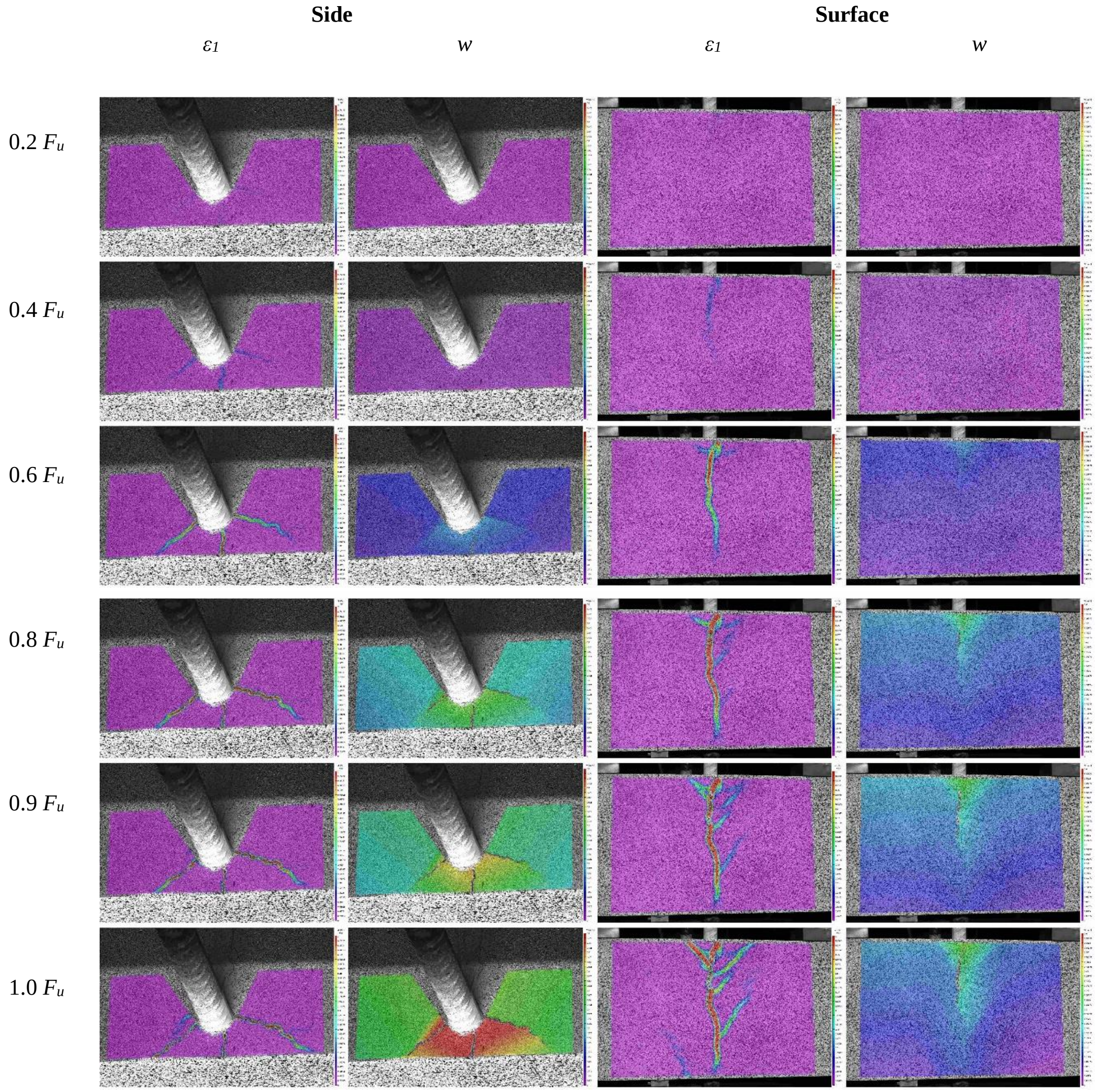

<u>ML10D20-12 (bottom bar, c = 20 mm, ϕ = 20 mm)</u>

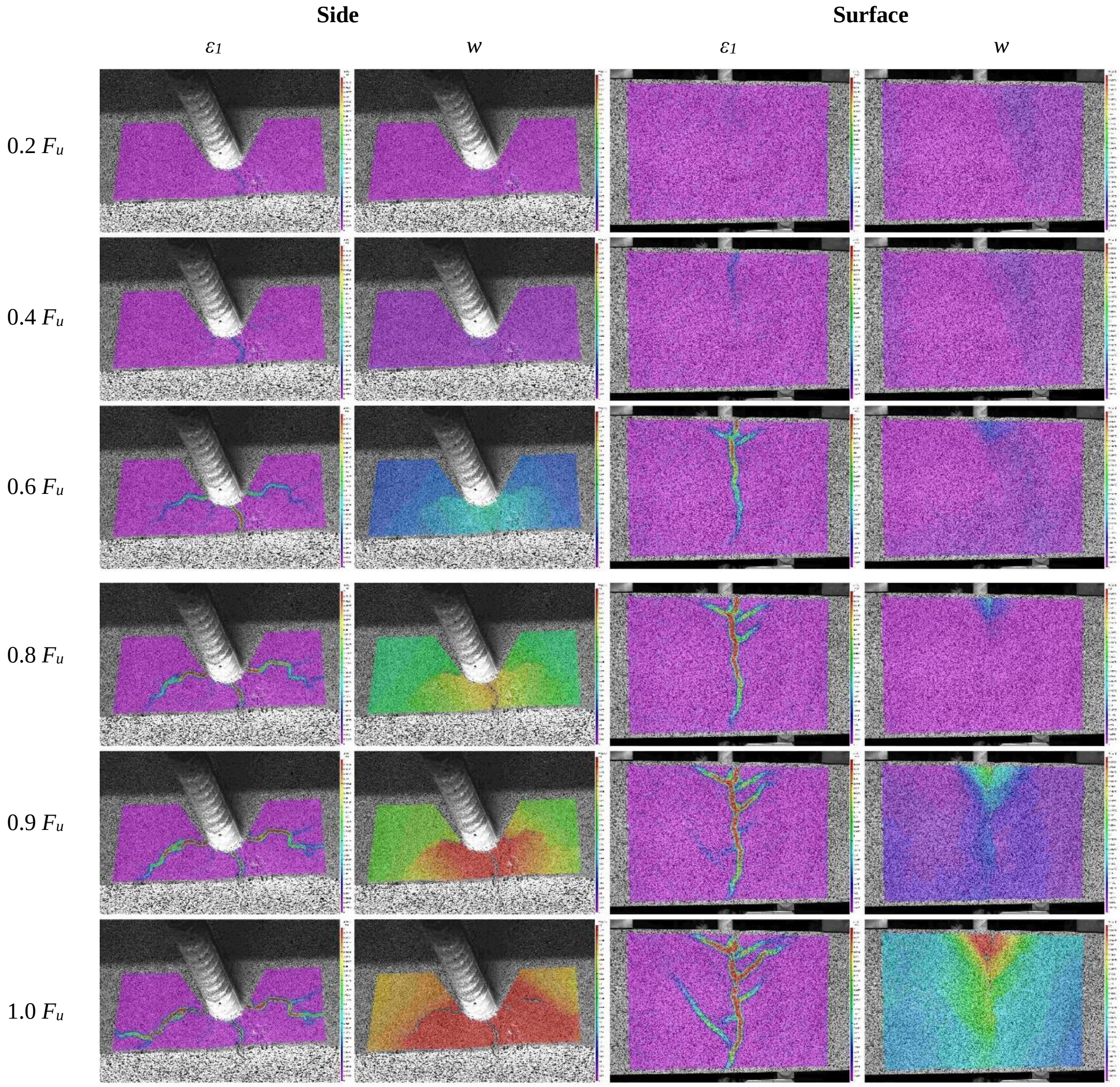

<u>ML10D14-15 (top bar, c = 0 mm, ϕ = 14 mm)</u>

	Side		Surface	
	ε_1	w	ε_1	w

0.2 F_u

0.4 F_u

0.6 F_u

0.8 F_u

0.9 F_u

1.0 F_u

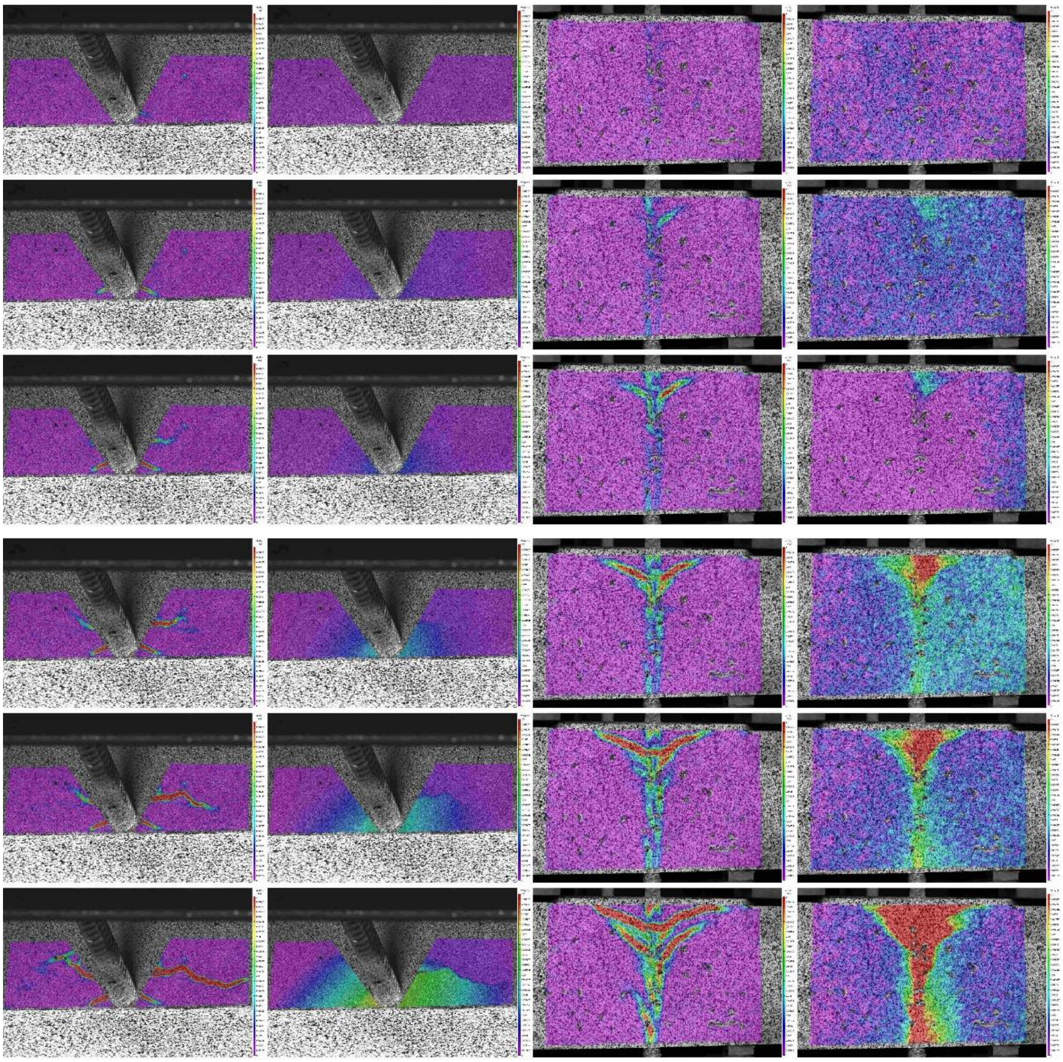

<u>ML10D14-16 (top bar, c = 3.5 mm, ϕ = 14 mm)</u>

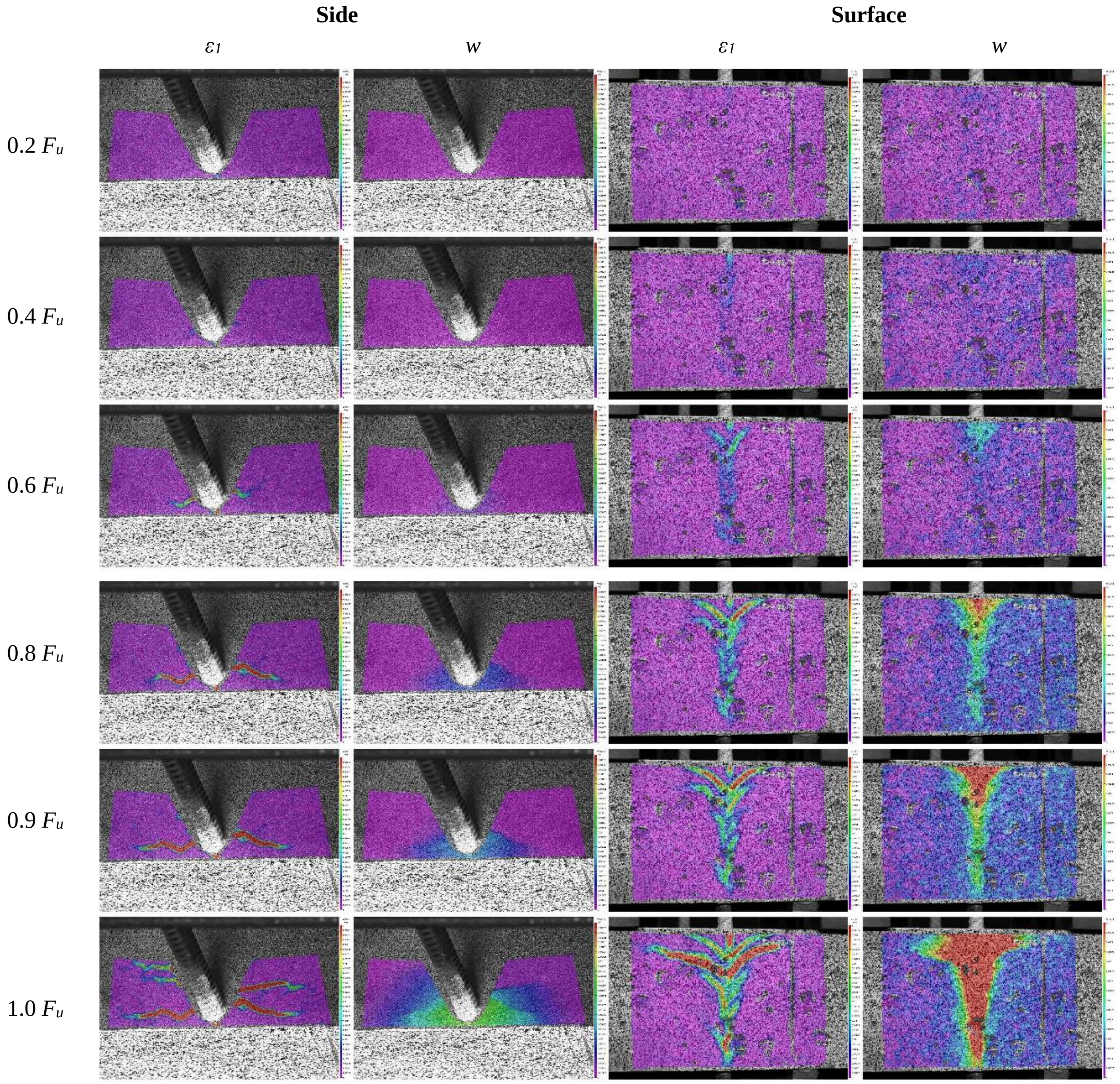

ML10D14-17 (top bar, c = 7 mm, ϕ = 14 mm)

Side **Surface**

ε_1 w ε_1 w

0.2 F_u

0.4 F_u

0.6 F_u

0.8 F_u

0.9 F_u

1.0 F_u

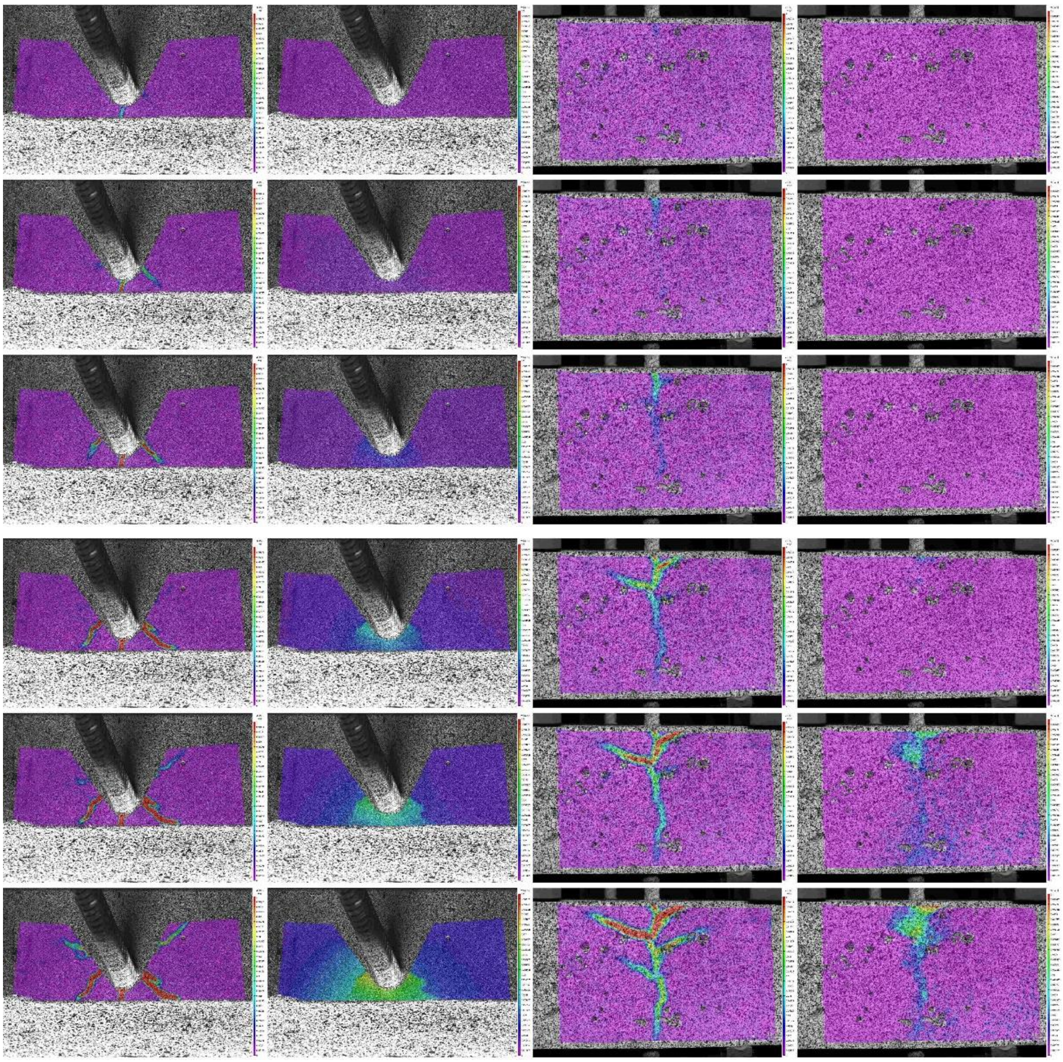

<u>**ML10D14-18 (top bar, c = 10.5 mm, ϕ = 14 mm)**</u>

	Side		**Surface**	
	ε_1	w	ε_1	w
0.2 F_u				
0.4 F_u				
0.6 F_u				
0.8 F_u				
0.9 F_u				
1.0 F_u				

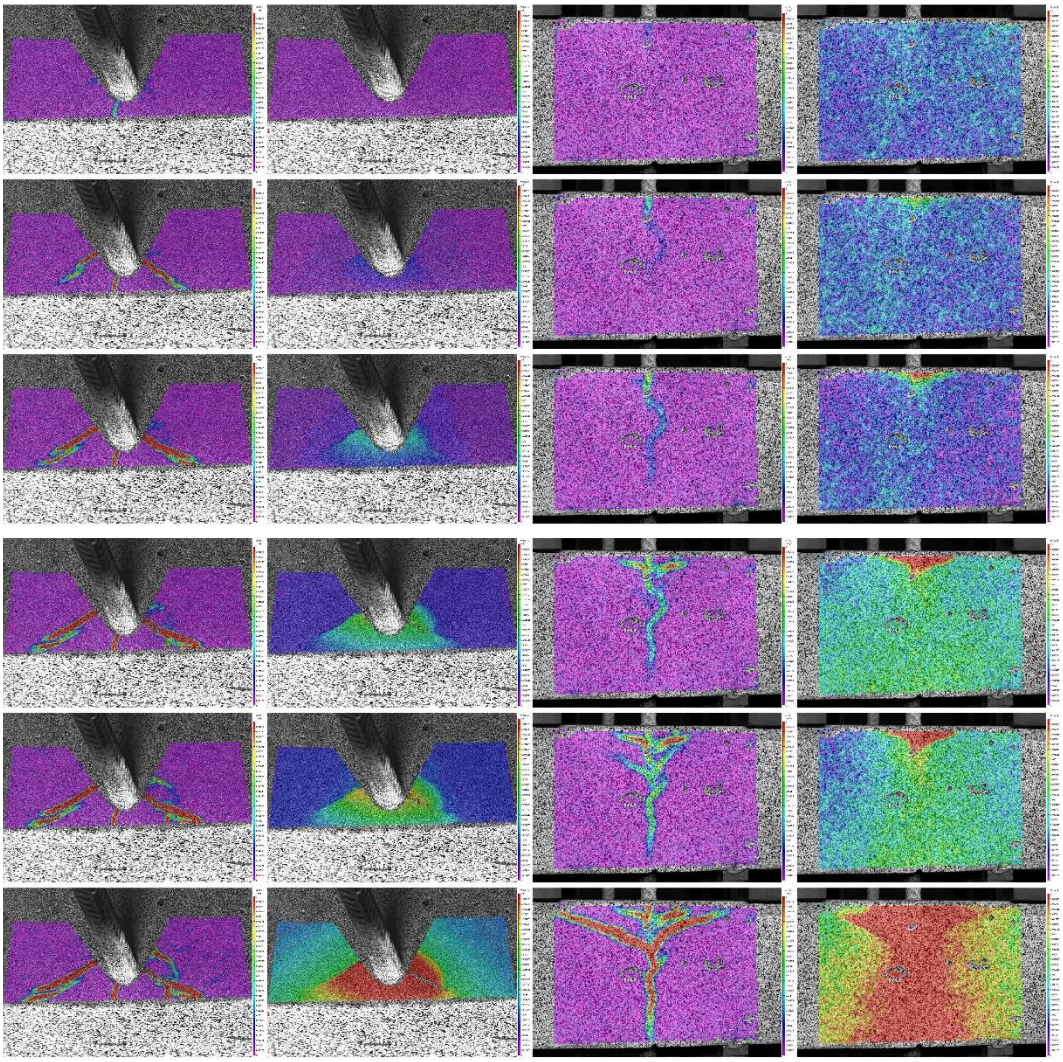

ML10D14-19 (top bar, c = 14 mm, ϕ = 14 mm)

Side **Surface**

ε_1 w ε_1 w

0.2 F_u

0.4 F_u

0.6 F_u

0.8 F_u

0.9 F_u

1.0 F_u

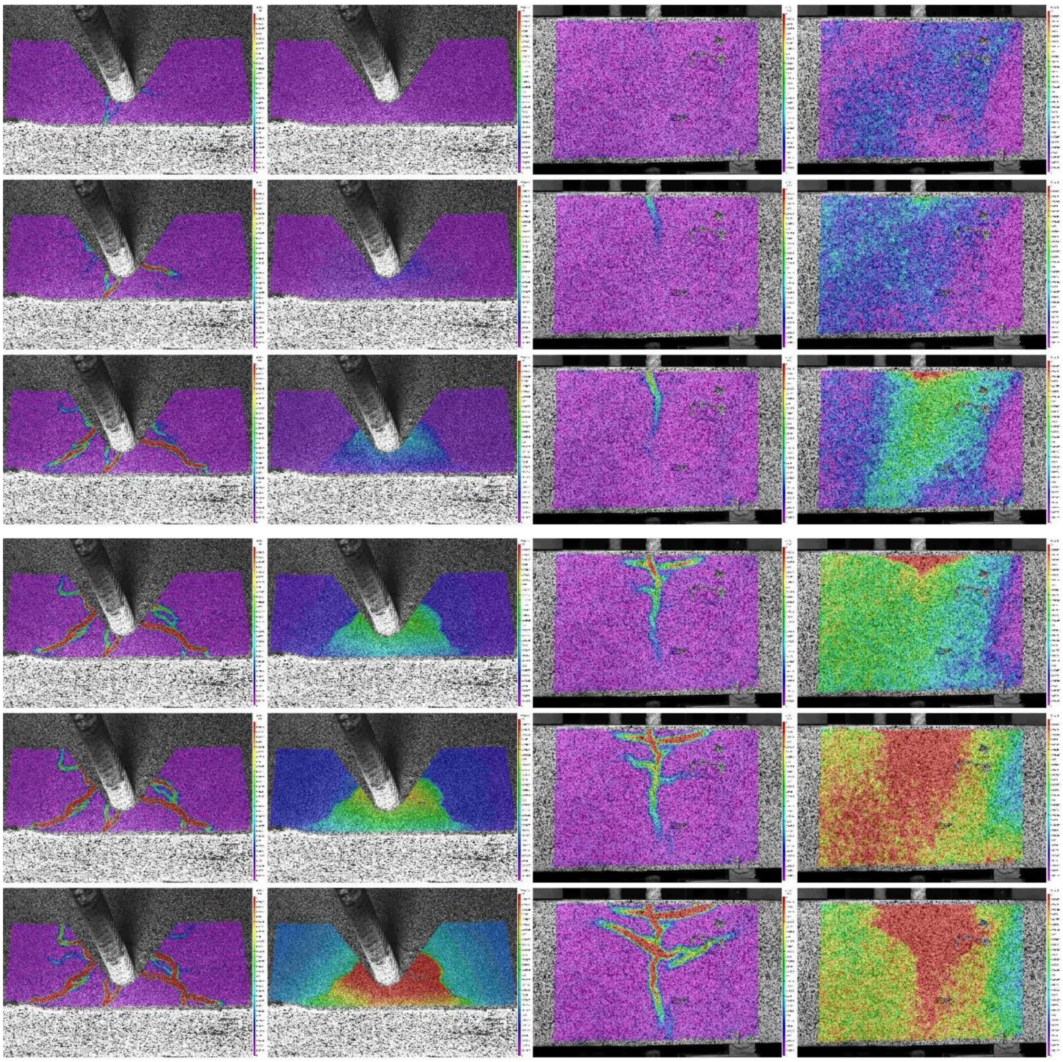

<u>ML10D14-20 (top bar, *c* = 21 mm, ϕ = 14 mm)</u>

Side **Surface**

ε_1 w ε_1 w

0.2 F_u

0.4 F_u

0.6 F_u

0.8 F_u

0.9 F_u

1.0 F_u

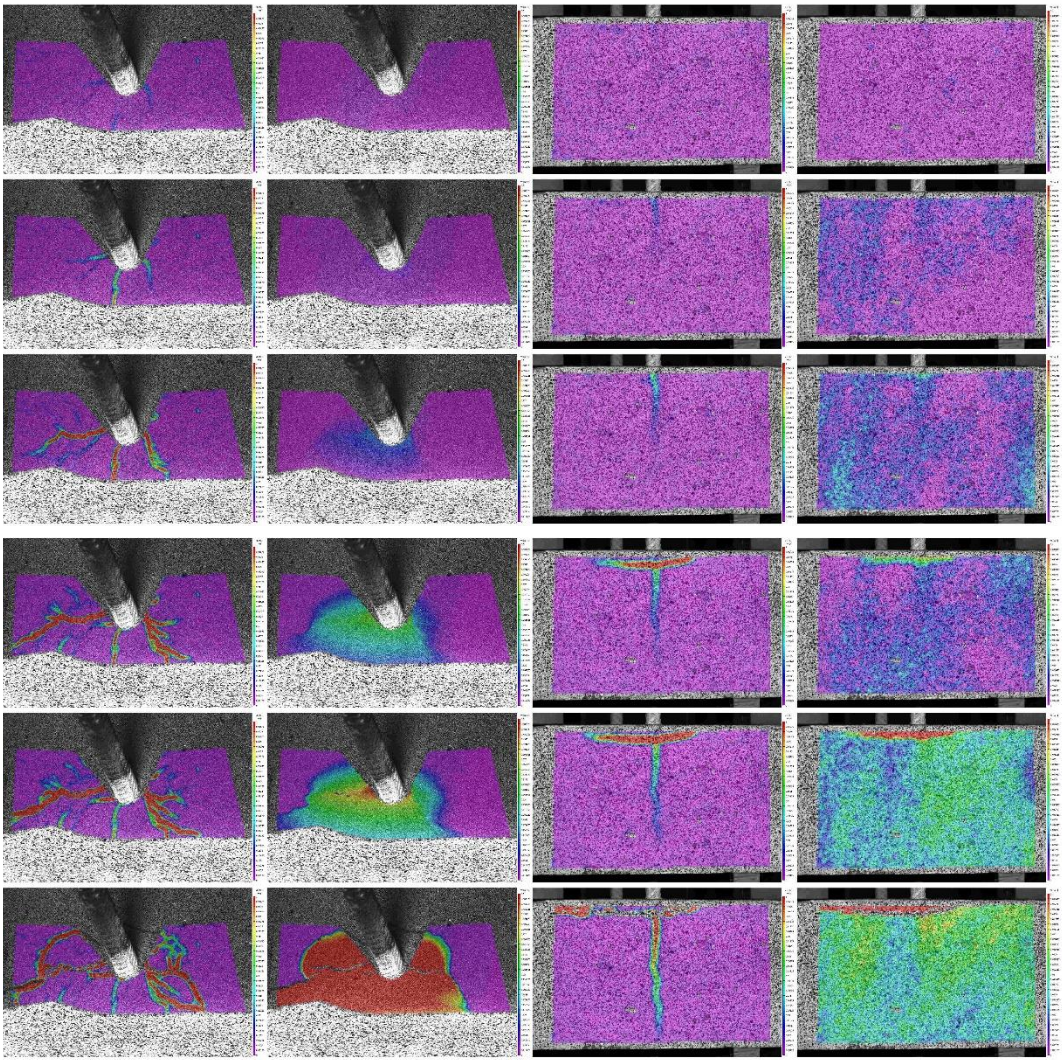

<u>ML10D14-21 (top bar, c = 28 mm, ϕ = 14 mm)</u>

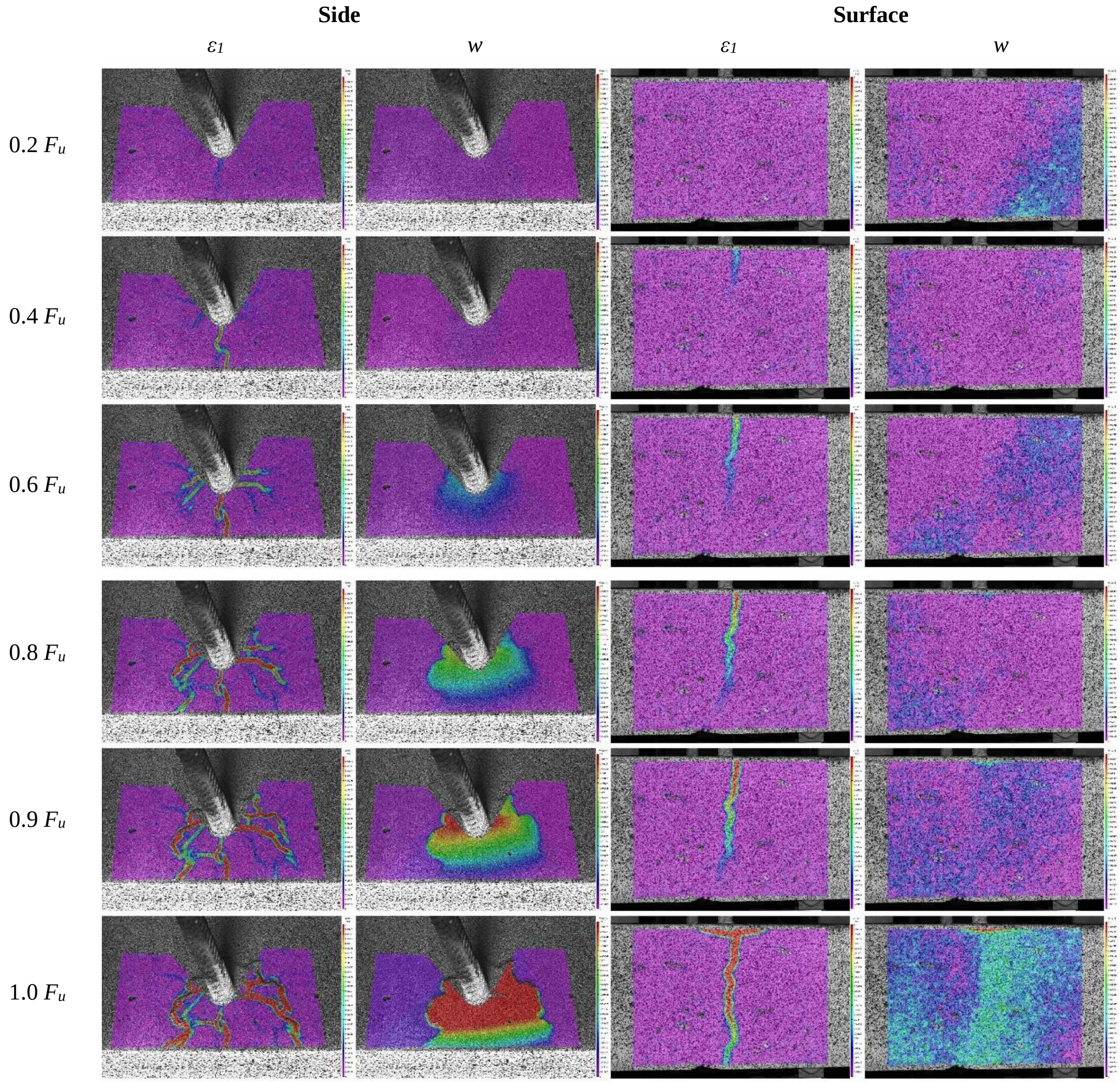

ML10D14-22 (bottom bar, c = 0 mm, ϕ = 14 mm)

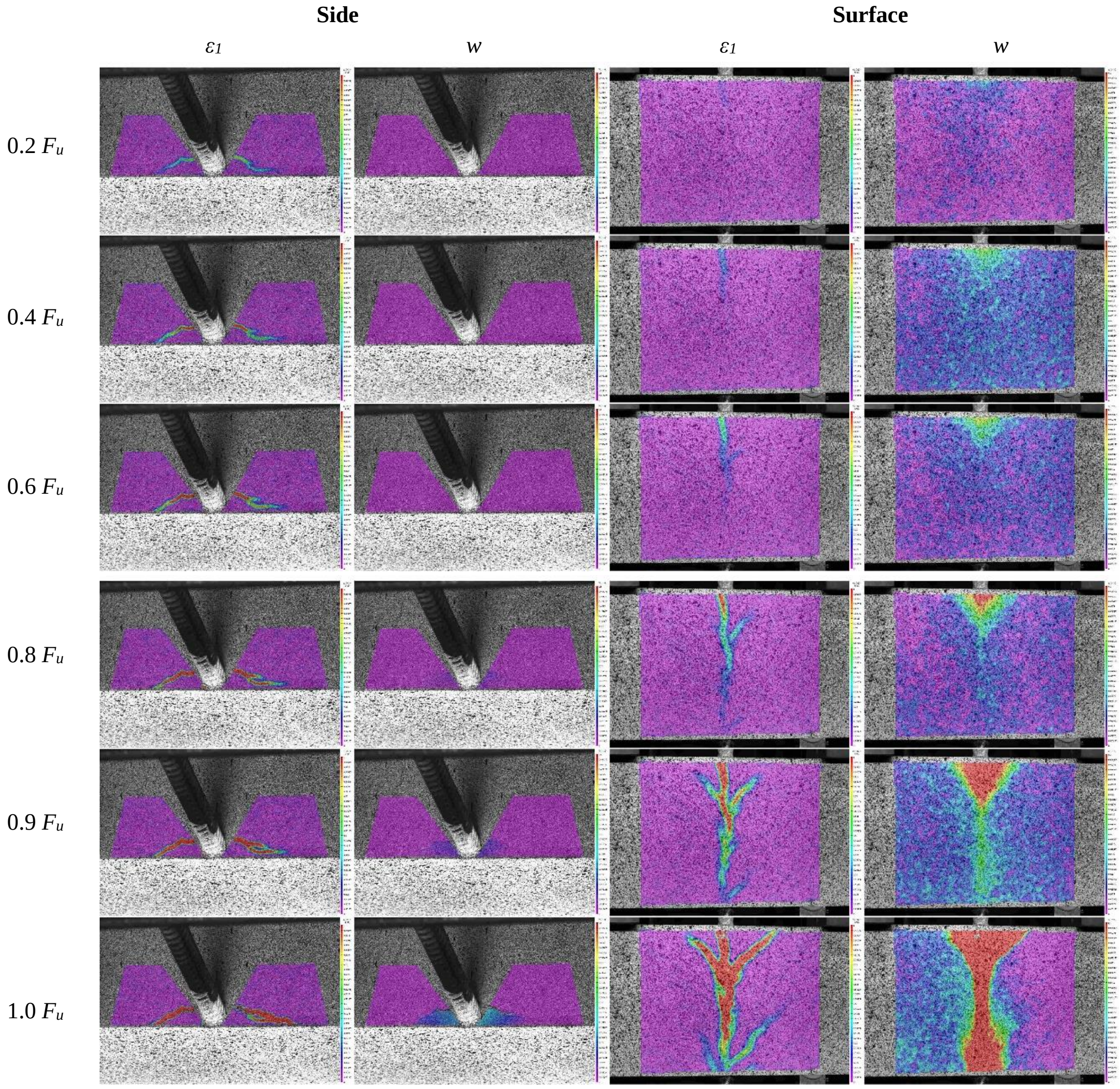

<u>ML10D14-23 (bottom bar, c = 3.5 mm, ϕ = 14 mm)</u>

	Side		Surface	
	ε_1	w	ε_1	w
0.2 F_u				
0.4 F_u				
0.6 F_u				
0.8 F_u				
0.9 F_u				
1.0 F_u				

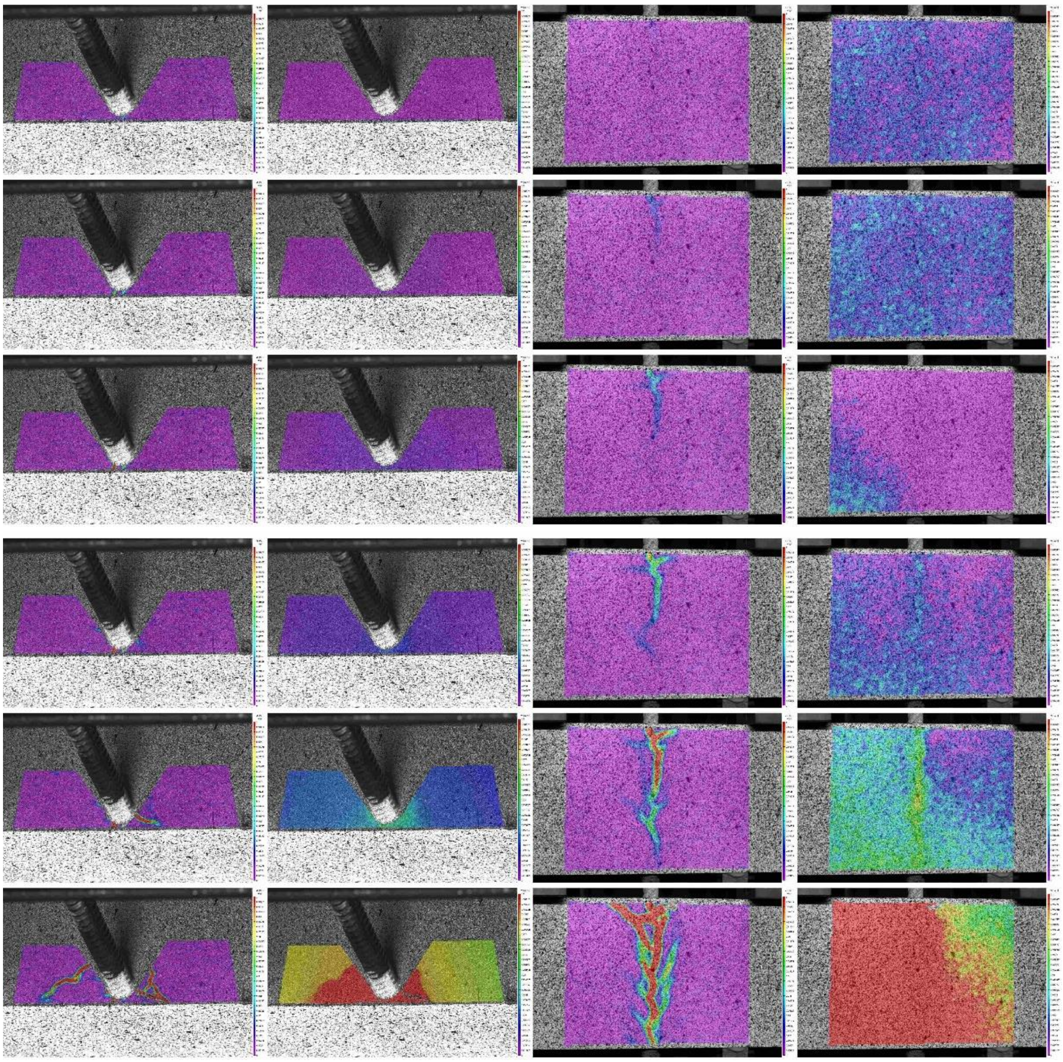

<u>ML10D14-24 (bottom bar, c = 7 mm, ϕ = 14 mm)</u>

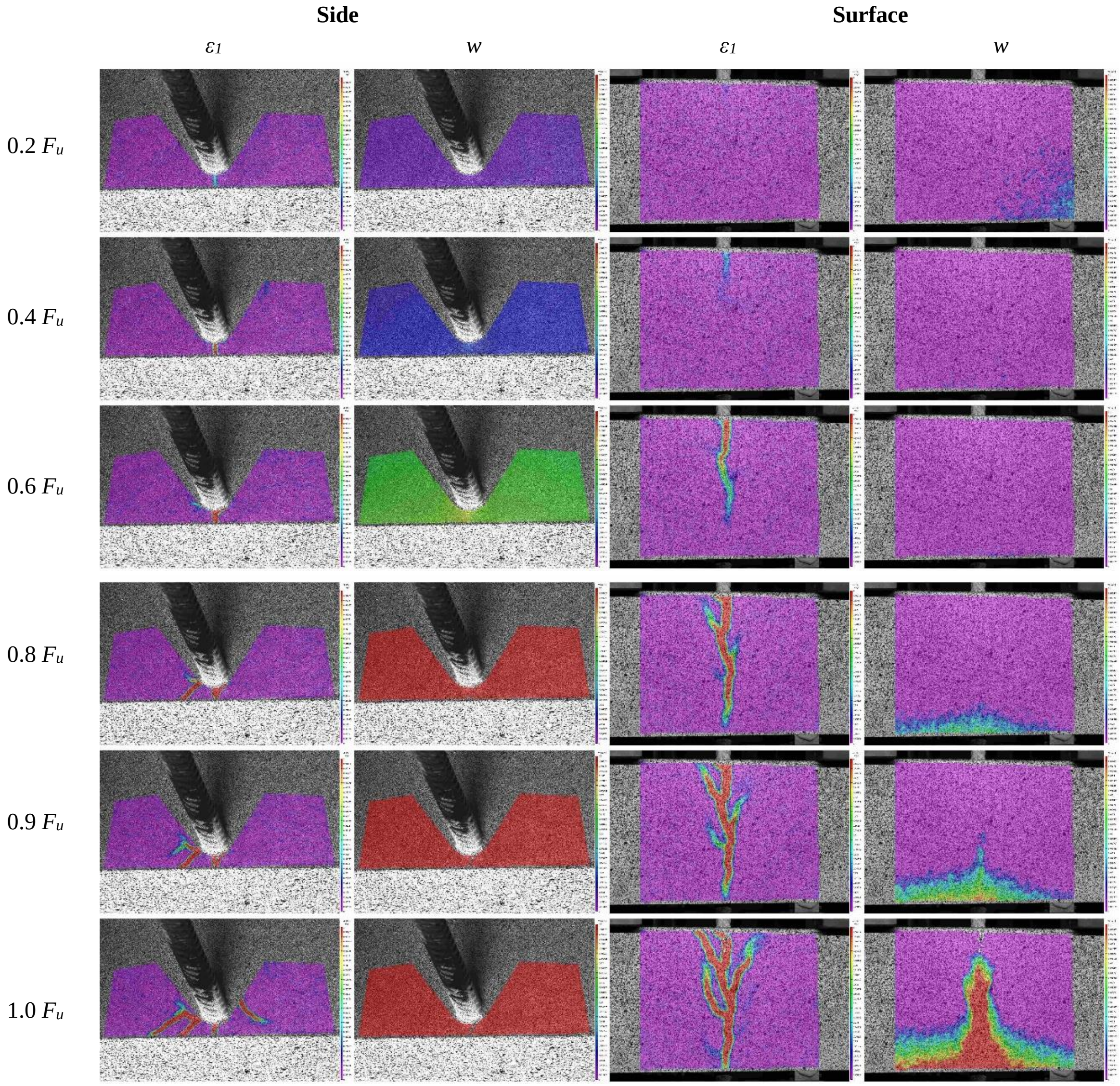

ML10D14-25 (bottom bar, c = 10.5 mm, ϕ = 14 mm)

	Side		Surface	
	ε_1	w	ε_1	w
0.2 F_u				
0.4 F_u				
0.6 F_u				
0.8 F_u				
0.9 F_u				
1.0 F_u				

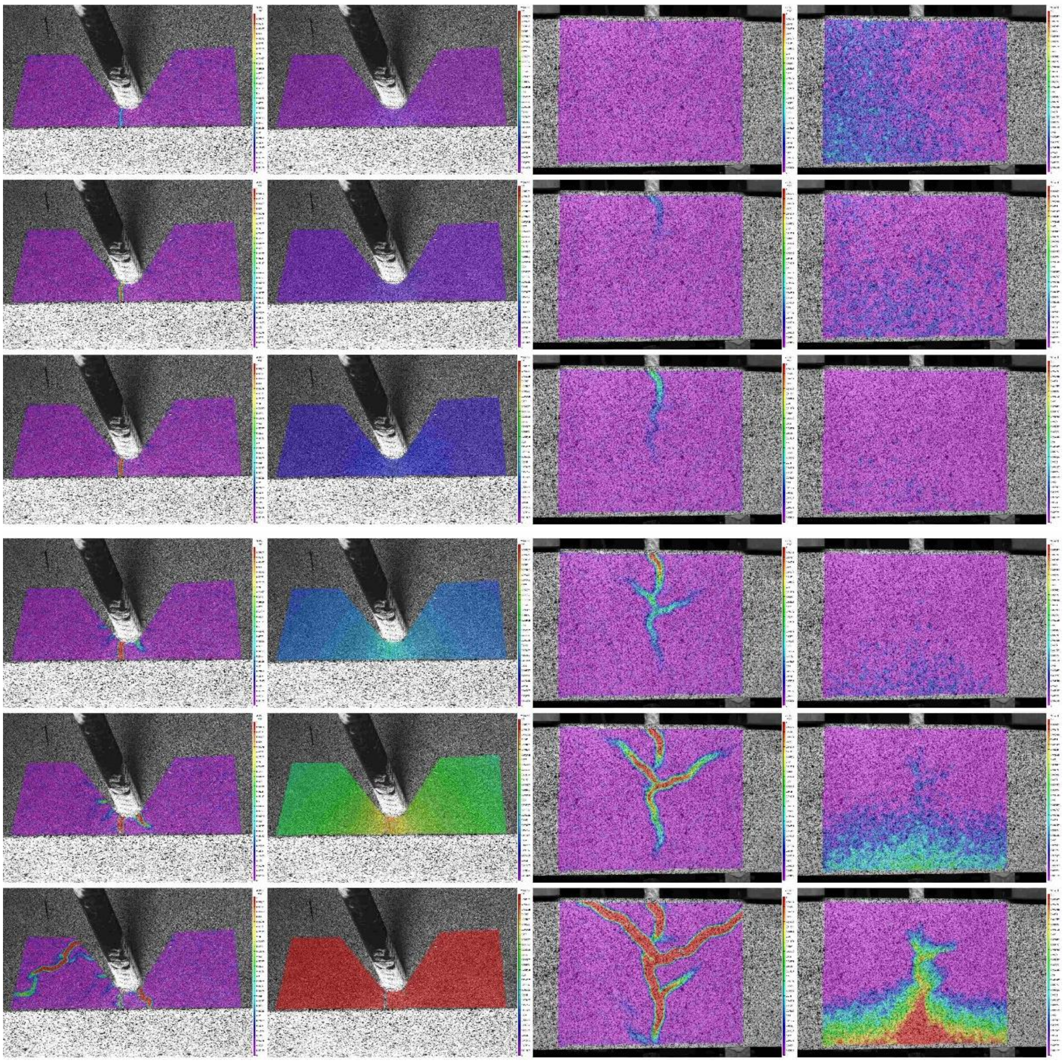

<u>ML10D14-26 (bottom bar, c = 14 mm, ϕ = 14 mm)</u>

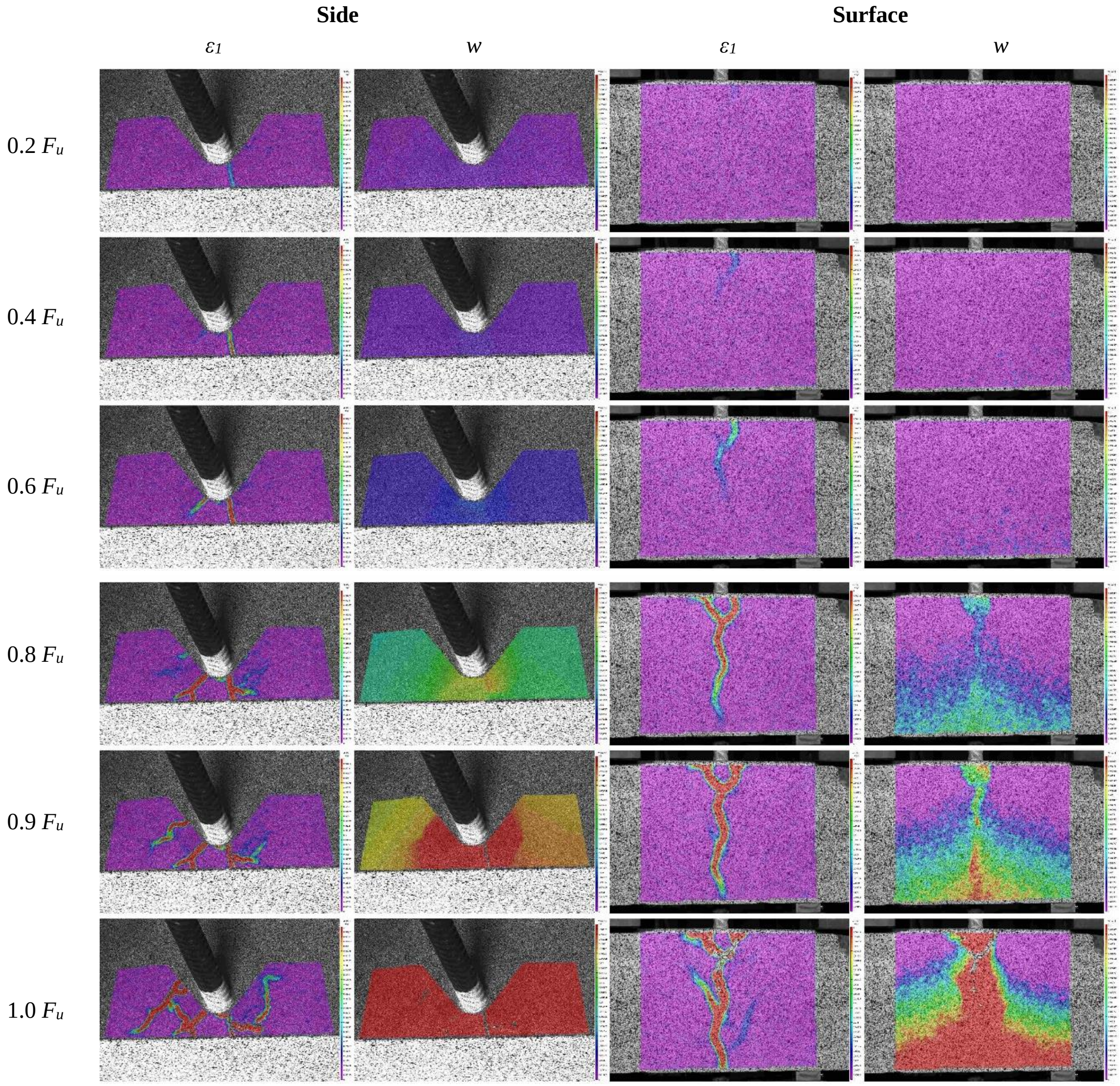

<u>ML10D14-27 (bottom bar, c = 21 mm, ϕ = 14 mm)</u>

	Side		Surface	
	ε_1	w	ε_1	w
0.2 F_u				
0.4 F_u				
0.6 F_u				
0.8 F_u				
0.9 F_u				
1.0 F_u				

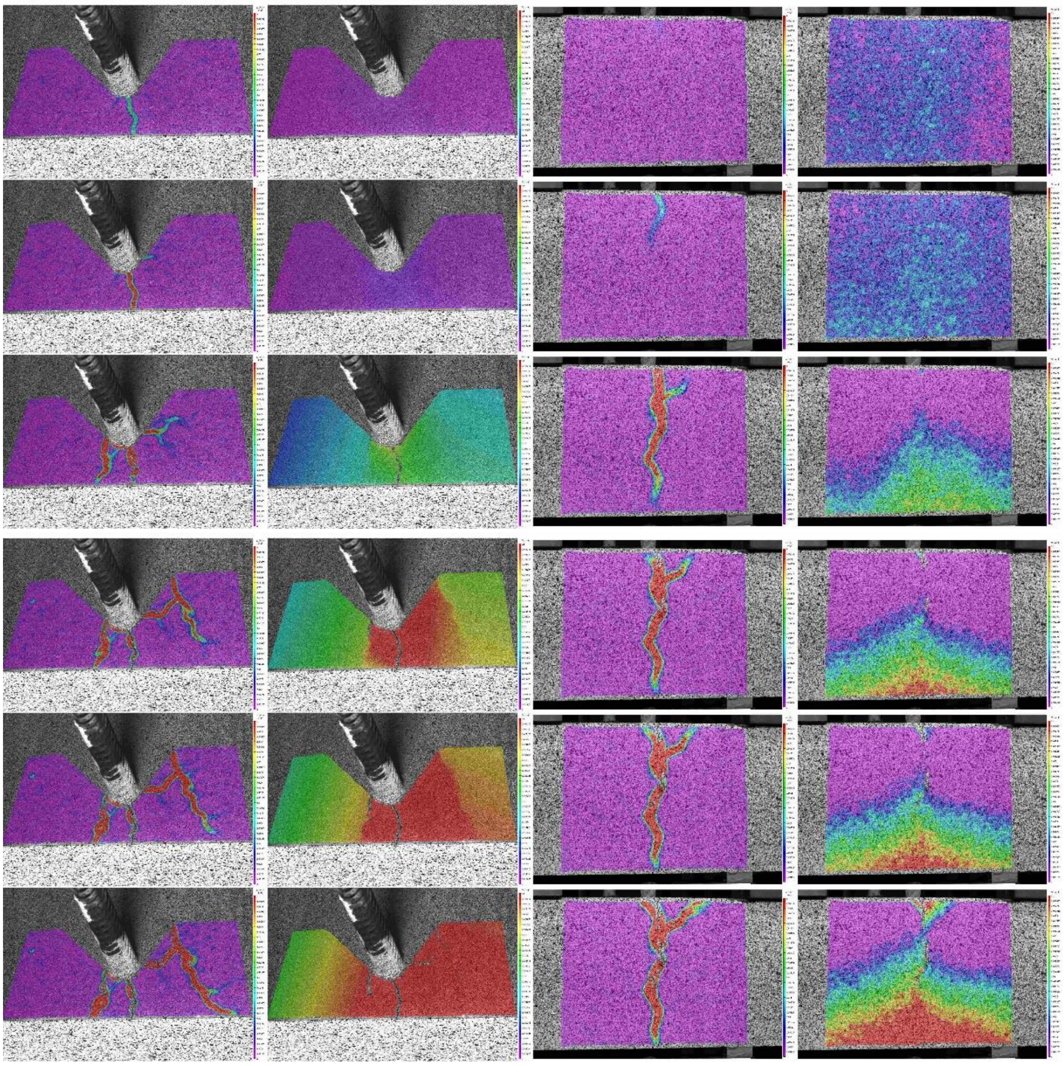

ML10D14-28 (bottom bar, c = 28 mm, ϕ = 14 mm)

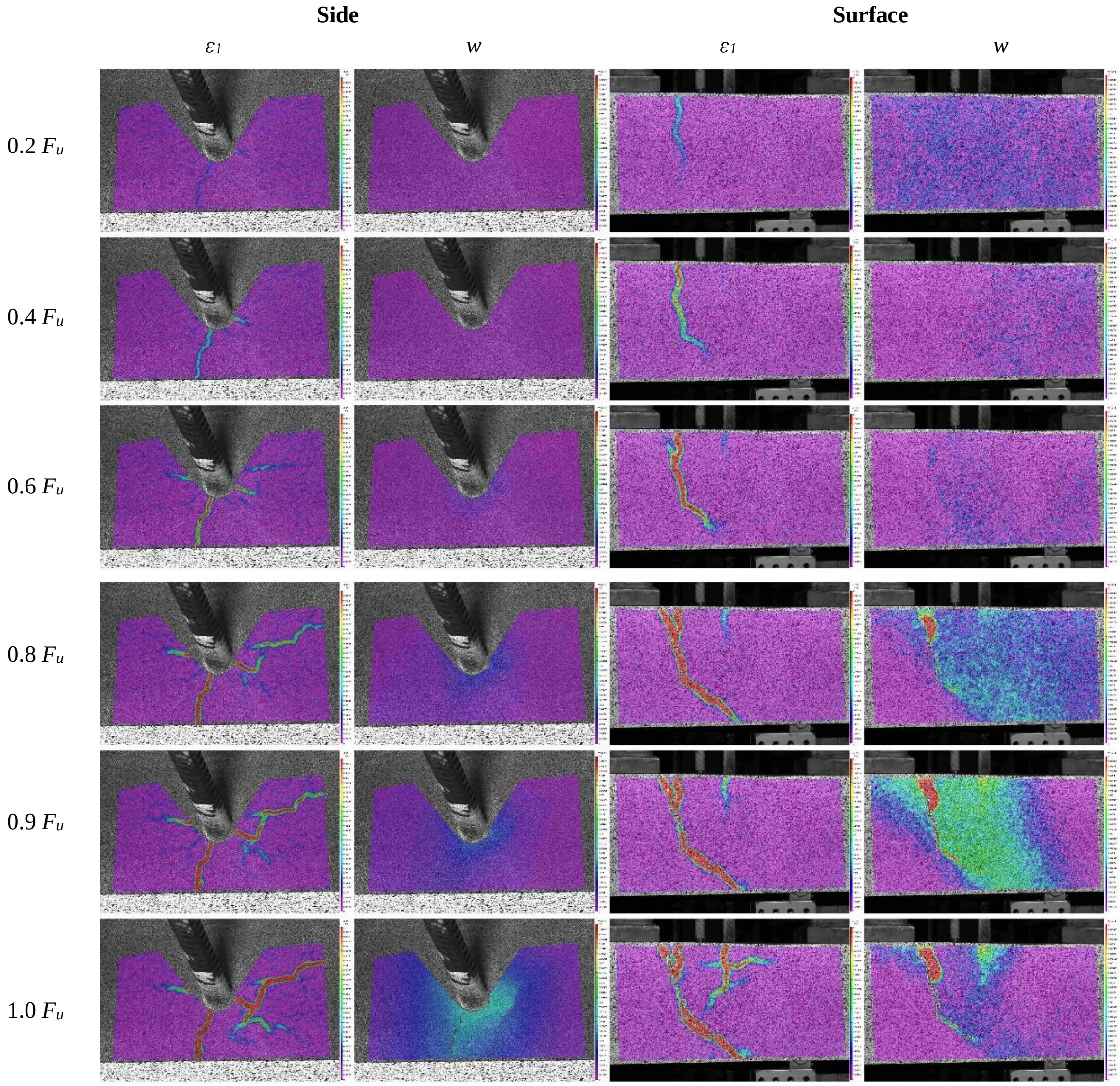

Curriculum Vitae

Francesco MOCCIA

francescomoccia1991@gmail.com
Chemin de Montelly, 18
1007 Lausanne

Born: 28th January 1991 in Locarno (Switzerland), Swiss nationality
Languages: Italian (native speaker), French and English (fluent), German (basic)

EDUCATION

2013-2015	**Master of Science MSc in Civil Engineering, Ecole Polytechnique Fédérale de Lausanne** First prize of the Holcim Junior Trophy for the most outstanding Master Thesis on reinforced concrete structures. Grade point average 5.66 out of 6.
Spring 2015	**Master Thesis at The University of Texas at Austin** Investigation of shear strength of post-tensioned girders, supervised by Profs. O. Bayrak and A. Muttoni.
2010-2013	**Bachelor of Science BSc in Civil Engineering, Ecole Polytechnique Fédérale de Lausanne** Grade point average 5.37 out of 6.

PROFESSIONAL EXPERIENCE

Jan. 2016 – Nov. 2020	**PhD Research Assistant, Structural Concrete Laboratory IBETON, EPFL** Experimental and theoretical work on the evaluation of the compressive and bond strength using detailed measurement techniques (supervised by Prof. A. Muttoni and Dr M. Fernández Ruiz).
2017	Reviewer of **Structural Concrete**, Journal of the *fib*
2013	**Thomas Jundt Ingénieurs Civils SA**, Geneva and Bern, Internship (2 months)
2010-2012	**Locarno Film Festival,** Staff for the “Prix du public UBS”
2008-2009	**Casé Woodworking, Minusio,** furniture manufacturing and assembling (2 months)

COMPUTER SKILLS

Calculation	Matlab, JConc, Cubus, Axis VM, Excel
Drafting	Adobe Illustrator, Audesk AutoCAD
Others	LaTex, Word, PowerPoint, Adobe Lightroom

PUBLICATIONS

2020	F. Moccia, M. Fernández Ruiz, A. Muttoni, *Spalling of concrete cover induced by reinforcement,* Engineering Structures [submitted for review].
2020	F. Moccia, M. Fernández Ruiz, G. Metelli, A. Muttoni, G. Plizzari, *Casting position effects on bond performance of reinforcement bars*, Structural Concrete [submitted for review].
2020	F. Moccia, Q. Yu, M. Fernández Ruiz, A. Muttoni, *Concrete compressive strength: from material characterization to a structural value*, Structural Concrete, pp. 1-20.
2020	F. Moccia, X. Kubski, M. Fernández Ruiz, A. Muttoni, *The influence of casting position and disturbance induced by reinforcement on the structural concrete strength*, Structural Concrete, pp. 1-28.
2018	A. Muttoni, M. Fernández Ruiz, F. Moccia, *Strength reduction factor for concrete in compression*, Background document to prEN 1992-1-1:2018, European Committee for Standardization (CEN), Brussels, Belgium, pp. 9-26.
2018	F. Moccia, M. Fernández Ruiz, A. Muttoni, *Efficiency Factors for Plastic Design in Concrete: Influence of Brittleness in Compression*, High Tech Concrete: Where Technology and Engineering Meet, Springer International Publishing, pp. 1234-1242.